The biocompatible and antimicrobial properties of Ag-$SrPO_4$-Mg

Dr. Jizhou Cheng

BSc, MChD

A thesis submitted for the Doctorate of Philosophy of the Australian National University

Trauma and Orthopaedic Research Unit, the Canberra Hospital, the Australian National University Medical School, Canberra, Australia

Declaration

This thesis presents research undertaken at the Trauma and Orthopaedic Research Unit (TORU), The Canberra Hospital and the John Curtin School of Medical Research, Australian National University, Canberra, Australia.

The research project was conducted under the supervision and guidance of Associate Professor Rachel Li, Professor Paul Smith, Dr. Karina Kennedy, and Dr. Anindita Das.

I hereby certify that the work in this thesis is the result of original research and has not been submitted for a higher degree at any other university or institution. To the best of my knowledge and belief, the thesis contains no material previously published or written by another person except where reference is made. The thesis is under 100000 words.

Signed:

Jizhou Cheng

Principle supervisor

Rachel Li

Acknowledgments

I will forever be grateful to my primary supervisor, Associate Professor Rachel W Li and the chair of my supervisory panel, Professor Paul Smith, for their guidance, inspiration, and support throughout the project. I would also like to thank my parents and my wife Ella for their unwavering support. In addition, I would like to thank the following people for the enormous help they have offered that made this project possible:

- **Patients who agreed to participate in this study.**
- **Dr. Donghai Zhang**
- **Department of Orthopaedic Surgery, the Canberra Hospital**
- **Theatre team, Calvary John James Hospital**
- **Trauma Orthopaedic Research Unit**
- **John Curtin School of Medical Research**
- **The Canberra Hospital Microbiology Laboratory**
- **Centre of Advanced Microscopy, Australian National University**
- **Dr. Karina Kennedy**
- **Dr. Anindita Das**

Abstract

The utilization of novel biomaterials in the field of orthopaedic surgery is ever increasing. Prosthetic joint infections however remain a significant cause of mortality and morbidity for patients undergoing orthopaedic procedures, as well as being a significant economic burden to healthcare systems, with *S. aureus,* coagulase-negative Staphylococci such as *S. epidermidis* and Gram-negative bacilli such as *E. coli* and *P. aeruginosa* being the most common offending organisms. Therefore, biomaterials that are bioactive, biodegradable and prevent infection are required. In addition, the host capsular tissue response to prosthetic joint infections at a genetic level, which ultimately culminates in septic loosening around the prosthesis, requires further understanding.

This study sought to examine the anti-bacterial and bioactive effects of a novel biomaterial, silver strontium phosphate magnesium (Ag-$SrPO_4$-Mg). This study tested Ag-$SrPO_4$-Mg against the aforementioned four bacterial species using LIVE/DEAD viability assay and found that *S. aureus, S. epidermidis, E. coli* and *P. aeruginosa* were on average inhibited by 93.38%, 32.09%, 85.8% and 47.69%, respectively, compared to stainless steel. This was further confirmed by scanning electron microscopy whereby the surface of Ag-$SrPO_4$-Mg discs had scant bacterial attachment compared to confluent bacterial attachment on stainless steel.

The bioactivity and cytotoxicity of Ag-$SrPO_4$-Mg on primary human osteoblasts was tested using ALP assay as well as mineralization assay. We tested 24-hour, 48-hour, 7-day and 14-day extracts of Ag-$SrPO_4$-Mg at concentrations of 10 µL/mL, 1 µL/mL and 0.1 µL/mL. This study did not find a significant reduction in ALP expression or mineralization in osteoblasts treated with Ag-$SrPO_4$-Mg extracts compared to $SrPO_4$-Mg, Mg or PBS controls. The differences that did reach statistical significance have an unclear clinical significance but signified no additional cytotoxicity of Ag-$SrPO_4$-Mg.

The project also investigated the gene expression in response to infection by performing RNA extraction, cDNA synthesis and PCR array on capsular tissue obtained from patients at time of primary or reversion arthroplasty. Capsular tissue obtained from patients undergoing revision surgeries for prosthetic joint infections demonstrated significant upregulation of the genes CCL20, CXCL6 and IL27 compared to patients undergoing primary joint replacements at 6.58-fold, 6.81-fold, and 20.98-fold respectively while TNFRSF11B was significantly downregulated by 8.52-fold.

The project demonstrated that Ag-$SrPO_4$-Mg is a promising orthopaedic biomaterial in the prevention of prosthetic joint infections while conferring no additional toxicity to host osteoblasts.

List of abbreviations

A2M – Alpha-2-macroglobulin

AAP – Accumulation associated protein

ACT – Australian Capital Territory

ACTB – Actin, beta

AD – Alpha defensin

AgNP – Silver nanoparticle

AIMP1 – Aminoacyl tRNA synthetase complex-interacting multifunctional protein 1

ALP – Alkaline phosphatase

ANOVA – Analysis of variance

ANU – Australian National University

APC – Antigen presenting cell

Ar – Argon

AR-S – Alizarin red

AST – Antibiotic suppression therapy

ATCC – American Type Culture Collection

Au – Gold

AVN – Avascular necrosis

B2M – Beta-2-microglobulin

BBB – Blood brain barrier

Bbp – Bone sialoprotein-binding protein

BHI – Brain heart infusion broth

BMI – Body mass index

BMP – Bone morphogenic protein

BPH – Benign prostatic hypertrophy

BPI – Bactericidal permeability-increasing protein

Ca – Calcium

CALCR – Calcitonin receptor

CAM – Centre for Advanced Microscopy

CAMP/LL37 – Cathelicidin antimicrobial peptide

CCF – Congestive cardiac failure

CCL – Chemokine (C-C motif) ligand

CCR – Chemokine (C-C motif) receptor

CD40LG – CD40 ligand

cDNA – Complementary DNA

CFU – Colony forming unit

CKD – Chronic kidney disease

Co – Cobalt

CPC – Cetylpyridinium chloride

Cr – Chromium

CRISPR – Clustered regularly interspaced short palindromic repeats

CRP – C-reactive protein

CSF – Colony stimulating factor

CVA – Cerebrovascular accident

CVC – Central venous catheter

CX3CL – Chemokine (C-X3-C) motif ligand

CXCL – Chemokine (C-X-C) motif ligand

CXCR – Chemokine (C-X-C) motif receptor

ddH_2O – Double distilled water

DAIR – Debridement, antibiotics and implant retention

DEF – Defensin

DNA – Deoxyribonucleic acid

DVT – Deep vein thrombosis

EBP – Elastin-binding protein

ECG – Electrocardiogram

EBI3 – Epstein-Barr virus induced gene 3

eDNA – Extracellular DNA

ELA-2 – Neutrophil elastase 2

ELANE – Neutrophil elastase

ELISA – Enzyme-linked immunosorbent assay

EMBP – Extracellular matrix binding protein

ESR – Erythrocyte sedimentation rate

EPS – Extracellular polymeric substance

ESD – Leukocyte esterase

ETT – Endotracheal tube

EUCAST – European Committee on Antimicrobial Susceptibility Testing

FASLG – Fas ligand

FBS – Fetal bovine serum

Fe – Iron

FESEM – Field Emission Scanning Electron Microscope

FGF – Fibroblast growth factor

FCGR1A – Fc fragment of IgG receptor Ia

FNB – Fibronectin binding protein

GAPDH – Glyceraldehyde-3-phosphate dehydrogenase

G-CSF – Granulocyte colony stimulating factor

GORD – Gastroesophageal reflux disease

H_2O_2 – Hydrogen peroxide

HA – Hydroxyapatite

HbA1c – Glycosylated haemoglobin

HBV – Hepatitis B virus

HCAI – Healthcare-associated infections

HCV – Hepatitis C virus

HEPES – 2% N-2-hydroxyethylpiperazine-N-2-ethane sulfonic acid

HIV – Human immunodeficiency virus

hMSC – Human mesenchymal stem cell

HPRT – Hypoxanthine phosphoribosyltransferase

HR – Hazard ratio

HSP – Heat shock protein

HTN – Hypertension

IBD – Inflammatory bowel disease

ICM – International Consensus Committee

ICAM – Intercellular adhesion molecule

IDC – Indwelling catheter

IHD – Ischaemic heart disease

IFNA – Interferon alpha

IFNG – Interferon gamma

IL – Interleukin

ILR – Interleukin receptor

LDH – Lactate dehydrogenase

LE – Leukocyte esterase

LPS – Lipopolysaccharide

LRTI – Lower respiratory tract infection

LTA – Lymphotoxin alpha

LTB – Lymphotoxin beta

LTF – Lactotransferrin

MIF – Macrophage migration inhibitory factor

MBL – Mannose-binding lectin

MCP – Monocyte chemoattractant protein

Mg – Magnesium

MIC – Minimal inhibitory concentration

MMP – Matrix metalloproteinase

mRNA – Messenger RNA

miRNA – Micro RNA

MRO – Muti-resistant organism

MRP – Myeloid related protein

MRSA – Methicillin-resistant *Staphylococcus aureus*

MSCRAMM – Microbial surface component recognizing adhesive matrix molecules

MSIS – Musculoskeletal Infection Society

MSSA – Methicillin-sensitive *Staphylococcus aureus*

NAMPT – Nicotinamide phosphoribosyltransferase

NGAL – Neutrophil gelatinase-associated lipocalin

NGS – Next generation sequencing

NfκB – Nuclear factor kappa-light-chain-enhancer of activated B-cells

OPG – Osteoprotegerin

OSA – Obstructive sleep apnea

OSM – Oncostatin M

PAMP – Pathogen-associated molecular patterns

PBS – Phosphate buffered saline

PBMC – Peripheral blood mononuclear cells

PC – Physical containment

PE – Pulmonary embolus

PGE – Prostaglandin E

PI – Peptidase inhibitor

piRNA – piwi-interacting RNA

PJI – Prosthetic joint infection

PIA – Polysaccharide intercellular adhesin

PMMA – Polymethylmethacrylate

PMN – Polymorphonuclear neutrophils

*p*NPP – para-Nitrophenylphosphate

PRR – Pattern recognition receptors

PSA – Capsular polysaccharide

PSM – Phenol-soluble modulin

PSN – Penicillin-streptomycin-neomycin

PVD – Peripheral vascular disease

qPCR – Quantitative polymerase chain reaction

RA – Rheumatoid arthritis

RANK – Receptor activator of NfκB

RANKL – Receptor activator of NfκB ligand

RCF – Relative centrifugal force

RETN – Resistin

RPLP0 – Ribosomal protein, large, P0

ROS – reactive oxygen species

R-TSA – Reverse total shoulder arthroplasty

RT-qPCR – Real time quantitative polymerase chain reaction

SEM – Scanning electron microscopy

SFRP – Secreted frizzled-related proteins

Sdr – Serine aspartate repeat proteins

SLE – Systemic lupus erythematosus

SNP – Single nucleotide polymorphism

snRNA – Small nuclear RNA

SPP – Secreted phosphoprotein

Sr – Strontium

SSI – Surgical site infection

SWCNT – Single walled carbon nanotube

Ta – Tantalum

TEA – Total elbow arthroplasty

TEM – Transmission electron microscopy

TGFβ – Transforming growth factor β

THA – Total hip arthroplasty

THBS – Thrombospondin

Ti – Titanium

TIMP – Tissue inhibitor of metalloproteinase

TKA – Total knee arthroplasty

TLC – Total lymphocyte count

TLR – Toll-like receptor

TMS – Trimethysilane

TNF – Tumor necrosis factor

TNFRSF – Tumor necrosis factor receptor superfamily, member

TNFSF – Tumor necrosis factor ligand superfamily

tRNA – Transfer RNA

TSA – Total shoulder arthroplasty

UHMWPE – Ultra high molecular weight polyethylene

USA – United States of America

UTI – Urinary traction infection

VAP – Ventilator associated pneumonia

VEGF – Vascular endothelial growth factor

VWF – von Willebrand Factor

WNT – Wingless and Int-1

W/V – Weight/volume %

Y – Yttrium

ZnO – Zinc oxide

Table of Contents

List of Tables

List of Figures

Chapter 1: Introduction

1.1 - Healthcare-associated infections

Healthcare-associated infections (HCAIs) are associated with enormous patient morbidity and mortality and pose a huge financial burden on healthcare services. HCAIs can occur in residential care homes, hospitals or in the patients' own homes, at a prevalence of approximately 6.4%. Aside from increased patient morbidity and mortality, HCAIs are the cause of significant economic burden [1].

The most prevalent HCAIs in healthcare systems include lower respiratory tract infections (LRTI) and ventilator-associated pneumonia (VAP) (22.8% of cases), urinary tract infections (UTI) associated with indwelling catheters (IDC) (17.2% of cases) and surgical-site infections (SSI) (15.7% of cases) [1]. The Centers for Disease Control and Prevention (CDC) have identified the most commonly identified pathogens in HCAI as *Escherichia coli (E.coli)*, *Staphylococcus aureus* (*S.aureus*), selected *Klebsiella* species, *Pseudomonas aeruginosa* (*P.aeruginosa*), *Enterococcus faecalis* (*E.faecalis*), and coagulase-negative staphylococci such as *Staphylococcus epidermidis* (*S.epidermidis*) [2, 3]. Risk factors for acquiring HCAIs include prolonged hospital stay, immunocompromised patient, invasive surgery and wound management at home [4]. Routes of transmission for micro-organisms include human skin as well as water and food sources. Infective agents can reach the new host through ingestion, inhalation, breaks in the skin barrier following surgical procedures or insertion of intravenous lines, as well as through mucous membranes, including eyes, mouth, and nose.

1.1.1 - Central venous catheters

Central venous catheters (CVC) are used to deliver medications, fluids, blood products, parenteral nutrition, and dialysis. The in-situ duration of the CVC impacts the degree and location of bacterial colonization, which can occur both in the lumen and on the outside of the device [5]. Anaissie et al found that microbial colonization occurred as early as one day after CVC insertion in adult cancer patients and that it was independent of the clinical status of the patient or the microbiological findings from the CVC [6].

1.1.2 - Urinary catheters

IDC are silicone or latex devices used to measure urine output, prevent urinary retention, control urinary incontinence as well as collect urine during surgical procedures. To prevent infections, clinicians must utilize catheters only when necessary and avoid prolonged catheterization as the risk of infection increases by 10% for each day the IDC is left in situ [7]. The micro-organisms that colonize the periurethral skin and contamination of the urine in the catheter draining bag are sources

of infection that can penetrate the mucoid layer which forms between the epithelial surface of the urethra and the catheter and enter the bladder [8]. In addition to this, frequent disruption and replacement of the catheter can cause shedding of bacteria from the biofilm from indwelling devices which enables dispersion of infecting bacteria to previously uncolonized sites.

1.1.3 - Ventilator associated pneumonia and endotracheal tubes

VAP is a common HCAI and has been reported to be prevalent in patients who have been intubated and ventilated mechanically for longer than 48-72 hours [9], with an increased risk of 6 to 20-fold with mortality rates ranging from 24-76% [10]. Endotracheal tubes (ETTs) are a risk factor for VAP acquisition, with reports of biofilms forming on ETTs within 24 hours of intubation. Numerous micro-organisms can colonize ETTs, including methicillin-resistant *Staphylococcus aureus* (MRSA) and Gram-negative bacilli such as *E.coli*, *K.pneumoniae*, *P.aeruginosa* and *Acinetobacter spp* [11]. VAP has major implications for patient morbidity and mortality as well as a significant burden on the healthcare system leading to prolonged hospital stay and increased costs [12].

1.1.4 - Surgical site infections

Surgical site infections (SSIs) are wound infections that occur following surgical procedures that can be due to the patient's own skin flora, the most common of which is *S.aureus* [13]. Kathju et al found that the microbiome profile found on suture materials of uninfected wounds different from those of infected wounds: *Corynebacterium* and *Bacillus spp* were the most commonly isolated micro-organism isolated from non-infected wounds whereas infected wounds were more likely to be colonized by *S.aureus, S.epidermidis,* MRSA and *P.aeruginosa* [14].

1.2 - Orthopaedic prosthetic joint infections

Since the introduction of joint prosthesis replacement surgery, patients with debilitating degenerative joint diseases have had significant symptom-relief, improved functionality, and quality of life. Approximately 120000 Australians underwent primary joint replacement surgery of the hip, knee and shoulder in 2017 and this number is set to increase with an aging population [15]. Despite the overall success of surgery, prosthetic joint infections (PJIs) remain a devastating and dreaded complication. The incidences of PJI for primary total hip arthroplasty (THA) and for primary total knee arthroplasty (TKA) ranged 0.5-2%, 0.5% to 2.9% for primary anatomic total shoulder arthroplasty (TSA) and 5% for primary reverse total shoulder arthroplasty (R-TSA) [16]. Infection remains one of the leading causes of revision surgery. Infection is associated with significant patient morbidity and twice the

relative mortality risk in patients undergoing revision surgery for infected hip arthroplasty compared to patients undergoing revision for other causes [17]. Moreover, PJIs are a significant economic burden: the annual cost of treatment of PJIs in the United States is projected to exceed $1.62 billion US by the year 2020 [18].

Prostheses-related infections are now thought to be biofilm-associated infections [19, 20]. which are highly resistant to antibiotic treatment [21]. The most common pathogens to establish biofilm infections on orthopaedic implants are *S.aureus, S.epidermidis, E.coli* and *P.aeruginosa*. These pathogens express their own unique proteins called microbial surface components recognizing adhesive matrix molecules (MSCRAMMs) during the attachment phase and maturation phase of biofilm formation. Current management of prosthesis infection involves antibiotics and surgical debridement, washout, removal of the prosthesis or in some cases, amputation of the affected limb.

In more recent times, the study of biomaterials to prevent and treat bacterial biofilms has seen the application of these biomaterials to the surface of implant devices. Silver nanoparticles (AgNPs) are one of the most promising and have been shown to have bactericidal effects in multiple studies. The exact mechanism through which AgNPs exert their bactericidal effect is unclear but may implicate the formation of reactive oxygen species. It must be noted however, that AgNPs may also have cytotoxic effects on the body's own cells. Moreover, there is scarce literature on how AgNPs affect the expression of adhesion proteins in bacteria. Hence, it is unclear if AgNPs inhibit biofilm formation via bactericidal activity alone or also interfere with the expression of MSCRAMMs in *S.aureus, S.epidermidis, E.coli* and *P.aeruginosa*.

1.2.1 - Risk factors for PJI

A number of operative and patient factors have been implicated in the development of PJIs. A literature review by Eka and Chen [22] has identified a number of patient factors which predispose to PJIs of the hip and knee:

- Obesity. Patients with a body mass index (BMI) of greater than 30 have an increased risk of PJIs, with a hazard ratio (HR) of 1.73 after THA and 1.22 after TKA. The risk of PJIs in patients with a BMI > 40 increased by 3.3 times while those with a BMI > 50 were 21 times more susceptible [23].
- Malnutrition. Malnutrition may be defined as a serum transferrin level < 200 mg/dL, serum albumin level < 3.5 g/dL, serum prealbumin < 15 mg/dL and a total lymphocyte count (TLC) < 1500 cells/mm^3 [24]. The risk of PJIs was 5 times greater in in patients with a preoperative TLC < 1500 cells/mm^3 and 7 times greater in patients with an albumin level < 3.5g/dL [25].
- Hyperglycaemia and uncontrolled diabetes mellitus. Diabetes mellitus is an independent, well-established risk factor for developing PJI [26]. The elevated risk of PJIs in diabetic and

hyperglycaemic patients may be due to a dysfunctional immune system against bacteria such as reduced vascular permeability, oxygen delivery, chemotaxis and phagocytosis, neutrophil adherence as well as impaired function of antibody responses and the complement system [27]. Uncontrolled diabetes is defined as blood sugar levels greater than 200 mg/L or glycosylated haemoglobin (HbA1c) levels greater than 7%. Marchant et al found that patients with uncontrolled diabetes had a significantly increased risk of developing post-operative wound infection with an adjusted odds ratio of 2.28 [28].

- Rheumatoid arthritis (RA). Several studies have reported RA as being an independent risk factor for the development of PJI, with a HR of 1.71 after THA and HR of 1.18 after TKA [26]. The underlying mechanism for this increased susceptibility is still under investigation but it is postulated to be caused by the synovial and intra-articular destruction of the disease itself, as well as associated comorbid conditions and immunosuppressive medications [29].
- Preoperative anaemia. Preoperative anaemia is defined as a haemoglobin level less than 120 mmol/L in women and less than 130 mmol/L in men. Patients with preoperative anaemia have greater risk of developing PJIs: hazard ratio (HR) of 1.36 after THA and HR of 1.26 after TKA [26]. A plausible explanation for this association may be that patients with preoperative anaemia are more likely to receive post-operative allogeneic blood transfusions, which increases the risk of infection [30].
- Cardiovascular diseases. Bozic et al [26] have reported a number of cardiovascular disorders which predispose patients to PJIs: pulmonary circulation disorders (HR = 1.42), congestive cardiac failure (CCF, HR=1.28), valvular disease (HR = 1.15) and peripheral vascular disease (PVD, HR = 1.13). Pulido et al also reported that myocardial infarction and atrial fibrillation are independent comorbid risk factors for PJIs. It is postulated that the increased risk of infection is attributable to patients with cardiovascular patients receiving more aggressive anticoagulation, which subsequently increases the risk of post-operative haematoma and is a risk for infection [31].
- Chronic renal disease (CKD). Patients with chronic renal failure who require haemodialysis or have undergone renal transplant have an increase in relative risk of 5-6 times to require joint replacement surgery than the general population. This is because long-term haemodialysis patients often accumulate β2-microglobulin amyloid deposition in the joints which invades the synovium, capsule and cartilage to cause arthropathy [32]. Patients on renal replacement therapy are also at a greater risk of developing PJI with a HR of 1.38 and the risk of infection seems to be higher in haemodialysis patients than immunocompromised transplant patients. The exact cause for this elevated risk is yet to be elucidated but is most likely multifaceted from multiple medical comorbidities and the use of use of immunosuppressive therapies [33].

- Depression. Bozic et al have identified depression as an independent risk factor for acquiring PJI post-operative (HR = 1.28) as depression may be associated with malnutrition and subsequent need for blood transfusions. Furthermore, depression has a direct effect on impairment of the immune system, making patients more susceptible to PJIs [34].

Aside from the patient-related risk factors for PJIs above, Zhu et al have also listed the following operative factors that increase the risk of PJIs: presence of a wound drain, SSI, prolonged operative time and revision surgery [35].

1.2.2 - Individual susceptibility to PJIs

In more recent times, individual differences in genetic polymorphism that predispose patients to PJIs have been gaining momentum in the research community. Interindividual differences in protein and cytokine production have been observed and accordingly, functional polymorphisms in these genes may be implicated in the development of PJIs, such as mounting an impaired response of the innate immune system [36]. To date, several studies have investigated the role of heritable factors in the pathogenesis of PJIs, including mutation of proteins, receptors, intracellular mediators, enzymes, and cytokines [37-42].

Stahelova et al [43] postulated that patients with PJI mount an immune response that is a deviation from those seen in those without infections, namely, with a decrease in the production of inflammatory cytokines, notably, interleukin-1β (IL-1β), IL-18 which trigger the inflammatory response together with other inflammatory cytokines such as IL-6 and TNF-α. Six single nucleotide polymorphisms (SNPs) were selected for each of IL-1β, IL-18, IL-6 and tumor necrosis factor α (TNF-α). Blood was extracted from study subjects consisting of patients with PJIs and healthy individuals. DNA was isolated from the blood and subjected to PCR. It was found that a particular *IL-1β* gene promoter polymorphism was nominated as a risk factor for PJI as it was more commonly found in patients with PJI. It was speculated that patients with this SNP differed in the way they produced inflammatory cytokines.

Malik et al [39] investigated the SNPs in the RANK/RANKL/OPG system and by collecting venous blood and extracting DNA from a total of 312 successive patients: 71 with PJI, 91 with aseptic loosening and 150 controls. In the group with confirmed PJI, the frequency of the A allele (p=0.001, OR=3.42, 95% CI=1.98–5.91) and homozygous genotype A/A (p=0.001) for the OPG-163 SNP were statistically significant. No other significant relationship was found between the RANK/OPG SNPs. Malik et al [38] also investigated the role of mannose-binding lectin (MBL), a liver-synthesized serum protein which is increased 4-fold during the acute phase of an infection. It can opsonize bacteria, as

well as activating the complement pathway. MBL deficiency is associated with 4 SNP within the MBL gene on chromosome 10. Like their previous study, venous blood taken from the 312 patients were used to extract deoxyribonucleic acid (DNA). With regard to the septic group, as compared with the control group, the frequency of the C allele (P= .01; OR = 1.90; 95% CI = 1.14-3.16) and that of the genotype C/C (P= .05) for the 550SNP were statistically significant.

Five polymorphisms for Toll-like receptors (TLR) have been investigated concentrating on severe infection and total joint arthroplasty failure [37, 44]. One study has shown that variants at TLR9-1486 were marginally or significantly associated with an elevated risk of PJIs. All other SNPs of TLR investigated were not significantly associated with increased PJI susceptibility. El-Helou et al [37] have shown that the R753Q SNP paralyses the TLR2-dependent immune signaling, which mediates binding to peptidoglycan in cell walls, in response to *S.aureus* in vitro. However, the presence of this SNP was not necessarily translatable in the clinical setting, as serum samples have shown the prevalence of the SNP was 23 (30%) in the 76 patients with PJIs in this study, compared to 83 (40%) in the non-infected patients in that study.

Malik et al investigated the role of four common polymorphisms of four matrix metalloproteinases (MMP): MMP1-1, MMP1-2, MMP1-3 and MMP 1-4, involved in the breakdown of interstitial collagen. It was postulated that the local production and activation of MMP1 involved in inflammation and neovascularization may suggest its role in the development of deep infection in PJI. In this study, there was no statistical difference in the SNPs of MMP1-1, MMP1-3 or MMP1-4 [40].

1.2.3 - Incidence of hip and knee prosthesis infections

Deep infection rates for THAs and TKAs are 1-2% over a 2-year post-op period and the Australian National Joint Replacement Registry (45) reported the revision rates for THA and TKA are 6.2% and 5.7% respectively, for any cause, at 10 years post implantation. Infection is the second leading cause of revision for THA at 22.3%, with the most common causes being dislocation and loosening. For TKA, it is the leading cause at 26.4%. However, interpretation of revision rates is complicated as many revision cases attributed to aseptic loosening are likely to be low-grade biofilm infections [46]. A 15-year prospective study in the United Kingdom by Phillips et al demonstrated lower rates of deep infection following hip replacements and knee replacements were 0.57% and 0.86% respectively [47].

1.2.4 - Incidence of upper limb prosthesis infections

The reported incidence of infection in R-TSA is higher than that of anatomic shoulder arthroplasty. The higher rates of infection seen in R-TSA compared to anatomical shoulder replacements include a

larger dead space, increased implant surface, patient factors and the complexity of certain indications [48]. The reported infection rate of R-TSA is 1-15%. In a meta-analysis by Zumstein et al, the mean infection rate of R-TSA was 3.8%, compared to 0.7% for anatomic arthroplasty [49].

Total elbow arthroplasty (TEA) has the highest reported incidence of infection among all arthroplasties. The reported infection rate of deep prosthetic infection in TEA is between 1.5% and 12% [50]. The higher incidence of PJI in TEA compared with THA and TKA may be due to lack of soft tissue covering from bone to skin [51]. Whereas there is a greater understanding of the management of PJI in THA and TKA, fewer studies in literature have been dedicated to the management of PJI in TEA [52]. The most encountered pathogens in PJIs are illustrated in **Table 1.1**.

Table 1.1 – **Common infectious agents in prosthetic joint infections.**

Organism	Incidence
Gram positive • *Staphylococcus aureus* • Coagulase-negative staphylococcus	>50%
Gram negative • *Enterobacter* spp • *Pseudomonas* spp • *Escherichia coli* • *Klebsiella* spp • *Proteus* spp	3-10%
Anaerobes	2-4%
Mycobacterium	0.7%
Fungi	1.2%
Polymicrobial	10%

Gram positive pathogens accounted for more than 50% of PJIs with *S.aureus* being the most common infective organism at 24-43%. Gram-negative organisms were the next most common group:

Enterobacter, *Pseudomonas* and *E.coli* were the predominant infective organisms in this group [47-49].

1.3 - Bacterial biofilms

Biofilms are aggregations of microorganisms attached to surfaces which have been attracting the interest of researchers, in part because they cause 65% or more of infections, including chronic infections. Biofilms are particularly problematic to eradicate due to their resistance to host defenses and conventional antibiotic therapy [54]. While bacteria are usually perceived as unicellular organisms, there is mounting evidence that they predominately exist as adherent multicellular biofilms in diverse environments including chronic infections. The transition from a planktonic state to a biofilm state, typically triggered by a stress signal secondary to unfavorable environmental changes, triggers the dysregulation of multiple regulatory pathways [55]. To avoid death, the stress-response must be mounted more quickly than the stress signal. Therefore, the process is a rapid and extremely efficient process. The expression of a differential set of important genes takes place, which can occur through adhesion organelles including pili, flagella or immobilization of the bacteria [56]. As bacteria accumulate and attach firmly, they trigger quorum-sensing circuits and secrete signal molecules to trigger profound regulatory changes [57].

Bacterial infections pose the risk of biofilm formation on prosthesis surfaces leading to persistent infections which are virtually impossible to eradicate due to their inert nature [58]. The most common culprits being *S.aureus*, coagulase-negative *Staphylococci, E.coli*, *P.aeruginosa, enterococci*, *P.mirabilis*, and *Streptococcus viridans* (*S.viridans*) [59]. Biofilms represent bacterial communities embedded in a self-produced extracellular polymeric substance (EPS) with bacteria undergoing multiple changes in physiology, gene expression and protein profile following attachment which confers on the associated organism a marked reduction in antimicrobial susceptibility.

Biofilm matrices of most bacteria species are formed through at least five developmental stages listed below [60], shown graphically in **Figure 1**:

- Initial reversible attachment of planktonic cells.
- Transition from reversible to irreversible attachment.
- Early development of biofilm architecture.
- Development of micro-colonies into a mature biofilm.
- Seeding of cells from the biofilm which return to the planktonic state.

The formation of a viable biofilm requires factors that disrupt cell-cell interactions in order to create nutrient channels which can penetrate into the deeper layers of the biofilm [61]. These factors can lead to the shedding of cells and cell clusters from biofilms and therefore, control thickness of the biofilm as well as expansion [62]. Cell detachment is vital for biofilm infections as dispersion will lead to the establishment of new infections elsewhere via dissemination. In *S.aureus*, detachment is mediated by

the quorum-sensing Agr system [63] but the mediators of detachment remain undefined. There is only preliminary evidence of polymer degrading enzymes in *S.aureus* and other staphylococci. In contrast, there is emerging evidence that bacteria can utilize surfactant-like molecules to detach of portions of biofilms for dispersal, including *P.aeruginosa* rhamnolipid [64], *Bacillus subtilis* (*B.subtilis*) surfactin [65] and *S.epidermidis* phenol-soluble modulin (PSM) [66].

The exact mechanisms for resistance to antimicrobials in biofilm-associated bacterial are multifactorial and may be intrinsic (decreased growth rates, diffusion of antibiotics through the EPS matrix, surrounding cells within the biofilm may provide conditions that further protect bacterial cells), extrinsic (horizontal exchange of plasmids encoding antimicrobial resistance is several orders higher in biofilms compared to in planktonic bacteria) or both. There are at least 3 factors that contribute to the intrinsic antibacterial resistance of biofilms:

- EPS matrix. The bacteria are typically embedded in a matrix of extracellular DNA (eDNA), polysaccharides and proteins [67]. The matrix provides structural stability but also protects cells from antibiotics. The matrix can inhibit diffusion either by chemical inactivation of the antibiotics or by slowing down their rate of diffusion and transport. Hoyle et al demonstrated that the EPS of *P.aeruginosa* bound to tobramycin and that planktonic *P.aeruginosa* bacteria were 15 times more susceptible to this agent compared to intact biofilm cells [68]. Moreover, the EPS can facilitate an accumulation of antibiotic-degrading enzyme such as β-lactamases [69]. Exposure of bacteria to eDNA in the matrix induces the accumulation of spermidine on the cell surface to confer a protective effect against oxidative stress [70].
- Biofilm-associated organisms have altered physiology with lower growth rates, significantly reducing the rate of uptake of antimicrobial agents into the cell and therefore affecting inactivation kinetics. DuGuid et al found that an increase in growth rate subsequently resulted in more susceptible *S.epidermidis* biofilms and that ciprofloxacin activity was influenced by the cell cycle [71]. Moreover, gene regulatory changes seen during starvation conditions induced complex regulatory pathways for antibiotic resistance.
- Heterogeneous population. The biofilm is typically comprised of communities of complex and heterogeneous cells in different states of growth. This differentiation is due to the consequence of decreasing oxygen and nutrient gradients between the superficial and deeper surface layers within biofilm. Thus, the metabolically active cells in the surface layers and the more dormant cells in the deeper layers display markedly different responses when exposed to antibiotics. Persister cells are a subpopulation of cells more commonly found in biofilms compared to planktonic populations [72]. Persister cells can withstand otherwise inhibitory concentrations of antibiotics and to overcome stressful

conditions including antibiotics due to programming. The possession of large populations of persister cells is one of the most significant resistance mechanisms in *S.epidermidis* [73].

As such, it was found that *E.coli* found in biofilms required more than 500 times the minimum inhibitory concentration (MIC) of antibiotic to provide a 3-log reduction and that *S.aureus* biofilms required more than 10 times the minimum bactericidal concentration of vancomycin to provide a 3-log reduction.

Surface characteristics also affect biofilm formation, with bacteria having greater affinity for rougher and more hydrophobic materials [74]. The situation becomes more complicated when a substratum is immersed in a fluid environment such as the synovial fluid or the bloodstream, where proteinaceous material may confer chemical properties that completely mask the substratum.

Bacterial biofilms are clinically relevant for the reasons described above and can be summarized into 4 points:

- Biofilms are highly resistant to antibiotics.
- Biofilms may be a source of chronic and persistent infection.
- Biofilms may harbor pathogenic organisms.
- Biofilms may enable the development of antimicrobial resistance through the exchange of resistance plasmids.

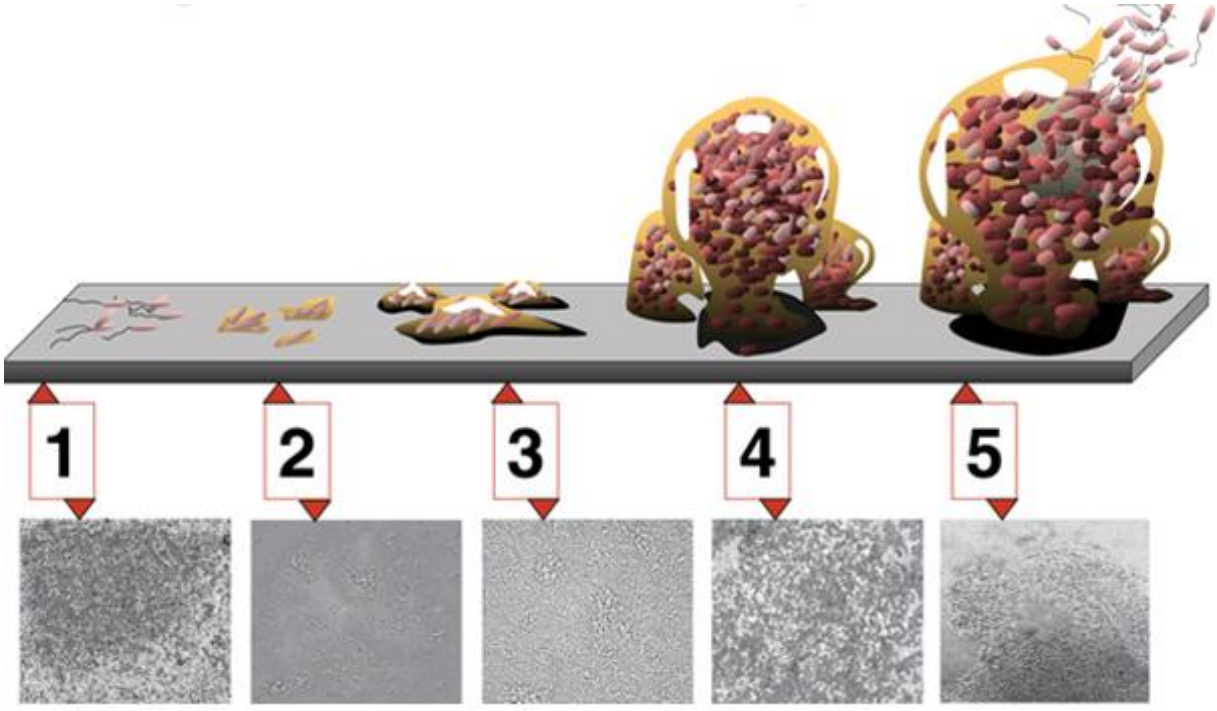

Figure 1.1 – **The five stages of bacterial biofilm development**

The five stages of biofilm development. Stage 1: planktonic (free-floating) bacteria attach to the biomaterial surface. Stage 2: cell aggregate, form micro colonies and excrete extracellular polymeric substances (EPS). The attachment becomes irreversible. Stage 3: a biofilm is formed. It matures and cells form multi-layered clusters. Stage 4: three-dimensional growth and further maturation of the biofilm, providing protection against host defense mechanisms and antibiotics. Stage 5: the biofilm reaches a critical mass and disperses planktonic bacteria to colonize other surfaces.

1.3.1 – Surface properties influencing bacterial attachment

There is a substantial body of research undertaken to elucidate whether certain surface characteristics promote or deter the adhesion of bacteria. A few of these characteristics are listed below:

- Surface charge. Charge has been long known to affect biofilm formation, as van der Waals forces and electrostatic interactions mediate bacterial adhesion. Positively charged surfaces promote adhesion more than negatively charged ones because most bacteria are negatively charged [76]. However, *P.aeruginosa* on negatively charged surfaces has a tendency to produce more EPS. In addition, a barrier comprised of dead bacterial cells can reduce the surface charge and facilitates adhesion of other cells. Therefore, charge alone may not be sufficient to repel bacteria. Various studies have shown that in general, bacteria prefer hydrophilic surfaces to hydrophobic ones although the preference for surface hydrophobicity differs among bacterial species [76]. More recent research has shown both ultra hydrophobic and ultra hydrophilic surfaces can prevent biofilm formation [77].
- Roughness and topography. In general, rougher surfaces promote bacterial adhesion due to an increase in contact surface between the surface and the bacterial cells [78] and shield the bacteria from shear forces [79]. Making a surface smoother can reduce biofilm formation and a surface roughness of 0.2 μm was reported to be the threshold for the maximum reduction on adhesion [80]. However, the exact effect is once again dependent on the size and shape of the bacteria, as well as other environmental factors.
- Topographic patterns. Aside from surface roughness, the distribution of elevations and troughs is also essential for biofilm formation [81]. Certain topographic patterns on the micrometer and nanometer-scale have been shown to inhibit biofilms compared to flat surfaces of the same material, such as cone-shaped patterns on silicone, circular poles on polystyrene [82], as well as others. Furthermore, nanoscale pillars can stretch the bacterial cell membrane in the regions suspended between the pillars to cause membrane damage and even death to bacteria [83].
- Stiffness. Lichter et al found that the attachment of *S.epidermidis* to polyelectrolyte multilayer thin films composed of poly(allylamine hydrochloride) and poly(acrylic acid) was associated with the stiffness of the material with Young's modulus of 0.8 to 80 MPa [84]. Furthermore, *E.coli* and *Lactococcus lactis* grew faster on soft than hard polyelectrolyte multilayer thin films [85].

1.3.2 – Staphylococci biofilm formation: *S.aureus* and *S.epidermidis*

Biofilm-associated infections with *staphylococci* are usually not mixed with other species [86]. Moreover, it is uncommon to find more than one strain of the same bacteria in an infection. One

possible explanation is interspecies inhibition from virulence factor expression. Many biofilm-forming organisms show a propensity for a two-step biofilm formation process with initial attachment and a subsequent maturation process, which are different from other species and factors specific to that phase [87]. A final step involving dispersion enables dissemination of bacteria to infect other parts of the body.

Attachment is mediated by MSCRAMMS (microbial surface components recognizing adhesive matrix molecules) which show selective binding to fibronectin and fibrinogen. Staphylococci have the ability to attach to plastic surfaces but whether direct attachment plays in a role in the development of infections is unclear, as device surfaces are rapidly covered by host matrix upon insertion it is the interaction between MSCRAMMS and these proteins that plays a more significant role [87].

Maturation is characterized by the production of a variety of molecules, adhesive proteins and exopolymers of polysaccharide, culminating in adhesion between cells in the biofilm and structuring forces that lead to the typical appearance of biofilms with cell towers surrounding fluid-filled channels. The main intercellular adhesion molecule is polysaccharide intercellular adhesin (PIA) encoded by the ica locus. It, in combination with other polymers such as teichoic acid and proteins form the major part of the 'slime', the extracellular matrix of biofilm-forming staphylococci. De-acetylation of PIA introduces a positive charge to an otherwise neutrally charged molecule and acts as an adhesive for negatively charged bacterial cell surface [87]. After colonization is achieved, there is increasing activity of the agr quorum-sensing system which subsequently negates the expression of adhesion factors that are no longer required [88]. Staphylococcal biofilms are characterized by physiological changes including a down regulation of active cell processes such as the synthesis of cell wall, DNA and proteins.

1.3.3 – *Staphylococcus aureus* biofilms

S.aureus is a gram positive coccus with an ecological niche in the anterior nares of humans [89] and approximately 20% of the population are persistently colonized with the bacteria while 70-80% are intermittently colonized or have never been colonized. Differences in the rates of colonization are not clearly understood but undiscovered host and bacterial factors that predispose to *S.aureus* colonization may play a role [87]. Nasal colonization of *S.aureus* provides the possibility of dissemination throughout the body following an epithelial breach. The bacteria are then either removed by the innate host immune system in circulation or attach to host extracellular proteins to form a biofilm [89]. *S.aureus* has a propensity to produce a multilayered biofilm within a heterogeneous slime layer composed of glycocalyx and protein expression throughout. The solid component of host and staphylococci proteins as well as teichoic acids (80%).

S.aureus is a major pathogen involved in the infection of implanted medical devices. *S.aureus* has been known to attach and form chronic biofilm most often on orthopaedic implants including intramedullary nails, fixation plates, external fixators, wires and prosthetic joints, as well as other non-orthopaedic devices. In Australia, MRSA is responsible for 26% of prosthetic joint infections. The device becomes coated in host extracellular matrix proteins, providing a surface for bacterial attachment. Whether infected during haematogenously, subsequent trauma or at the time of implantation, the outcome is the same and the device must be completely removed.

A specific antigen involved in the formation of *S.aureus* is PIA produced in vitro via products of the intercellular adhesion (ica) locus. Several methods of biofilm formation in *S.aureus* have been proposed:

- PIA-dependent biofilm formation: the proteins encoded by the genes of the *ica* locus have been shown to be instrumental for biofilm formation and are upregulated in the presence of an anaerobic environment [89], a condition which is frequently seen in the biofilm environment. Other environmental factors, such as temperature, osmolarity, ethanol and glucose, also play a role in the regulation of *ica*.
- PIA-independent biofilm formation: proteins with adhesive properties substitute for PIA. The most important of these proteins is *Aap*. Other adhesins include proteins that bind fibronectin (*FnbA, FnbB*), a collagen binding protein (*I*), three fibrinogen-binding proteins (*ClfA, ClfB, EfB*), elastin-binding protein (*EbpS*) and the bone sialoprotein-binding protein (*Bbp*). A study by Arciola et al found that the *I* gene was present, respectively, in 36% of strains derived from internal fixation devices, 40% from those on knee arthroplasties, 43% of those from hip arthroplasties and 52% from external fixation devices [86].
- eDNA and biofilm formation: eDNA is another important component of biofilm formation. The important role of eDNA in biofilm formation was first made apparent in *P.aeruginosa* and was supported by the finding that DNase treatment could eradicate only early, immature biofilms. Success in treating biofilms was shown when DNAse was used concurrently with antibiotics to treat cystic fibrosis patients. Studies have demonstrated that the mutation of *cidA*, a gene encoding an effector of murein hydrolase activity and regulating cell death, led to a lower levels of eDNA and subsequently a less adherent. In addition, biofilm formation in cidA mutants were minimally inhibited by treatment with DNase.

Phenol-soluble modulins are staphylococcal peptides with an alpha-helical, amphipathic structure that gives them surfactant properties. Mutants in the quorum sensing region *Agr* lack PSM production because *psm* operon transcription is under strict control of the *AgrA* DNA binding protein [90]. Periasamy et al [62] demonstrated, with MRSA strains USA300 and USA400, that *Agr* and PSM mutants had generated larger volume biofilms with smoother surfaces: this

indicated that *Agr* not only controlled biofilm detachment as previously thought but also biofilm structuring. Moreover, it also indicated that PSMs represent key molecular factors contributing in biofilm structuring and detachment in *S.aureus*. In addition, Periasamy et al also demonstrated expression of *Agr* and PSM differed when biofilms were grown in static conditions compared to in a dynamic medium: although *Agr* and PSM were expressed throughout the biofilm, they were more concentrated in the outer layers in a dynamic environment, hence indicating their role in dispersion.

1.3.4 – *Staphylococcus epidermidis* biofilm formation

S.epidermidis can be found in the commensal skin flora of every individual. In its natural niche, it maintains local homeostasis, the exact mechanism of which is still not clearly understood [91]. Recent light has been shed that *S.epidermidis* can inhibit the colonization of *S.aureus* via the expression of a serine-type protease called *Esp* [92]. Due to the abundance of *S.epidermidis* found on skin, it can often be a challenge to distinguish between clinically relevant and contaminating isolates.

S.epidermidis is a significant pathogen of infection of prosthetic joints. The paucity of non-invasive management options for infection of prosthetic joint implants necessitates surgery and replacement of the infected prosthesis. In the UK, coagulase-negative staphylococci and *S.epidermidis* were isolated in 36% of total hip replacements and 49% of total knee arthroplasty infections [47]. In another study of infected total knee and hip arthroplasty, 77% of the isolated coagulase-negative staphylococci were identified to be *S.epidermidis*. Heilmann et al identified that bacterial binding to unmodified polystyrene is mediated by *AtlE*, a member of bacterial peptidoglycan hydrolase which normally plays a role in bacterial cell wall degradation [93]. Proteins with extracellular matrix (ECM)-binding capacity are important in initiating device infection since foreign bodies are covered by ECM materials (*FN* for fibrinogen, *Fg* for fibronectin, *Cn* for collagen and *VN* for vitronectin) after being inserted into the body [94]. Similar to *S.aureus*, *S.epidermidis* also expresses MSCRAMMs, a group of serine-aspartate (Sdr) repeat proteins that mediate ECM-bacterial interactions. In *S.epidermidis*, three Sdr proteins referred to as *SdrF, SdrG* and *SdrH* have been identified [95]. *SdrG* is crucial for adherence of *S.epidermidis* to fibrinogen-coated surfaces and the gene encoding *S.epidermidis* is commonly found in clinical isolates. *SdrF* has organizational similarity to *SdrG* and binds to collagen. Similar to *S.aureus*, eDNA also plays a role in biofilm formation although studies do show there are clear functional differences [96]. eDNA is expressed post cell-lysis by the action of the *AltE* autolysin as mentioned earlier.

Extracellular polysaccharide adhesins are essential to adherence of bacteria to surface and between bacterial cells. Two particular adhesins of interest are capsular polysaccharide (*PSA*) and

polysaccharide intercellular adhesion (*PIA*), both of which are encoded by the *ica* (intercellular adhesion) operon [97]. In the two-step model, initial attachment and adhesion is mediated by *PSA*, while subsequent accumulation of bacterial cells is mediated by *PIA*. Commensal strains of *S.epidermidis* can be differentiated from invasive isolates that cause joint infections by the presence of the *ica* operon, the only genetic marker to differentiate the strains [98].

Accumulation associated protein (*aap*) and extracellular matrix binding protein (*embp*) are multi-functional with important functions during the various phases of biofilm formation and surface adhesion for *S.epidermidis*. *Embp* and its ortholog in *S.aureus* designated *Ebh* were identified during studies aimed at identifying staphylococcus proteins with fibrinogen-binding activities [99]. In collections of clinically significant *S.epidermidis* isolates *embp* was detected in more than 90% of strains [100]. Experimental evidence illustrated that *embp*-fibrinogen interactions were necessary for accumulation on plastic surfaces that did not otherwise promote binding as well as an intercellular adhesion [101]. The functional importance of *Aap* was first recognized after mutant strains of *S.epidermidis* that did not express *Aap*, as well strains that did express *Aap* but were treated with antibodies against *Aap*, were unable to form biofilms [102]. The isolated expression of mature *Aap* alone is not sufficient to mediate adhesion but requires proteolytic removal of the A-domain to become a functionally active intercellular adhesin [100]. Although the intercellular adhesive properties of *Aap* were recognized first, there is now increasing evidence that *Aap* is also involved in primary attachment to natural epithelial cells or artificial surfaces [103].

Most of the studies aimed at understanding the relevance of biofilm formation and the individual roles and contribution of specific factors for colonization and establishment of chronic infections are studied using either in vitro models or animal models rather than in-vivo human studies.

1.3.5 – *Escherichia coli* biofilm formation

Biofilm formation in the early stages requires the production of bacterial surface adhesins including flagella to enable reversible initial adhesion. Following this, flagella production is inhibited and the expression of adhesion organelles including type I fimbriae, encoded by *fim* genes, and curli fimbriae, encoded by the *csg* operon, are important for irreversible attachment in chronic biofilms [104]. Type I mannose-sensitive fimbriae also affect adherence and promotes antibiotic-resistant pod formation. Bundle-forming pili and *EspA* filament are important for biofilm formation by enteropathogenic *E.coli*. Conjugation plasmids increase biofilm formation in a manner independent of flagella, type I fimbriae and curli. One common finding is the role of stress genes in *E.coli* biofilm formation. Several stress-induced genes (*hslST*, *hha*, *soxS* and *ycfR*) were identified in 7 hour *E.coli* cells and that stress promotes the formation of *E.coli* biofilm [105]. Moreover, envelope stress response genes, such as *rpoE* , *pspABCDE*, *rseA* and *cpxAR*, were induced in 8 day old *E.coli* biofilm cells and not

exponentially-growing planktonic cells regardless of whether conjugation plasmids were present or not [106]. Various transcriptome profiling studies have also identified the importance of the *YmgB/AriR* by inducing the expression of acid-resistance genes (to survive low-pH of the stomach) which promotes biofilm formation.

1.3.6 – *Pseudomonas aeruginosa* biofilm formation

Three important polysaccharides (alginate, *Pel* and *Psl*) secreted by *P.aeruginosa* determine the stability of the biofilm [107]. Alginate is a linear, unbranched polymer that enables the retention of water and nutrients, which contributes to the structural stability and protection of biofilms [108]. *Pel* and *Psl* are polysaccharides and contribute to the structural scaffold for biofilm development and are involved in the early stages of biofilm formation [109]. As with many other bacteria, eDNA also constitutes an important functional component of the biofilm matrix. Organelles such as flagella, fimbriae and type IV pili play a role in not only bacterial motility flagella but also play an important role in adhesion in cell-cell interactions [110].There are two major quorum-sensing systems in *P.aeruginosa* (*las* and *rhl*) which drive production and perception of autoinducer signaling molecules. A third quorum-sensing system, based on quinolone signals (PQS system) interacts with acyl homoserine lactones systems. Compared with wild type biofilm, *las* mutants were undifferentiated and were quick to disperse after exposure to sodium dodecyl sulfate [111]. The production of rhamnolipids is regulated by the *rhl* system and contributes to multiple functions in biofilm formation including formation of microcolonies, maintaining open channels that prevent bacterial colonization by disrupting cell-cell and cell-surface interactions, promoting the formation of 3-D structures in *P.aeruginosa* biofilms, as well as promoting cell detachment, as *P.aeruginosa* variants which produce more rhamnolipids than wild-type *P.aeruginosa* exhibit hyper-detaching properties [64].

1.4 – Implant involvement in PJI and periprosthetic osteolysis

1.4.1 – Biofilm formation on the implant

The orthopaedic implant itself represents a risk factor for the formation of biofilms leading to the progression of osteomyelitis. The type of material is a minor risk factor regarding the susceptibility of a device to colonization. In-vitro studies have shown that *S.epidermidis* displayed a greater degree of adherence to stainless steel compared to titanium (Ti) but this difference was not observed in in-vivo, hence the protein coating of the implant is more important for attachment than the type of material involved [112]. The synthetic material is covered by host proteins, including fibrinogen, laminin and fibronectin, as soon as it is introduced into the body and these proteins act as mediators of bacterial adherence. Implant-associated infections never heal without intervention. Hence, the implantation of

the prosthesis represents a race against time between integration into host tissue and adherence by bacteria.

These findings can be explained by the fact that the implant impairs the local immune response to invading organisms by activation of polymorphonuclear neutrophils (PMNs) and the complement system which in turn creates a cytotoxic local environment to cause tissue damage as well as host cell death [113]. The paradox is that although there is an abundance of PMNs and proinflammatory cytokines, the clearance of bacteria in this environment is compromised and bacteria gain the additional advantage of the foreign surface acting as a site of attachment to facilitate the transition from planktonic state to biofilm. It is postulated that the interactions between granulocytes and the surface of the implant or implant wear particles, impair the function of granulocytes, termed frustrated phagocytosis [114]. Studies with guinea pigs showed that the introduction of foreign material decreased the required inoculum dose from 10^8 colony forming units (CFUs) of *S.aureus* to 10^2 to establish infection [115]. Other in-vivo studies using rats demonstrated that *S.aureus* inoculum as low as 10^2 CFUs were sufficient to establish hardware-associated bone infections without further promoting factors such as bony injury or soft tissue injury [116].

Zimmerli et al [115] inserted subcutaneous tissue implants into guinea pigs and demonstrated that granulocytes around these tissue cages were unable to efficiently kill *Staphylococci* despite adequate opsonization and opsonized particles were phagocytosed inefficiently with partial degranulation and reduced production of ROS. In addition to this, Chang et al exposed PMNs to different biomaterials and found that there was enhanced ROS production which induced nonapoptotic death in the PMNs resulting in impaired microbial clearance around the implant [117]. The implantation of devices also leads to the activation of complement and attract PMNs and complement activation around prostheses and wear particles may therefore act as the trigger for aseptic loosening around joint prosthesis.

1.4.2 – Immune response to chronic implant-related bone infections

PMNs and macrophages infiltrate the site of infection in the presence of planktonic bacteria. The cells are activated by binding to pathogen-associated molecular patterns (PAMPs) to pattern recognition receptors (PRRs) such as TLRs resulting in the activation of NfκB and subsequently produces a pro-inflammatory environment from the generation of reactive oxygen species (ROS), nitrogen species (NOS), antimicrobial peptides, enhanced phagocytosis and pro-inflammatory cytokines [118]. In addition, PMNs form extracellular fibril matrices of DNA and granule proteins that ensnare bacteria for degradation and the planktonic bacteria are usually eliminated by the innate immune system before progression to irreversible attachment and biofilm formation [119].

In the case of implant-associated infection however, the implant is recognized as foreign by the innate immune system to stimulate the secretion of ROS, NOS, anti-microbial peptides and inefficient phagocytosis and reduced granulocyte function as described above, culminating in immune cell exhaustion, cell death and tissue damage without eradicating the infecting microorganisms [118]. In-vivo mice studies of implant-based *S.aureus* osteomyelitis showed that bacterial adherence commence on the first day after surgery, with strong proliferation of bacteria and biofilm taking place between postoperative days 3 to 7 and maximum biofilm mass being achieved by day 14 and a subsequent decline in proliferation thereafter as dispersion begins to take place [120]. In effect, this indicates that the window of opportunity in which planktonic bacteria clearance could take place is very brief and that the immune system is attempting to clear the biofilm phase in almost the entire duration of the infection. Mature biofilms consist of a dense EPS component which is difficult to penetrate and engulf by phagocytes [121]. Although the EPS expresses PAMPs to normally stimulate a pro-inflammatory response

1.4.3 – Minimizing noxious interactions

Improving the biocompatibility of implantable devices and prosthesis refers to the biomaterial performing its intended function in the body without unwanted adverse local and systemic side-effects to harm the host. Vitamin E is incorporated into UHMWPE to provide oxidative resistance without compromising the fatigue strength or physical properties and Massaccesi et al [122] found that Obs receiving treatment of UHMWPE blended with vitamin E induced a decrease in the RANKL/OPG ratio compared to OB treated with UHMWPE without vitamin E. In addition, there have been no shortage of studies to increase the biocompatibility of joint prostheses and internal fixation devices with nanoparticle coating to enhance OB proliferation and osteointegration into the body such that it no longer elicits a foreign body immune response once incorporated into the body [123-125]. Nanotechnology has also be studied for its role in the activation of the complement system: Ferraz et al [126] have shown that complement activation is less pronounced when the blood is in contact with 20 nm compared to 200 nm pore-sized membranes. Other modification techniques include coating the surface with compounds to induce the attachment of host fibroblasts [127] and modification of surface charge to inhibit bacterial attachment [128]. Nanoscale coatings of interleukin 12 (IL-12), a major cytokine that stimulates T-helper cells (Th) to secrete Th1 cytokines to attract macrophages, have been shown to reduce infection rates in open fractures in rat models [129]. However, the effect of nanoscale coat of IL-12 on osteolysis remains to be seen.

1.5 – Clinical presentation and management of orthopaedic implant infections

1.5.1 – Clinical classification and presentation of orthopaedic implant infections

Orthopaedic implant infections are classified as follows by Zimmerali et al [130]:

- Early: within 3 months following implantation.
- Delayed: between 3 to 24 months following implantation.
- Late: occurring 24 months after surgery.
- Haematagenous: typically 24 months or later after surgery but can occur at any time.

Early implant infections typically present with erythema of the wound, purulent discharge from the wound and swelling of the affected joint in contrast to the patient complaining of gradually worsening pain seen in chronic infections. Haematagenous infections are typically associated with a history of a well-functioning joint for months to years post-operatively before a sudden onset of pain and erythema of the affected joint as well as systemic symptoms such as fever.

1.5.2 – Diagnostic criteria for PJI

The diagnosis of PJIs can present a challenge to clinicians as the presenting signs and symptoms and elevation of inflammatory biomarkers, such as ESR and CRP, may be equivocal in the most delayed, indolent or chronic infections, as well as in patients who have been administered antibiotics. In recent years, clinical research has focused on the biomarkers found in synovial fluid as breakthrough diagnostic biomarkers in equivocal cases of PJIs. In addition to this, chronic inflammatory diseases and metallosis can also mimic the clinical and biochemistry profile of PJI. Since 2011, the definition derived from the Musculoskeletal Infection Society (MSIS) is now taken as the gold standard [131] definition for PJIs and is based on the proposed criteria that, PJI is definite when:

1. There is a cutaneous sinus communicating with the prosthesis; or
2. The same pathogen is isolated from two or more separate tissue or fluid samples obtained from the prosthetic joint; or
3. Four of the six following criteria are met:
    a. Elevated C-reactive protein (CRP) or erythrocyte sedimentation rate (ESR)
    b. Elevated synovial leukocyte count
    c. Elevated synovial neutrophil percentage (PMN %)
    d. Presence of pus in the joint
    e. Isolation of a microorganism in one culture of periprosthetic tissue or fluid
    f. More than 5 neutrophils per high-power field in 5 high-power fields (400 x magnification) from histological analysis of periprosthetic tissue

As of 2018 however, emergence of new diagnostic markers prompted the development of an evidence-based and updated version of the criteria [132]. The two major criteria diagnostic of PJI (a sinus tract, two or more positive cultures of the same organism) remain unchanged. For the minor criteria, the calculated weights of an elevated D-dimer (>860 ng/mL), CRP (>1 mg/dL) and ESR (>30 mm/h) were 2, 2 and 1 points, respectively. An elevated synovial fluid white cell count (> 3000 cells/μL), alpha defensin (AD) (signal-to-cutoff ratio >1), leukocyte esterase (++), polymorphonuclear percentage (>80%), and synovial CRP (> 6.9 mg/L) received 3, 3, 3, 2 and 1 points, respectively. Patients with an accumulated score of greater than or equal to six were infected. A score of between 4 and 5 were inconclusive, and a score of 3 or less were not infected. The new diagnostic criteria had a sensitivity of 97.7% compared with the previous MSIS scoring system with a sensitivity of 79.3%. Both versions had a specificity of 99.5%.

It is imperative that 3 to 5 tissue or fluid samples representative of periprosthetic tissue be obtained in a sterile manner with sterile instruments. Moreover, evidence indicates that certain traditional tests, such as the Gram stain, are not sensitive in diagnosis of PJIs [133]. CRP values of greater than 10 mg/L and ESR greater than 30 mm/hour represent elevated levels. The synovial leukocyte count and PMN % for a chronically infected TKA is reported to be 1100 to 4000 cells/μL and 64-69%, respectively [134] while the corresponding values for an acute infection are much higher at 20000 cells/μL and 89% respectively [135].

The diagnostic criteria for PJI of TSA and R-TSA were developed by the International Consensus Meeting (ICM) and are slightly different due to a higher incidence of infections caused by less virulent organisms such as *Cutibacterium acnes* thus the MSIS criteria for TKA and THA may not be applicable to the shoulder [136]. The ICM criteria [137] divides shoulder PJIs into four categories: definite infection, probable infection, possible infection, and unlikely infection.
A definite infection is characterized by one or more of the following:

- Presence of a cutaneous sinus tract to the prosthesis
- Macroscopic intra-articular pus
- Two positive cultures of the same high virulence organism, such as *S.aureus*. This is in contrast to low-virulence organisms such as *C.acnes* or coagulase-negative Staphylococci.

Aside from the major criteria, several minor criteria were also established:

- Unexpected wound discharge and drainage
- Single positive tissue culture with a virulent organism
- Single positive tissue culture with a low-virulence organism
- Second positive tissue culture (identical low-virulence organism)

- Humeral loosening
- Positive frozen section (5 neutrophils in > 5 high-powered fields)
- Positive pre-operative aspirate culture
- Synovial neutrophil percentage > 80%
- Synovial white blood cell count > 3000 cells/μL beyond 6 weeks from surgery
- ESR > 30 mm/h
- CRP > 10 mg/L
- Elevated synovial AD
- Cloudy synovial fluid.

The ICM defined the presence of 6 or more minor criteria with an identified organism as a probable infection. Infection is possible when there are 6 or more minor criteria without an identified organism, or fewer than 6 minor criteria with a single positive culture with a virulent organism, or fewer than 6 minor criteria with 2 positive cultures with a low-virulence organism. An infection was deemed unlikely with fewer than 6 minor criteria with no positive cultures or a single positive culture with a low-virulence organism.

1.5.3 – Culture-negative PJIs

Culture-negative PJIs are extremely difficult to eradicate and are a dilemma for the surgeon, the infectious diseases team, as well as the patient. In recent years, the incidence of culture-negative PJIs have been increasing. Traditionally, they accounted for up to 45% of PJIs in some series [138]. The sensitivity of routine culture methods for identifying the correct infective organisms in PJI is low and ranges between 39-70% in reported studies [139, 140]. Culture-negative infections can be attributed to antibiotics prior to samples being taken, failure to use enrichment media for bacterial growth, infection with a low-virulence organism that require special growth media and longer incubation periods [141]. In theory, the premature administration of antibiotics may compromise the yield of the culture and should therefore be withheld until an organism is shown on the culture. However, several studies have demonstrated that pre-operative administration of antibiotics had no influence on the culture yield [139, 142, 143]. Despite multiple studies however, the International Consensus Meeting on PJI recommends that the mandatory withholding of antibiotics is not justified but “in cases in which PJI is diagnosed or suspected and a pathogen has yet to be identified, the use of prophylactic antibiotics is dependent on clinical judgement” [139].

Indolent organisms such as *Propionibacterium acnes* (*P.acnes*) and coagulase-negative Staphylococci may also yield a false-negative culture result depending on the culture technique. Several studies have shown that blood culture bottles increase the yield of positive cultures for tissue and synovial fluid samples compared with conventional agar and broth growth media [142]. In addition to this, it is

imperative to obtain an adequate number of intraoperative tissue samples (typically 3-5) for both aerobic and anaerobic culture, and that as many as 10 samples should be obtained when a low-virulence organism is suspected [144]. The duration of incubation also plays an important role: *P.acnes* requires a prolonged culture duration with a median time of 6 days before it can be identified on routine cultures [143].

1.5.4 – Fungal infections

Fungal PJIs account for approximately 1% of all PJIs and the diagnosis of these infections may be more difficult compared to bacterial PJIs due to the highly diverse presentations. The diagnosis and management of fungal PJIs pose unique challenges for clinicians due to a number of reasons. There are no standardized guidelines that have been developed for fungal PJIs due to their rarity and the patients tend to be immunocompromised. In addition to this, it is not known if the well-established treatment algorithms for bacterial PJIs can be applied to fungal PJIs since there is inconsistent data regarding the use of systemic, local and oral antifungal agents [145].

Patients presenting with fungal PJIs can present with varying signs based on pre-existing co-morbidities and may also have a superimposed bacterial infection. Risk factors include intravenous drug use, immunosuppressive medications, prolonged or inappropriate use of antibiotics, rheumatoid arthritis, diabetes mellitus, tuberculosis, underlying cardiac disease, hepatic and renal disease, as well as indwelling catheters [146, 147]. Of these risk factors, immunosuppression has the highest association with fungal infections as innate immune pattern recognition receptor cells are responsible for mounting an immune response via TLRs, C-type receptors and pentraxin-3 [148]. Patients often present with a low-grade indolent infection with chronic pain without the classic signs of erythema, effusion or swelling. Systemic signs such as fevers chills and malaise are not routinely present in cases of fungal PJI [148].

The MSIS definition for diagnosis of PJIs may not be applicable to fungal PJIs as the definition was based on bacterial infections. The initial workup for fungal PJIs should begin with a CRP and ESR. With regards to the accuracy of these tests, a multicenter study of 31 fungal PJI cases reported an average ESR and CRP of 54 mm/h and 17.5 mg/L, respectively [149]. However, two recent meta-analyses demonstrated that in patients with confirmed fungal PJI of the hip and knee, only half had elevated inflammatory markers including CRP and ESR, as well as leukocytosis [146, 147]. Synovial fluid analysis and culture should also be considered. However, there is insufficient evidence on whether certain ranges of synovial white cell counts are more indicative of fungal PJIs. In addition, synovial fluid biomarkers such as leukocyte esterase and AD, although useful tests in bacterial PJIs, aided in the diagnosis of only six fungal PJIs and therefore found no threshold levels for AD for

fungal infections [150, 151]. The identification of the correct organism is vital for selection of appropriate antibiotic therapy but up to 46% of fungal PJIs are culture negative due to difficulty of isolating organisms. Fungal cultures should be continued for a minimum of 5 to 14 days, and up to 4 weeks because of their indolent growth [149]. Other efforts to improve the diagnostic accuracy of fungal PJIs included next-generation sequencing (NGS). Two emerging tests in clinical practice for identifying infective organisms are the 16S RNA PCR for bacteria and internal transcribed spacer for fungi. Although NGS appears to be a highly promising tool, no studies have reported on the diagnosis of fungal PJIs. Diagnosis using frozen-section histopathology, which can help diagnose bacterial PJIs with a specificity of 94%, similarly has a low diagnostic value of 50% in fungal PJIs, as fungal infections a usually present in immunocompromised patients and the predicted inflammatory response seen in bacterial PJIs is unlikely to be present in fungal infections [152].

1.5.5 – Novel biomarkers for diagnosis of PJIs

In more recent years, research on diagnostic biomarkers for PJIs found in synovial fluid have greatly increased. Deirmengian et al [153] identified and investigated 16 potential synovial biomarkers for PJI diagnosis in 95 samples of synovial fluid used to classify 29 PJIs and 66 aseptic joints. The biomarkers included: IL-1a, IL-1, IL-6, IL-8, IL-10, IL-17, vascular endothelial growth factor (VEGF), CRP, neutrophil elastase 2 (ELA-2), lactoferrin, granulocyte colony-stimulating factor (G-CSF), neutrophil gelatinase-associated lipocalin (NGAL), resistin, thrombospondin, bactericidal permeability-increasing protein (BPI) and AD. Of these 16 markers, five demonstrated very high sensitivity and specificity for PJI. These were: AD 1-3, ELA-2, BPI, NGAL and lactoferrin [153, 154].

The synovial biomarker with the highest sensitivity and specificity for PJI of TKA and THA is AD [155-157]. AD is an antimicrobial peptide secreted by neutrophils in response to bacterial infections [158]. It's role in antimicrobial support of the immune system is that it integrates into the pathogen's cell membrane to induce lysis and rapid death by depolarization of the target cell. In addition to this, AD levels did not seem to suffer a decrease following the administration of antimicrobial agents [155]. Leukocyte esterase (LE) is an enzyme that is produced by activated neutrophils at a site of infection and was originally utilized as a diagnostic marker in UTIs. LE present in the synovial fluid of suspected PJI cases is detected via colorimetric strip tests whereby a color change indicates the presence of LE. A meta-analysis by Chen et al [159] examining the reliability of AD and LE in the diagnosis of PJIs found that AD had sensitivity and specificity of 87% and 97% respectively while LE had sensitivity and specificity of 79% and 96% respectively, indicating that both markers performed better than other serological and synovial markers.

1.5.6 – Current management of PJI

The ultimate goal of treatment is to eradicate biofilm from the indwelling device whilst preserving joint functionality and improving quality of life for the patient. Surgical interventions to manage PJIs include the following (**Figure 1.2**):

- Debridement, antibiotics and implant retention (DAIR) of the prosthesis in conjunction with antibiotic therapy.
- One-stage or two-stage revision for patients who don't qualify for debridement and implant retention.
- Excisional arthroplasty with or without arthrodesis.
- Amputation of the affected limb.
- Chronic suppression of the infection with antibiotics without surgical intervention. This option never eliminates the infection and is associated with high rates of recurrence.

The DAIR procedure is preserved for only acute post-operative infections or acute haematogenous infections to reduce the infective organism load and to treat with antibiotics prior to the formation of the bacterial biofilm. The surgical procedure involves excision of skin edges and any sinuses as well as radical synovectomy and exchange of removable parts of the implant such as the polyethylene (PE) insert. Success rates for the DAIR are 28-62% for late chronic or established PJIs and 31-100% for acute infections [160]. The risk factors for failure of the DAIR procedure are no different to other procedures and are dependent on patient factors, surgical factors, and duration of symptoms. DAIR is contraindicated in those with a persisting wound sinus [161] and may not be an appropriate option in immunocompromised patients [162]. Multiple studies have shown that an infection with *S.aureus*, in particular MRSA, is an independent risk factor for failure of the DAIR and the duration of post-operative antibiotics remains an area of controversy [163, 164]. The current recommendation for a DAIR is an acute post-operative within 4 weeks or acute haematogenous infection within 2 weeks performed open with PE exchange and post-operative antibiotics for 6 weeks with monitored progress with clinical examination and inflammatory markers. Patients who are immunocompromised, have a MRSA infection or poor local soft tissues or previous failure of DAIR should undergo revision instead [160].

Surgical practices in revision arthroplasty differ worldwide (**Figure 1.3)**: exchange procedures are favored in North America whereas DAIR is preferred in Australia and Europe in acute infections [104]. The two-stage revision is still considered as the gold standard for revision of PJIs of TKAs. The two-stage revision involves removal of the prosthesis and insertion of an antibiotic cement spacer for 6 weeks, during which time the patient receives antibiotics before a new prosthesis is put back. This causes prolonged hospitalization and increased morbidity to the patient. The single stage revision

involves removal of all prosthetic components and cement with aggressive debridement of non-bleeding scar tissue and bone with intramedullary reaming if required followed by copious lavage and re-scrubbing of the entire surgical team prior to re-implantation of new instruments [165]. Recent literature suggests that the single stage revision is an alternative to the two-stage revision with the main advantages being a single surgical procedure, shorter duration of hospitalization, lower costs, and a shorter duration of antibiotics. Correct patient selection is crucial in the decision-making of choosing between single-stage or two-stage revision. The Infectious Disease Society of America guidelines patients with a THA PJI, good soft tissue, good bone stock, known micro-organism with susceptibility to oral anti-microbial agents with high oral bioavailability are suitable for single-stage revisions whereas those with poor soft tissue, difficult to treat organisms and where delayed reimplantation is technically feasible, a two-stage revision may be more appropriate. The reported success rates of single-stage revisions are 67-100% with an average of 87.1%, whereas those for two-stage revision are 54-100% with an average of 84.8% with comparable functional outcomes [166].

There are patients in whom surgical interventions for PJI may be contraindicated. These may include significant medical co-morbidities that pose unacceptably high anesthetic and surgical risks, poor bone stock, advanced patient age, anticipation of poor outcomes, surgeon decision and patient refusal to undergo any further surgeries. Antibiotic suppressive therapy (AST) is utilized in these patients with the aim of suppressing the clinical manifestations of the infection rather than eradicating it. A multi-centered, retrospective study [167] involving 302 patients was conducted with a mean follow-up period of 25 months. Tetracyclines were the most prescribed oral antibiotics for suppression, followed by cotrimoxazole. AST was considered successful in 58.6% of patients and failed in 41.4%. Success rates at 2- and 5-years post commencement of therapy were 75% and 50% respectively. Other studies have quoted success rates of AST of 23-86% [168, 169]. Variables associated with failure of AST and lower chance of survival include *S.aureus* infection, age above 85, female gender, hypoalbuminaemia, presence of a sinus tract, tumor prosthesis and rheumatoid arthritis [170].

1.5.7 – Antibiotic-impregnated cement and spacer

Due to the limited efficacy of antibiotics in preventing or treating biofilms, the use of antimicrobials alone is inadequate. Antibiotics in polymethylmethacrylate (PMMA) cements and antibiotic-coated implants are increasingly being utilized to prevent PJI as well as in the management of open fractures with bone defects as well as in the treatment of osteomyelitis.

Appropriate selection of the antibiotic with the desirable pharmacokinetics and physical properties is essential: it must be thermostable to prevent breakdown during the exothermic polymerization reaction, it must be active against the causative agent, and it must be a form that is compatible with PMMA [171]. The most common antibiotic-impregnated PMMA formulations contain

aminoglycosides, such as gentamicin and tobramycin, and vancomycin as well as cephalosporins. Gentamicin and tobramycin are bactericidal against aerobic Gram-negative bacilli but also have a synergistic effect against Gram-positive bacteria including *Staphylococci* and *Enterococci* [172]. Vancomycin is highly efficacious against gram-positive bacteria including MRSA and displays excellent elution properties from calcium sulphate and PMMA [173].

Dosing of antibiotics in PMMA can be divided into low-dose, containing less than 2 g of antibiotics per 40 g of cement, or high-dose, containing greater than 3.6 g of antibiotics per 40 g of cement. Further increase in antibiotic dose is discouraged and will weaken the cement construct. Low-dose formulations are typically used for prophylaxis in primary arthroplasty whereas high-dose is typically used in established infections [171]. The rate and duration of antibiotic release are affected by the concentration of the antibiotic, surface area of the cement/beads, vacuum-mixing and the conditions of the local environment. Antibiotics elute through small pores in the surface of the cement and is characterized by rapid release in the first 24 hours followed by a period in which the rate decreases rapidly and then reaches a steady declining rate [174] with the entire process taking up to 5 weeks for tobramycin and vancomycin and combining these two antibiotics increased the elution of tobramycin by 68% and vancomycin by 103% compared to if either were used alone [175].

One of the limitations of antibiotic-impregnated implant coating like hydroxyapatite (HA) is burst drug release due to weak binding forces between HA surface and the drugs. Recent developments in material science have shown the utility of slowly biodegradable polymer coatings that contain antibiotics to ensure the sustained release of antibiotics [176]. However, this would only be insufficient to solve the problem as the use of antibiotics would also cause resistance.

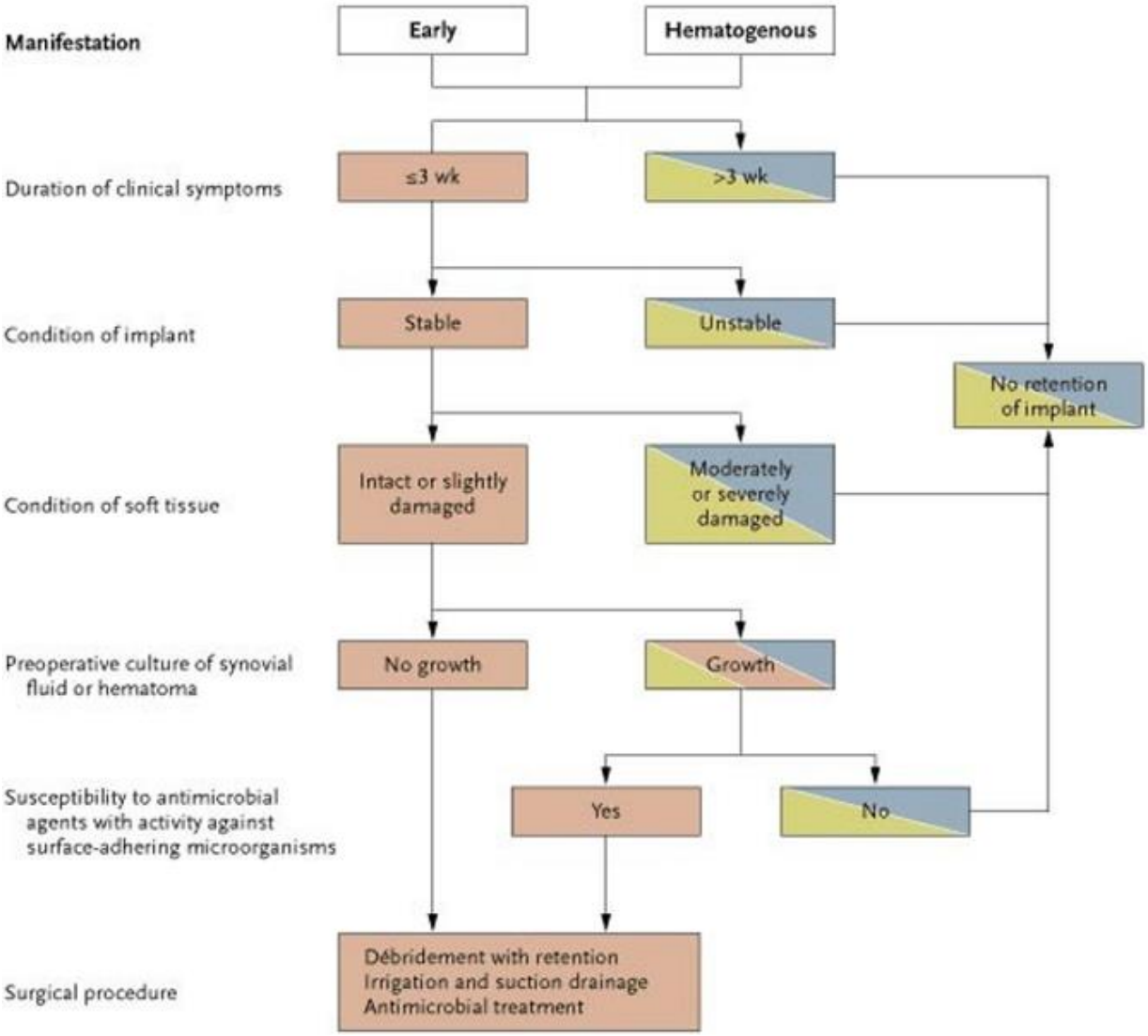

Figure 1.2 – **Algorithm for the treatment of early and haematogenous PJIs.**

This treatment algorithm is used in the management of PJIs involving TKAs and THAs. PJIs greater than 3 weeks in duration tend to have established biofilms on the implants and the failure rate of DAIR is very high. Prosthesis that are mechanically loose or unstable and are moderately or severely damaged must also be removed.

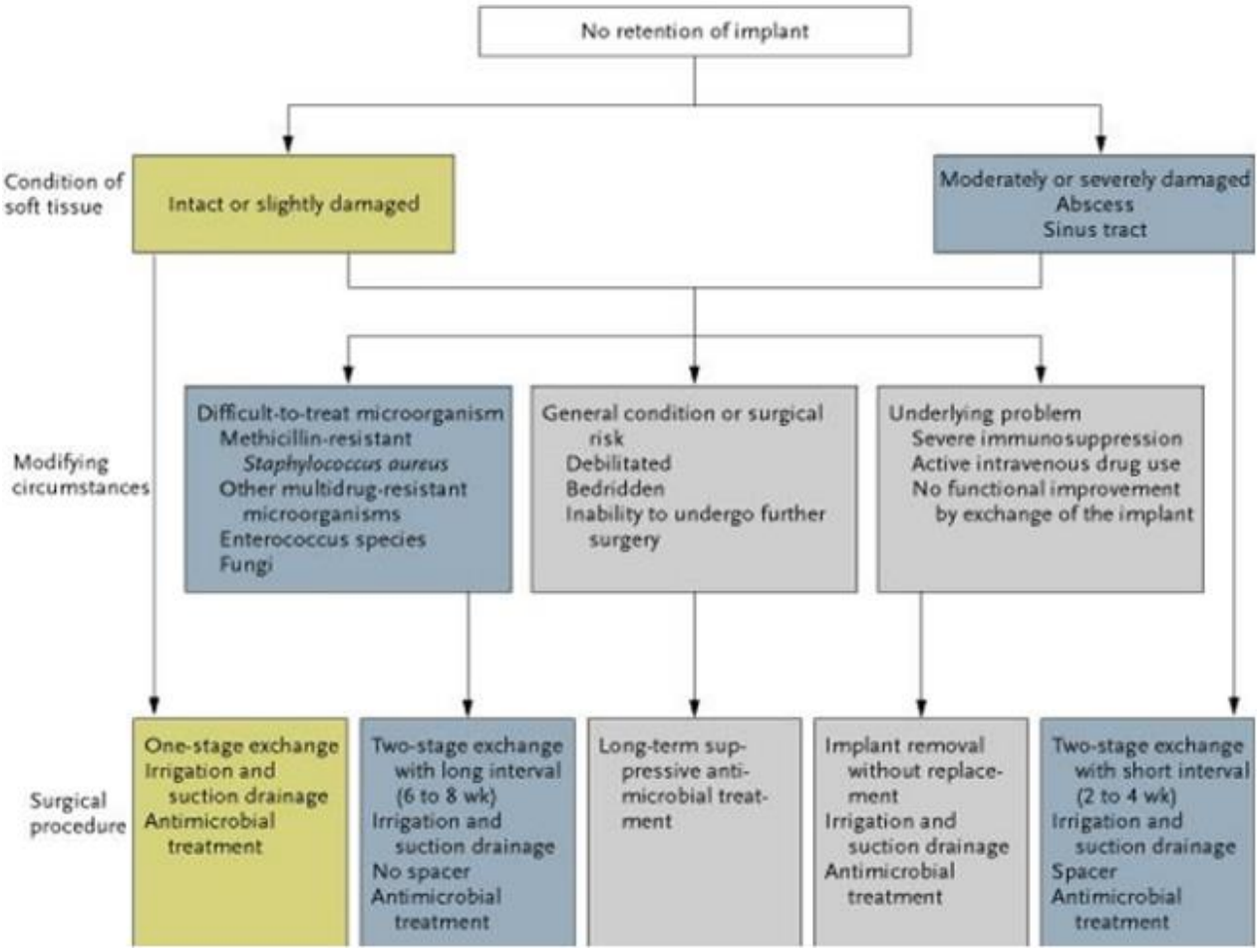

Figure 1.3 – **Algorithm for the treatment of patients with PJIs who do not qualify for implant retention.**

Patients with a TKA and THA who have delayed or late infection, infection with difficult-to-treat microorganisms, severe medical morbidities and severely compromised soft tissue are not suitable for DAIR due to high failure rates. In patients with a knee prosthesis, arthrodesis is performed after resection arthroplasty. If the soft tissue is intact or only slightly damaged, a one-stage revision may be possible. In patients with compromised soft tissue or difficult-to-treat microorganisms, a two-stage exchange (blue boxes) is preferred. Permanent explantation or joint arthrodesis are usually performed in severely immunocompromised patients, those with active intravenous drug use, and those in whom arthroplasty will not provide any functional benefit.

1.6 - Biomaterials in the combat against biofilms

1.6.1 - Biomaterials to inhibit biofilm formation

Novel anti-biofilm technologies such as the modification of biomaterials for use in medical devices to inhibit the formation of biofilms have been developed, including the use of nanoparticles to functionalize the surface of biomaterials, which have been attracting researchers [22]. Materials that have been studied include trimethylsilane, zinc oxide (ZnO) nanoparticles and silver nanoparticles (AgNPs). The biofilm formation of *S.epidermidis* on stainless steel and titanium decreased when the metals were coated with trimethylsilane (TMS). The inhibition can be attributed to coating smoothness, low surface free energy, coating chemical inertness, surface bound CH3 groups. Furthermore, not only did TMS decrease *S.epidermidis* biofilm formation, bacterial cells on TMS-coated surfaces were also more susceptible to antibiotic treatment than their counterparts in biofilms on uncoated surfaces [177].

A study by Lee et al investigated the role in heavy metal ions in the inhibition of pyocyanin production, and hence biofilm formation, by *P.aeruginosa* without inhibiting planktonic growth and that zinc nanoparticles inhibited *P.aeruginosa* biofilm formation without exhibiting cytotoxicity. The group also examined the genetic mechanism by which ZnO nanoparticles exhibited these inhibitory effects by evaluating the change in RBC lysis by *P.aeruginosa* pre and post incubation with ZnO as well as the differential RNA load and gene expression in *P.aeruginosa* samples treated with ZnO compared with non-treated controls [178]. In addition, other in vitro studies have also demonstrated that ZnO nanoparticles also inhibited biofilm formation of enterohaemorrhagic *E.coli*, *MSSA* and *MRSA* at 5 mM [179].

1.6.2 - AgNPs

Among metal nanoparticles with proven bactericidal activity, silver is one of the most effective [180]. Two antibacterial mechanisms are mentioned in literature: ion-mediated killing and contact killing [181].

It has been demonstrated that AgNPs adhere and anchor to the cell wall of bacteria before infiltration into the cell. The positive charge of AgNPs confers a strong electrostatic attraction with negatively charged groups in bacterial cell walls such as carboxyl, phosphate and amino groups present in bacterial cell walls. This culminates in physical changes in the bacterial membrane, leading to damage and leakage of cellular contents ultimately resulting in bacterial death [182]. There is large difference in the thickness of cell walls between Gram-positive bacteria (30 nm) and Gram-negative bacteria (3-4 nm), with most of the difference attributable to peptidoglycan. Because of this, AgNPs have a more potent antibacterial effect on Gram-negative bacteria compared to Gram-positive bacteria [183].

Following adhesion and infiltration to bacterial cell wall, AgNPs can infiltrate into the cell. There is a size-dependent antibacterial effect: smaller nanoparticles have a larger surface area and reach the cytoplasm more readily than larger nanoparticles. Once inside the cell, AgNPs can interact with cellular structures and macromolecules such as proteins, lipids and nucleic acids. These interactions between cellular structures and AgNPs will lead to bacterial dysfunction and cell death. AgNP interaction with ribosomes lead to protein denaturation and inhibition of translation [181].

In addition, AgNPs can generate an abundance of reactive oxygen species (ROS) and free radicals including hydrogen peroxide (H_2O_2), superoxide anion, hydroxyl radical, hypochlorous acid and singlet oxygen. Reactive oxygen species are normally removed by bacterial homeostasis and antioxidant systems, but AgNPs exerts an addition effect of inactivating antioxidant systems culminating in excess ROS generation [184].

1.6.3 - Ag antibacterial mechanism mediated by Ag+ ions

The mechanism of antibacterial action of Ag^+ is associated with its interaction with sulfhydryl groups in proteins and enzymes. Ag^+ can bind to proteins in membrane-bound proteins, involved in transmembrane ATP generation, resulting in protein deactivation [185]. Ag^+ have also been described to uncouple respiratory electron transport from oxidative phosphorylation and limit the respiratory enzymes [186]. In addition, Ag^+ is able to intercalate between purines and pyrimidine base pairs and disrupt base pairs of DNA strands [187]. Like AgNPs, Ag^+ can increase cellular oxidative stress in microbes. Although AgNPs can kill bacteria through the two different modes of action mentioned above, the antibacterial mechanism is usually a synergistic effect generated by AgNPs and Ag^+.

More recently, transcriptome analysis demonstrated that AgNPs repressed the expression of *icaA*, a key intracellular adhesion protein as well as various other adhesins [188]. In addition to this, Singh el al performed transcriptome analysis on *S.aureus* treated with AgNPs and showed that a number of genes involved in metabolic processes, quorum sensing as well as cell transporters were differentially expressed compared to *S.aureus* treated with control samples [189].

1.6.4 - Anti-biofilm activity of AgNPs

Several studies have demonstrated the antibiofilm activity of AgNPs. Franci et al [190] have shown that AgNPs are detrimental to the formation and maturation of *Pseudomonas putida* biofilms. Other studies have shown at AgNPs at concentrations up to 10 µg/mL exhibited antibiofilm effect against *E.coli* [191]. In addition, van Hengel et al incorporated AgNPs into porous titanium implants and subsequent antimicrobial assays showed strong antibacterial activity against MRSA including

prevention of biofilm formation and surface antimicrobial activity [192]. The findings from these studies illustrated that the incorporation of AgNP into implants can functionalize the implants and bestow upon them an antibacterial function. Similarly, Kalishwaralal et al [193] demonstrated almost complete inhibition of biofilm formation by *P.aeruginosa* and *S.epidermidis* with AgNPs at a concentration of 100 nM.

1.7 - Cytotoxicity of silver nanoparticles

1.7.1 - Health concerns regarding AgNPs

The strong oxidative properties of AgNPs releases Ag^+ ions resulting in several detrimental effects on biological organisms by inducing genotoxicity, cytotoxicity, immunological response and apoptosis [194]. Because the use of AgNPs carry a number of concerns with regards to their biological interactions, AgNPs raise concerns in human exposure as they can pass through the blood brain barrier (BBB) via transcytosis of endothelial cells [195]. It is postulated that Ag^+ ions have greater toxicity than elemental Ag or AgNPs. However, the magnitude of toxicity is difficult to ascertain due to the myriad of studies with different methodologies for AgNP synthesis, the use of capping agents and different toxicity tests. However, it can be stated that the physiochemical properties of AgNPs can control the toxicity pathways [196].

1.7.2 - Mechanism of AgNP toxicity

The precise toxicological mechanism of AgNP on human cells is still unclear, although a number of both *in vitro* and *in vivo* studies are available. Physicochemical factors such as particle size, concentration, as well as exposure time and the presence of surface coating agents contribute to the overall cytotoxic and genotoxic effect of AgNPs. AgNPs are toxic at particle sizes of 10-100 nm at concentrations ranging from 5-10 µg/mL [197].

The most probable cause of biochemical disruption is probably mediated by AgNP-induced oxidative stress and the generation of ROS, which has been shown in several *in vitro* studies [198]. The presence of AgNPs and Ag^+ ions generate ROS including superoxide radical (O_2^-) and H_2O_2 which are essential for maintaining physiological cellular processes, but excess ROS generation will overwhelm the antioxidant defense to damage macromolecules including nucleic acids (DNA and RNA), proteins and lipids, especially in human cell lines. Intracellular oxidative stress activates matrix metalloproteinase 3 (MMP3) to secrete an extracellular matrix digester protease [199]. In conjunction with this, the depletion of glutathione and antioxidant enzyme activity, as well as elevated levels of lipid peroxidation and protein carbonylation occurs to promote apoptosis signaling pathways such as

p53, AKT and MAPK [200, 201]. Several studies have reported that the release of Ag^+ from AgNPs is responsible for cytotoxic effect of AgNPs on cells and found that AgNPs can act as a transport vehicle for delivering Ag^+ into cells via a 'Trojan-horse' mechanism [202].

1.7.3 - Cellular uptake of AgNPs

The rate of the translocation of AgNPs, as well as the destination inside the cell, may be size-dependent. Zielinska et al [204] visualized osmiophilic granular aggregates of AgNPs (18 nm in diameter) localized in cellular vacuoles using transmission electron microscopy (TEM). Along similar lines, Sengstock et al demonstrated that human mesenchymal stem cells treated with AgNPs for 24 hours showed aggregates of the nanoparticles in the endo-lysosomal areas but not inside the nuclei [205]. Berry et al [206] observed that gold nanoparticles (AuNPs) with a diameter of 5 nm were found in the nuclei of human fibroblasts whereas AuNPs 30 nm or larger in diameter were commonly found in the cytoplasm. This finding, however, is not consistent. Another study demonstrated that the exposure of OB to AgNPs 5 nm in size resulted in the localization of these NPs inside the lysosomes but not the nucleus [207] whereas conversely, nuclear presence was detected for AgNPs with a diameter of 30 nm in keratinocyte (HaCaT cell lines) and AgNPs over 50 nm were detected in the nuclei of human mesenchymal cells [208, 209]. To further complicate the matter, human gingival fibroblasts treated with AgNPs caused their uptake and localization in the mitochondria, the same AgNPs were not detected at all by TEM when incubated with human osteoarthritis chondrocytes [210, 211]. The discrepancy of all these findings indicated that the cellular uptake of AgNPs is not merely a function of particle size but is also dependent on cell-type, time of incubation, zeta potentials as well as concentration.

1.7.4 - Physicochemical properties of AgNPs on cytotoxicity

The genotoxicity and cytotoxicity of AgNPs is influenced by particle size and a number of studies have supported the hypothesis that smaller particles induce greater cytotoxicity on a number of cell lineages, as smaller particles have greater surface area and surface reactivity compared to larger particles [212-214]. Similarly, Carlson et al found that smaller hydrocarbon-coated AgNP (15 nm) generated higher levels of ROS and displayed more toxicity to macrophages than larger AgNPs (55 nm) [215].

Different methods of synthesis result in diverse types of AgNPs with varying shapes; the shape of AgNPs may influence cellular uptake, which in turn may modulate cytotoxicity. However, different cell lines such as macrophages (RAW 264.7, J774.1), A549, A498, HepG2, and neurons (Neuro 2A) showed selective toxicity to certain shapes over others [216]. Stoeher et al demonstrated that spherical

AgNPs exhibited minimal adverse effects against A549 cells whereas thin, wire-shaped AgNPs induced detrimental outcomes [217].

1.7.5 - Effect of capping agents and coating

The presence of coating or capping agents can also significantly affect the cytotoxicity of AgNPs on cells, possibly due to limited direct contact the nanoparticle surface with cellular components [218] or decreases the rate at which Ag^+ ions are released into the surroundings, although the exact effects have not been completely elucidated. However, this is another area of contention as not all studies showed that coating agents reduce the cytotoxicity of AgNPs and may be in part attributed to the properties of the coating agents used. For instance, Suresh et al showed that poly(diallydimethylammonium)-coated AgNPs, biogenic-Ag and oleate-AgNPs were in fact more toxic to macrophages and lung epithelial cells compared to uncoated AgNPs [219]. Similarly, others have shown that AgNPs at a diameter of 10 nm exerted cytotoxicity towards human lung cells and this toxicity was independent of the surface coating [220].

1.7.6 - Cytotoxicity of AgNPs on human osteoblast (OBs) and osteoclasts (OCs)

Silver nanoparticles, similar to most other NPs, can generate ROS and reactive nitrogen species to induce oxidative damage. However, information regarding cytotoxic concentrations of AgNPs in literature is often conflicting and unclear. Albers et al [221] described toxicity of AgNPs obtained from $AgNO_3$ on OBs and OCs. OBs and OCs were cultured in α-MEM supplemented to 10% FBS for 72 hours. After this period, the culture media was changed and treated with Ag microparticles and nanoparticles (average sizes of 50 nm, 3 µm and 30 µm at concentrations of 8-500 µg/mL) for a further 72 hours. Titanium microparticles and nanoparticles (average sizes of 50 nm and 30 µm) were used as negative controls. The results indicate that Ag treatment decreased cell viability and cell differentiation in both OBs and OCs and that cell differentiation was impaired at lower concentrations than cell viability for both cell groups. Furthermore, OBs were more sensitive to Ag than OCs and proliferation and differentiation were affected at lower concentrations. The MIC for OBs and OCs were as follows; OB viability 128 µg/mL; OB differentiation: 64 µg/mL; OC viability: 256 µg/mL; OC differentiation 128 µg/mL. In addition to this, the degree of cytotoxicity was dependent on particle size, with nanoparticles (average size 50 nm) demonstrating greater toxicity on OB and OC than microparticles (average size 3 µm). Larger microparticles (average size 30 µm) did not demonstrate toxicity.

Alternatively, Pauksch et al suggested that a therapeutic window for AgNPs exists and that mesenchymal stem cells and OBs incubated with AgNPs at a concentration of 10 µg/mL demonstrated impaired cell viability after 21 days. However, information regarding cytotoxic

concentrations to OBs and OCs found in literature is sometimes contradictory and there is no clear consensus on the molecular mechanism of silver toxicity in bone [207]. Zielinska et al incubated human fetal osteoblast cells (hFOB 1.19) with uncoated AgNPs 18 nm in diameter at concentrations of 30 µg/mL and 60 µg/mL for 24 hours and 48 hours of exposure [204]. The group observed that uptake of AgNPs by OBs, by way of TEM, was associated with alterations in the ultrastructure of the cell and signs of cellular injury such as swelling of the endoplasmic reticulum, clumping and marginalization of condensed heterochromatin in the nucleus, reduced cell volume, increased nuclear to cytoplasm ratio, plasma membrane blebbing and apoptotic body formation.

1.7.7 - Effect of AgNPs on OB differentiation

The effect of nanoparticles, including AgNPs, on the maturation and differentiation of OBs has been investigated. Whilst evidence exists to suggest that AgNPs are cytotoxic to OBs, Mahmood et al [222] have demonstrated that AgNPs may stimulate and promote OB differentiation and mineralization. The group performed in-vitro mineralization tests on MC3T3 cells using AgNPs 23.0 ± 2.0 nm in diameter (synthesized by borohydrate mediated reduction of silver nitrate), hydroxyapatite nanoparticles nanoparticles, titanium dioxide nanoparticles (TiO_2) as well as single walled carbon nanotubes (SWCNTs), all at a concentration of at a concentration of 20 µg/mL. On day 24, the concentration of alizarin red stain (AR-S) was the highest for AgNP-treated cells at 2.1 mmol/mg, compared to 1.5 mmol/mg for hydroxyapatite nanoparticles, 1.2 mmol/mg for TiO_2, 0.9 mmol/mg for SWCNTs and 0.75 mmol/mg for controls. In addition to this, the increase in ARS also appeared to be time-dependent: the ARS in AgNP-treated cells was the same as control cells on day 6, two times greater at day 15 and approximately 2.5 times greater at day 24. The group also found that alkaline phosphatase (ALP) activity at day 6 in AgNP-treated cells was more than twice that found in controls.

Genetic sequencing has also been employed to elucidate the role of AgNPs in the maturation and differentiation of OBs [222, 223]. Mahmood et al performed micro-RNA (miRNA) microarrays on OBs and found that many multifunctional bone-forming growth factors were observed in AgNP-treated cells but not controls, including BMP2, BMP3, BMP6 BMP7 and BMP8. In addition, several transcriptional factors involved in bone formation including Smad1, Smad5, Runx2, Dlx3 and Msx2 were affected by the correspondent miRNAs only in AgNP-exposed cells. Runx2 is a common target of BMP2 and transforming growth factor β (TGF-β), and cooperation between Smad2 and Runx2 selects for OB-specific gene expression in pluripotent mesenchymal precursor cells. Following these findings, Qing et al [223] performed transcriptome analysis via RNA sequencing on AgNP-treated OBs and found that 179 genes were upregulated while 58 genes were downregulated compared to controls. The dysregulation in most of these genes occurred on the day one group of AgNP treatment, but minimal changes were observed after the first day of AgNP treatment. The enriched pathways

affected genes associated with phase I and II drug metabolism (metabolism of xenobiotics by cytochrome P450, drug metabolism-cytochrome P450 and glutathione metabolism) and to a smaller extent, bone mineralization and formation and the extracellular matrix interaction pathway. One upregulated gene was BMP6, which initiates OB differentiation: the expression of BMP6 was 3.8 times higher in AgNP-treated cells compared to controls. The authors concluded that although there was minimal influence was observed of AgNP on genes associated with differentiation when compared with the control population, there were many differentially expressed genes involved in metabolism pathways, particularly metabolism of glutathione and xenobiotics. The results seemed to also indicate that AgNP-induced toxicity at the molecular level may not be apparent in phenotypic assays such as mineralization assay and ALP activity assay when an apparent non-toxic dose is used. Moreover, the large number of differentially expressed genes on day 1 indicates that AgNPs induce an acute cytotoxicity.

Therefore, the utility of the antimicrobial effects of AgNPs in biomaterials is limited and offset by their cytotoxic effects and the option of coupling AgNPs with other elements to reduce their toxicity on host cells must be further explored.

1.8 - Osseointegration properties of biomaterials

1.8.1 – Optimal properties of orthopaedic prostheses

The utilization of novel biomaterials in the field of orthopaedic surgery is ever increasing, with a projected annual number of orthopaedic procedures approaching 28.3 million in the year 2022. Accordingly, the synthesis of biomaterials with multi-modal functions is a rapidly evolving field. Approximately 70-80% of prostheses are composed of metal biomaterials. At the most fundamental level, a biomaterial requires a Young's elastic modulus similar to that of bone to prevent stress-shielding induced bone-resorption and subsequent device-failure, as well as allowing integration to promote fracture healing [224]. In addition to this, the biomaterial should be inert and not elicit an immune response to harm the surrounding tissue nor jeopardize the longevity of the implant [225]. Due to the rapid developments in material designs however, the qualities alone are no longer adequate. The expected requirements of a 'smart' biomaterial in orthopaedics should be one that is bioactive, biodegradable and possesses antibacterial properties.

1.8.2 - Current biomaterials in use in orthopaedic surgery

The most common metallic biomaterials in orthopaedic implants are stainless steel, cobalt (Co)-chromium (Cr) alloys, Ti and its alloys [226]. Of these, Ti alloys possess the highest corrosion resistance, biocompatibility and specific strength compared with Co-Cr alloys and stainless steel, but

the least stiffness. Co-Cr alloys have the highest wear resistance and higher strength whereas stainless steel had higher ductility and cyclic twist strength. Other biomaterials, such as magnesium (Mg) alloys, iron (Fe) and tantalum (Ta) are also important, but are found less commonly in orthopaedic implants and prostheses. Although Ti and CoCr alloys are frequently used in orthopaedic implants and arthroplasty, they are not without disadvantages. The Young's elastic moduli of these metals are much greater than that of bone, leading to stress shielding and decreased bone formation and remodeling around the implant leading to subsequent stem loosening and a propensity for periprosthetic fractures [227]. In addition to this, Ti granules at concentrations of 100 μg/mL and above inhibited OB viability and increased the concentration of intracellular ROS levels [228]

More recently, Niinomi et al [226] have developed a novel Ti alloy consisting of Ti, niobium (Nb), tantalum (Ta) and zirconium (Zr), termed TNTZ. This alloy has a Young's modulus similar to that of human bone and therefore reduces the degree of stress shielding and therefore bone resorption and subsequent implant loosening and fracture.

1.8.3 - Role of magnesium on osteogenic differentiation

Magnesium (Mg) is the fourth most abundant cation in the human body and is essential to human metabolism and is naturally occurring in bone. Magnesium serves as a co-factor in many biochemical processes in the body, including but not limited to regulating cardiac rhythm, muscle and nerve function, protein synthesis and regulation of blood pressure and glycaemic control [229]. Approximately 60% of total Mg in the body is stored in bone, 39% stored intracellularly and the remaining 1% is free in plasma. The homeostasis of Mg is a balance between intestinal absorption, storage in bone and cells and excretion by the kidneys. In addition to the aforementioned functions, Mg alloys are suitable for use in orthopaedic implants due to their bioactive properties and has already been utilized in the design of biomedical devices such as stents, plates and screws [230]. With a density of 1.74 g/cm^3, Mg is an exceptionally light metal and is 4.5 times less dense than steel. Although light, the toughness of Mg is higher than that of hydroxyapatite while the Young's elastic modulus and compressive yield strength are closer to that of human bone than other commonly used metal implants. This in turn reduces the risk of stress-shielding and in turn enhances implant longevity [231, 232]. In addition, Mg has been found to have a stimulatory role in osteogenesis [233]. It is thought that Mg and its alloys can be applied as degradable, lightweight, load-bearing orthopaedic implants which would maintain mechanical integrity over 12-18 weeks while the bone tissue heals, after which it is replaced by the body's own tissue and this property has a clear advantage of obviating the need for removal of the implant after fracture union. Li et al [234] have shown that Mg and alloys of Mg, in particular Mg-Y (yttrium), promoted osteogenic differentiation and mineralization in hMSC

and upregulated genes involved in osteogenic differentiation such as TGFβ-1, BMP-2, SMAD4, FGF-2 and FGF-10.

However, the major drawback of Mg is the rapid corrosion of pure Mg, particularly in electrolytic, aqueous environments in physiological pH (7.4-7.6) resulting in loss of mechanical integrity before the tissue has healed and rapid production of hydrogen gas that is too fast to be dealt with by the host [235]. Additional concerns include adverse host reactions, the accumulation of toxic corrosion products and the formation of cavities around the implant [236, 237]. Some studies have demonstrated the presence of cavities near the site of the implant, of which the cause remains unclear but has been postulated that degradation granules might attract OCs to the implant site and subsequently enhance resorption [238, 239]. Wang et al demonstrated that Mg particle concentrations of up to 100 μg/mL increased OB viability and even offset the toxic effects of Ti particles but Mg concentrations above 200 μg/mL were associated with OB toxicity [228]. The seeming contradiction that Mg promotes osteogenic differentiation and increases OB viability, whilst forming cavities around implants may be explained by the different effect of Mg ions compared to Mg degradation granules: Maradze et al demonstrated that Mg ions increased OB viability whilst Mg degradation products impaired viability [236].

In addition to concerns of toxicity to OB, clinicians must also be cognizant of potential systemic toxicity due to hypermagnesaemia. The definition of hypermagnesaemia is a serum Mg level greater than 30 μg/mL [240]. As Mg concentration approaches 60-120 μg/mL, electrocardiogram (ECG) changes (prolonged PR-interval, widened QRS complex) occur. At 120 μg/mL, there is a loss of deep tendon reflexes and muscle weakness; cardiac conduction abnormalities at the sinoatrial and atrioventricular nodes, as well as respiratory depression are observed at 180 μg/mL and cardiac arrest results at 240 μg/mL [229]. Although Mg toxicity is uncommon and achieving such supra-physiological serum concentrations of Mg is unlikely, patients with CKD, those with a creatinine clearance less than 30 ml/minute, are at risk given that Mg is excreted by the kidneys. Given that approximately 15% of the adult population in the United States have CKD, and that approximately 1.2% of patients undergoing TKA and THA suffer from acute exacerbation of CKD resulting in severe renal dysfunction post-operatively, efforts to limit Mg release from biomaterials is crucial [241, 242]. Rare elements may be added to alloys to control Mg degradation and one such option is the trace element strontium (Sr).

1.8.4 - Osteobanabolic effect of strontium

Strontium ions (Sr^{2+}) is a trace element of the body and have the same physiological and chemical properties as calcium ions (Ca^{2+}), a major constituent of mineralized bone, and can be incorporated

into bone by ionic substitution for Ca^{2+} [243]. It never occurs free in nature due to oxidation to form strontium oxide. In human biology and pathology, this element has attracted less attention the two other divalent metals calcium and magnesium, although awareness is mounting as strontium ranelate has been shown to reduce the incidence of fragility fractures in osteoporotic patients [244, 245]. Bonnelye et al [246] demonstrated that mouse calvaria cells exposed to strontium ranelate treatment had an increased expression of the OB markers ALP, bone sialoprotein (BSP) and osteocalcin (OCN), as well as increased bone nodules. Conversely, the number of mature OCs was greatly reduced after strontium ranelate treatment. Ding et al [247] developed a $SrPO_4$ coating for the aforementioned TNTZ and found that $SrPO_4$-TNTZ had the following effect on OBs and OCs compared with uncoated controls:

- Higher expression of ALP and OCN, and therefore proliferation and differentiation, in OBs.
- Overexpression of transcriptional factors involved in bone formation pathway such as RUNX2, SMAD4, TGFβ1 and β-catenin.
- Inhibition of progression from OC progenitors or peripheral blood mononuclear cells (PBMCs) to mature OCs.

Such a novel compound has the promising potential for utilization in a large range of orthopaedic implants, in particular, for osteopenic and osteoporotic patients. Current clinical applications include the incorporation of Sr into PMMA bone cement and modification of bioceramics with Sr, with encouraging results showing increased OB proliferation and apatite precipitation to improve bone strength at the bone-implant interface [248, 249]. Furthermore, utilization of Sr coating to control Mg degradation may confer superior prosthesis longevity compared to conventional hydroxyapatite (HA; $Ca_{10}(PO_4)_6(OH)_2$) coating via plasma spray due to low adhesion strength and potential delamination of the hydroxyapatite coating [250]. Chen et al [251] were able to slow down Mg degradation by incorporation of Mg into a SrP conversion coating. This study demonstrated that not only was the corrosion of Mg much slower in coated samples compared to uncoated samples, but the degradation products of samples also containing the SrP conversion coating induced greater osteogenic proliferation and differentiation compared to pure Mg.

1.9 - Inflammatory gene expression in capsular tissue of patients

1.9.1 - Background on RNA expression

The keystone of molecular biology, first discovered by Watson and Crick, is the flow of information stored in genes in the form of DNA, transcription into RNA, followed by translation into proteins. The phenotypic expression of this genetic information is modified by various environmental factors.

Transcription of a small group of genes into complementary DNA (cDNA) subsequently determines the identity of the cell and regulates activities within the cell [252]. Collectively, these DNA molecules are termed the transcriptome and are vital interpreting normal function of the cell as well as the development of pathology.

The transcriptome is very complex and encompasses both coding and non-coding RNA. Messenger RNA (mRNA) was previously the most studied form of RNA species as it was the intermediate between genes and proteins. In more recent times, a diverse group of noncoding RNA (ncRNA) were discovered to be functional. In addition to ribosomal RNA (rRNA) and transfer RNA (tRNA) which are involved in protein translation and small nuclear RNA (snRNA) involved in splicing, novel classes of RNA including microRNA (miRNA) and piwi-interacting RNA (piRNA) are both involved with gene regulation at the posttranscriptional level [253].

1.9.2 - Process of lytic damage in aseptic loosening and PJIs

Aseptic loosening of THA and TKA are slow processes that take years to develop and is driven by chronic, low-grade inflammation caused by biomaterial wear debris at the implant bearing surface and/or the interfaces between the bone, bone cement and the implant surface [254, 255]. The molecular mechanisms surrounding aseptic loosening of prosthetic implants because of the interactions between the innate immune system and PMMA, ultra-high molecular weight polyethylene (UHMWPE) and metal debris is well documented. Macrophages are the key mediators in this indolent form of chronic inflammation and are activated by PMMA and UHMWPE to secrete proinflammatory cytokines to recruit other macrophages, promote osteoclastogenesis and inhibition of osteoblast function [256]. Macrophages are activated by debris particles by way of TLR, in particular TLR2, TLR2/1 dimers as well as TLR4 to activate proinflammatory signaling [257].

Periprosthetic tissue obtained from intra-operative samples with aseptic loosening have demonstrated the upregulation of macrophage mediators such as iNOS, TNF-α, IL-1β, IL-6, PGE-2, IL-8 and CCL3, via immunohistochemical staining [258]. Traditionally, aseptic loosening has been defined as osteolysis in the absence of microbial involvement, but this distinction is becoming questionable as it is becoming clear that bacterial components are detected in some seemingly aseptic samples [259, 260]. Pajarinen et al analyzed the histological and immunohistochemical differences between aseptic loosening and septic loosening and found that in aseptic loosening, large infiltrates of CD68-positive and CD163-positive monocytes/macrophages, foreign body giant cells as well as some scattered CD3-positive T-cells and HSP47-positive fibroblasts with very few CD2-positive B-lymphocytes and CD138-positive plasma cells. In contrast to this, synovial membrane samples from septic loosening samples were more heterogeneous with large numbers of CD68-positive and CD163-positive

monocytes/macrophages, neutrophil infiltrates as well as high numbers of CD3-positive T-lymphocytes and CD20-positive B-lymphocytes. Septic loosening is different from aseptic loosening in several aspects: TLR immunoreactive neutrophils play a prominent role septic loosening whereas these cells are less common in aseptic loosening, more plasma cells were present in peri-implant tissue in septic loosening indicating lymphocyte activation and production of antibodies, and TLR-positive lymphocytes seem to play a role in septic loosening whereas such cells are relatively few in aseptic loosening [261]. Bacteria can stimulate an upregulation of RANKL expression in PMNs, as well as producing a large panel of cytokines and chemokines which contributes to a pro-inflammatory environment leading to the activation of OCs [262].

Dapunt et al compared the expression, by way of RNA expression, of cathepsin K, MMP1, MMP9, CXCL8 (IL-8), IL-1β, receptor activator of NfκB (RANK), its ligand (RANKL), TNFα, CXCL2 [macrophage inflammatory protein (MIP)-2α], CCL2 (monocyte chemoattractant protein MCP-1), myeloid related protein (MRP)-14 (S100A9) and CXCL10 [interferon gamma induced protein (IP)-10)] in periprosthetic tissue in cases of aseptic loosening and PJIs, as these genes are involved in the process of osteoclast induction, promotion of the proinflammatory cascade and activation of monocytes and T-cells. The group found that cathepsin K was upregulated in areas of osteolysis in both the aseptic and infected groups, but the infected group had significantly higher expression of CXCL8 compared to the aseptic group (>10-20 times). The induction of CXCL8 is two-fold: it is a direct inducer of OC generation, but it also acts as a chemokine to attract monocytes to further promote OC generation.

Chapter 2: Project aim and significance

2.0 - Clinical relevance

Infections of implants, in particular prosthetic joint infections, are a major cause for morbidity and mortality in the field of orthopaedic surgery, as well as a significant economic burden. We propose to investigate the antibacterial effects of the novel biomaterial Ag-$SrPO_4$-Mg. We hypothesize that this novel compound will inhibit proliferation of common Gram-positive and Gram-negative organisms implicated in PJIs including *S.aureus*, *S.epidermidis*, *E.coli* and *P.aeruginosa*. In addition, an additional benefit for this compound to display osseointegration and promote OB proliferation and differentiation will make it a promising option for use in future orthopaedic implants.

2.1 - Research questions

- Will Ag-$SrPO_4$-Mg reduce bacterial adhesion and biofilm formation of *S.aureus*, *S.epidermidis*, *E.coli* and *P.aeruginosa* compared to the stainless-steel control?
- Will Ag-$SrPO_4$-Mg inhibit Gram-negative bacteria (*E.coli*, *P.aeruginosa)* to a greater extent than Gram-positive bacteria (*S.aureus*, *S.epidermidis*)?
- Will Ag-$SrPO_4$-Mg display biocompatibility to OBs? Does the benefit of biofilm inhibition outweigh the harm of cytotoxicity and therefore is the use of Ag-$SrPO_4$-Mg in orthopaedic implants justified?
- Which genes in the inflammatory pathway are activated in the synovial and capsular tissue during a PJI?

2.2 – Aims

Our aims for this project were:

- To test the antibacterial properties of Ag-$SrPO_4$-Mg extracts in reducing bacterial adhesion and biofilm formation against the Gram positive strains *S.aureus* and *S.epidermidis.*
- To test the antibacterial properties of Ag-$SrPO_4$-Mg extracts in reducing bacterial adhesion and biofilm formation against the Gram negative strains *E.coli* and *P.aeruginosa*.
- To compare if Ag-$SrPO_4$-Mg extracts inhibit Gram negative strains, namely *E.coli* and *P.aeruginosa*, to a greater extent than Gram positive strains, namely *S.aureus* and *S.epidermidis.*
- To assess the biocompatibility of Ag-$SrPO_4$-Mg extracts on human OBs and to ascertain if the benefit of any antibacterial effect of the extract is not offset by potential cytotoxicity on human OBs.

- To understand the cellular and molecular mechanisms in response to PJIs, and differences in patients' genetic makeup in inflammatory and infection pathways in responding to implant materials by investigating patients' synovial and capsular tissue during a PJI.

2.3 – Hypotheses

We hypothesize that Ag-$SrPO_4$-Mg will inhibit bacterial adhesion and biofilm formation compared to stainless steel for all 4 strains of bacteria and inhibit the Gram-negative strains to a greater extent than Gram-positive strains. We also hypothesize that Ag-$SrPO_4$-Mg will be biocompatible to OB and that genes of the pro-inflammatory pathway will be upregulated culminating in the activation of osteoclasts.

Chapter 3: Materials and methods

3.1 - Ethics approval

Ethics was obtained from Australian Capital Territory (ACT) Health in conjunction with the Australian National University (ANU) titled 'Proposed collection and storage of operative tissue samples for research purposes be considered a part of normal clinical practice in the ACT', reference number ETH.9.07.865. This ethics application enabled the collection of tissue considered to be operative waste, tissue that would otherwise be discarded, for the purposes of research and therefore does not pose any risks to the patients in addition to the standard operative and anesthetic risks. Patients are informed at the time of initial contact that refusal to participate will not affect the quality or timing of their care. Patients were initially contacted via phone one week prior to their surgery and then again in person on the day of the operation. Tissue collected included capsular tissue and bone around the hip and knee during both primary and revision arthroplasty (both aseptic revision and infected revision).

3.2 - Materials design and characterization

3.2.1 - Synthesis of Ag-SrPO4-Mg and SrPO4-Mg coated discs

The metal discs used in our experiments were bare stainless steel (316L), Mg, Ag-$SrPO_4$-Mg and $SrPO_4$-Mg coated discs. The Ag-$SrPO_4$-Mg and $SrPO_4$-Mg coated discs were designed and synthesized in conjunction with our collaborators at the RMIT University, Melbourne, Australia.

High purity Mg ingots (>99.9%, Fe ≤ 40 ppm) were supplied by August Metal and Alloy Co. (AMAC), Victoria, Australia. Square Mg disc samples of 10 mm in length, 10 mm in width, and 5 mm in thickness were cut from high-purity Mg ingots using electrical discharge machining. The samples were then ground up to a 1200 grit finish using silicon carbide sandpaper to remove surface oxides and contaminants. Surface cleaning was performed in an ultrasonic bath for 5 minutes in acetone and 5 minutes in absolute ethanol at room temperature, followed by drying in cold flow for subsequent $SrPO_4$ coating growth.

Following this, a clear solution containing 0.1 M strontium nitrate, $Sr(NO_3)_2$ and 0.06M ammonium dihydrogen phosphate, $NH_4H_2PO_4$ was prepared for coating growth by dissolving chemicals in deionized water with stirring and pH was adjusted to 3.0 by the addition of nitric acid HNO_3. A one-step conversion coating process was conducted by immersing Mg specimens in the coating solution at 80 ^oC for 5 minutes. Coated Mg samples were removed from the coating bath, rinsed with running distilled water and dried in cold air flow and stored in a desiccator for further sputtering and

characterization. All chemicals were of analytical grade and obtained from Sigma-Aldrich, Sydney, Australia.

Silver nanoparticles were deposited on the $SrPO_4$-coated Mg pieces via radio-frequency magnetron sputtering at the Melbourne Centre for Nanofabrication. A high purity Ag target (99.99%, Ezzi Vision, Australia) was used as the Ag source. Bare and $SrPO_4$ coated Mg square pieces were attached to the stage in the sputtering chamber with double-sided tape to ensure their stability during sputtering. The chamber was vacuumed overnight to reach 3.0×10^{-7} torr prior to sputtering. Argon (Ar) gas (99.99% pure) was purged into the chamber with a flow rate of 20 sccm during the sputtering process. 100W DC power was used to generate plasma and lasted for 10 minutes. A constant distance of 12 cm between the Mg specimens and Ag target was set and the temperature of the stage was set as 17 ^{o}C during the entire deposition process. The samples were removed from the chamber with care and stored in a portable vacuum container for transfer to the laboratory for subsequent characterization.

3.2.2 - Ag-SrPO4-Mg characterization

The surface morphologies and chemical compositions of the Ag-$SrPO_4$-Mg and $SrPO_4$-Mg disc samples before and after immersion in α-MEM for 24 hours were analysed using scanning electron microscopy coupled with energy dispersive X-ray spectroscopy (SEM-EDS).

3.2.3 - Reagent, assay, and instrument information

Reagents

- Brain-heart infusion broth (BHI) for culture of bacteria: Thermo Fisher Scientific, Australia.
- Oxacillin sodium (200 mg/mL stock) for positive control against Gram-positive bacteria: Sigma-Aldrich, Australia
- Gentamicin sulphate (200 mg/mL stock) for positive control against Gram-negative bacteria: Sigma-Aldrich, Australia
- Glutaraldehyde solution for preparation of samples for SEM: Sigma-Aldrich, Australia
- Sodium cacodylate for fixation of SEM slides: Sigma-Aldrich, Australia
- Osmium tetroxide for fixation of SEM slides: Sigma-Aldrich, Australia
- α-MEM for OB cell culture: Thermo Fisher Scientific, Australia
- Fetal bovine serum (FBS) for OB cell culture: Corning, Australia
- 2% N-2-hydroxyethylpiperazine-N-2-ethane sulfonic acid 20 mM (HEPES) for OB cell culture: Thermo Fisher Scientific, Australia

- Penicillin-streptomycin-neomycin 100 μM (PNS) for OB cell culture: Thermo Fisher Scientific, Australia
- L-ascorbic acid for OB cell culture: Thermo Fisher Scientific, Australia
- TrypLE™ Express Enzyme for dissociating adherent cells and sub-culture: Thermo Fisher Scientific, Australia
- Alizarin red (AR-S) for staining calcium: Sigma-Aldrich, Australia
- Cetylpyridinium chloride (CPC) for extraction of AR-S: Sigma-Aldrich, Australia
- 2% chlorhexidine gluconate and 70% ethanol Surgi-Prep C Pink for surgical skin prep: Joya Medical Supplies, Australia
- TRIzol reagent for RNA extraction: Thermo Fisher Scientific, Australia
- Chloroform for RNA extraction: Sigma-Aldrich, Australia
- Ioban 2 Antimicrobial Incise Drapes for keeping skin in surgical site sterile: 3M, Australia

Bacterial strains

- *Staphylococcus aureus* subsp. *aureus* Rosenbach 29213: American Type Culture Collection (ATCC), USA
- *Staphylococcus epidermidis* (Winslow and Winslow) Evans 12228: ATCC, USA
- *Escherichia coli* (Migula) Castellani and Chalmers 25922: ATCC, USA
- *Pseudomonas aeruginosa* (Schroeter) Migula 27853: ATCC, USA

Human cells and tissues with ethics approval

- Primary human OBs: OBs from patients rev 82, rev 104 and rev 117 between cell passages 2 and 6.
- Hip and knee capsular tissue obtained from time of DAIR or revision surgery.

Assay kits

- LIVE/DEAD BacLight Bacterial Viability Kit for assessing percentage of live bacterial cells post treatment: Thermo Fisher Scientific, Australia
- SensoLyte *p*NPP Alkaline Phosphatase Assay Kit for detecting ALP levels in OB cell cultures: AnaSpec, United States of America (USA)
- RNeasy Mini Kit for RNA isolation: Qiagen, Australia
- RT^2 First Strand Kit for cDNA synthesis: Qiagen, Australia
- RT^2 Profiler PCR array Human Inflammatory Cytokines and Receptors for quantitative PCR of all genes available in PCR array panel against sample DNA: Qiagen, Australia

Laboratory instruments

- Hummer BC-20DC/RF Sputter System for synthesis of Ag-$SrPO_4$-Mg and $SrPO_4$-Mg, Anatech, USA
- DensiCHEK Plus instrument for detecting number of bacteria in suspension, bioMérieux, France

- Bactosonic BS 14.2 ultrasonic bath for ultrasonication of discs: Bandelin, Germany
- Infinite M200 PRO plate reader for detecting fluorescent signal of LIVE/DEAD assay, ALP assay and mineralization assay: Tecan, USA
- Ultra Plus Field Emission Scanning Electron Microscope (FESEM) for visualizing bacterial biofilms on the surface of discs: ZEISS, Australia
- Olympus IX71 fluorescence microscope for visualizing bacteria stained with LIVE/DEAD stain: Olympus Life Science, USA
- Olympus TH4-200 lamp for visualizing bacteria stained with LIVE/DEAD stain: Olympus Life Science, USA
- Ohaus pH Meter Model ST300 for preparation of AR-S solution at pH 4.2: Sigma-Aldrich, Australia
- NanoDrop One microvolume UV-Vis spectrophotometer for detecting concentration of extracted RNA: Thermo Fisher Scientific, Australia
- Centrifuge 5810R for RNA extraction: Eppendorf, Germany
- Centrifuge 5425R for cDNA synthesis: Eppendorf, Germany
- Mastercycler EP Gradient S PCR Thermal Cycler 5345 for cDNA synthesis: Eppendorf, Germany
- 7900HT Fast Real-Time PCR thermal cycler for performing PCR array: Thermo Fisher Scientific, Australia

3.2.4 – Metal extract preparation for cell viability assay

Degradation extracts of test samples, namely pure Mg, Ag-$SrPO_4$-Mg and $SrPO_4$-Mg were prepared by placing the metal discs into 12-well plates and sterilizing the discs with UV for 30 minutes per side. After this, the discs were transferred to a 50 mL centrifuge tubes and submerged in 5 mL of sterile double-distilled water (ddH_2O) for 24 hours, 72 hours, 7 days, and 14 days. At the end of these periods, the supernatant was collected and further sterilized by filtering with a Sterile Millex syringe-driven filter unit prior to use.

3.3 – Antibacterial testing

3.3.1 - Bacterial strains and clinical breakpoints

All bacterial strains were obtained from the Department of Microbiology, ACT Pathology, Canberra Hospital, ACT, Australia. The strains were *Staphylococcus aureus* ATCC 29213, *Staphylococcus epidermidis* ATCC 12228, *Escherichia coli* ATCC 25922 and *Pseudomonas aeruginosa* ATCC 27853.

The two antibiotics used in the positive control samples were oxacillin sodium (200 mg/mL stock) for the Gram-positive bacteria and gentamicin sulphate (200 mg/mL stock) for Gram-negative bacteria.

The positive control samples in the experiment contained the antibiotics at half the minimal inhibitory concentration (MIC), at the MIC and twice the MIC. The MIC for the four strains of bacteria were obtained from the European Committee on Antimicrobial Susceptibility Testing (EUCAST) clinical breakpoints [263]. The MICs for the four strains are shown below in **table 3.1**:

Table 3.1 – Minimal inhibitory concentration of *S.aureus, S.epidermidis, E.coli* and *P.aeruginosa*.

Bacteria	Positive control sample	Oxacillin concentration
Staphylococcus aureus	½ MIC	1 mg/L
	MIC	2 mg/L
	2x MIC	4 mg/L
Staphylococcus epiderimidis	½ MIC	0.125 mg/L
	MIC	0.25 mg/L
	2x MIC	0.50 mg/L

Bacteria	Positive control sample	Gentamicin concentration
Escherichia coli	½ MIC	1 mg/L
	MIC	2 mg/L
	2x MIC	4 mg/L
Pseudomonas aeruginosa	½ MIC	2 mg/L
	MIC	4 mg/L
	2x MIC	8 mg/L

Gram-positive bacteria are tested against oxacillin and Gram-negative bacteria are tested against gentamicin. Concentrations used in experiments were at ½ MIC, MIC and 2x MIC. The MIC values were obtained from the EUCAST clinical breakpoints.

3.3.2 - Bacterial culture

Bacterial colonies were transferred from blood agar plates using cotton swabs and suspended in 5 mL of 0.45% sodium chloride inhalation solution (USP, pH 5) to achieve a concentration of 0.5 McFarland standard. The density of the bacterial suspension was determined using a DensiCHEK Plus instrument. The different test conditions in the experiment were as follows:

- Quality control: stainless steel 316L disc, no bacteria inoculum and no antibiotic, to ensure no contamination of brain-heart infusion broth.
- Negative control: stainless steel 316L disc, bacteria, no antibiotic.
- ½ MIC antibiotic: stainless steel 316L disc, bacteria, and antibiotic at ½ MIC concentration.
- MIC antibiotic: stainless steel 316L disc, bacteria, and antibiotic at MIC concentration.
- 2x MIC: stainless steel 316L disc, bacteria, and antibiotic at 2x MIC concentration.
- Experimental sample 1: Ag-$SrPO_4$-Mg disc, bacteria, no antibiotics.
- Experimental sample 2: $SrPO_4$-Mg disc, bacteria, no antibiotics.

Each test condition was performed in replicates to give a total of 14 individual samples for each experimental set and the antibacterial assays were repeated in triplicates, twice. The metal disc, inoculation of bacteria, volume of BHI and antibiotics in the 14 samples for each of the 4 bacterial strains tested are shown below in **table 3.2.** Samples 1 and 2 were duplicates of the quality control sample with stainless steel 316L discs with no bacteria and no antibiotics. Samples 3 and 4 were duplicates of the negative control. Samples 5 and 6 were duplicates of the ½ MIC antibiotic positive control samples. Samples 7 and 8 were duplicates of the MIC antibiotic positive control samples. Samples 9 and 10 were duplicates of the 2x MIC antibiotic positive control samples. Samples 11 and 12 and samples 13 and 14 were duplicate samples of the Ag-$SrPO_4$-Mg and $SrPO_4$-Mg test samples respectively. All test samples were seeded with approximately 1 x 10^6 CFU/well. Following inoculation, the bacteria were incubated for 24 hours at 37 ^oC and 5% CO_2.

Table 3.2 – Volume of reagents for bacterial viability testing.

Sample	Metal disc	*S.aureus* stock volume (1 x 10^8 CFU/mL) (µL)	BHI volume (µL)	Oxacillin 500 µg/mL stock volume (µL)
1, 2	Nil	0	2000	0
3, 4	Stainless steel 316L	10	1990	0
5, 6	Stainless steel 316L	10	1986	4
7, 8	Stainless steel 316L	10	1982	8
9, 10	Stainless steel 316L	10	1974	16
11, 12	Ag-$SrPO_4$-Mg	10	1990	0
13, 14	$SrPO_4$-Mg	10	1990	0

Sample	Metal disc	*S.epidermidis* stock volume (1 x 10^8 CFU/mL) (µL)	BHI volume (µL)	Oxacillin 50 µg/mL stock volume (µL)
1, 2	Nil	0	2000	0
3, 4	Stainless steel 316L	10	1990	0
5, 6	Stainless steel 316L	10	1985	5
7, 8	Stainless steel 316L	10	1980	10
9, 10	Stainless steel 316L	10	1970	20

11, 12	Ag-$SrPO_4$-Mg	10	1990	0
13, 14	$SrPO_4$-Mg	10	1990	0

Sample	**Metal disc**	***E.coli* stock volume (1×10^8 CFU/mL) (µL)**	**BHI volume (µL)**	**Gentamicin 500 µg/mL stock volume (µL)**
1, 2	Nil	0	2000	0
3, 4	Stainless steel 316L	10	1990	0
5, 6	Stainless steel 316L	10	1986	4
7, 8	Stainless steel 316L	10	1982	8
9, 10	Stainless steel 316L	10	1974	16
11, 12	Ag-$SrPO_4$-Mg	10	1990	0
13, 14	$SrPO_4$-Mg	10	1990	0

Sample	**Metal disc**	***P.aeruginosa* stock volume (1×10^8 CFU/mL) (µL)**	**BHI volume (µL)**	**Gentamicin 500 µg/mL stock volume (µL)**
1, 2	Nil	0	2000	0
3, 4	Stainless steel 316L	10	1990	0
5, 6	Stainless steel 316L	10	1982	8

7, 8	Stainless steel 316L	10	1974	16
9, 10	Stainless steel 316L	10	1958	32
11, 12	Ag-$SrPO_4$-Mg	10	1990	0
13, 14	$SrPO_4$-Mg	10	1990	0

The quality control sample wells contained 2 mL of BHI without bacteria. The negative controls, Ag-$SrPO_4$-Mg and $SrPO_4$-Mg samples contained 1990 µL of BHI while the positive control samples contained the volumes of antibiotic solutions corresponding to ½ MIC, MIC and 2x MIC, in addition to the appropriate volumes of BHI broth such that all wells contained a total of 2 mL.

3.3.3 - Bacterial viability assay using fluorescence labelling

Bacterial cultures were incubated at 37 ^oC and 5% CO_2 for 24 hours as described above. Following this, the plates were removed from the incubator and the BHI broth from each well was aspirated and discarded. Each disc was washed once with 1 mL of sterile phosphate buffered saline (PBS), taking care not to direct the PBS onto the surface of the disc to minimize disruption to the bacteria on the surface of the discs. Each disc was then transferred into a 15 mL Eppendorf conical tube containing 1 mL of PBS and the tubes were ultrasonicated for 5 minutes using a Bandelin Bactosonic ultrasonicator. Following this, the discs were removed, and the remaining 1 mL of bacterial suspension was stained with 3 µL of LIVE/DEAD BacLight Bacterial Viability Kit as per the manufacturer's instructions.

The LIVE/DEAD BacLight Bacterial Viability Kit utilizes a mixture of SYTO 9 green-fluorescent nucleic acid stain and propidium iodide, a red-fluorescent nucleic acid stain. These stains differ in their ability to penetrate healthy bacterial cells as well as their spectral characteristics. When SYTO 9 is used alone, it will stain all cells in the population: those with intact membranes as well as damaged membranes. Propidium iodide penetrates only cells with damaged cell membranes, and this weakens the SYTO 9 signal when both dyes are present. Therefore, when both dyes are used simultaneously, only live bacteria with intact membranes will stain green.

The bacterial suspension stained with the LIVE/DEAD stain were incubated for 10 minutes at room temperature in the dark as per the user's manual and then vortexed for 10 seconds. Two 200 µL aliquots from each sample were pipetted into the wells of a flat black 96-well plate and covered with tin foil to minimize the effect of photo-bleaching. The plate was then inserted into an Infinite M200

PRO plate reader and incubated for a further 10 minutes in the dark. The i-control 1.9 program was utilized with the excitation and emission wavelengths set at 470 nm and 550 nm respectively. The emission intensities were obtained, and these corresponded to the number of live bacteria in the samples.

The intensity reading of the empty wells, representing background signal, were averaged and deducted from the readings of the 14 test samples. The quality control signal intensities, containing PBS without bacteria, were then averaged, and subtracted from the remaining 12 test samples containing bacteria.

The average intensity readings of the negative control duplicates containing only stainless steel 316L and no antibiotics were used in the following equation to derive the percentage growth inhibition of all test samples:

$$\textbf{Percentage growth inhibition (\%)} = 1 - \left(\frac{\textbf{Test sample intensity reading}}{\textbf{Negative control intensity reading}} \right) \textbf{ x 100}$$

The percentage growth inhibition values of the duplicates for each test condition were averaged and expressed graphically using GraphPad Prism 7.

3.3.4 - Bacterial viability assay using confocal fluorescence microscopy

Bacterial culture was performed as described in section 3.3.2. After 24 hours of incubation, the plates were removed from the incubator and the BHI broth was aspirated from the wells. The discs were washed once with 1 mL of sterile PBS, taking care not to disrupt the bacteria on the surface. Each disc was then transferred into a 15 mL tube containing 1 mL of PBS and ultrasonciated for 5 minutes using BactoSonic ultrasonicator. The 1 mL of bacterial suspension was then stained with 3 µL of LIVE/DEAD dye. After an incubation period of 10 minutes in the dark, the solution was vortexed and 7 µL of each sample was loaded onto a 25.4 x 76.2 mm microscope slide with a 22 x 50 mm coverslip and sealed with nail polish. The slides were then viewed under a confocal fluorescence microscope on filter 6 (Alexa 888) using the DP controller program. The slides were shielded from light during transfers to prevent photo-bleaching.

3.3.5 - Visualization of bacterial biofilm using scanning electron microscopy

Bacterial culture was repeated as per section 3.3.2. After 24 hours of incubation, the plates were removed from the incubator. The BHI broth was aspirated from the wells and discarded. Each disc was washed once with 1 mL of sterile PBS, taking care not to direct the PBS onto the bacteria to

minimize disruption of attachment. The PBS was then aspirated, and the discs were transferred into a new 12-well cell culture plate and prepared for scanning electron microscopy (SEM). The discs were fixed with 2% glutaraldehyde in 0.1 M sodium cacodylate buffer for 2 hours at room temperature. The following steps of sample preparation were performed by the Centre of Advanced Microscopy (CAM), Australian National University (ANU). The discs were washed 3 times with 0.1 M cacodylate buffer then fixed with 1% osmium tetroxide for 1 hour. Subsequently, the samples were washed 3 times with distilled water followed by serial dehydration with 10%, 50%, 70% and 90% ethanol and then 3 times with 100% ethanol. Following this, the samples were dehydrated by the critical point dryer and gold-coated (coating approximately 20 nm thick with 15 mA for 2 minutes). The discs were then viewed using FESEM at 500x, 2000x, 10000x and 30000x magnification and the density of the bacterial biofilms on the surface of the discs was noted.

3.4 – Osteoblast cytotoxicity testing

3.4.1 - Isolation and culture of human primary OB cells from trabecular bone

Human OBs were obtained from femoral heads collected at the time of elective primary THA (ACT Health Ethics Approval ID: ETH 9.07.865). All steps described were carried out in a laminar tissue culture hood. The surface of the femoral head cut by the surgical saw at the time of operation was not utilized due to thermal necrosis of the underlying tissue was excised using a bony curette. Small bone chips 1-2 mm in size were then excised using a scalpel blade and scissors. The bone chips were washed 5 times with sterile PBS and transferred into a sterile 50 mL centrifuge tube and vortexed to remove contaminating red blood and fat. Following this, 8-10 pieces of bone chips were transferred into a T75 tissue culture flask containing 20 mL of OB media containing α-MEM supplemented by 10% fetal bovine serum (FBS), 2% N-2-hydroxyethylpiperazine-N-2-ethane sulfonic acid 20 mM (HEPES), 1% penicillin-streptomycin-neomycin 100 μM (PSN) and 1% L-ascorbic acid. The flask was then placed in a tissue culture incubator with 5% CO_2 at 37 ^oC for 1 week. Following one week of incubation, the culture media was removed, and fresh media added without disrupting the bone chips. The flask was viewed under the microscope to visualize OB cells in the flask and cell culture media was changed every 48 hours until the cells reached 80-90% confluence.

3.4.2 - Culture of OB cells from trabecular bone

The OBs were grown and in T75 flasks in 20 mL of cell culture media containing α-MEM, 10% FBS, 2% HEPES buffer (20 mM), 1% L-ascorbic acid (100 μM) and 1% PSN and incubated at 37 ^0C in a humidified atmosphere containing 5% CO_2. Cell media was changed every 48 hours until the cells were 80-90% confluent. At 80-90% confluence, the cells were washed with 10 mL and 5 mL of

recombinant enzyme TrypLE™ Express Enzyme was added to detach the cells and placed in the cell incubator for 5 minutes until the cells were completely detached under the microscope and then used for either subculture or seeding of OB cells for experiments.

For ALP assays and mineralization assays, after the OB cells have been detached with TrypLE™ and incubated for 5 minutes, the cells were suspended using a pipette and 5 mL of OB cell culture media was added to neutralize the TrypLE™. The cell suspension was then transferred to a 50 mL centrifuge tube and centrifuged at 1200 rpm at 4 °C for 6 minutes. The supernatant was then aspirated, and the resulting cell pellet was resuspended in 3 mL of OB cell culture media by pipetting. To further break up any cell clusters to create a fine cell suspension, the cell suspension was passed through a 10 mL syringe with a 21-gauge needle 5-6 times. Fifty microliters of this cell suspension were added to 50 µL of 0.2% trypan blue and the concentration of the OBs in suspension was determined by a haemocytometer and a cell counter and OBs were seeded at a concentration of 4000 cells/cm^2. Primary osteoblasts from patients with patient IDs rev 82, rev 104 and rev 117 between cell passages 2-6 were used for subsequent experiments. Osteoblasts from these patients were collected by other members of our research group (R.W Li, D.H Zhang) for other OB experiments unrelated to this project.

3.4.3 - OB alkaline phosphatase assay

Primary human OBs were cultured in T75 flasks until 80-90% confluent and then seeded into T25 flasks at 4000 cells/cm^2 or 100000 cells per flask in 5 mL of OB media. Culture media was changed every 48 hours. Treatment was first added on day 3 and then on day 9. Treatment comprised of pure Mg extract, Ag-$SrPO_4$-Mg and $SrPO_4$-Mg at concentrations of 0.1 µL/mL, 1 µL/mL and 10 µL/mL or PBS as the negative control. The ALP assay was performed on day 11 using the SensoLyte *p*NPP Alkaline Phosphatase Assay Kit as per the manufacturer's instructions. Reactants provided in the kit include para-Nitrophenylphosphate (*p*NPP) colorimetric alkaline phosphate substrate, 10x assay buffer, stop solution, triton X-100 and alkaline phosphate standard. The 10x assay buffer is diluted to a working 1x assay buffer by dilution with double distilled water (ddH_2O). Lysis buffer was made by adding 20 µL of triton X-100 to 10 mL of 1x assay buffer and the ALP standard was serially diluted in 1x assay buffer to achieve concentrations of 100, 50, 25, 12.5, 6.2, 3.1 and 0 ng/mL.

The culture media was aspirated, and the cells were washed twice with 1x wash buffer. The cells were then lysed by adding 2 mL of the triton X-100 lysis buffer. The cells were scraped off the flask using a cell scraper and transferred to a 15 mL centrifuge tube and incubated at 4 °C for 10 minutes under gentle agitation and subsequently centrifuged at 4 °C, 2500 *g* for 10 minutes. Following this, 1.5 mL of the supernatant from each tube was pipetted in triplicates of 50 µL into the wells of a clear 96-well

plate, along with the ALP standards also in triplicates and volume of 50 μL of the *p*NPP substrate was then added to each well. The plate was shaken for 30 seconds then incubated at room temperature for 45 minutes covered by tin foil to prevent photobleaching. Following the incubation period, 50 μL of stop solution was added to each well. The plate was placed on a plate shaker again for one minute before absorbance was measured at a wavelength of 405 nm using the Infinite M200 PRO plate reader and i-control 1.9 program.

3.4.4 - OB mineralization assay

In preparation for the assay, 40 mM AR-S solution was made by dissolving alizarin red (AR-S) in ddH_2O and adjusting the pH to 4.2, as determined by a pH meter. Sodium phosphate buffer was made by adding equal volumes of Na_2HPO_4 solution, pH 9 and NaH_2PO_4 solution, pH 4 and adjusted to a pH of 7.0. Following this, the appropriate amount of cetylpyridinium chloride (CPC) was added to the sodium phosphate buffer of pH 7.0 to make 10% weight/volume (w/v) CPC extraction buffer. An AR-S solution of 1 mM was made by diluting the 40 mM AR-S solution 1 in 40 in 10% w/v CPC extraction buffer and serially diluted in CPC extraction buffer to create AR-S standard solutions of concentrations 333, 111, 37, 12, 0.4 and 0.1 μM.

Primary human OBs were cultured in T75 flasks until 80-90% confluent and then seeded into 6-well culture plates at 4000 cells/cm^2 or 36000 cells per well in 3 mL of OB media. Culture media was changed every 48 hours. Treatment was first added on day 3 and then on days 9 and 15. Treatment comprised of pure Mg extract, Ag-$SrPO_4$-Mg and $SrPO_4$-Mg at concentrations of 0.1 μL/mL, 1 μL/mL and 10 μL/mL or PBS as the negative control, added to the wells in triplicates. Mineralization assay was performed on day 21. The cells were washed once with PBS and fixed by addition of 1 mL/well of ice-cold 70% ethanol and incubated at 4 ºC for a minimum of 1 hour. Following this, the cells were washed once with ddH_2O before adding 1 mL/well of 40 mM pH 4.2 AR-S solution for 10 minutes at room temperature on a rocking platform. The cultures were then washed 5 times with ddH_2O and then once with PBS while on a rocking platform for 15 minutes. After this wash, photographs of the plates were taken and 1 mL/well of CPC extraction buffer was added and reacted at room temperature for 15 minutes. The CPC buffer from each well containing the extracted AR-S was pipetted into the wells of a clear 96-well plate and the AR-S concentration was determined by absorbance measurement at 562 nm using the Infinite M200 PRO plate reader and i-control 1.9 program.

3.5 - Patient capsular tissue response to periprosthetic joint infections

3.5.1 - Patient selection and recruitment

Eligible patients undergoing primary arthroplasty at Calvary John James Hospital, Deakin, ACT, 2600, Australia and patients with PJIs undergoing DAIR/revision surgery at The Canberra Hospital, Garran, ACT, 2605, Australia were recruited to the study. All patients were over the age of 18 and were recruited after obtaining informed consent by the primary researcher (J Cheng). Patients with PJIs undergoing DAIR/revision arthroplasty were selected based on clinical signs (erythema, swelling, pain, discharge), radiological findings (such as joint effusions) as well as serological/microbiological markers based on the MSIS criteria score over 6 for minor criteria or the presence of a major criteria (same bacteria isolated on two or more joint fluid aspirates or presence of sinus) and informed patient consent was obtained once the decision was made by the surgeon to proceed with surgical intervention. Patients undergoing primary arthroplasty were recruited as controls and were contacted via phone approximately one week prior to their scheduled surgery to obtain phone consent and then again on the morning of the surgery for written consent. Control patients were selected based on their age, gender, and profile of their medical conditions to match those in the PJI cohort. Patients undergoing TKA and THA only were recruited due to the greater incidence of these surgeries compared to primary arthroplasty of other joints. All patients were given a patient information sheet, at the time of consent, outlining the nature of the research as well as a project donor questionnaire to screen for exclusion criteria. Exclusion criteria for patients included:

- Positive for blood-borne viruses, including hepatitis B virus (HBV), hepatitis C virus (HCV) and human immunodeficiency virus (HIV) due to risk to researchers during handling of tissue.
- Cancer treatment, including chemotherapy, radiotherapy and immunotherapy.
- Long term corticosteroids and anabolic steroids.
- Avascular necrosis (AVN) of bone in region of interest.
- Autoimmune disorders including but not limited to rheumatoid arthritis, systemic lupus erythematosus (SLE), seronegative spondyloarthropathies, scleroderma, inflammatory bowel disease (IBD).
- Metabolic bone diseases including but not limited to Paget's disease, osteopetrosis.
- Refusal to give consent.

All documentation containing patient signatures and confidential patient information are stored in a secure, designated locked filing cabinet at the John Curtin School of Medical Research accessible only to those directly involved in the project. Patient information was also stored on an electronic database whereby patient names were de-identified and coded with only the date of birth and unit

record number visible. The electronic database was stored on a secure JCSMR computer protected by a password that only those directly involved in the project can access.

3.5.2 - Surgical procedure and collection of tissue

All surgeries were undertaken in laminar flow operating theatres. All personnel in the operating theatre wore the appropriate sterile theatre attire including sterile surgical gown, sterile gloves, face shield and surgical balaclava. All patients undergoing surgery of the hip were in a lateral position with the standard posterior approach to the hip; those undergoing knee surgery were positioned supine with bolsters and a tourniquet inflated to 300 mmHg with the standard medial parapatellar approach to the knee. The skin over the surgical site was prepped with 2% chlorhexidine gluconate and 70% ethanol Surgi-Prep C Pink and covered with antimicrobial incise drapes. A prophylactic dose of antibiotic (Cephazolin, 2g) was given intravenous within 30 minutes of the skin incision for primary arthroplasty patients and withheld for PJI patients, unless already commenced on antibiotic treatment after identification of the infecting organism from joint aspiration. The skin incision was made with a scalpel and further dissection made with either the scalpel or electrocautery knife at the surgeon's discretion. The scalpel was used for the capsulotomy and extraction of capsular tissue and synovial tissue to prevent thermal necrosis of the tissue sample. The capsular tissue was then placed in a sterile container and taken immediately for further processing and mRNA isolation.

3.5.3 - Tissue processing

The preparation of the capsular tissue was carried out in a laminar flow cabinet using sterile technique. The tissue was sectioned into pieces less than 1 mm in diameter with a scalpel, fast frozen with liquid nitrogen and then ground into a fine powder using a sterile porcelain mortar and pestle. This tissue was then transferred into a sterile 1.5 mL Eppendorf tube to which 1 mL of TRIzol reagent was added and incubated at room temperature for 10 minutes. Any tissue contaminated by touch or surrounding equipment was discarded. All excess tissue was transferred into cryovials, fast frozen in liquid nitrogen and stored in a -80 ^{o}C freezer.

3.5.4 - mRNA isolation

TRIzol reagent was added to the pulverized capsular tissue and incubated for 10 minutes. After this, 200 μL of chloroform was added and the tube was shaken vigorously for 15 seconds. The tube was then rested at room temperature for 3 minutes before being centrifuged at 12,000 relative centrifugal force (RCF or *g*) for 15 minutes at 4 ^{o}C. Following this, the colorless aqueous layer, usually 500 μL,

was transferred to another sterile 1.5 mL tube, to which an equal volume of 70% ethanol was added, and the tube was shaken vigorously by hand and 700 µL of the resultant mixture is transferred to a RNeasy mini spin column, in a 2 mL collection tube. mRNA was then extracted from this solution using the RNeasy Mini Kit according to the manufacturer's instructions. The spin column was centrifuged at 8500 *g* at room temperature for 15 seconds and the flow through was discarded. If sample volume exceeded 700 µL, successive aliquots were centrifuged in the same RNeasy spin column. Three hundred and fifty microlitres of Buffer RW1 was then added to the column and centrifuged again (8500 *g*, 15 seconds) and the flow through discarded. Eighty microlitres of DNaseI solution, containing 10 µL of DNAse I stock solution and 70 µL of Buffer RDD, were added onto the spin column silica gel membrane and incubated at room temperature for 15 minutes. Following this, 350 µL of Buffer RW1 was added onto the column and centrifuged at 8500 *g* for 15 seconds and the flow through discarded. The spin column was then placed into a new collection tube and 500 µL of Buffer RPE was added to the column and centrifuged again as before. A second wash with 500 µL of Buffer RPE was performed and spun at 8500 *g* for 2 minutes. The spin column was then spun again at 8500 *g* for 2 minutes to dry the membrane. The spin column was then placed into a new 1.5 mL tube and 50 µL of RNase-free water was added to the membrane and incubated at room temperature for 1 minute, before centrifuging at 8500 *g* for 1 minute.

3.5.5 - Measurement of mRNA quality and quantity assessment

The quantity and quality of the isolated mRNA was assessed using the NanoDrop One microvolume UV-Vis spectrophotometer. The platform was cleaned with nuclease-free water and 1 µL of nuclease-free water was loaded to 'blank' the spectrophotometer. Following this, 1 µL of the mRNA sample was loaded. The concentration of the mRNA sample was expressed as ng/µL and the quality of the mRNA was expressed as A260/A280 and A260/A230 ratios. Only mRNA with an A260/A280 ratio greater than 2 and an A260/230 ratio greater than 1.8 were deemed to be good quality and utilized for cDNA synthesis and PCR array.

3.5.6 - cDNA synthesis

The patient mRNA samples from step 3.5.5 of good quality were used. A total of 1 µg of mRNA per patient was used for cDNA synthesis using the RT^2 First Strand Kit as per the manufacturer's instructions. The genomic DNA elimination mix was prepared by adding 2 µL of Buffer GE, a volume of mRNA containing 1 µg of mRNA and a volume of RNase-free water such that the total volume of was 10 µL. This genomic DNA elimination mix placed in a PCR Thermal Cycler was incubated at 42 ^{o}C for 5 minutes and then at 4 ^{o}C for at least one minute. Following this, a 10 µL of

reverse-transcription mix containing 4 µL of 5x buffer BC3, 3 µL RNase-free water, 2 µL of RE3 reverse transcriptase mix and 1 µL of control P2, was added to the genomic DNA elimination mix and incubated at 42 ºC for 15 minutes followed by 95 ºC for 5 minutes. The cDNA samples were then stored at -80 ºC until further use for PCR array.

3.5.7 - RT Profiler PCR Array on human inflammatory cytokine pathway

The cDNA was thawed and 91 µL of nuclease-free water was added to each cDNA sample. The PCR component was then prepared by adding 650 µL of 2x RT^2 SYBR Green Mastermix, 548 µL of nuclease-free water and 102 µL of the cDNA sample per patient and the solution mixed thoroughly by pipetting up and down. This was then loaded into a reservoir and a multi-channel pipette used to load 10 µL of the PCR mix into each well of a 384-well plate (4x96, format E) plate of the RT^2 Profiler PCR array Human Inflammatory Cytokines and Receptors. The full panel of genes included in this PCR array is shown in **table 3.3** below. Each 384-well plate was used for the cDNA of 4 patients. The plate was then centrifuged at 277 *g* for 2 minutes before being loaded into a 7900HT Fast Real-Time PCR thermal cycler using the SDSv4 program. The thermal cycler program was set as per the manufacturer's instructions to include 1 cycle at 95 ºC lasting 10 minutes and 40 cycles consisting of 95 ºC for 15 seconds and 60 ºC for 1 minute. The data was exported from the program and transferred onto an Excel spreadsheet and uploaded to the Qiagen GeneGlobe website for analysis. The expression of genes was normalized to the housekeeping glyceraldehyde 3-phosphate dehydrogenase (GAPDH) gene. An absolute threshold of 1.5-fold was applied to exclude background noise. Relative mRNA expression was determined using the $2^{-\Delta\Delta Ct}$ method in the Qiagen data analysis portal (http://www.qiagen.com/geneglobe). Results were expressed relative to the control group. RNA samples with threshold cycle (Ct) values that were deemed as outliers were excluded and data analysis was performed again for each gene without outliers.

Table 3.3 – Panel of genes found in the Qiagen human inflammatory cytokines and receptors RT^2 Profiler^{TM} PCR array.

Gene symbol	Name	Description/function of encoded gene
AIMP1	Aminoacyl tRNA synthetase complex-interacting multifunctional protein 1	Cytokine induced by apoptosis and is involved in the regulation of angiogenesis, inflammation, and wound healing.
BMP2	Bone morphogenetic protein 2	Involved in morphogenesis of bone and cartilage.
C5	Complement component 5	Component of the complement system, a part of the innate immune system in inflammation, host homeostasis, and host defense against pathogens.
CCL1	Chemokine (C-C motif) ligand 1	Secreted by activated T-cells and displays chemotactic activity for monocytes but not neutrophils.
CCL11	Chemokine (C-C motif) ligand 11	Displays chemotactic activity for eosinophils, but not mononuclear cells or neutrophils.
CCL13	Chemokine (C-C motif) ligand 13	Displays chemotactic activity for monocytes, lymphocytes, basophils and eosinophils, but not neutrophils.
CCL15	Chemokine (C-C motif) ligand 15	Chemotactic for T cells and monocytes, and acts through C-C chemokine receptor type 1.
CCL16	Chemokine (C-C motif) ligand 16	Displays chemotactic activity for lymphocytes and monocytes but not for neutrophils.
CCL17	Chemokine (C-C motif) ligand 17	Displays chemotactic activity for T lymphocytes, but not monocytes or granulocytes.
CCL2	Chemokine (C-C motif) ligand 2	Displays chemotactic activity for monocytes and basophils but not for neutrophils or eosinophils.
CCL20	Chemokine (C-C motif) ligand 20	Displays chemotactic activity for lymphocytes and can repress proliferation of myeloid progenitors.
CCL22	Chemokine (C-C motif) ligand 22	Displays chemotactic activity for monocytes, dendritic cells, natural killer cells and for chronically activated T lymphocytes.
CCL23	Chemokine (C-C motif) ligand 23	Displays chemotactic activity on resting T lymphocytes and monocytes, lower activity on neutrophils and no activity on activated T lymphocytes.
CCL24	Chemokine (C-C motif) ligand 24	Displays chemotactic activity on resting T lymphocytes, a minimal activity on neutrophils, and is negative on monocytes and activated T lymphocytes.

CCL26	Chemokine (C-C motif) ligand 26	Displays chemotactic activity for normal peripheral blood eosinophils and basophils and has antimicrobial activity against *S.pneumoniae*, *S.aureus*, non-typeable *H.influenzae* and *P.aeruginosa*.
CCL3	Chemokine (C-C motif) ligand 3	Also known as macrophage inflammatory protein 1 alpha, plays a role in inflammatory responses through binding to the receptors CCR1, CCR4 and CCR5.
CCL4	Chemokine (C-C motif) ligand 4	Mitogen-inducible monokine and is one of the major HIV-suppressive factors produced by CD8+ T-cells. The encoded protein is secreted and has chemokinetic and inflammatory functions.
CCL5	Chemokine (C-C motif) ligand 5	Chemoattractant for blood monocytes, memory T helper cells and eosinophils. It causes the release of histamine from basophils and activates eosinophils.
CCL7	Chemokine (C-C motif) ligand 7	Attracts macrophages during inflammation and metastasis.
CCL8	Chemokine (C-C motif) ligand 8	Chemotactic activity for monocytes, lymphocytes, basophils and eosinophils.
CCR1	Chemokine (C-C motif) receptor 1	Member of the beta chemokine receptor family. Ligands include macrophage inflammatory protein 1 alpha (MPIF-1), regulated on activation normal T expressed and secreted protein (RANTES), monocyte chemoattractant protein 3 (MCP-3) and myeloid progenitor inhibitory factor-1 (MPIF-1). Mediates signal transduction and recruitment of effector immune cells to site of inflammation.
CCR2	Chemokine (C-C motif) receptor 2	Receptor for monocyte chemoattractant protein-1, a chemokine which specifically mediates monocyte chemotaxis.
CCR3	Chemokine (C-C motif) receptor 3	Receptor may contribute to the accumulation and activation of eosinophils and other inflammatory cells in the allergic airway
CCR4	Chemokine (C-C motif) receptor 4	Receptor for the CC chemokine - MIP-1, RANTES, TARC and MCP-1. Belongs to G-protein coupled receptor family.
CCR5	Chemokine (C-C motif) receptor 5	Member of beta chemokine receptor family and expressed by T cells and macrophages. Known to be an important co-receptor for macrophage-tropic virus, including HIV, to enter host cells.
CCR6	Chemokine (C-C motif) receptor 6	Expressed by immature dendritic cells and memory T cells, has been shown to be important for B-lineage maturation and antigen-driven B-cell differentiation, and may regulate the migration and

		recruitment of dendritic and T cells during inflammatory and immunological responses.
CCR8	Chemokine (C-C motif) receptor 8	Regulation of monocyte chemotaxis and thymic cell apoptosis and may contribute to the proper positioning of activated T cells within the antigenic challenge sites and specialized areas of lymphoid tissues.
CD40LG	CD40 ligand	Expressed on the surface of T cells to regulate B cell function by engaging CD40 on the B cell surface.
CSF1	Colony stimulating factor 1 (macrophage)	Cytokine that controls the production, differentiation, and function of macrophages.
CSF2	Colony stimulating factor 2 (granulocyte-macrophage)	Cytokine that controls production, differentiation, and function of granulocytes and macrophages.
CSF3	Colony stimulating factor 3 (granulocyte)	Cytokine that controls the production, differentiation, and function of granulocytes.
CX3CL1	Chemokine (C-X3-C motif) ligand 1	Plays a role in a wide range of diseases, including cancer, vasculitis, neuropathies, atherosclerosis, inflammatory diseases, and in human immunodeficiency virus infections
CX3CR1	Chemokine (C-X3-C motif) receptor 1	Receptor for fractalkine, a transmembrane protein and chemokine involved in the adhesion and migration of leukocytes.
CXCL1	Chemokine (C-X-C motif) ligand 1 (melanoma growth stimulating activity, alpha)	Plays a role in inflammation and as a chemoattractant for neutrophils.
CXCL10	Chemokine (C-X-C motif) ligand 10	Chemokine of the CXC subfamily and ligand for receptor CXCR3 and binding results in stimulation of monocytes, natural killer and T-cell migration, and modulation of adhesion molecule expression.
CXCL11	Chemokine (C-X-C motif) ligand 11	Induces a chemotactic response in activated T-cells and is the dominant ligand for CXC receptor-3.
CXCL12	Chemokine (C-X-C motif) ligand 12	This antimicrobial gene encodes a stromal cell-derived alpha chemokine. Plays a role in many diverse cellular functions, including embryogenesis, immune surveillance, inflammation response, tissue homeostasis, and tumor growth and metastasis.
CXCL13	Chemokine (C-X-C motif) ligand 13	B lymphocyte chemoattractant and preferentially promotes migration of B lymphocytes over T cells and macrophages.

CXCL2	Chemokine (C-X-C motif) ligand 2	This chemokine is expressed at sites of inflammation and may suppress hematopoietic progenitor cell proliferation.
CXCL3	Chemokine (C-X-C motif) ligand 3	This protein plays a role in inflammation and as a chemoattractant for neutrophils.
CXCL5	Chemokine (C-X-C motif) ligand 5	Proposed to recruit neutrophils, to promote angiogenesis and to remodel connective tissues.
CXCL6	Chemokine (C-X-C motif) ligand 6 (granulocyte chemotactic protein 2)	Chemotactic for neutrophil granulocytes and has antibacterial action against gram-negative and gram-positive bacteria.
CXCL9	Chemokine (C-X-C motif) ligand 9	Involved in T cell trafficking, chemoattractant for lymphocytes but not for neutrophils.
CXCR1	Chemokine (C-X-C motif) receptor 1	Binds to IL8 with high affinity, and transduces the signal through a G-protein activated second messenger system.
CXCR2	Chemokine (C-X-C motif) receptor 2	Binds to IL8 with high affinity, and transduces the signal through a G-protein activated second messenger system.
FASLG	Fas ligand (TNF superfamily, member 6)	The primary function of the encoded transmembrane protein is the induction of apoptosis triggered by binding to FAS.
IFNA2	Interferon, alpha 2	Member of the type I interferon family produced in response to viral infection as a key part of the innate immune response with potent antiviral, antiproliferative and immunomodulatory properties
IFNG	Interferon, gamma	Secreted by cells of both the innate and adaptive immune systems. Binds to the interferon gamma receptor which triggers a cellular response to viral and microbial infections.
IL10RA	Interleukin 10 receptor, alpha	Receptor to IL-10 and mediates the immunosuppressive signal of IL-10, and thus inhibits the synthesis of proinflammatory cytokines.
IL10RB	Interleukin 10 receptor, beta	Co-expression of this and IL10RA proteins has been shown to be required for IL10-induced signal transduction.
IL13	Interleukin 13	Produced primarily by activated Th2 cells and is involved in several stages of B-cell maturation and differentiation.
IL15	Interleukin 15	Regulates T and natural killer cell activation and proliferation.
IL16	Interleukin 16	Functions as a chemoattractant, a modulator of T cell activation, and an inhibitor of HIV replication.

IL17A	Interleukin 17A	Proinflammatory cytokine produced by activated T cells, mediates downstream pathways induce the production of inflammatory molecules, chemokines, antimicrobial peptides, and remodeling proteins.
IL17C	Interleukin 17C	Stimulates the release of tumor necrosis factor alpha and interleukin 1 beta from a monocytic cell line.
IL17F	Interleukin 17F	Expressed by activated T cells, stimulates the production of several other cytokines, including IL6, IL8, and CSF2/GM_CSF and induces angiogenesis of endothelial cells.
IL1A	Interleukin 1, alpha	Pleiotropic cytokine involved in various immune responses, inflammatory processes, and hematopoiesis. Produced by monocytes and macrophages as a proprotein, which is proteolytically processed and released in response to cell injury, and thus induces apoptosis.
IL1B	Interleukin 1, beta	Important mediator of the inflammatory response, involved in a variety of cellular activities, including cell proliferation, differentiation, and apoptosis.
IL1R1	Interleukin 1 receptor, type I	Receptor for interleukin-1 alpha, interleukin-1 beta, and interleukin-1 receptor antagonist. Important mediator involved in many cytokine-induced immune and inflammatory responses.
IL1RN	Interleukin 1 receptor antagonist	Inhibits the activities of IL1A and IL1B and modulates a variety of IL-1 related immune and inflammatory responses.
IL21	Interleukin 21	Active in innate and adaptive immune responses by inducing differentiation, proliferation and activity of multiple target cells including macrophages, natural killer cells, B cells and cytotoxic T cells.
IL27	Interleukin 27	A subunit of a heterodimeric cytokine complex to drive the rapid expansion of naïve but not memory CD4 T cells and triggers IFNG production.
IL3	Interleukin 3 (colony-stimulating factor, multiple)	Supports the proliferation of a broad range of hematopoietic cell types and involved in cell growth, differentiation and apoptosis.
IL33	Interleukin 33	Involved in the maturation of Th2 cells and the activation of mast cells, basophils, eosinophils and natural killer cells.
IL5	Interleukin 5 (colony-stimulating factor, eosinophil)	Acts as a growth and differentiation factor for both B cells and eosinophils. Plays a major role in the regulation of eosinophil formation, maturation, recruitment and survival.

IL5RA	Interleukin 5 receptor, alpha	An interleukin 5 specific subunit of a heterodimeric cytokine receptor.
IL7	Interleukin 7	Important for B and T cell development. Essential for lymphoid cell survival and maintenance of naïve and memory T cells.
IL8	Interleukin 8	Functions as a chemotactic factor by guiding the neutrophils to the site of infection.
IL9	Interleukin 9	Regulator of a variety of hematopoietic cells and stimulates cell proliferation and prevents apoptosis.
IL9R	Interleukin 9 receptor	Ligand binding of this receptor leads to the activation of various JAK kinases and STAT proteins, which connect to different biologic responses.
LTA	Lymphotoxin alpha (TNF superfamily, member 1)	Mediates a large variety of inflammatory, immunostimulatory, and antiviral responses, is involved in the formation of secondary lymphoid organs during development and plays a role in apoptosis.
LTB	Lymphotoxin beta (TNF superfamily, member 3)	An inducer of the inflammatory response system and involved in normal development of lymphoid tissue.
MIF	Macrophage migration inhibitory factor (glycosylation-inhibiting factor)	Involved in cell-mediated immunity, immunoregulation, and inflammation.
NAMPT	Nicotinamide phosphoribosyltransferase	Involved in many important biological processes, including metabolism, stress response and aging.
OSM	Oncostatin M	Cytokine and growth regulator that inhibits the proliferation of a number of tumor cell lines.
SPP1	Secreted phosphoprotein 1	Involved in the attachment of OCs to the mineralized bone matrix. The encoded protein is secreted and binds hydroxyapatite with high affinity.
TNF	Tumor necrosis factor	Mainly secreted by macrophages. It can bind to, and thus functions through its receptors TNFRSF1A/TNFR1 and TNFRSF1B/TNFBR. This cytokine is involved in the regulation of a wide spectrum of biological processes including cell proliferation, differentiation, apoptosis, lipid metabolism, and coagulation.
TNFRSF11B	Tumor necrosis factor receptor superfamily, member 11b	This protein is an OB-secreted decoy receptor, osteoprotegerin (OPG) that functions as a negative regulator of bone resorption.

TNFSF10	Tumor necrosis factor (ligand) superfamily, member 10	Belongs to the tumor necrosis factor (TNF) ligand family. Preferentially induces apoptosis in transformed and tumor cells, but does not appear to kill normal cells.
TNFSF11	Tumor necrosis factor (ligand) superfamily, member 11	Encodes ligand for OPG and functions as a key factor for OC differentiation and activation.
TNFSF13	Tumor necrosis factor (ligand) superfamily, member 13	This protein is a ligand for TNFRSF17/BCMA, a member of the TNF receptor family and is important for B cell development.
TNFSF13B	Tumor necrosis factor (ligand) superfamily, member 13b	Expressed in B cell lineage cells, and acts as a potent B cell activator. Plays an important role in the proliferation and differentiation of B cells.
TNFSF4	Tumor necrosis factor (ligand) superfamily, member 4	Functions in T cell antigen-presenting cell (APC) interactions and mediates adhesion of activated T cells to endothelial cells.
VEGFA	Vascular endothelial growth factor A	Induces proliferation and migration of vascular endothelial cells, and is essential for both physiological and pathological angiogenesis.
ACTB (Housekeeping gene)	Actin, beta	Major constituent of the contractile apparatus and one of two non-muscle cytoskeletal actins that are ubiquitously expressed.
B2M (Housekeeping gene)	Beta-2-microglobulin	Antimicrobial protein that displays antibacterial properties in amniotic fluid.
GAPDH (Housekeeping gene)	Glyceraldehyde-3-phosphate dehydrogenase	Catalyzes an important energy-yielding step in carbohydrate metabolism.
HPRT1 (Housekeeping gene)	Hypoxanthine phosphoribosyltransferase 1	Plays a central role in the generation of purine nucleotides through the purine salvage pathway.
RPLP0 (Housekeeping gene)	Ribosomal protein, large, P0	This gene encodes a ribosomal protein that is a component of the 60S subunit.

The PCR array contains 84 genes involved in the inflammatory pathway, as well as 5 housekeeping genes: ACTB, B2M, GAPDH, HPRT1 and RPLP0. The gene symbol, gene name and the function of the protein produced are shown.

3.6 - Statistical analysis

3.6.1 – Measurement of variability

One-way analysis of variance (ANOVA) was used to test if there were any significant differences between sets of means between test groups in an experiment. In all the bioassays of this project, including bacterial viability assay, as well as primary human OB assays such as the ALP assay and mineralization assay, the Kruskhal-Wallis ANOVA on ranks was used to estimate if there was a difference between all groups as the data points did not form a Gaussian distribution and therefore a non-parametric test was needed instead of a standard ANOVA. The difference between any two treatment groups was analyzed using the Mann-Whitney U test. All calculations were performed using GraphPad Prism 9.3.1. Results were presented as mean +/- standard error of the mean (s.e.m). Results were accepted as statistically significant for *p*-values less than 0.05.

3.6.2 – Inter-experimental variability of OB ALP assay and mineralization assay.

The ALP assay was routinely used to check the bioactivity, namely proliferation and maturation, of primary human OBs exposed to various biomaterials in our laboratory with different batches of the ALP assay kit. The variability between the ALP activity of the standard control samples between different batches of ALP assay kits as seen in experiments conducted by other members of the TORU unit and by me were analyzed using ANOVA.

In addition, the standards for the different OB mineralization assays conducted, which corresponded to different Ca concentrations, from which we extrapolated the Ca concentrations of the test samples, were also compared and ANOVA calculated to measure the inter-experimental variability. Differences were accepted as statistically significant for *p*-values less than 0.05.

3.6.3 – Inter-group variability of patient demographics

A total of 12 patients were recruited to this study with 6 in the PJI group and 6 in the control group. Control patients were matched based on age and gender to those in the PJI group to minimize the confounding effect of gender and age on gene expression. The age in the two groups formed Gaussian distribution and we performed student's t-test to ascertain if there were differences in the age and gender between the PJI group and control group, with *p*-values < 0.05 deemed statistically significant.

Chapter 4: Patient Recruitment

4.1 - Patient demographics

A total of 15 patients were recruited to the study after obtaining informed consent between 21/02/21 and 23/07/2021 at Calvary John James Hospital, Deakin, and The Canberra Hospital, Woden, both located in the ACT. The recruitment process had to be discontinued in late August 2021 due to lockdown in the ACT in response to the COVID-19 pandemic. The 7 patients undergoing primary TKA and THA (control group) had their surgeries at the Calvary John James Hospital whereas the 8 patients with PJIs undergoing DAIR and revision arthroplasty all had their surgeries at The Canberra Hospital.

The average age of the entire cohort of patients was 65.8. Four patients were female and 11 were male. Ten of the operations were on the hip and 5 were on the knee.

Three patients of the 15 recruited patients were excluded from the final PCR array analysis: 2 had an unacceptably low yield of RNA from their joint capsule tissue (1 control, 1 PJI) and the third (PJI group) did not have a definitive diagnosis of PJI, with a MSIS score of 5 and no culture positive samples. This left a total of 12 patients, with 6 each in the primary arthroplasty and PJI groups. The average age of the remaining cohort was 67.17 years, with an average age of 66 years in the control group 68.33 years in the PJI group with no statistically significant difference. Of the control group, 2 were female and 4 were male, compared to the PJI group which had 1 female and 5 males, with no statistically significant difference between the groups. The surgical procedures in the control group were 3 TKA and 3 THA. In the PJI group, 1 operation was on the knee (DAIR) and 5 were on the hip (3 DAIR, 2 first stage revision). The patients' age, gender and medical comorbidities are listed in **Table 4.1** below.

4.2 - Microbiology profile

All 6 cases of PJI patients were classified as definitive infections after either fulfilling the major MSIS criteria or scoring more than 6 on minor criteria. All cases yielded positive cultures from tissues isolated at time of surgery. The most common causative organism was *S.aureus* (MSSA), which was identified in 2 cases. The organisms identified in the other 4 cases were *Klebsiella aerogenes, Enterobacter bugandensis, Streptococcus gallolyticus* and *Escherichia coli* (**Table 4.1A)**.

Table 4.1 – Patients recruited in the study.

A

Patient ID	Gender	Age	Group	Infective organism	Medical history
1	Female	63	Control	N/A	Obesity, hypertension (HTN), hypercholesterolaemia, anxiety
2	Female	76	Control	N/A	HTN
3	Male	71	Control	N/A	Aortic stenosis, asthma, gastroesophageal reflux disease (GORD), gout, ischaemic heart disease (IHD), obesity
4	Male	59	Control	N/A	HTN, obesity, OA, obstructive sleep apnea (OSA)
5	Male	73	Control	N/A	Coronary artery bypass graft (CABG), depression, IHD, pacemaker
6	Male	54	Control	N/A	HTN, hypercholesterolaemia
7	Female	65	PJI	*Klebsiella aerogenes*	Depression, GORD, bilateral THA, obesity
8	Male	79	PJI	*Enterobacter bugandensis*	HTN
9	Male	49	PJI	*Staphylococcus aureus*	Benign prostatic hypertrophy (BPH), cerebral palsy, epilepsy, GORD, right subcapital neck of femur (NOF) fracture with fixation December 2020 with failure and conversion to THA (infected side), schizophrenia
10	Male	68	PJI	*Streptococcus gallolyticus*	Atrial fibrillation (AF), HTN, hypercholesterolaemia IHD, peripheral vascular disease (PVD) type 2 diabetes mellitus (T2DM)
11	Male	75	PJI	*Staphylococcus aureus*	GORD, HTN, hypercholesterolaemia, bilateral THA (sampled side revised once for dislocation)

12	Male	74	PJI	*Escherichia coli*	BPH, DVT, HTN, hypercholesterolaemia IHD, T2DM, previous left THA revision for dislocation (sampled side)

B

	Controls	**PJI**	***P*-value**
Age (mean ± s.d)	66 ± 8.67	68.33 ± 10.73	0.69
Gender (male/female)	4/2	5/1	0.20
Procedure (hip/knee)	3/3	5/1	N/A

A. The age, gender, group and past medical history of all recruited patients are listed. In addition, the infective organisms in the PJI group are also listed. **B.** The mean age of the control and PJI groups are expressed as mean age ± standard deviation (s.d). There was no statistically significant difference in age or distribution of gender between the control and PJI groups.

Chapter 5: Antibacterial Effects of Ag-SrPO4-Mg

5.1 - Introduction

Several studies in existing literature support the antibacterial role of AgNPs in solution in the prevention of bacterial attachment and biofilm formation. This chapter will focus on the inhibition of adhesion and proliferation of the bacterial strains *S.aureus, S.epidermidis*, *E.coli* and *P.aeruginosa*. We explored this topic by addressing the following:

1. Visualizing the difference in the number of live bacteria on different test samples using confocal fluorescence microscopy.
2. Evaluation of bacterial viability by fluorescent LIVE/DEAD staining signal.
3. Visualization of the metal disc surfaces, and the layer of bacteria attached using scanning electron microscopy.

5.2 - Detection and characterization of Ag-SrPO4-Mg using SEM

The chemical constituents of the Ag-$SrPO_4$-Mg disc were analyzed using SEM. The surface topography of the Ag-$SrPO_4$-Mg discs used in this study are presented in **Figure 5.1**. The Ag-$SrPO_4$-Mg sample was immersed in α-MEM culture media for 24 hours and detection of the chemical constituents using electron microscope were analyzed using Energy Dispersive X-ray Spectroscopy, as shown in **Figure 1C-D**, which confirmed the presence of Ag and Mg present on the surface of the discs. The average size of the AgNPs generated was 100 nm in diameter. The surface coating of the Ag-$SrPO_4$-Mg discs had an average thickness of 130 nm to 150 nm.

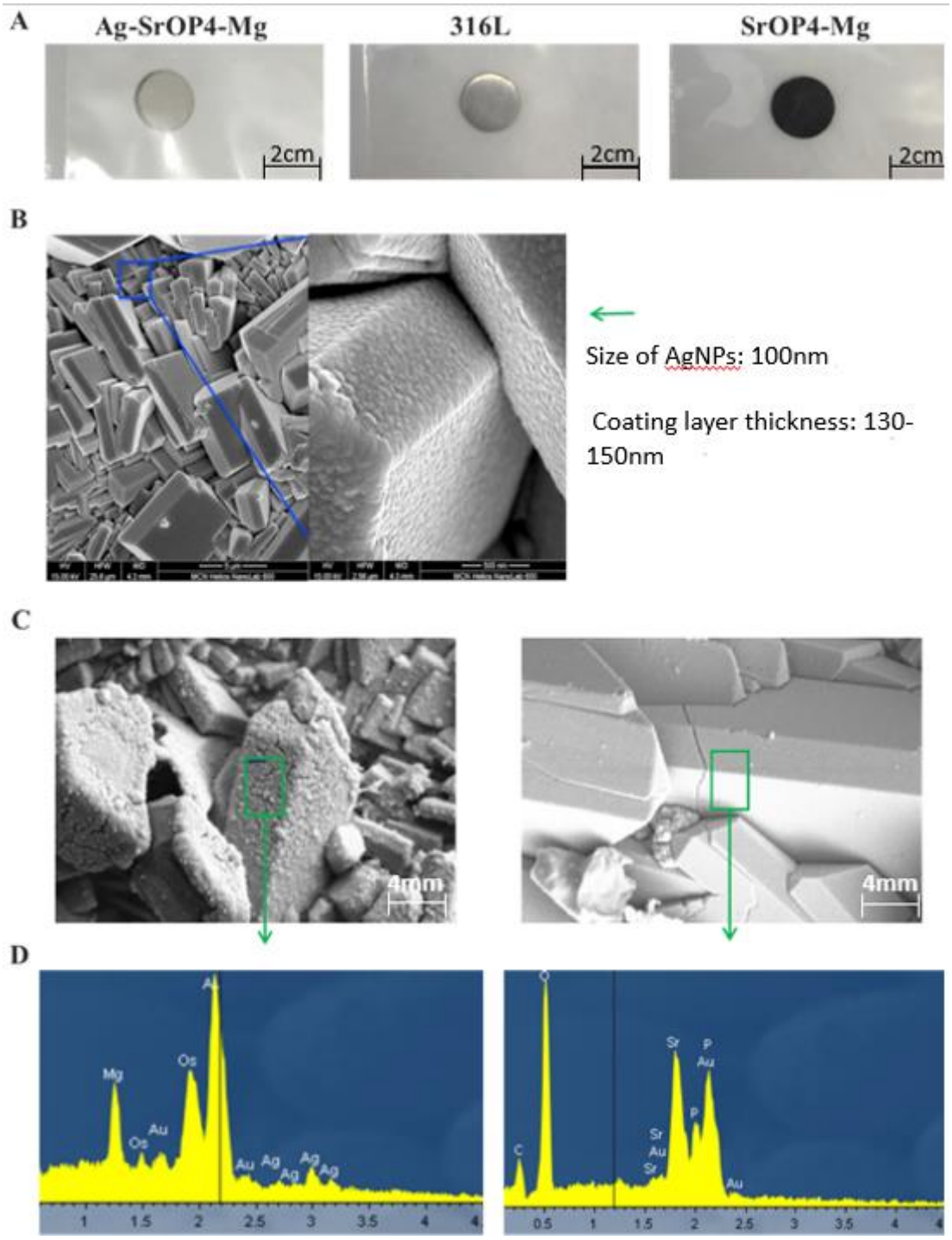

Figure 5.1 – **SEM-EDS analysis results of sample surfaces.**

(**A**) Macroscopic appearance of Ag-$SrPO_4$-Mg, stainless steel and $SrPO_4$-Mg discs. (**B**) SEM images of Ag-$SrPO_4$-Mg sample surface. (**C**) SEM images of Ag-$SrPO_4$-Mg and $SrPO_4$-Mg sample surfaces after immersion in α-MEM culture media for 24 hours (**D**) EDS profiles showing the chemical compositions of the areas marked in (**C**).

5.3 – Inhibition of *E.coli*

5.3.1 - *E.coli* bacterial viability assay

The Kruskal-Wallis ANOVA test *p*-value between all groups was 0.009, indicating a statistically significant difference between groups. There was not a significant difference between the growth inhibitions of the samples treated with the three concentrations of gentamicin: the mean growth inhibition for the positive control samples at ½ MIC, MIC and 2x MIC were 60.85 ± 8.68%, 48.41 ± 5.83% and 56.37 ± 5.83% respectively. The Ag-$SrPO_4$-Mg samples had highest inhibition at 85.8 ± 2.60% and this was statistically significant with *p*-values of 0.026, 0.002 and 0.002 when compared to ½ MIC, MIC and 2x MIC gentamicin, respectively. It was noted that $SrPO_4$-Mg also inhibited growth of *E.coli* by 46.45 ± 6.23%, similar to MIC gentamicin but was statistically significantly less than Ag-$SrPO_4$-Mg, *p*-value 0.002 (**Figure 5.2**)**.** This was supported by the confocal fluorescence microscopy photos, showing *E.coli* treated with Ag-$SrPO_4$-Mg had not only the fewest number of live bacteria but also the greatest number of dead bacteria.

Table 5.1 – Growth inhibition percentage of *E.coli* (n=6).

Sample	Inhibition of growth percentage mean ± s.e.m
½ MIC gentamicin	60.85 ± 8.68
MIC gentamicin	48.41 ± 5.83
2x MIC gentamicin	56.37 ± 7.99
Ag-$SrPO_4$-Mg	85.8 ± 2.60
$SrPO_4$-Mg	46.46 ± 6.23

E.coli were treated with ½ MIC, MIC and 2x MIC gentamicin as well as Ag-$SrPO_4$-Mg and $SrPO_4$-Mg.

5.3.2 - Visualization of *E.coli* biofilm using SEM

We further characterized the extent of bacterial attachment to the surface of the discs, as well as the fine structural differences of the discs using SEM. At 10000x magnification, the negative control stainless steel 316L disc had confluent aggregates of *E. coli* on the surface. Similarly, the $SrPO_4$-Mg disc also had dense collections of *E. coli*, in contrast to the Ag-$SrPO_4$-Mg disc on which no *E. coli* bacilli were definitively visualized (**Figure 5.3**). Furthermore, the surface structure of the Ag-$SrPO_4$-Mg disc had an almost cotton-wool appearance after incubation with *E. coli*, which was not observed after incubation with any other strain. The three gentamicin-treated samples had progressively fewer bacilli as the gentamicin concentration increased.

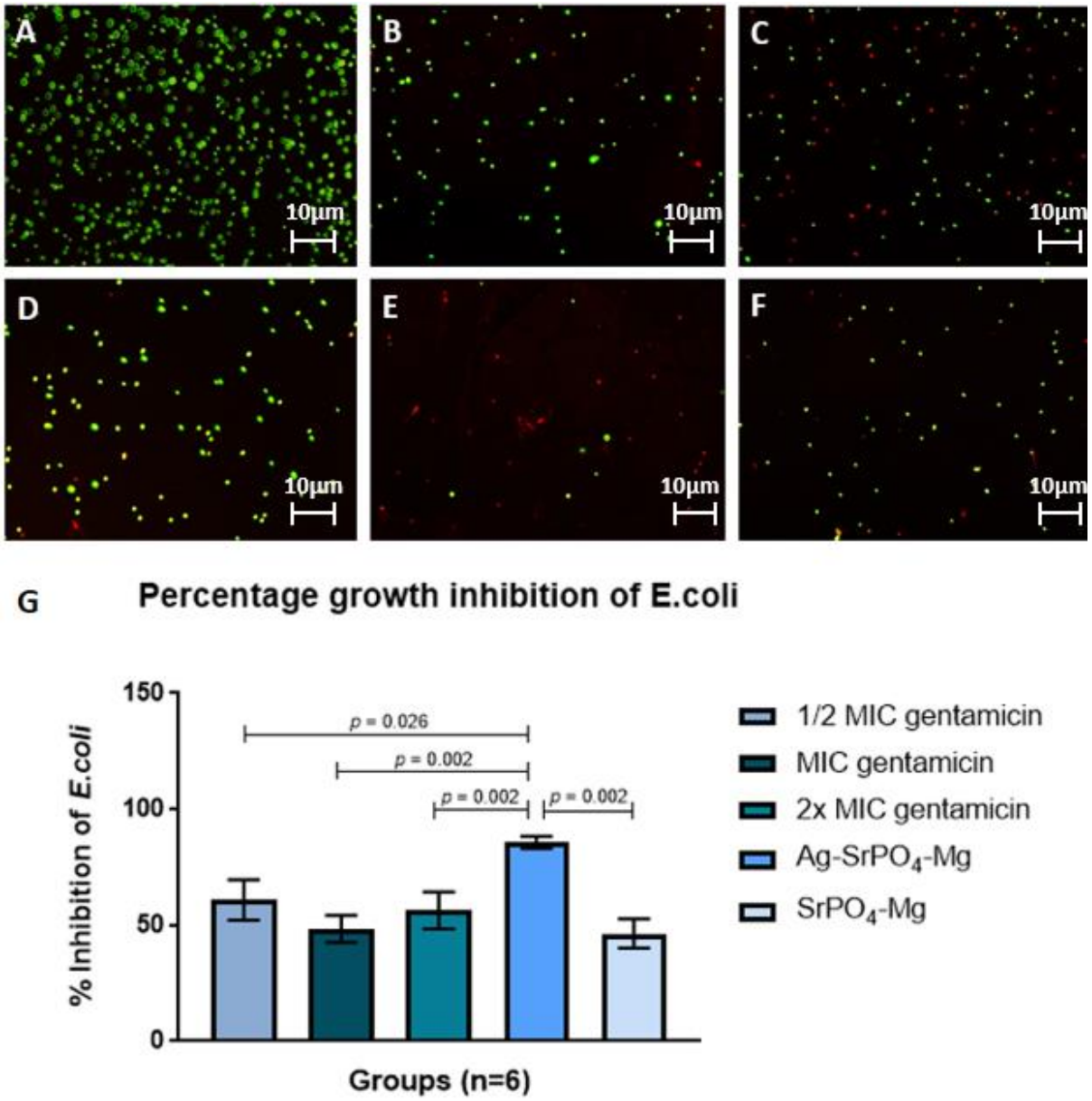

Figure 5.2 – **Confocal fluorescence microscopy images of E. coli with LIVE/DEAD staining (n=6).**

Live bacteria stain green and dead bacteria stain red. (**A**) Negative control. (**B**) ½ MIC gentamicin. (**C**) MIC gentamicin. (**D**) 2x MIC gentamicin. (**E**) Ag-$SrPO_4$-Mg. (**F**) $SrPO_4$-Mg. (**G**) Percentage growth inhibition of *E. coli* of samples when compared to the negative control sample. The values are the means ± s.e.m of six replicates. The ½ MIC gentamicin, MIC gentamicin and 2x gentamicin samples inhibited growth by 60.85 ± 8.68%, 48.41 ± 5.83% and 56.37 ± 7.99% respectively. Ag-$SrPO_4$-Mg inhibited growth by 85.8 ± 2.60% while $SrPO_4$-Mg inhibited growth by 46.46 ± 6.23%. Inhibition by Ag-$SrPO_4$-Mg was significantly greater than ½ MIC gentamicin, MIC gentamicin, 2x MIC gentamicin and $SrPO_4$-Mg with *p*-values of 0.026, 0.002, 0.002 and 0.002 respectively.

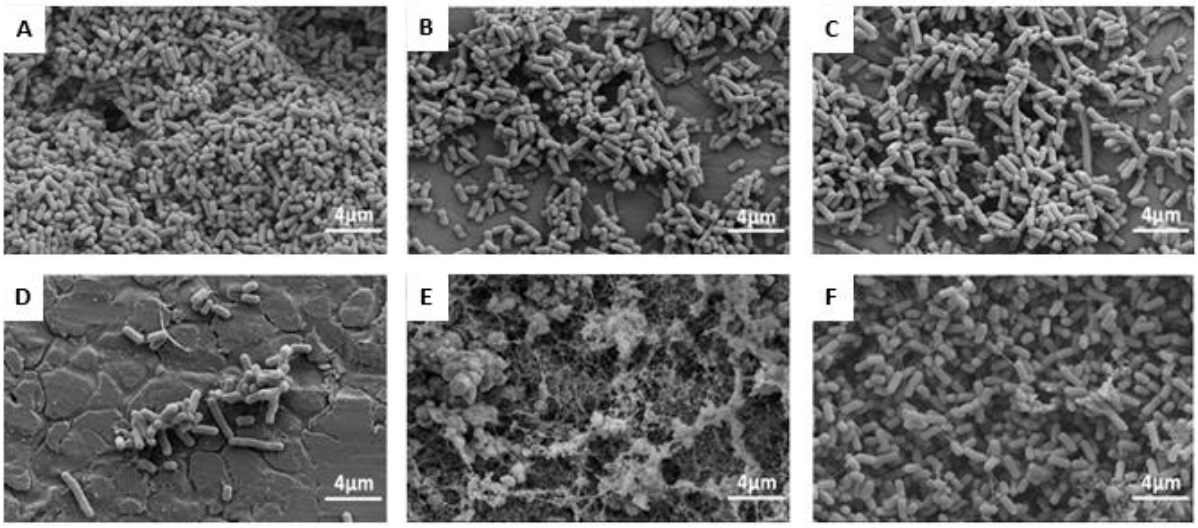

Figure 5.3 – **SEM images of the surface of metal discs at 10000x magnification following 24 hours incubation with E. coli.**

(**A**) Negative control of stainless steel 316L, bacteria and no gentamicin. (**B**) ½ MIC gentamicin: stainless steel 316L, bacteria and ½ MIC gentamicin. (**C**) MIC gentamicin: stainless steel 316L, bacteria and MIC gentamicin (**D**) 2x MIC gentamicin: stainless steel 316L, bacteria and 2 x MIC gentamicin. (**E**) Ag-$SrPO_4$-Mg, bacteria, and no gentamicin. (**F**) $SrPO_4$-Mg, bacteria, and no gentamicin.

Dense aggregates of *E.coli* were seen covering the entire surface of the negative control disc whereas only parts of the $SrPO_4$-Mg disc were covered with confluent bacteria while others were not. Stainless steel discs treated with ½ MIC and MIC gentamicin had similar confluence of bacteria and were less confluent compared to those treated with the negative control while sparse bacteria were visualized on the surface of stainless steel treated with 2x MIC gentamicin. No *E.coli* were visualized definitively on the surface of the Ag-$SrPO_4$-Mg disc but the surface appeared very different after 24 hours of immersion in BHI broth.

5.4 – Inhibition of *P.aeruginosa*

5.4.1 - Viability assay of *P.aeruginosa*

The Kruskal-Wallis ANOVA test *p*-value between all groups was <0.001, indicating a statistically significant difference between groups. Gentamicin at concentrations of ½ MIC, MIC and 2x MIC inhibited the growth of *P.aeruginosa* by 16.09 ± 10.33%, 90.11 ± 1.76% and 99.53 ± 0.11%. In contrast, Ag-$SrPO_4$-Mg inhibited the growth of *P.aeruginosa* by 47.69 ± 13.27% but fluorescent microscopy demonstrated a greater number of dead bacteria compared to the other samples, while $SrPO_4$-Mg inhibited growth modestly by only 7.25 ± 2.68%. (**Figure 5.4**). Although Ag-$SrPO_4$-Mg inhibited *P.aeruginosa* to a greater extent than ½ MIC, this was not statistically significant (*p*-value 0.102). The degree of inhibition by MIC and 2x MIC concentrations of gentamicin were significantly higher than that of Ag-$SrPO_4$-Mg (both *p*-values of 0.002) while Ag-$SrPO_4$-Mg demonstrated a statistically significant increase in inhibition compared to $SrPO_4$-Mg (*p*-value 0.041).

Table 5.2 – Growth inhibition percentage of *P.aeruginosa* (n=6).

Sample	Inhibition of growth percentage mean ± s.e.m
½ MIC gentamicin	16.09 ± 10.33
MIC gentamicin	90.11 ± 1.76
2x MIC gentamicin	99.53 ± 0.11
Ag-$SrPO_4$-Mg	47.69 ± 13.27
$SrPO_4$-Mg	7.25 ± 2.68

P.aeruginosa were treated with ½ MIC, MIC and 2x MIC gentamicin as well as Ag-$SrPO_4$-Mg and $SrPO_4$-Mg.

5.4.2 - Visualization of *P.aeruginosa* biofilm using SEM

At 10000x magnification, there were a similar number of bacteria seen in the negative control, positive control 1 and $SrPO_4$-Mg samples (**Figure 5.5**). However, it must be noted that the distribution of bacteria on the Ag-$SrPO_4$-Mg sample was not uniform across the entire disc and certain areas were more confluent. We noted that while the surface of the Ag-$SrPO_4$-Mg disc had less *P. aeruginosa* bacteria attached overall compared to the negative control, ½ MIC gentamicin sample and $SrPO_4$-Mg, the surface structure of the Ag-$SrPO_4$-Mg disc influenced the number of *P. aeruginosa* attached on different regions of that disc. **Figure 5.6** illustrates that the large, rough lattice structure of certain regions (**Figure 5.6 A-B**) accommodated a layer of *P. aeruginosa* bacilli while the irregular floral patterned surface of other regions did not (**Figure 5.6 C-D**).

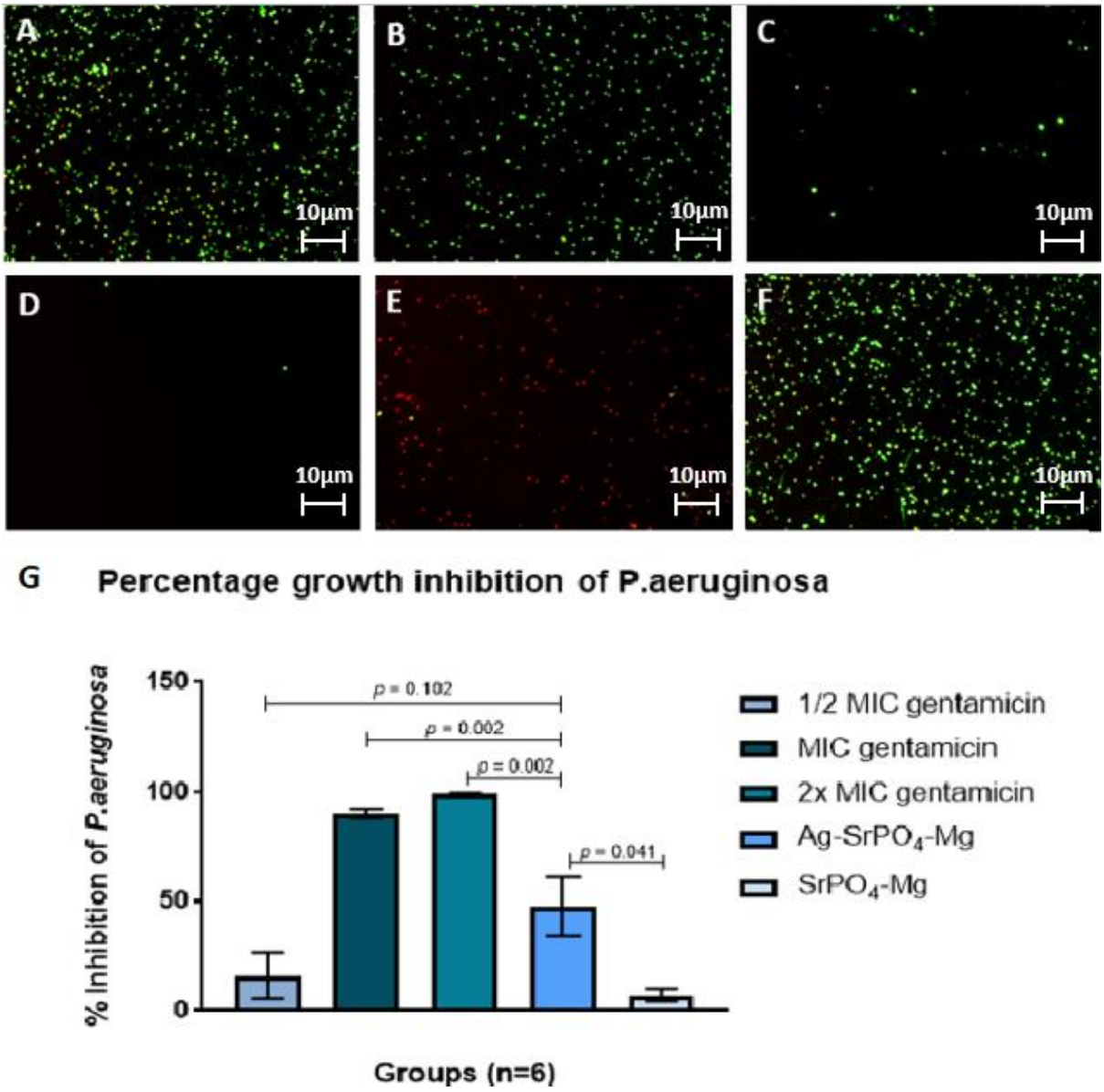

Figure 5.4 – **Confocal fluorescence microscopy images of P.aeruginosa with LIVE/DEAD staining (n=6).**

Live bacteria stain green and dead bacteria stain red. (**A**) Negative control. (**B**) ½ MIC gentamicin. (**C**) MIC gentamicin. (**D**) 2x MIC gentamicin. (**E**) Ag-$SrPO_4$-Mg. (**F**) $SrPO_4$-Mg. (**G**) Percentage growth inhibition of *P.aeruginosa* of samples when compared to the negative control sample. The values are the means ± s.e.m of six replicates. The ½ MIC gentamicin, MIC gentamicin and 2x gentamicin samples inhibited growth by 16.09 ± 10.33%, 90.11 ± 1.76% and 99.53 ± 0.11% respectively. Ag-$SrPO_4$-Mg inhibited growth by 47.69 ± 13.27% while $SrPO_4$-Mg inhibited growth by 7.25 ± 2.68%. Ag-$SrPO_4$-Mg inhibited growth significantly more than $SrPO_4$-Mg (*p*-value 0.041) but significantly less than MIC and 2x MIC gentamicin (*p*-values 0.002). Although Ag-$SrPO_4$-Mg inhibited growth more than ½ MIC gentamicin, this was not statistically significant (*p*-value 0.102).

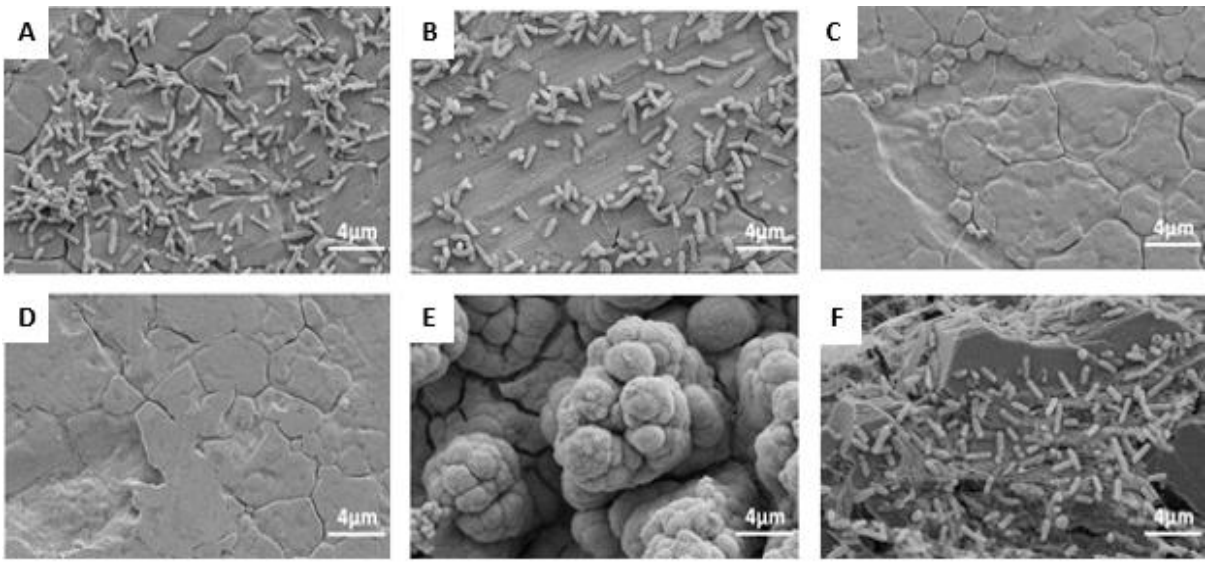

Figure 5.5 – SEM images of the surface of metal discs at 10000x magnification following 24 hours incubation with *P.aeruginosa*.

(**A**) Negative control: stainless steel 316L, bacteria, no gentamicin. (**B**) ½ MIC gentamicin: stainless steel 316L, bacteria and ½ MIC gentamicin. (**C**) MIC gentamicin: stainless steel 316L, bacteria and MIC gentamicin. (**D**) 2x MIC gentamicin: stainless steel 316L, bacteria and 2 x MIC gentamicin. (**E**) Ag-$SrPO_4$-Mg, bacteria, no gentamicin. (**F**) $SrPO_4$-Mg, bacteria, no gentamicin.

Confluent bacteria were seen on the surface of the negative control stainless steel disc as well as the $SrPO_4$-Mg disc. A less confluent layer of bacteria is seen on the surface of the ½ MIC gentamicin stainless steel disc while no bacteria were visualized on the MIC and 2x MIC gentamicin stainless steel discs.

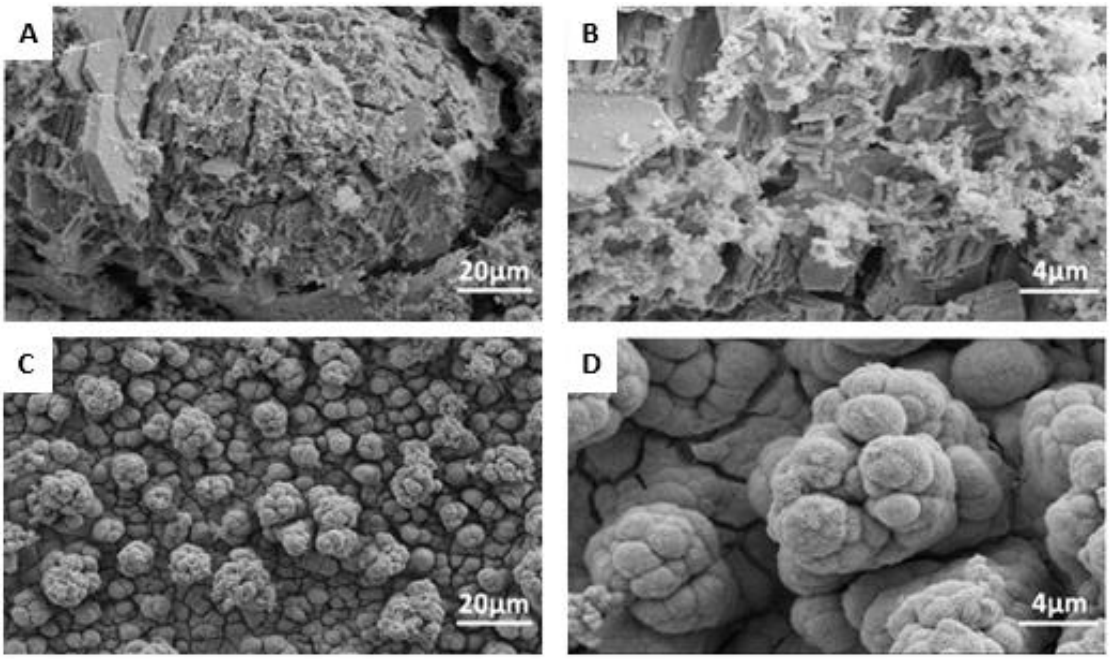

Figure 5.6 – **SEM images of two regions on one Ag-$SrPO_4$-Mg disc incubated with P. aeruginosa at 2000x and 10000x magnification.**

(**A**) and (**B**) are the 2000x and 10000x magnifications of region one with rough large protruding lattice structures, with large numbers of *P. aeruginosa* bacteria attached, while (**C**) and (**D**) are the corresponding magnifications of region two with an irregular, floral pattern surface with scarce bacteria.

5.5 – Inhibition of *S.aureus*

5.5.1 - Viability assay of *S.aureus*

The Kruskal-Wallis ANOVA test *p*-value between all groups was 0.002, indicating a statistically significant difference between groups. For *S.aureus* ATCC 29213, all concentrations of oxacillin used strongly inhibited bacterial growth and the degree of inhibition increased with increasing concentrations of oxacillin. The mean growth inhibition at ½ MIC, MIC and 2x MIC oxacillin were 91.1 ± 5.93%, 94.4 ± 3.75% and 99.4 ± 0.32% respectively. The Ag-$SrPO_4$-Mg samples also strongly inhibited *S.aureus* growth by 93.38 ± 1.31% whereas $SrPO_4$-Mg s inhibited growth by 41.3 ± 4.47%. There was no statistically significant difference between Ag-$SrPO_4$-Mg, ½ x MIC and MIC (*p*-values 0.394 and 0.386 respectively). Although the difference between 2x MIC oxacillin and Ag-$SrPO_4$-Mg was small, it was statistically significant (*p*-value 0.009). The mean growth inhibition percentage values are shown in the table below**.** These values were supported by the images obtained using confocal fluorescence microscopy where only the negative control and $SrPO_4$-Mg samples had large numbers of live bacteria and the Ag-$SrPO_4$-Mg sample had the highest number of dead bacteria (**Figure 5.7**).

Table 5.3 – Growth inhibition percentage of *S.aureus* (n=6).

Sample	Inhibition of growth percentage mean ± s.e.m
½ MIC antibiotic (oxacillin)	91.10 ± 5.93
MIC antibiotic (oxacillin)	94.38 ± 3.75
2x MIC antibiotic (oxacillin)	99.40 ± 0.32
Ag-$SrPO_4$-Mg	93.38 ± 1.31
$SrPO_4$-Mg	41.3 ± 4.47

S.aureus were treated with ½ MIC, MIC and 2x MIC oxacillin as well as Ag-$SrPO_4$-Mg and $SrPO_4$-Mg.

5.5.2 - Visualization of *S.aureus* biofilm using SEM

At 10000x magnification, the surface of the negative control stainless steel disc had a confluent layer of *S.aureus* across the surface while all three concentrations of oxacillin eliminated the bacteria and none were visualized. Most of the Ag-$SrPO_4$-Mg disc surface was free of bacteria but in small areas where the surface had retained the layered, metallic lattice structure, bacteria was still seen between the layers. The parts of the disc that had acquired an irregular floral pattern did not harbor any bacteria. Overall, these findings were consistent with the results from the viability assay. The 10000x magnification SEM photos are shown in **Figure 5.8**.

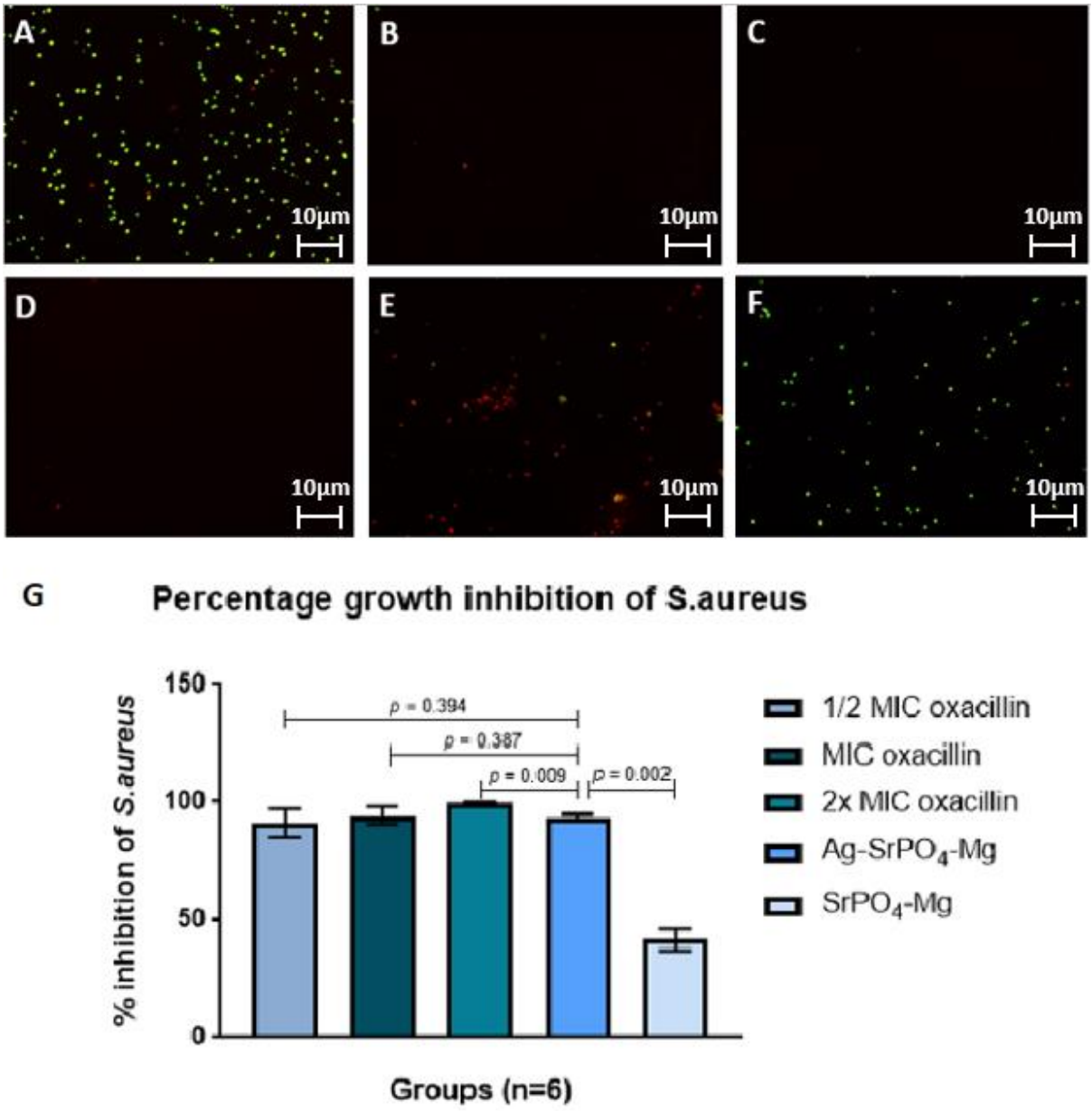

Figure 5.7 – Confocal fluorescence microscopy images of S.aureus with LIVE/DEAD staining (n=6).

Live bacteria stain green and dead bacteria stain red. (**A**) Negative control. (**B**) ½ MIC oxacillin. (**C**) MIC oxacillin. (**D**) 2x MIC oxacillin. (**E**) Ag-$SrPO_4$-Mg. (**F**) $SrPO_4$-Mg. (**G**) Percentage growth inhibition of *S.aureus* of samples when compared to the negative control sample. The values are the means ± s.e.m of six replicates. The ½ MIC oxacillin, MIC oxacillin and 2x oxacillin samples inhibited growth by 91.10 ± 5.93%, 94.38 ± 3.75% and 99.40 ± 0.32% respectively. Ag-$SrPO_4$-Mg inhibited growth by 93.38 ± 1.31%, more than twice that of $SrPO_4$-Mg at 41.3 ± 4.47% and this was statistically significant (*p*-value 0.002). There was no statistically significant difference in the inhibition of *S.aureus* by Ag-$SrPO_4$-Mg compared to ½ MIC and MIC oxacillin (*p*-values 0.394 and 0.387 respectively). Although there was only a modest difference in inhibition between 2x MIC oxacillin and Ag-$SrPO_4$-Mg, this was statistically significant (*p*-value 0.009).

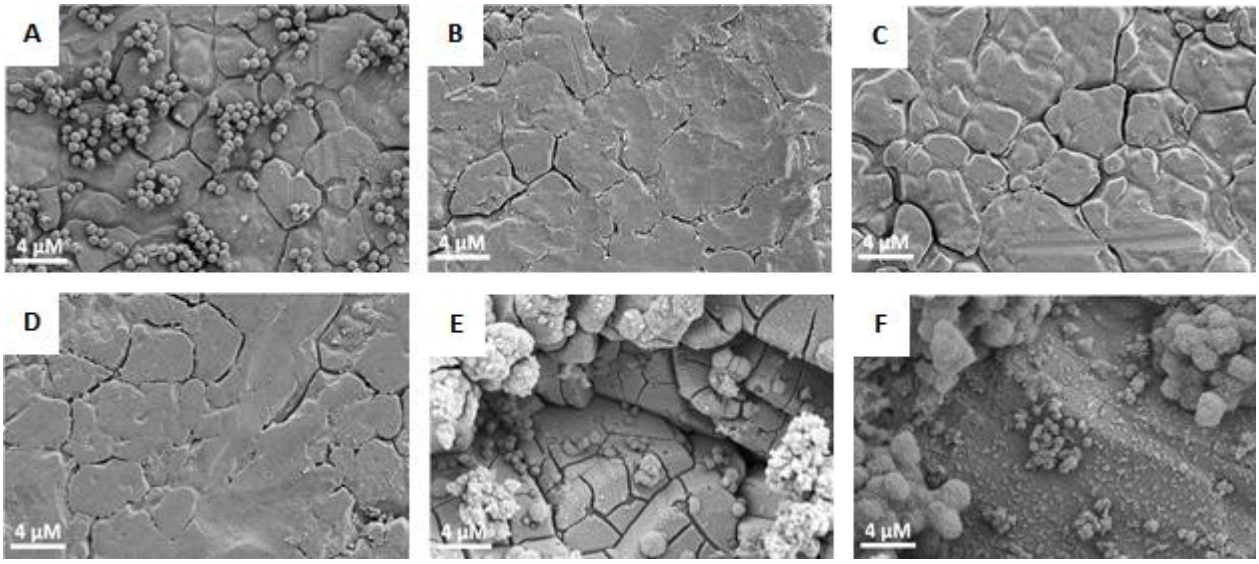

Figure 5.8 – **SEM images of the surface of metal discs at 10000x magnification following 24 hours incubation with S.aureus.**

(**A**) Negative control of stainless steel 316L, bacteria and no oxacillin, (**B**) ½ MIC oxacillin: stainless steel 316L, bacteria and ½ MIC oxacillin, (**C**) MIC oxacillin: stainless steel 316L, bacteria and MIC oxacillin, (**D**) 2x MIC oxacillin: stainless steel 316L, bacteria and 2 x MIC oxacillin, (**E**) Ag-$SrPO_4$-Mg, bacteria and no oxacillin, (**F**) $SrPO_4$-Mg, bacteria and no oxacillin.

5.6 – Inhibition of *S.epidermidis*

5.6.1 - Viability assay of *S.epidermidis*

The Kruskal-Wallis ANOVA test *p*-value between all groups was <0.001, indicating a statistically significant difference between groups. We found that Ag-$SrPO_4$-Mg demonstrated a modest inhibition in the growth of *S.epidermidis* with an inhibition of 32.09 ± 2.60%. This was significantly less than all three concentrations of oxacillin with the inhibition percentages of ½ MIC, MIC and 2x MIC being 90.9 ± 2.56%, 99.9 ± 0.03% and 99% respectively (*p*-values all 0.002). $SrPO_4$-Mg did not demonstrate any inhibition on the growth of *S.epidermidis* **Figure 5.9.**

Table 5.4 – Growth inhibition percentage of *S.epidermidis* (n=6).

Sample	Inhibition of growth percentage mean ± s.e.m
½ MIC antibiotic (oxacillin)	90.9 ± 2.56
MIC antibiotic (oxacillin)	99.9 ± 0.03
2x antibiotic (oxacillin)	99.9 ± 0
Ag-$SrPO_4$-Mg	32.09 ± 2.60
$SrPO_4$-Mg	0

S.epidermidis were treated with ½ MIC, MIC and 2x MIC oxacillin as well as Ag-$SrPO_4$-Mg and $SrPO_4$-Mg.

5.6.2 - Visualization of *S.epidermidis* biofilm using SEM

There was a confluent layer of *S.epidermidis* on the surface of the stainless steel 316L disc negative control samples in the absence of oxacillin but attachment of the bacteria was almost completely inhibited by all concentrations of oxacillin used in the experiment (**Figure 5.10**). The $SrPO_4$-Mg sample did not seem to inhibit *S.epidermidis* adhesion as there were a large number of cocci seen distributed evenly over the different regions of the disc. The surface of the Ag-$SrPO_4$-Mg disc had reduced number of cocci attached across the whole disc compared to the negative control but the degree of inhibition seemed to be influenced by the surface structure of the disc: small clusters of *S.epidermidis* were attached to the more regular, corrugated regions (**Figure 5.11 A-B**) of the disc while other regions with a more irregular and floral pattern harbored no bacteria (**Figure 5.11 C-D**). Interestingly, we found that certain surface formations on the Ag-$SrPO_4$-Mg disc accommodated certain bacterial strains while simultaneously being hostile to other strains. This comparison is demonstrated in **Figures 5.6**. The surface contour of the two discs appears similar but it is able to support *S.epidermidis* attachment while completely inhibiting *P.aeruginosa* adhesion.

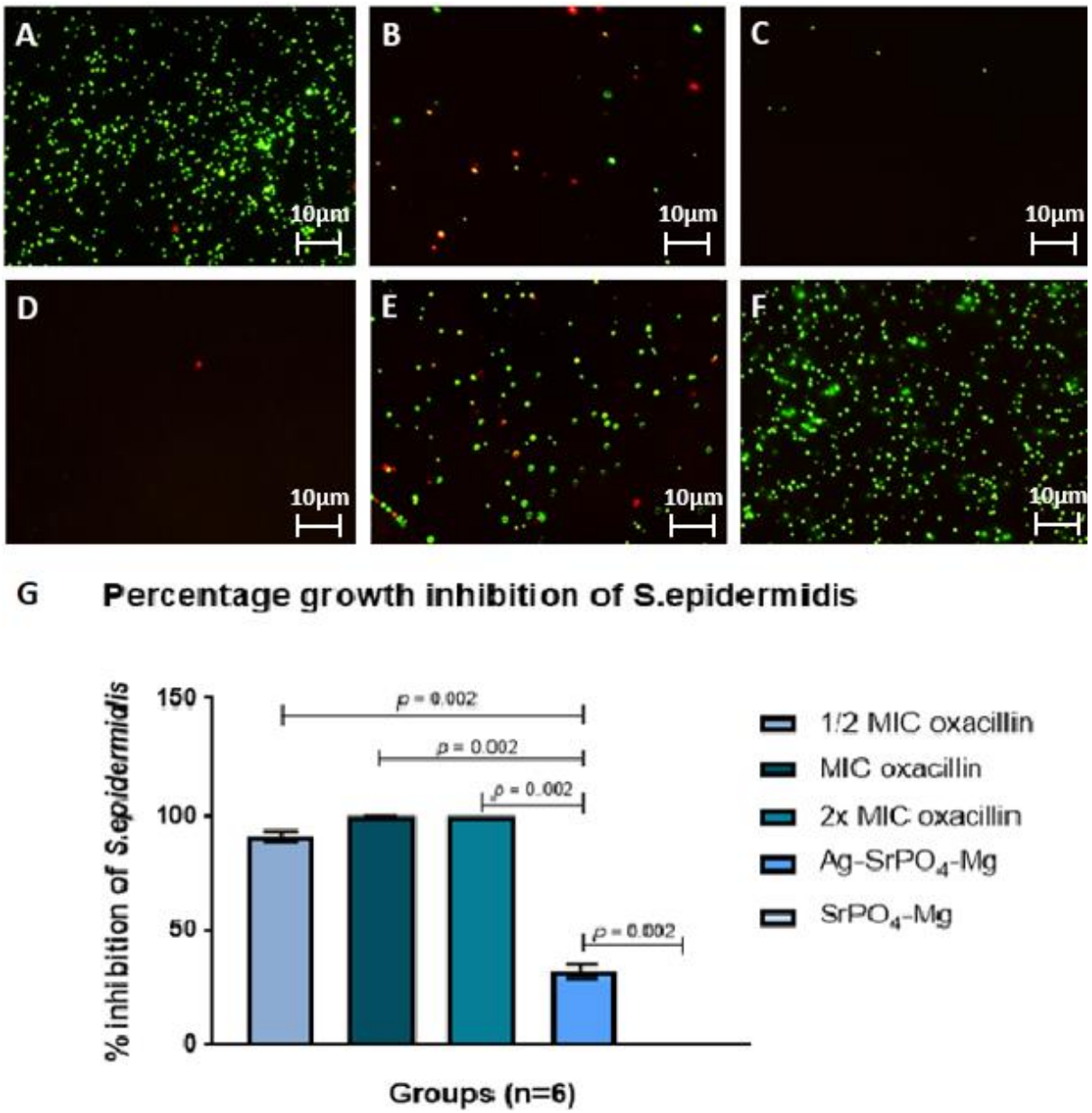

Figure 5.9 – **Confocal fluorescence microscopy images of S.epidermidis with LIVE/DEAD staining (n=6).**

Live bacteria stain green and dead bacteria stain red. (**A**) Negative control. (**B**) ½ MIC oxacillin. (**C**) MIC oxacillin. (**D**) 2x MIC oxacillin. (**E**) Ag-$SrPO_4$-Mg. (**F**) $SrPO_4$-Mg. (**G**) Percentage growth inhibition of *S.epidermidis* of samples when compared to the negative control sample. The values are the means ± s.e.m of six replicates. All three concentrations of oxacillin at ½ MIC, MIC and 2x MIC inhibited growth greatly by 90.9 ± 2.56%, 99.9 ± 0.03% and 99.9% respectively, significantly greater compared to modest inhibition by Ag-$SrPO_4$-Mg at 32.09 ± 2.60% (*p*-value 0.002). $SrPO_4$-Mg showed no inhibition of *S.epidermidis*.

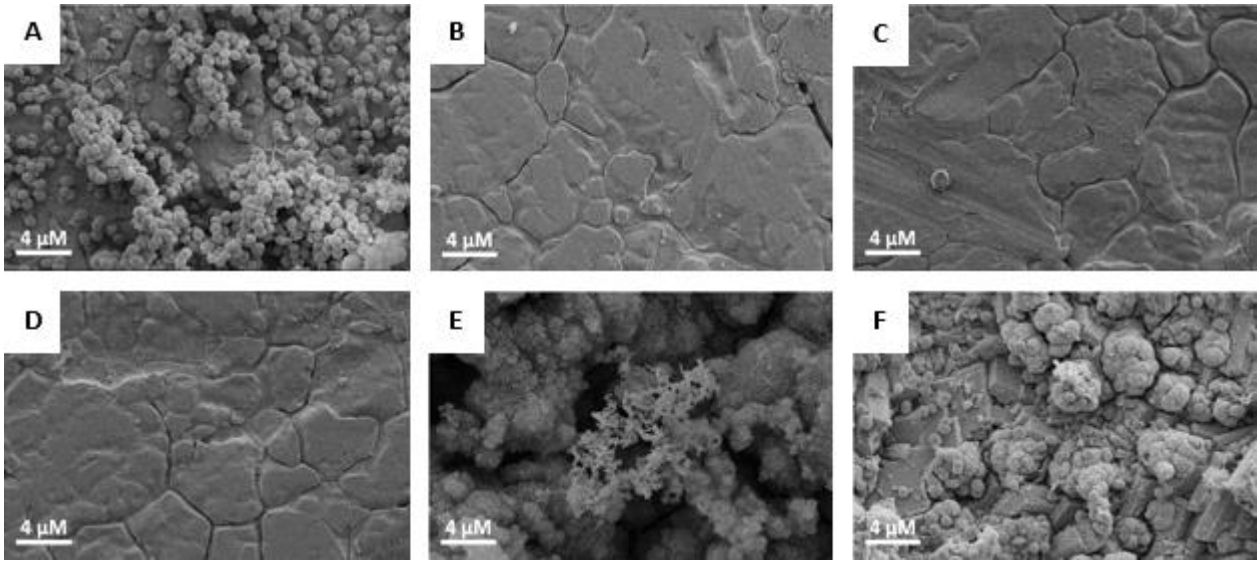

Figure 5.10 – **SEM images at 10000x magnification of test samples incubated with S.epidermidis.**

(A) Negative control of stainless steel 316L, bacteria and no oxacillin, (**B**) ½ MIC antibiotic: stainless steel 316L, bacteria and ½ MIC oxacillin, (**C**) MIC antibiotic: stainless steel 316L, bacteria and MIC oxacillin, (**D**) 2x MIC antibiotic: stainless steel 316L, bacteria and 2 x MIC oxacillin, (**E**) Ag-$SrPO_4$-Mg, bacteria, and no oxacillin, (**F**) $SrPO_4$-Mg, bacteria, and no oxacillin.

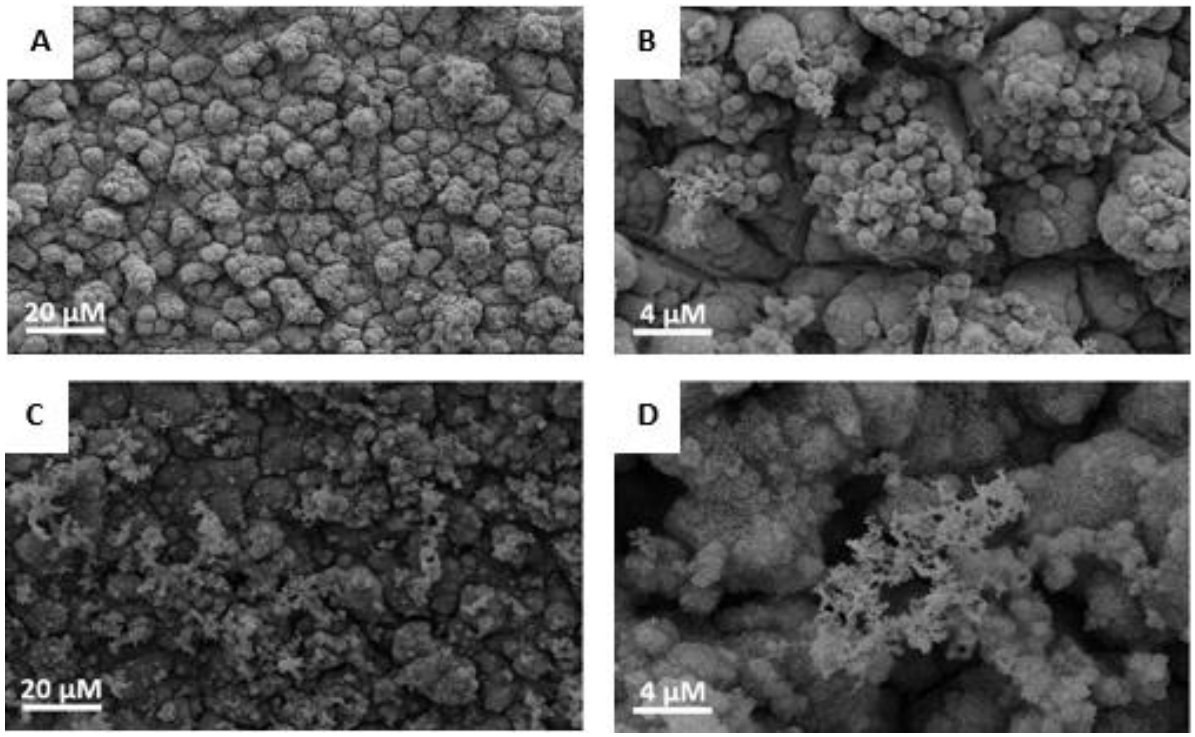

Figure 5.11 – **SEM images of two regions on one Ag-$SrPO_4$-Mg disc incubated with S.epidermidis at 2000x and 10000x magnification.**

(**A**) and (**B**) are the 2000x and 10000x magnification of region one with a rougher surface, with clusters of S.epidermidis attached, while (**C**) and (**D**) are the corresponding magnifications of region two with a more even, but irregular surface resembling cotton wool had fewer bacteria attached.

Chapter 6: Bioactivity of Ag-SrPO4-Mg on OB

6.1 - Introduction

Several studies in literature have been dedicated to investigating the cytotoxic effects of Ag on human cells. Albers et al [221] have demonstrated that 50 nm AgNPs synthesized from $AgNO_3$ displayed cytotoxicity to OB and OC. However, previous studies in our laboratory by Li et al and Ding et al have shown that both Mg and Sr induced proliferation and differentiation of OBs [234, 247]. This chapter investigates if the incorporation of Ag into the parent compound $SrPO_4$-Mg will affect the bioactivity to Sr to OBs. We determined the effects of pure Mg, $SrPO_4$-Mg and Ag-$SrPO_4$-Mg extracts at concentrations of 0.1 µL/mL, 1 µL/mL and 10 µL/mL, compared to PBS control, on OB proliferation, differentiation and mineralization by performing ALP assays and examining the extent of OB mineralization.

6.2 - OB cell differentiation assay

6.2.1 - OB ALP expression level following treatment with 24-hour extract

We did not observe a statistically significant difference in ALP expression in OBs treated with 24-hour extracts of Ag-$SrPO_4$-Mg, $SrPO_4$-Mg and Mg at concentrations of 10 µL/mL, 1 µL/mL and 0.1 µL/mL compared to those treated with PBS. The highest ALP expression was seen in OBs treated with $SrPO_4$-Mg at concentrations of 1 µL/mL and 0.1 µL/mL and were 1.41 ± 0.16 times and 1.48 ± 0.23 times higher than those treated with PBS, respectively, but neither reached a statistically significant difference (**Table 6.1 and Figure 6.1)**. There was no statistically significant difference between the test groups, with a Kruskal-Wallis ANOVA test *p*-value of 0.312.

Table 6.1 – Relative ALP expression of OBs treated with 24-hour extracts of Ag-$SrPO_4$-Mg, $SrPO_4$-Mg and Mg at concentrations of 10 µL/mL, 1 µL/mL and 0.1 µL/mL compared to PBS-treated OBs (n=6).

Treatment: 24-hour extract	Extract concentration (µL/mL)	Relative ALP level compared to control mean ± s.e.m	*p*-value
Ag-$SrPO_4$-Mg	10	1.00 ± 0.08	0.49
	1	1.06 ± 0.03	0.35
	0.1	1.03 ± 0.02	0.49

$SrPO_4$-Mg	10	1.15 ± 0.11	0.49
	1	1.41 ± 0.16	0.20
	0.1	1.48 ± 0.23	0.06
Pure Mg	10	1.09 ± 0.10	0.53
	1	0.97 ± 0.04	0.80
	0.1	0.96 ± 0.03	0.80

Figure 6.1 – **Relative expression of ALP in OBs treated with 24-hour extracts of Ag-$SrPO_4$-Mg, $SrPO_4$-Mg and pure Mg at concentrations of 10 µL/mL, 1 µL/mL and 0.1 µL/mL compared to PBS control (n=6).**

The relative ALP expression of OBs treated with Ag-$SrPO_4$-Mg at concentrations of 10 µL/mL, 1 µL/mL and 0.1 µL/mL were 1.00 ± 0.08, 1.06 ± 0.03 and 1.03 ± 0.02 respectively. Relative ALP expression of OBs treated with $SrPO_4$-Mg at concentrations of 10 µL/mL, 1 µL/mL and 0.1 µL/mL were 1.15 ± 0.11, 1.41 ± 0.16 and 1.48 ± 0.23 respectively. Relative ALP expression of OBs treated with pure Mg at concentrations of 10 µL/mL, 1 µL/mL and 0.1 µL/mL were 1.09 ± 0.10, 0.97 ± 0.04 and 0.96 ± 0.03 respectively. None of the differences in ALP expression of the extract-treated samples reached statistically significant difference compared to PBS-treated controls.

6.2.2 - OB ALP expression level following treatment with 72-hour extract

We did not observe a statistically significant difference in ALP expression in OBs treated with Ag-$SrPO_4$-Mg at concentrations of 10 µL/mL, 1 µL/mL and 0.1 µL/mL. We observed a statistically significant difference in ALP expression in OBs treated with $SrPO_4$-Mg and pure Mg both at concentrations of 0.1 µL/mL only, with a relative expression of 1.15 ± 0.07 times and 1.39 ± 0.13 times respectively, with *p*-values of 0.03 and 0.004 respectively (**Table 6.2 and Figure 6.2**). The variability between test groups did not reach statistical significance, with a Kruskal-Wallis ANOVA test *p*-value was 0.081.

Table 6.2 – Relative ALP expression of OBs treated with 72-hour extracts of Ag-$SrPO_4$-Mg, $SrPO_4$-Mg and Mg at concentrations of 10 µL/mL, 1 µL/mL and 0.1 µL/mL compared to PBS-treated OBs (n=6).

Treatment: 72-hour extract	Extract concentration (µL/mL)	Relative ALP level compared to control. Mean ± s.e.m	*p*-value
Ag-$SrPO_4$-Mg	10	0.95 ± 0.07	0.46
	1	1.15 ± 0.11	0.28
	0.1	1.05 ± 0.10	0.81
$SrPO_4$-Mg	10	0.96 ± 0.04	0.28
	1	1.06 ± 0.06	0.57
	0.1	1.15 ± 0.07	**0.03**
Pure Mg	10	0.96 ± 0.03	0.37
	1	1.11 ± 0.12	0.93
	0.1	1.39 ± 0.13	**0.004**

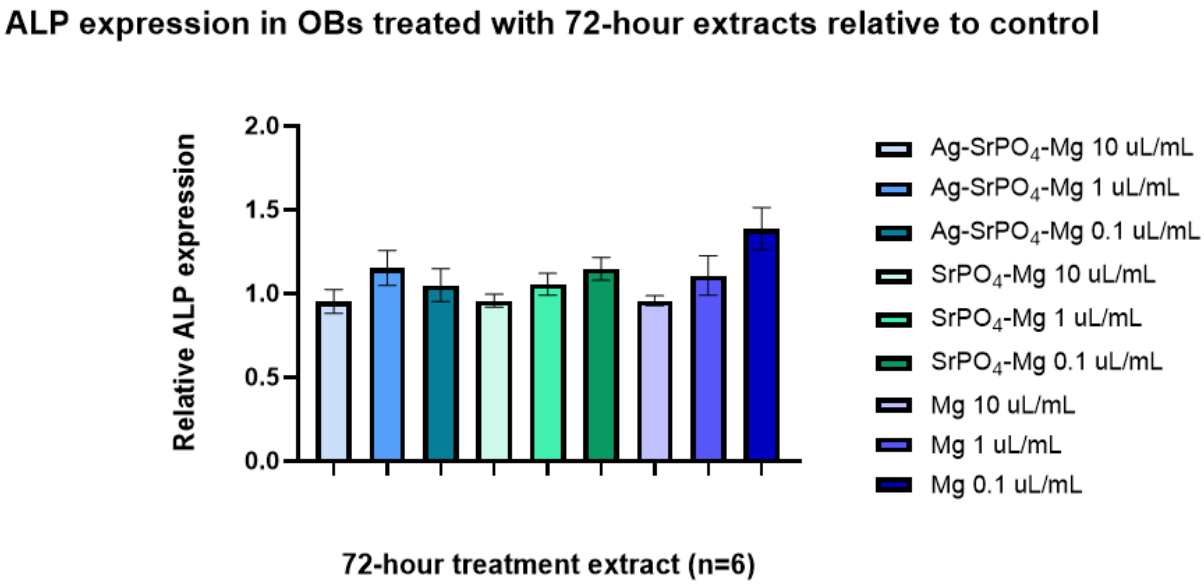

Figure 6.2 – **Relative expression of ALP in OBs treated with 72-hour extracts of Ag-$SrPO_4$-Mg, $SrPO_4$-Mg and pure Mg at concentrations of 10 µL/mL, 1 µL/mL and 0.1 µL/mL compared to PBS control (n=6).**

The relative ALP expression of OBs treated with Ag-$SrPO_4$-Mg at concentrations of 10 µL/mL, 1 µL/mL and 0.1 µL/mL were 0.95 ± 0.07, 1.15 ± 0.11 and 1.05 ± 0.10 respectively. Relative ALP expression of OBs treated with $SrPO_4$-Mg at concentrations of 10 µL/mL, 1 µL/mL and 0.1 µL/mL were 0.96 ± 0.04, 1.06 ± 0.06 and 1.15 ± 0.07 respectively. Relative ALP expression of OBs treated with pure Mg at concentrations of 10 µL/mL, 1 µL/mL and 0.1 µL/mL were 0.96 ± 0.03, 1.11 ± 0.12 and 1.39 ± 0.13 respectively. A statistically significant decrease in ALP expression was seen in OBs treated with $SrPO_4$-Mg at 0.1 µL/mL and pure Mg at 0.1 µL/mL.

6.2.3 - OB ALP expression level following treatment with 7-day extract

We observed a trend in reduced ALP expression in OBs treated with 7-day extracts of Ag-$SrPO_4$-Mg, $SrPO_4$-Mg and Mg at concentrations of 10 µL/mL, 1 µL/mL and 0.1 µL/mL compared to controls treated with PBS but not all reached statistical significance (**Table 6.3 and Figure 6.3**). A statistically significant reduction was seen with Ag-$SrPO_4$-Mg at 10 µL/mL and 1 µL/mL with relative expressions of 0.82 ± 0.06 and 0.79 ± 0.05 respectively (*p*-value 0.004), $SrPO_4$-Mg at 10 µL/mL and 0.1 µL/mL with relative expressions of 0.80 ± 0.06 and 0.83 ± 0.04 (*p*-value 0.004) and Mg at 10 µL/mL and 0.1 µL/mL with relative expressions of 0.76 ± 0.06 and 0.89 ± 0.04 respectively (*p*-value 0.004 and 0.02 respectively). The Kruskal-Wallis ANOVA test *p*-value for differences between test groups was 0.447 and did not reach statistical significance.

Table 6.3 – Relative ALP expression of OBs treated with 7-day extracts of Ag-$SrPO_4$-Mg, $SrPO_4$-Mg and Mg at concentrations of 10 µL/mL, 1 µL/mL and 0.1 µL/mL compared to PBS-treated OBs (n=6).

Treatment: 7-day extract	Extract concentration (µL/mL)	Relative ALP level compared to control. mean ± s.e.m	*p*-value
Ag-$SrPO_4$-Mg	10	0.82 ± 0.06	**0.004**
	1	0.79 ± 0.05	**0.004**
	0.1	0.90 ± 0.06	0.28
$SrPO_4$-Mg	10	0.80 ± 0.06	**0.004**
	1	0.86 ± 0.09	0.21
	0.1	0.83 ± 0.04	**0.004**
Pure Mg	10	0.76 ± 0.06	**0.004**
	1	0.91 ± 0.05	0.21
	0.1	0.89 ± 0.04	**0.02**

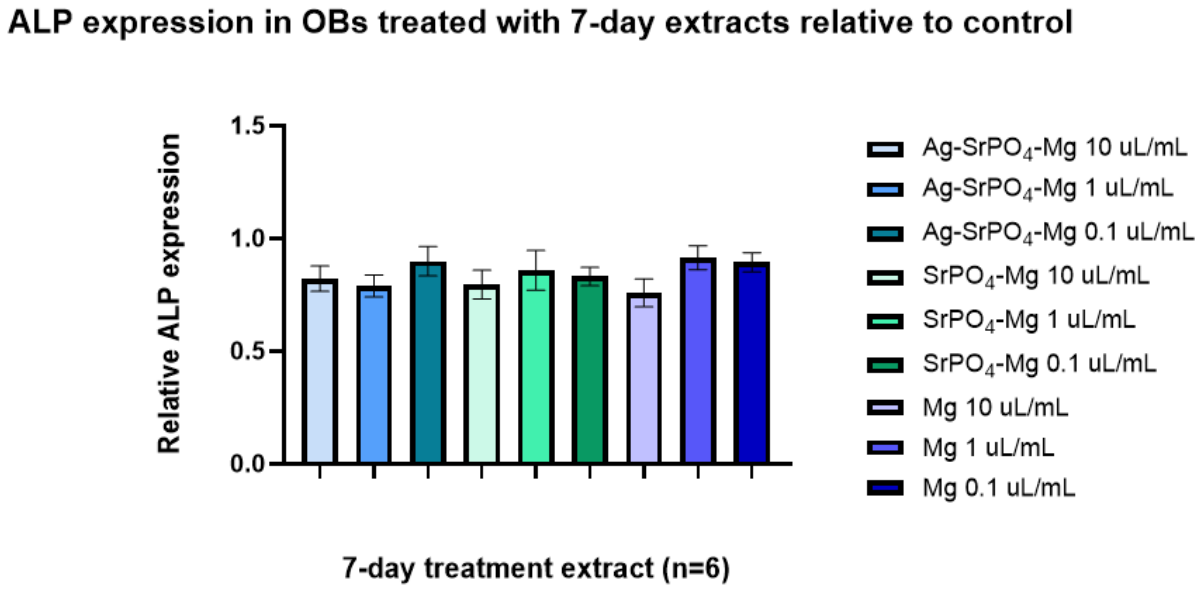

Figure 6.3 – **Relative expression of ALP in OBs treated with 7-day extracts of Ag-$SrPO_4$-Mg, $SrPO_4$-Mg and pure Mg at concentrations of 10 µL/mL, 1 µL/mL and 0.1 µL/mL compared to PBS control (n=6).**

The relative ALP expression of OBs treated with Ag-$SrPO_4$-Mg at concentrations of 10 µL/mL, 1 µL/mL and 0.1 µL/mL were 0.82 ± 0.06, 0.79 ± 0.05 and 0.90 ± 0.06 respectively. Relative ALP expression of OBs treated with $SrPO_4$-Mg at concentrations of 10 µL/mL, 1 µL/mL and 0.1 µL/mL were 0.80 ± 0.06, 0.86 ± 0.09 and 0.83 ± 0.04 respectively. Relative ALP expression of OBs treated with pure Mg at concentrations of 10 µL/mL, 1 µL/mL and 0.1 µL/mL were 0.76 ± 0.06, 0.91 ± 0.05 and 0.89 ± 0.04 respectively. A statistically significant decrease in ALP expression was seen in OBs treated with Ag-$SrPO_4$-Mg at 10 µL/mL and 1 µL/mL, $SrPO_4$-Mg at 10 µL/mL and 0.1 µL/mL and pure Mg at 10 µL/mL and 0.1 µL/mL.

6.2.4 - OB ALP expression level following treatment with 14-day extract

We did not observe a statistically significant difference in the expression of ALPs in OBs treated with 14-day extracts of Ag-$SrPO_4$-Mg and Mg at concentrations of 10 µL/mL, 1 µL/mL and 0.1 µL/mL (**Table 6.4 and Figure 6.4**). The only statistically significant difference in ALP expression compared to PBS-treated OBs was seen in those treated with 14-day extracts of $SrPO_4$-Mg at 0.1 µL/mL, with a relative expression of 0.74 ± 0.05 (*p*-value 0.03). Statistical significance was not reached for $SrPO_4$-Mg at 10 µL/mL and 1 µL/mL. The Kruskal-Wallis ANOVA test between the test groups had a *p*-value of 0.08 and did not reach statistical significance.

Table 6.4. – Relative ALP expression of OBs treated with 14-day extracts of Ag-$SrPO_4$-Mg, $SrPO_4$-Mg and Mg at concentrations of 10 µL/mL, 1 µL/mL and 0.1 µL/mL compared to PBS-treated OBs (n=6).

Treatment: 14-day extract	Extract concentration (µL/mL)	Relative ALP level compared to control. mean ± s.e.m	*p*-value
Ag-$SrPO_4$-Mg	10	1.03 ± 0.05	0.69
	1	0.85 ± 0.11	0.69
	0.1	0.89 ± 0.04	0.20
$SrPO_4$-Mg	10	1.12 ± 0.07	0.20
	1	0.93 ± 0.09	0.69
	0.1	0.74 ± 0.05	**0.03**
Pure Mg	10	1.04 ± 0.05	0.69
	1	0.98 ± 0.02	>0.99
	0.1	0.93 ± 0.09	0.69

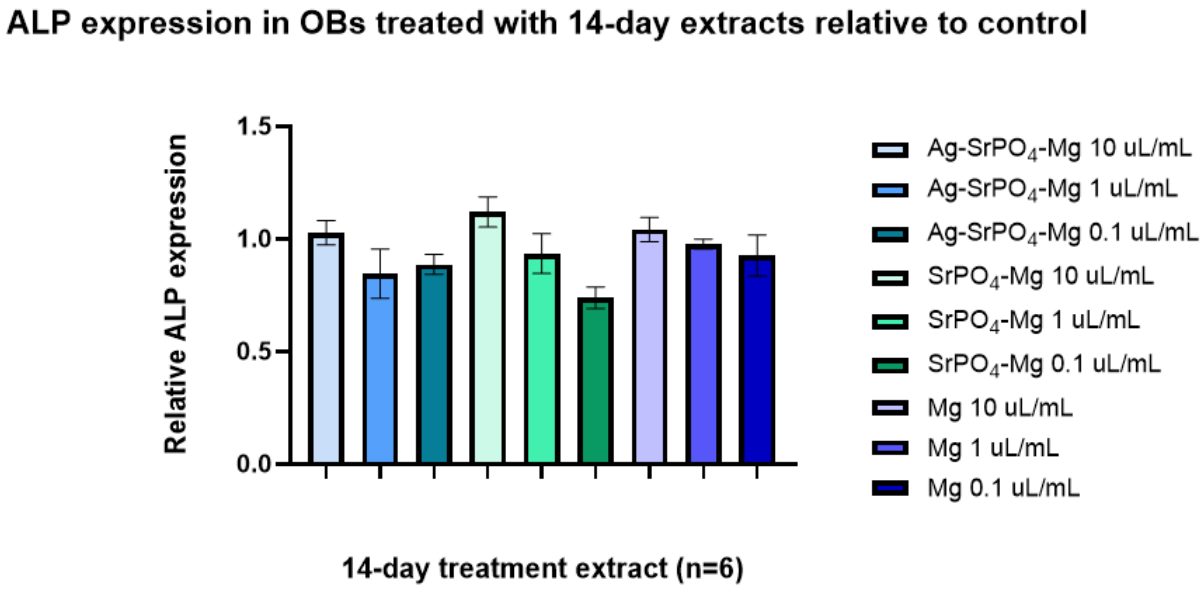

Figure 6.4 – **Relative expression of ALP in OBs treated with 14-day extracts of Ag-$SrPO_4$-Mg, $SrPO_4$-Mg and pure Mg at concentrations of 10 µL/mL, 1 µL/mL and 0.1 µL/mL compared to PBS control (n=6).**

The relative ALP expression of OBs treated with Ag-$SrPO_4$-Mg at concentrations of 10 µL/mL, 1 µL/mL and 0.1 µL/mL were 1.03 ± 0.05, 0.85 ± 0.11 and 0.89 ± 0.04 respectively. Relative ALP expression of OBs treated with $SrPO_4$-Mg at concentrations of 10 µL/mL, 1 µL/mL and 0.1 µL/mL were 1.12 ± 0.07, 0.93 ± 0.09 and 0.74 ± 0.05 respectively. Relative ALP expression of OBs treated with pure Mg at concentrations of 10 µL/mL, 1 µL/mL and 0.1 µL/mL were 1.04 ± 0.05, 0.98 ± 0.02 and 0.93 ± 0.09 respectively. A statistically significant decrease in ALP expression was seen in OBs treated with $SrPO_4$-Mg at 0.1 µL/mL.

6.2.5 – Inter-experiment variability between ALP assay standards

Two separate SensoLyte *p*NPP Alkaline Phosphatase assay kits purchased between 2017 and 2022 were used in the ALP experiments discussed in this thesis. Each experiment contained eight standards, corresponding to eight concentrations of ALP, used to construct the standard curve from which the test sample ALP concentrations were interpolated. We compared the standards from six sets of ALP assays with ANOVA and found there was no statistically significant inter-experiment variability between the standards, with a *p*-value of 0.794 (**Table 6.5)**.

Table 6.5 – Absorbance values of ALP standards.

Standard ALP concentration (ng/well)	Assay 1	Assay 2	Assay 3	Assay 4	Assay 5	Assay 6
10	3.273	3.457	3.238	3.619	3.286	3.202
5	2.738	2.756	2.026	2.935	2.274	2.412
2.5	1.726	1.749	1.135	2.013	1.431	1.381
1.2	0.975	1.279	0.605	1.410	0.820	0.683
0.6	0.504	1.115	0.325	0.981	0.476	0.379
0.3	0.249	0.684	0.166	0.719	0.219	0.196
0.15	0.129	0.703	0.094	0.751	0.125	0.111
0	0.024	0.637	0.025	0.632	0.01	0.024

The SensoLyte *p*NPP Alkaline Phosphatase Assay Kit contained ten standards corresponding to 10, 5, 2.5, 1.2, 0.6, 0.3, 0.15 and 0 ng/well of ALP with absorbance values measured at 405 nm using the Infinite M200 PRO plate reader and i-control 1.9 program. Inter-experiment variability between six assays had an ANOVA *p*-value of 0.794, showing no statistically significant difference between assays.

6.3 - OB Cell Mineralization Assay

6.3.1 - OB mineralization with 24-hour pure Mg extract

OBs treated with 24-hour pure Mg extract at concentrations of 0.1 and 1 μL/mL had higher Ca concentrations (231.3 ± 8.75 and 237.6 ± 8.57 μM) respectively compared to OBs treated with control (223.7 ± 6.23 μM) although neither reached statistical significance (*p*-values 0.55 and 0.13 respectively), while OBs treated with Mg extract at a concentration of 10 μL/mL had a decreased Ca concentration (218.7 ± 8.48) compared to control but this also did not reach statistical significance (*p*-value 0.77) **Table 6.6**. The Kruskal-Wallis ANOVA test *p*-value between test samples and control was 0.363. The appearance of the OBs treated with control and different concentrations of pure Mg extract, as well as the concentrations of Ca in each sample, are shown in **Figure 6.5**

OBs treated with 24-hour $SrPO_4$-Mg extracts at concentrations of 0.1, 1 and 10 μL/mL all demonstrated higher Ca concentrations (327.6 ± 23.35, 327.6 ± 33.6, 336.6 ± 20.93 μM respectively) compared to control treated OBs (324.7 ± 27.95 μM) although none reached statistical significance. The Kruskal-Wallis ANOVA test *p*-value between test groups and control was 0.951 **Figure 6.6**.

Similarly, OBs treated with 24-hour extracts of Ag-$SrPO_4$-Mg at concentrations of 0.1, 1 and 10 μL/mL all demonstrated a greater degree of mineralization with higher Ca concentrations (343.8 ± 25.95, 339.8 ± 33.2, and 343.8 ± 25.95 μM respectively) compared to control treated OBs (324.7 ± 27.95 μM) but none were statistically significant. The Kruskal-Wallis ANOVA test *p*-value between test groups and control was 0.909 **Figure 6.7**.

Table 6.6 – Calcium concentration in mineralization assays of OBs treated with 24-hour extracts at concentrations of 0.1, 1 and 10 μL/mL (n=6).

A

Treatment: 24-hour extract	Extract concentration (μL/mL)	Calcium concentration (μM) mean ± s.e.m	*p*-value
PBS	10	223.7 ± 6.23	N/A
Mg	0.1	231.3 ± 8.75	0.55
Mg	1	237.6 ± 8.57	0.13
Mg	10	218.7 ± 8.48	0.77

B

Treatment: 24-hour extract	Extract concentration (µL/mL)	Calcium concentration (µM) mean ± s.e.m	*p*-value
PBS	10	324.7 ± 27.95	N/A
$SrPO_4$-Mg	0.1	327.6 ± 23.35	0.95
$SrPO_4$-Mg	1	327.6 ± 33.6	0.68
$SrPO_4$-Mg	10	336.6 ± 20.93	0.85

C

Treatment: 24-hour extract	Extract concentration (µL/mL)	Calcium concentration (µM) mean ± s.e.m	*p*-value
PBS	10	324.7 ± 27.95	N/A
Ag-$SrPO_4$-Mg	0.1	343.8 ± 25.95	0.41
Ag-$SrPO_4$-Mg	1	339.8 ± 33.2	0.35
Ag-$SrPO_4$-Mg	10	343.8 ± 25.95	0.47

A. 24-hour Mg extract. **B.** 24-hour $SrPO_4$-Mg extract. **C.** 24-hour Ag-$SrPO_4$-Mg extract.

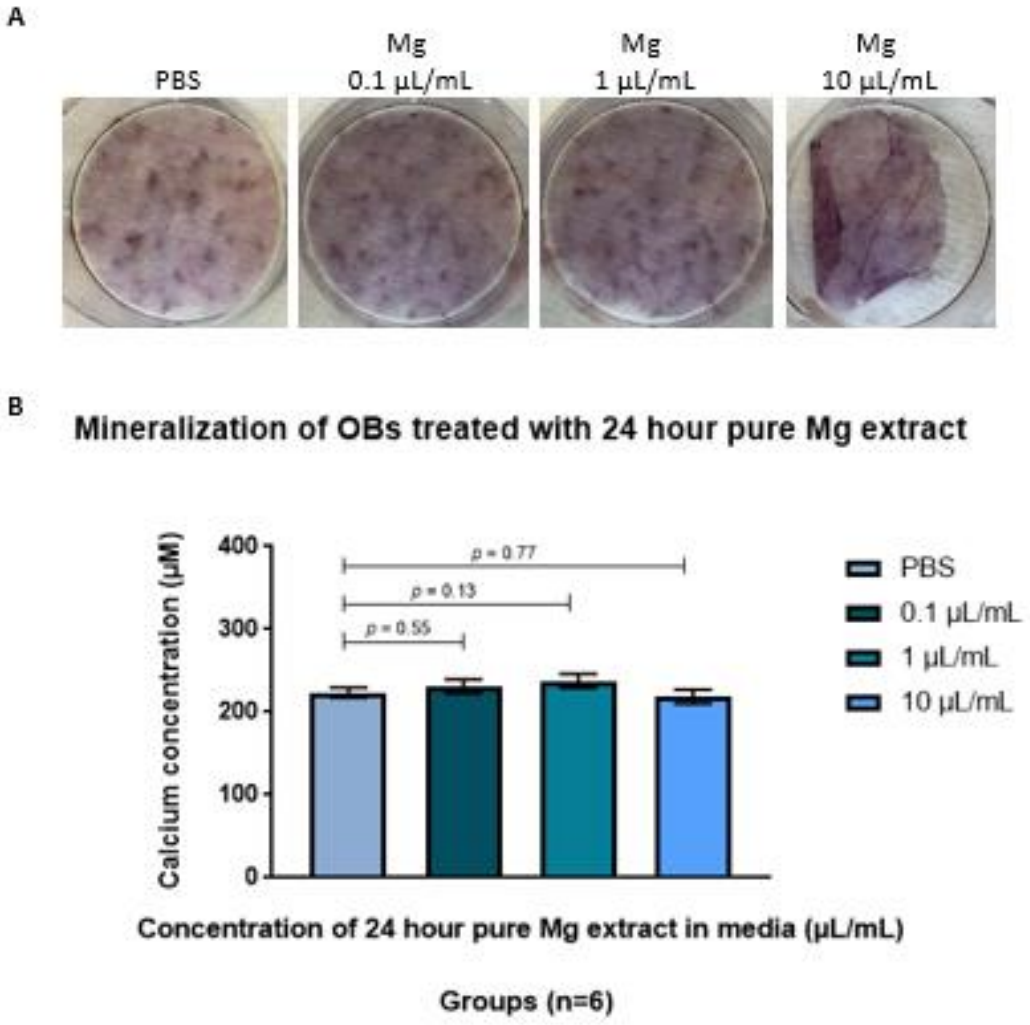

Figure 6.5 – **Mineralization of OBs treated with 24-hour pure Mg extracts (n=6).**

A. Photographs showing AR-S staining of OBs prior to the extraction step with CPC: OBs treated with PBS control and 24-hour pure Mg extracts at concentrations of 0.1, 1 and 10 µL/mL from left to right. **B.** Concentrations of Ca in OBs treated with control and 24-hour Mg extracts at concentrations of 0.1, 1 and 10 µL/mL were 223.7 ± 6.23, 231.3 ± 8.75, 237.6 ± 8.57 and 218.7 ± 8.48 µM respectively. None of the Mg-treated samples had a statistically significant difference compared to the control sample OBs with *p*-values of 0.55, 0.13 and 0.77 respectively. All treatments had 6 replicates, performed over two experiments.

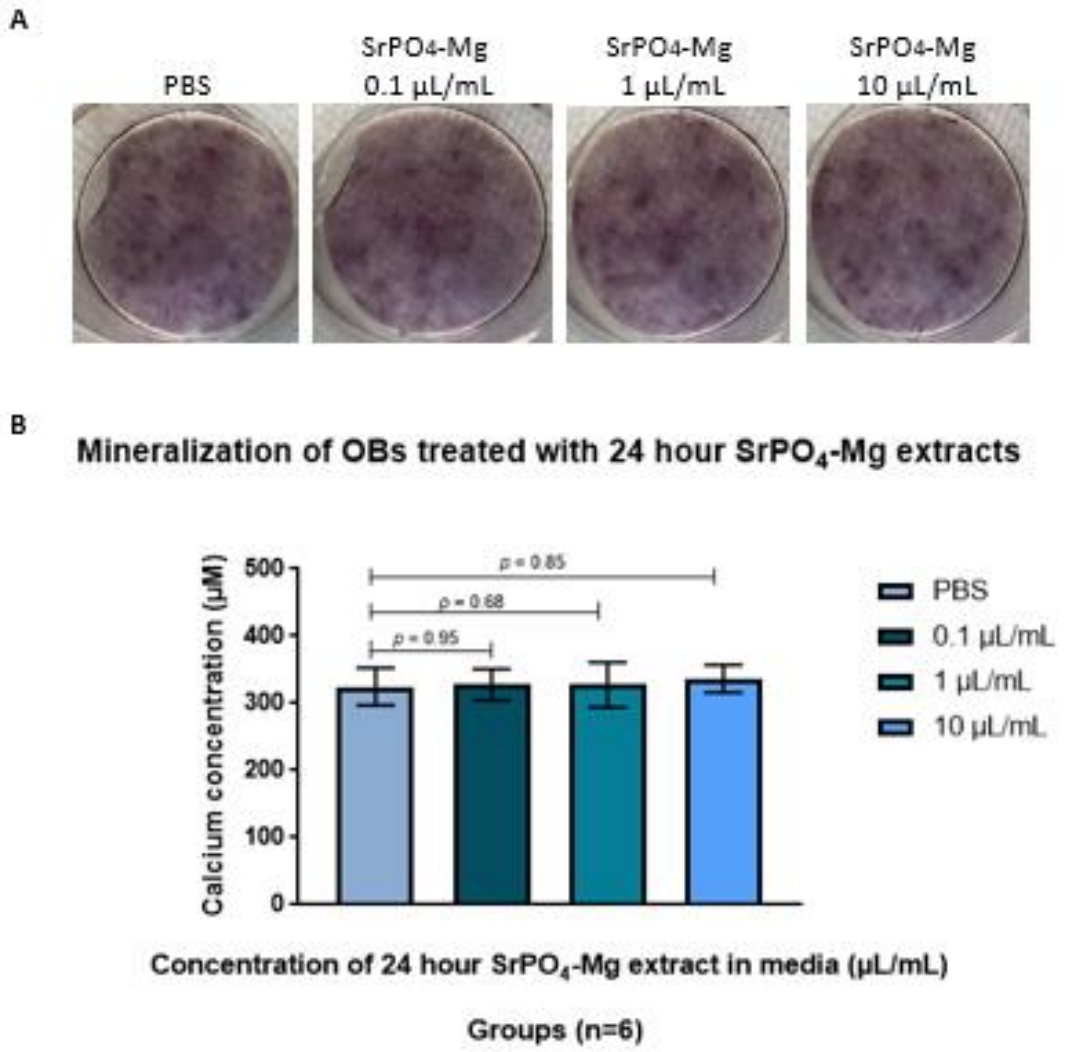

Figure 6.6 – **Mineralization of OBs treated with 24-hour $SrPO_4$-Mg extracts (n=6).**

A. Photographs showing AR-S staining of OBs prior to the extraction with CPC: OBs treated with PBS control and 24-hour $SrPO_4$-Mg extracts at concentrations of 0.1, 1 and 10 µL/mL from left to right. **B.** Concentrations of Ca in OBs treated with control and 24-hour $SrPO_4$-Mg extracts at concentrations of 0.1, 1 and 10 µL/mL were 324.7 ± 27.95, 327.6 ± 23.35, 327.6 ± 33.6 and 336.6 ± 20.93 µM respectively. Although the $SrPO_4$-Mg-treated OBs all had higher Ca concentrations compared to the control samples, none reached statistical significance with *p*-values of 0.95, 0.68 and 0.85 respectively. All treatments had 6 replicates, performed over two experiments.

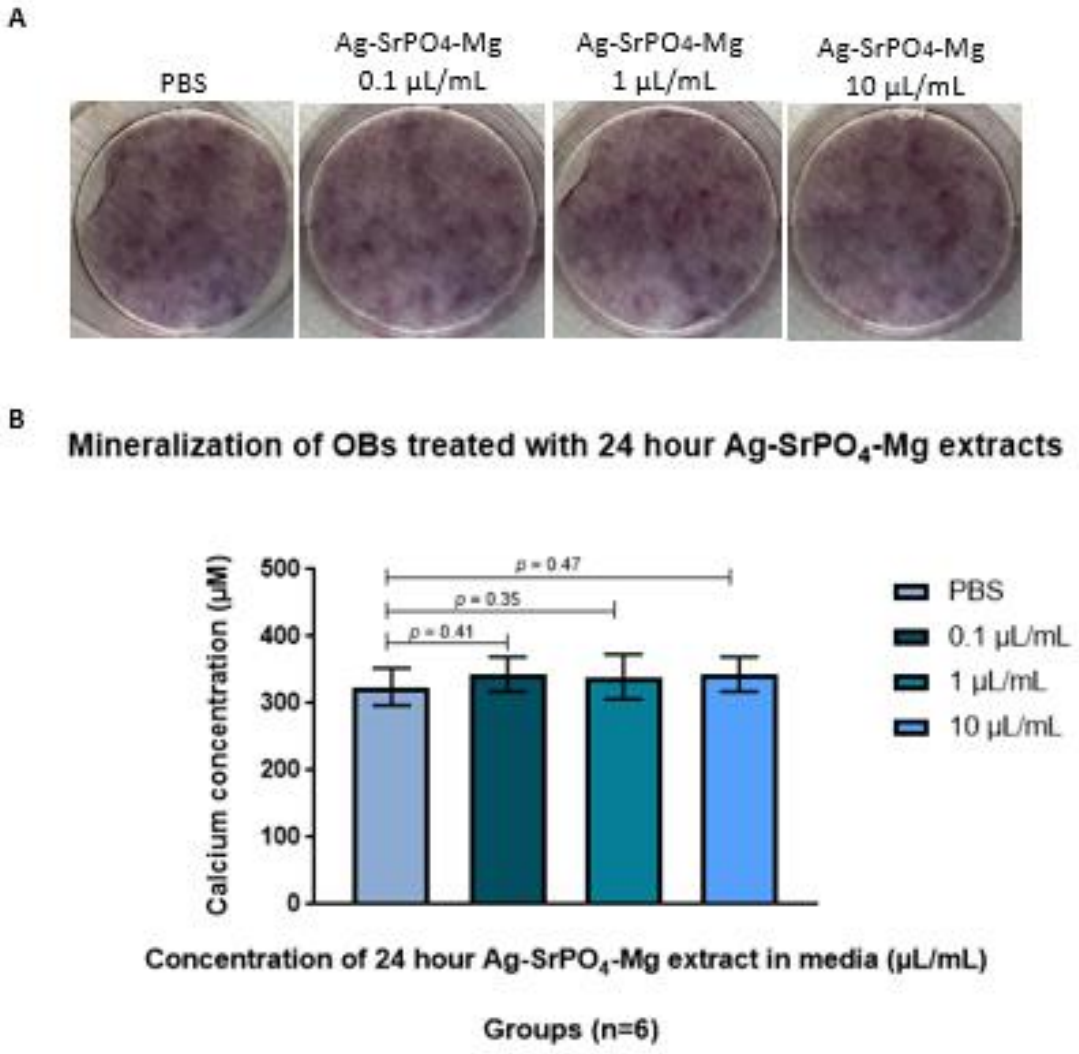

Figure 6.7 – **Mineralization of OBs treated with 24-hour Ag-$SrPO_4$-Mg extracts (n=6).**

A. Photographs showing AR-S staining of OBs prior to the extraction with CPC: OBs treated with PBS control and 24-hour Ag-$SrPO_4$-Mg extracts at concentrations of 0.1, 1 and 10 µL/mL from left to right. **B.** Concentrations of Ca in OBs treated with control and 24-hour Ag-$SrPO_4$-Mg extracts at concentrations of 0.1, 1 and 10 µL/mL were 324.7 ± 27.95, 343.8 ± 25.95, 339.8 ± 33.2 and 343.8 ± 25.95 µM respectively. Although the $SrPO_4$-Mg-treated OBs all had higher Ca concentrations compared to the control samples, none reached statistical significance with *p*-values of 0.42, 0.35 and 0.47 respectively. All treatments had 6 replicates, performed over two experiments.

6.3.2 - OB mineralization with 72-hour extracts

OBs treated with 72-hour pure Mg extract all had similar concentrations of Ca compared to control-treated OBs, irrespective of the Mg extract concentration (**Table 6.7**). The Ca concentration of the control, 0.1, 1 and 10 μL/mL samples were 223.7 ± 6.23, 221 ± 3.92, 224.7 ± 3.85 and 220.9 ± 8.13 μM respectively, and none reached statistical significance (*p*-value 0.96, 0.96 and 0.89 respectively). The Kruskal-Wallis ANOVA test *p*-value between test groups and control was 0.115 **Figure 6.8**.

Similarly, OBs treated with 72-hour $SrPO_4$-Mg extracts had very similar Ca concentrations compared to control-treated OBs irrespective of the concentration of the $SrPO_4$-Mg extracts with mean concentrations at 0.1, 1 and 10 μL/mL at 313.9 ± 28.24, 315.3 ± 29.82 and 315.4 ± 35.18 μM respectively, with the control Ca concentration at 314.8 ± 27.26 μM, with no treatment reaching statistical significance. The Kruskal-Wallis ANOVA test *p*-value between test groups and control was 0.951 **Figure 6.9**.

OBs treated with 72-hour Ag-$SrPO_4$-Mg extracts at 0.1 and 1 μL/mL had Ca concentrations of 317.4 ± 26.6 and 317.7 ± 27.58 μM, compared to the control concentration of 314.8 ± 27.26 μM. Although the extract at 10 μL/mL showed increased Ca concentration at 324.7 ± 30.34 μM, none of the concentrations showed statistical significance, with *p*-values of 0.48, 0.48 and 0.18 for concentrations of 0.1, 1 and 10 μL/mL respectively. The Kruskal-Wallis ANOVA test *p*-value between test groups and control was 0.812 **Figure 6.10**.

Table 6.7 – Calcium concentration in mineralization assays of OBs treated with 72-hour extracts at concentrations of 0.1, 1 and 10 μL/mL (n=6).

A

Treatment: 72-hour extract	Extract concentration (μL/mL)	Calcium concentration (μM) mean ± s.e.m	*p*-value
PBS	10	223.7 ± 6.23	N/A
Mg	0.1	221 ± 3.92	0.96
Mg	1	224.7 ± 3.85	0.96
Mg	10	220.9 ± 8.13	0.89

B

Treatment: 72-hour extract	Extract concentration (μL/mL)	Calcium concentration (μM) mean ± s.e.m	*p*-value

PBS	10	314.8 ± 27.26	N/A
$SrPO_4$-Mg	0.1	313.9 ± 28.24	0.73
$SrPO_4$-Mg	1	315.3 ± 29.82	0.94
$SrPO_4$-Mg	10	315.4 ± 35.18	> 0.99

C

Treatment: 72-hour extract	**Extract concentration (µL/mL)**	**Calcium concentration (µM) mean ± s.e.m**	***p*-value**
PBS	10	314.8 ± 27.26	N/A
Ag-$SrPO_4$-Mg	0.1	317.4 ± 26.6	0.48
Ag-$SrPO_4$-Mg	1	317.7 ± 27.58	0.48
Ag-$SrPO_4$-Mg	10	324.7 ± 30.34	0.18

A. 72-hour Mg extract. **B.** 72-hour $SrPO_4$-Mg extract. **C.** 72-hour Ag-$SrPO_4$-Mg extract.

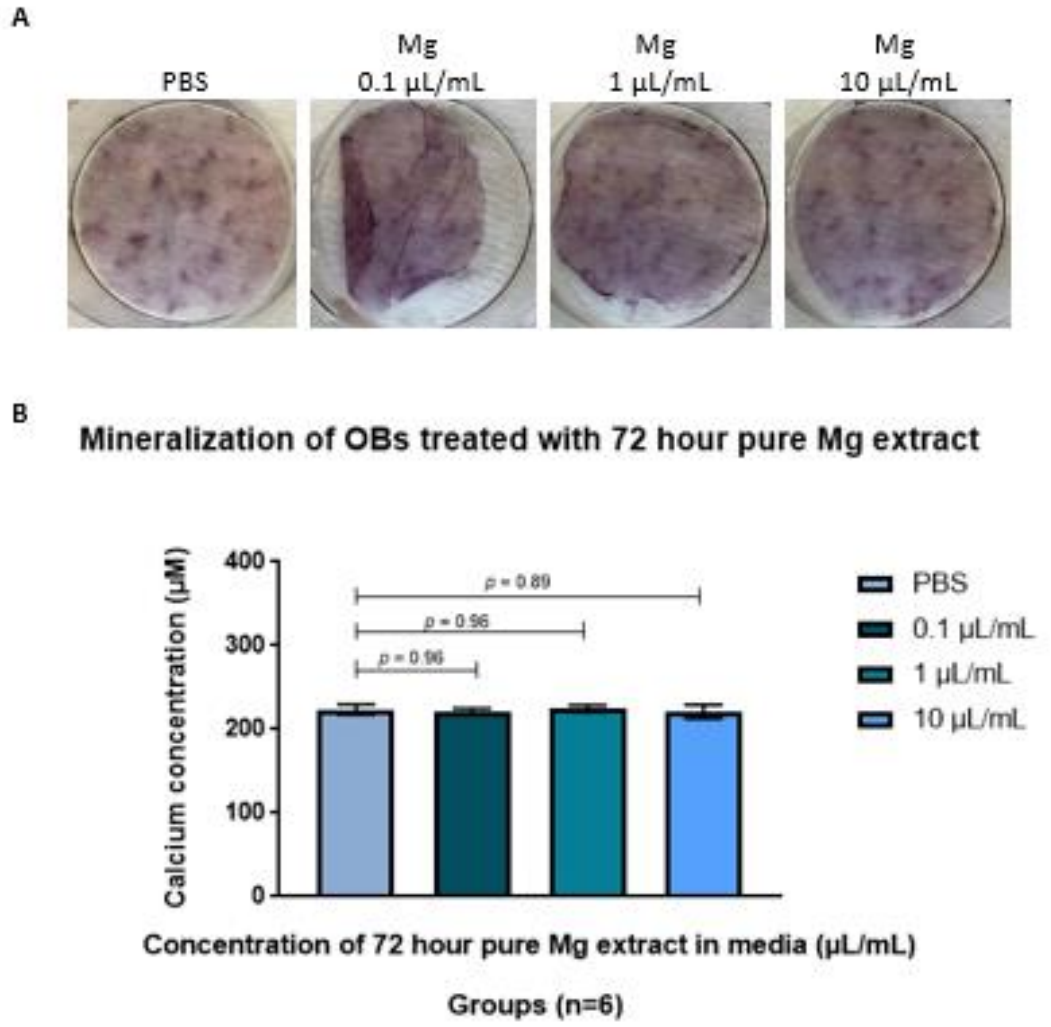

Figure 6.8 – **Mineralization of OBs treated with 72-hour pure Mg extracts (n=6).**

A. Photographs showing AR-S staining of OBs prior to the extraction with CPC: OBs treated with PBS control and 72-hour pure Mg extracts at concentrations of 0.1, 1 and 10 µL/mL from left to right. **B.** Concentrations of Ca in OBs treated with control and 72-hour Mg extracts at concentrations of 0.1, 1 and 10 µL/mL were 223.7 ± 6.23, 221 ± 3.92, 224.7 ± 3.85 and 220.9 ± 8.13 µM respectively. None of the Mg-treated samples had a statistically significant difference compared to the control sample OBs with *p*-values of 0.96, 0.96 and 0.89 respectively. All treatments had 6 replicates, performed over two experiments.

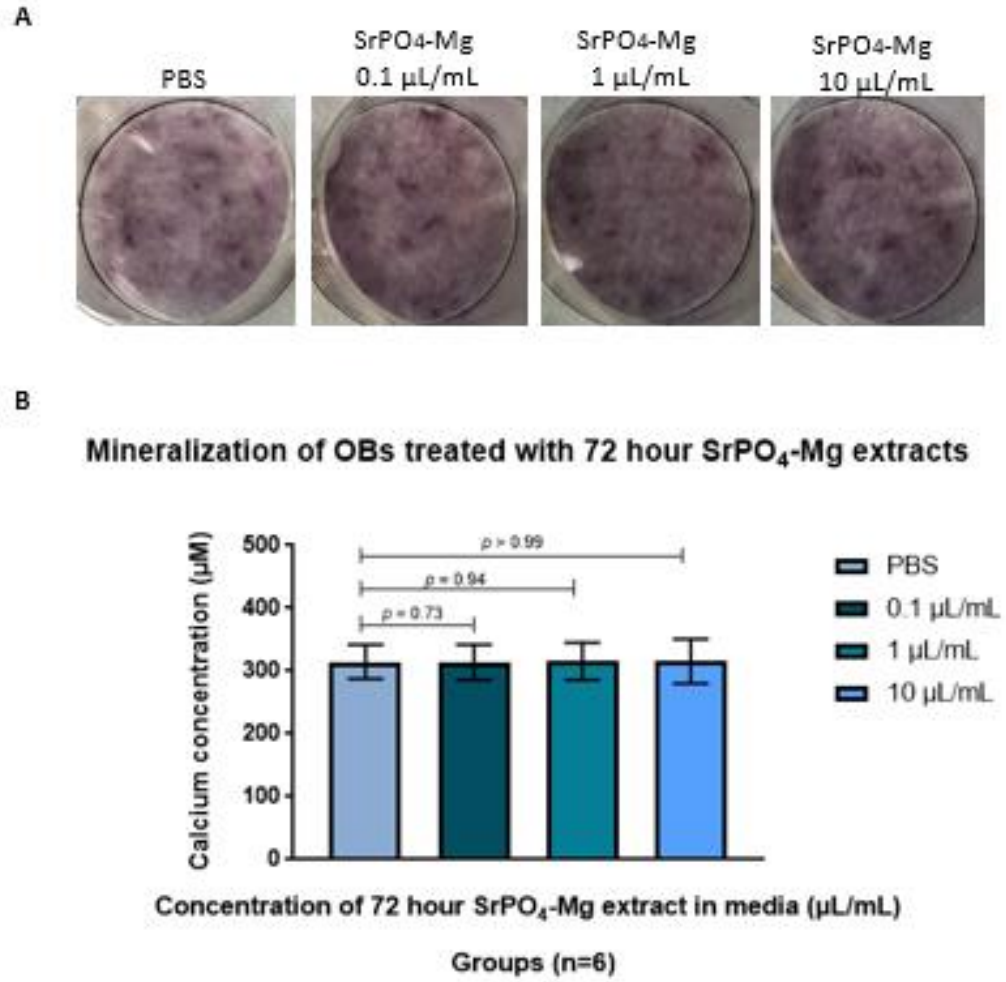

Figure 6.9 – **Mineralization of OBs treated with 72-hour $SrPO_4$-Mg extracts (n=6).**

A. Photographs showing AR-S staining of OBs prior to the extraction with CPC: OBs treated with PBS control and 72-hour $SrPO_4$-Mg extracts at concentrations of 0.1, 1 and 10 µL/mL from left to right. **B.** Concentrations of Ca in OBs treated with control and 72-hour $SrPO_4$-Mg extracts at concentrations of 0.1, 1 and 10 µL/mL were 314.8 ± 27.26, 313.9 ± 28.24, 315.3 ± 29.82 and 315.4 ± 35.18 µM respectively. None of the $SrPO_4$-Mg-treated samples had a statistically significant difference compared to the control sample OBs with *p*-values of 0.73, 0.94 and >0.99 respectively. All treatments had 6 replicates, performed over two experiments.

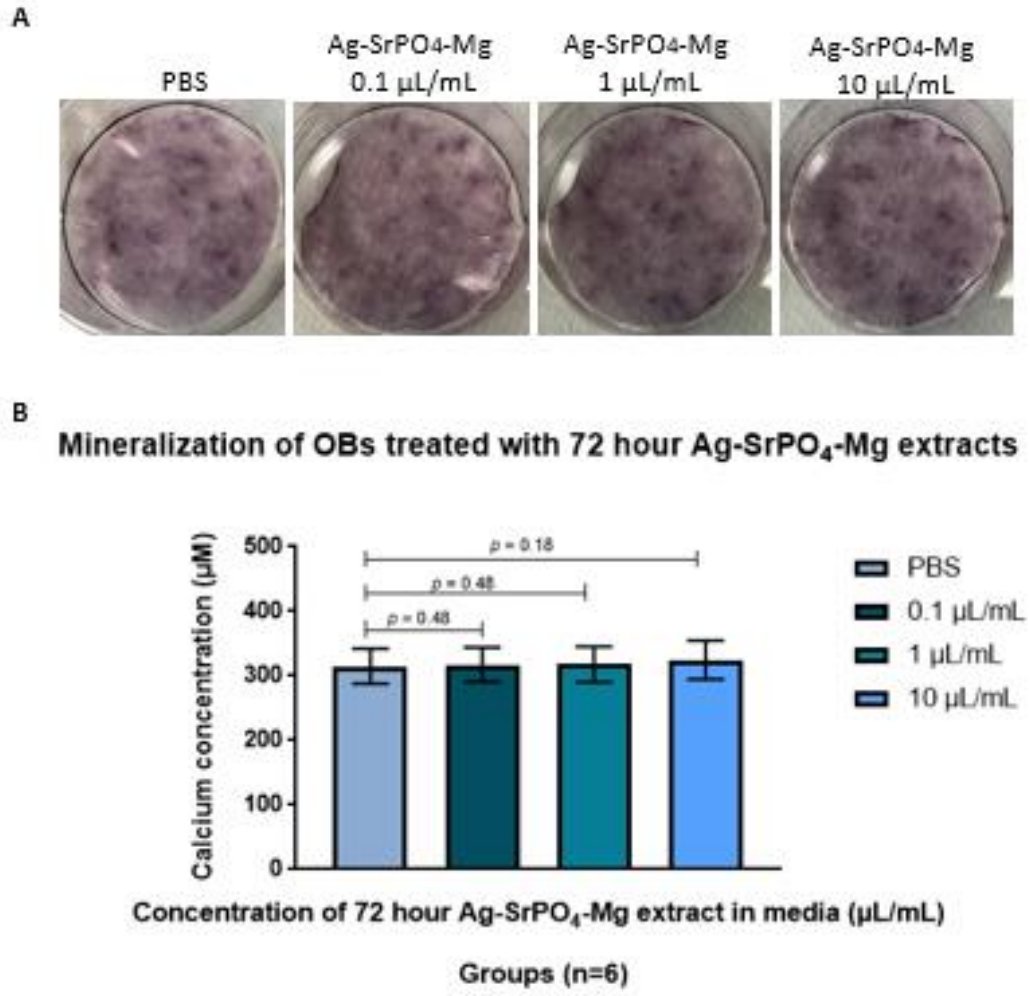

Figure 6.10 – **Mineralization of OBs treated with 72-hour Ag-$SrPO_4$-Mg extracts (n=6).**

A. Photographs showing AR-S staining of OBs prior to the extraction with CPC: OBs treated with PBS control and 72-hour Ag-$SrPO_4$-Mg extracts at concentrations of 0.1, 1 and 10 µL/mL from left to right. **B.** Concentrations of Ca in OBs treated with control and 72-hour Ag-$SrPO_4$-Mg extracts at concentrations of 0.1, 1 and 10 µL/mL were 314.8 ± 27.26, 317.4 ± 26.6, 317.7 ± 27.58 and 324.7 ± 30.34 µM respectively. There were no statistically significant differences between the Ag-$SrPO_4$-Mg-treated samples and the control with *p*-values of 0.48, 0.48 and 0.18, respectively. All treatments had 6 replicates, performed over two experiments.

6.3.3 - OB mineralization with 7-day extracts

OBs treated with 7-day pure Mg extract at concentrations of 0.1, 1 and 10 μL/mL all had higher Ca concentrations (238.1 ± 8.17, 233.4 ± 8.01 and 242.7 ± 10.16 μM) than control-treated OBs at 229.6 ± 8.12 μM but these differences were not statistically significant (*p*-value 0.44, 0.62 and 0.21 respectively). The Kruskal-Wallis ANOVA test *p*-value between test groups and control was 0.798 **Table 6.8, Figure 6.11**.

OBs treated with 7-day $SrPO_4$-Mg extracts had very similar Ca concentrations compared to control-treated OBs irrespective of the concentration of the $SrPO_4$-Mg extracts with mean concentrations at 0.1, 1 and 10 μL/mL of 201 ± 6.32, 205.8 ± 4.25 and 202.1 ± 7.96 μM respectively, with the control Ca concentration of 209.1 ± 7.04 μM with no treatment reaching statistical significance. The Kruskal-Wallis ANOVA test *p*-value between test groups and control was 0.965 **Figure 6.12**.

OBs treated with 7-day Ag-$SrPO_4$-Mg extracts at 0.1 and 1 μL/mL had similar Ca concentrations (208 ± 7.51 and 207.2 ± 5.14 μM) to the control concentration of 203.1 ± 7.04 μM and there was no statistically significant difference (*p*-value >0.99 and 0.75 respectively). Ag-$SrPO_4$-Mg extract at 10 μL/mL resulted in a decrease in mineralization, with a Ca concentration of 180 ± 8.54 μM but this did not reach statistical significance (*p*-value 0.129). The Kruskal-Wallis ANOVA test *p*-value between test groups and control was 0.157 **Figure 6.13**.

Table 6.8 – Calcium concentration in mineralization assays of OBs treated with 7-day extracts at concentrations of 0.1, 1 and 10 μL/mL (n=6).

A

Treatment: 7-day extract	Extract concentration (μL/mL)	Calcium concentration (μM) mean ± s.e.m	*p*-value
PBS	10	229.6 ± 8.12	N/A
Mg	0.1	238.1 ± 8.17	0.44
Mg	1	233.4 ± 8.01	0.62
Mg	10	242.7 ± 10.16	0.21

B

Treatment: 7-day extract	Extract concentration (μL/mL)	Calcium concentration (μM) mean ± s.e.m	*p*-value

PBS	10	203.1 ± 7.04	N/A
$SrPO_4$-Mg	0.1	201 ± 6.32	0.75
$SrPO_4$-Mg	1	205.8 ± 4.25	0.66
$SrPO_4$-Mg	10	202.1 ± 7.96	0.49

C

Treatment: 7-day extract	**Extract concentration (µL/mL)**	**Calcium concentration (µM) mean ± s.e.m**	***p*-value**
PBS	10	203.1 ± 7.04	N/A
Ag-$SrPO_4$-Mg	0.1	208 ± 7.51	>0.99
Ag-$SrPO_4$-Mg	1	207.2 ± 5.14	0.75
Ag-$SrPO_4$-Mg	10	180 ± 8.54	0.129

A. 7-day Mg extract. **B.** 7-day $SrPO_4$-Mg extract. **C.** 7-day Ag-$SrPO_4$-Mg extract.

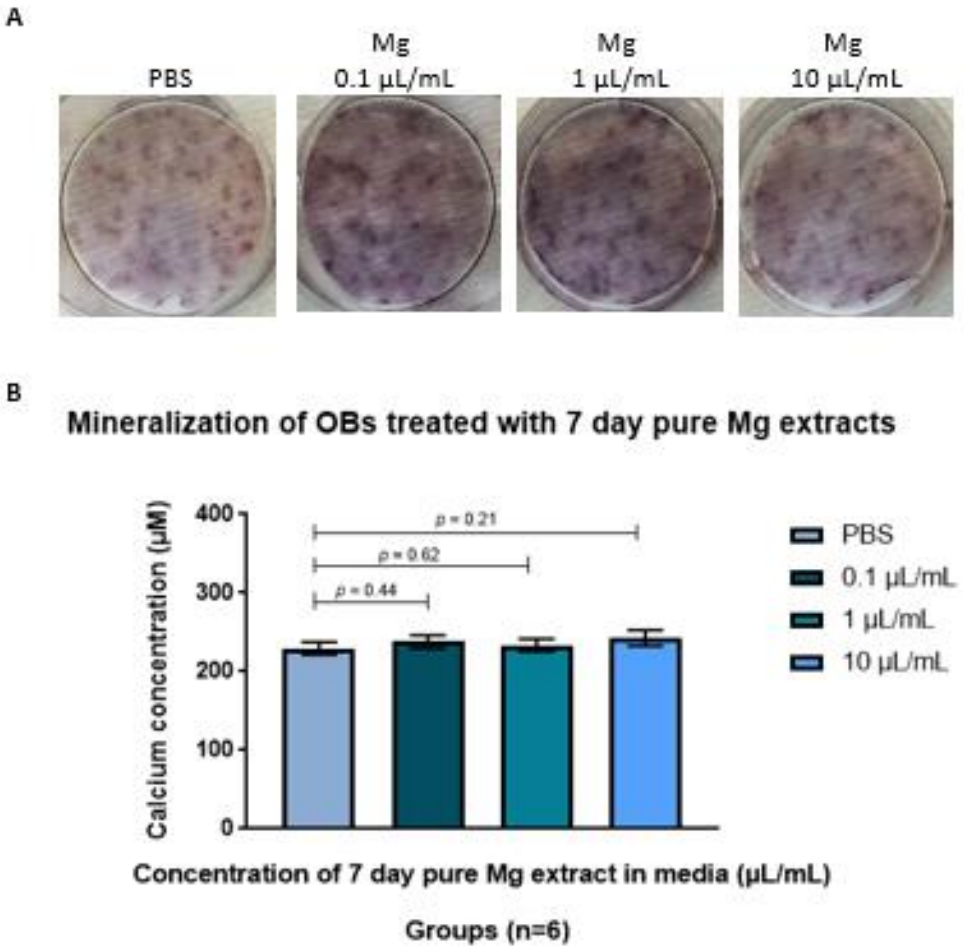

Figure 6.11 – **Mineralization of OBs treated with 7-day pure Mg extracts (n=6).**

A. Photographs showing AR-S staining of OBs prior to the extraction with CPC: OBs treated with PBS control and 7-day pure Mg extracts at concentrations of 0.1, 1 and 10 µL/mL from left to right. **B.** Concentrations of Ca in OBs treated with control and 7-day Mg extracts at concentrations of 0.1, 1 and 10 µL/mL were 229.6 ± 8.12, 238.1 ± 8.17, 233.4 ± 8.01 and 242.7 ± 10.16 µM respectively. None of the Mg-treated samples had a statistically significant difference compared to the control sample OBs with *p*-values of 0.44, 0.62 and 0.21 respectively. All treatments had 6 replicates, performed over two experiments.

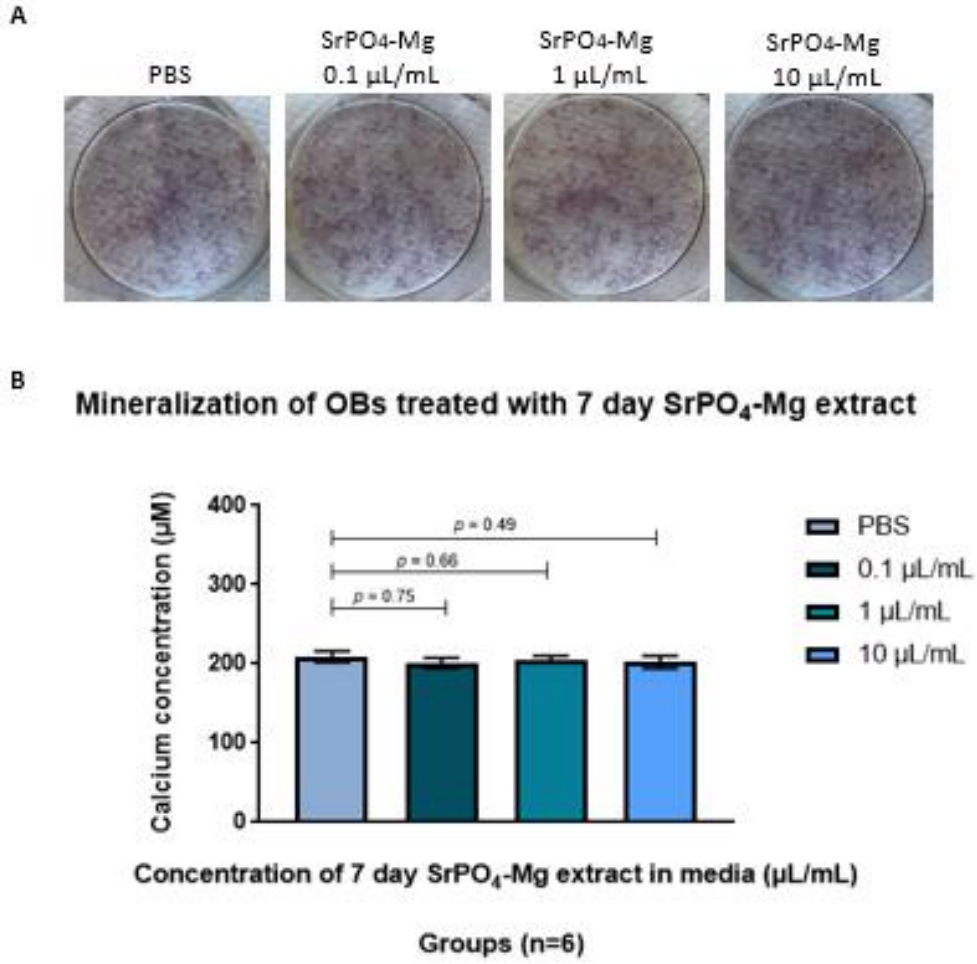

Figure 6.12 – **Mineralization of OBs treated with 7-day $SrPO_4$-Mg extracts (n=6).**

A. Photographs showing AR-S staining of OBs prior to the extraction with CPC: OBs treated with PBS control and 7-day $SrPO_4$-Mg extracts at concentrations of 0.1, 1 and 10 µL/mL from left to right. **B.** Concentrations of Ca in OBs treated with control and 7-hour $SrPO_4$-Mg extracts at concentrations of 0.1, 1 and 10 µL/mL were 209.1 ± 7.04, 201 ± 6.32, 205.8 ± 4.25 and 202.1 ± 7.96 µM respectively. None of the $SrPO_4$-Mg-treated samples had a statistically significant difference compared to the control sample OBs with *p*-values of 0.75, 0.66 and 0.49 respectively. All treatments had 6 replicates, performed over two experiments.

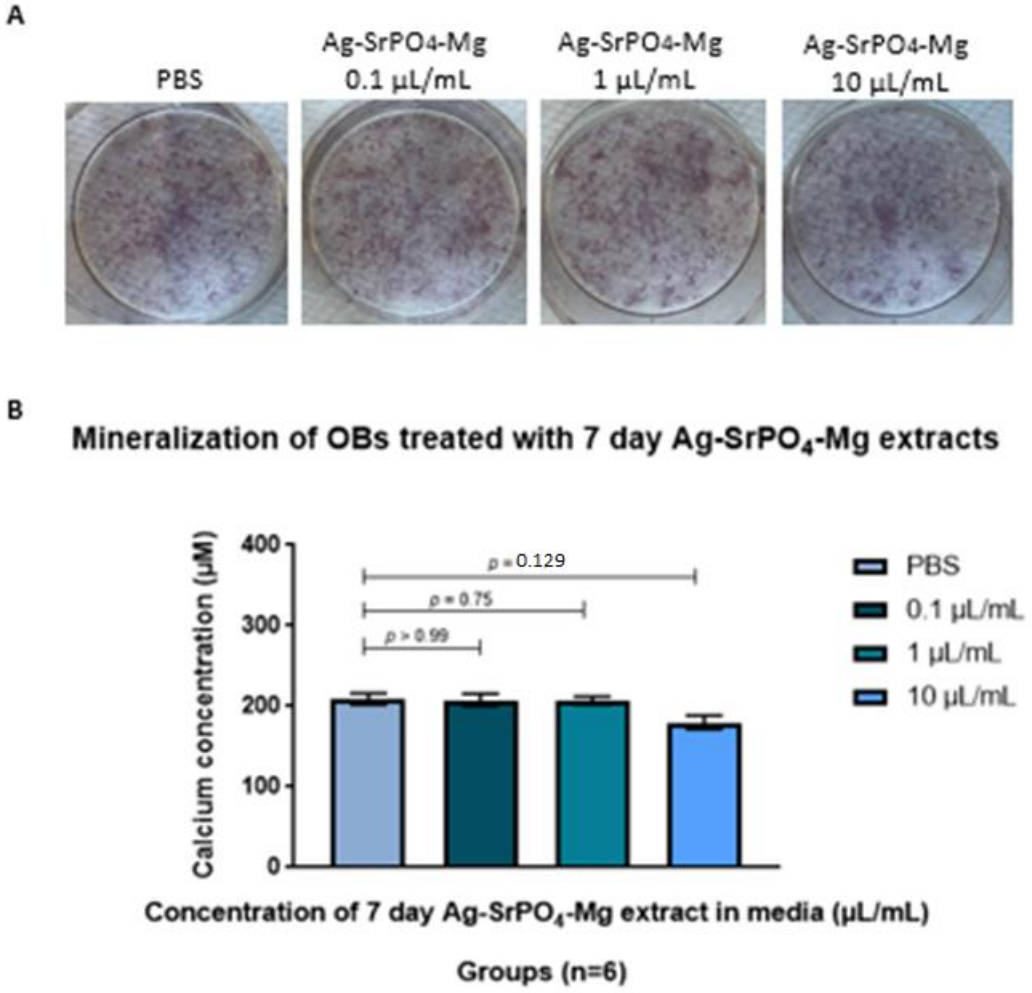

Figure 6.13 – **Mineralization of OBs treated with 7-day Ag-$SrPO_4$-Mg extracts (n=6).**

A. Photographs showing AR-S staining of OBs prior to the extraction with CPC: OBs treated with PBS control and 7-day Ag-$SrPO_4$-Mg extracts at concentrations of 0.1, 1 and 10 µL/mL from left to right. **B.** Concentrations of Ca in OBs treated with control and 7-day Ag-$SrPO_4$-Mg extracts at concentrations of 0.1, 1 and 10 µL/mL were 203.1 ± 7.04, 208 ± 7.51, 207.2 ± 5.14 and 180 ± 8.54 µM respectively. There was no statistically significant difference in Ca concentration between control and Ag-$SrPO_4$-Mg-treated at 10, 1 and 0.1 µL/mL compared to the control. All treatments had 6 replicates, performed over two experiments.

6.3.4 - OB mineralization with 14-day extracts

OBs treated with 14-day pure Mg extract at a concentration of 0.1 μL/mL had a slightly lower Ca concentration (221.8 ± 3.27 μM) compared to the control (229.7 ± 9.31 μM) whilst extract concentration at 1 and 10 μL/mL were higher than the control at 236.7 ± 8.54 and 236.5 ± 10.21 μM, respectively, although none of the differences were statistically significant. The Kruskal-Wallis ANOVA test *p*-value between test groups and control was 0.643 **Table 6.9**, **Figure 6.14**.

By comparison, OBs treated with 14-day $SrPO_4$-Mg extracts had concentration of 10 μL/mL had the lowest Ca concentration at 183.3 ± 10.26 μM whilst both the 0.1 and 1 μL/mL extracts had higher Ca concentrations of 195.2 ± 6.78 and 197.2 ± 5.68 μM respectively compared to a control concentration of 187.2 ± 4.26 μM. None of the differences between the test samples and control samples were of statistical significance. The Kruskal-Wallis ANOVA test *p*-value between test groups and control was 0.459 **Figure 6.15**.

14-day Ag-$SrPO_4$-Mg extract at a concentration of 1 μL/mL seemed to stimulate mineralization with a Ca concentration of 203.8 ± 7.4 μM compared to control Ca concentration of 187.2 ± 4.26 μM and this was narrowly below statistical significance with a *p*-value of 0.08. OBs treated with extract at concentrations of 0.1 and 10 μL/mL both had higher Ca concentrations (195.1 ± 8.48, 193 ± 10.68 μM, respectively) compared to the control, but neither reached statistical significance. The Kruskal-Wallis ANOVA test *p*-value between test groups and control was 0.481 **Figure 6.16**.

Table 6.9 – Calcium concentration in mineralization assays of OBs treated with 14-day extracts at concentrations of 0.1, 1 and 10 μL/mL (n=6).

A

Treatment: 14-day extract	Extract concentration (μL/mL)	Calcium concentration (μM) mean ± s.e.m	*p*-value
PBS	10	229.7 ± 9.31	N/A
Mg	0.1	221.8 ± 3.27	>0.99
Mg	1	236.7 ± 8.54	0.49
Mg	10	236.5 ± 10.21	0.49

B

Treatment: 14-day extract	Extract concentration	Calcium concentration (µM) mean ± s.e.m	*p*-value
PBS	10	187.2 ± 4.26	N/A
$SrPO_4$-Mg	0.1	195.2 ± 6.78	0.35
$SrPO_4$-Mg	1	197.2 ± 5.68	0.14
$SrPO_4$-Mg	10	183.3 ± 10.26	0.85

C

Treatment: 14-day extract	Extract concentration (µL/mL)	Calcium concentration (µM) mean ± s.e.m	*p*-value
PBS	10	187.2 ± 4.26	N/A
Ag-$SrPO_4$-Mg	0.1	195.1 ± 8.48	0.57
Ag-$SrPO_4$-Mg	1	203.8 ± 7.4	0.08
Ag-$SrPO_4$-Mg	10	193 ± 10.68	0.57

A. 14-day Mg extract. **B.** 14-day $SrPO_4$-Mg extract. **C.** 14-day Ag-$SrPO_4$-Mg extract.

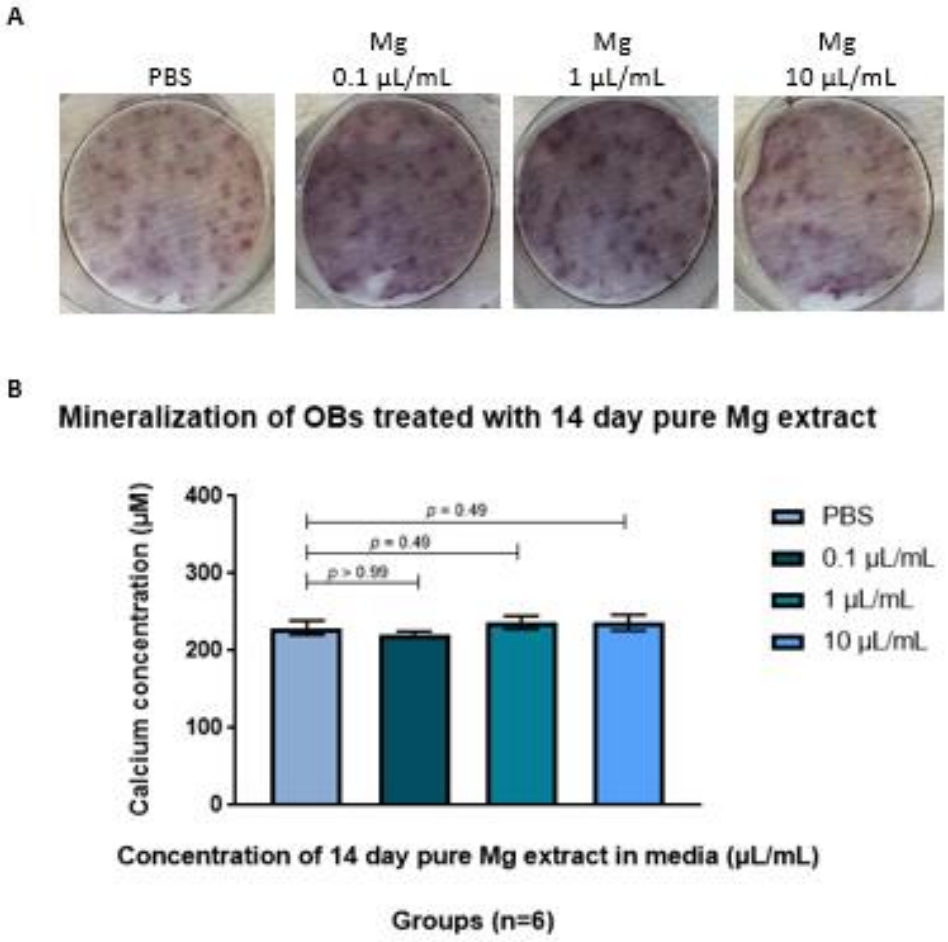

Figure 6.14 – **Mineralization of OBs treated with 14-day pure Mg extracts (n=6).**

A. Photographs showing AR-S staining of OBs prior to the extraction with CPC: OBs treated with PBS control and 14-day pure Mg extracts at concentrations of 0.1, 1 and 10 µL/mL from left to right. **B.** Concentrations of Ca in OBs treated with control and 14-day Mg extracts at concentrations of 0.1, 1 and 10 µL/mL were 229.7 ± 9.31, 221.8 ± 3.27, 236.7 ± 8.54 and 236.5 ± 10.21 µM respectively. None of the Mg-treated samples had a statistically significant difference compared to the control sample OBs with *p*-values of >0.99, 0.49 and 0.49 respectively. All treatments had 6 replicates, performed over two experiments.

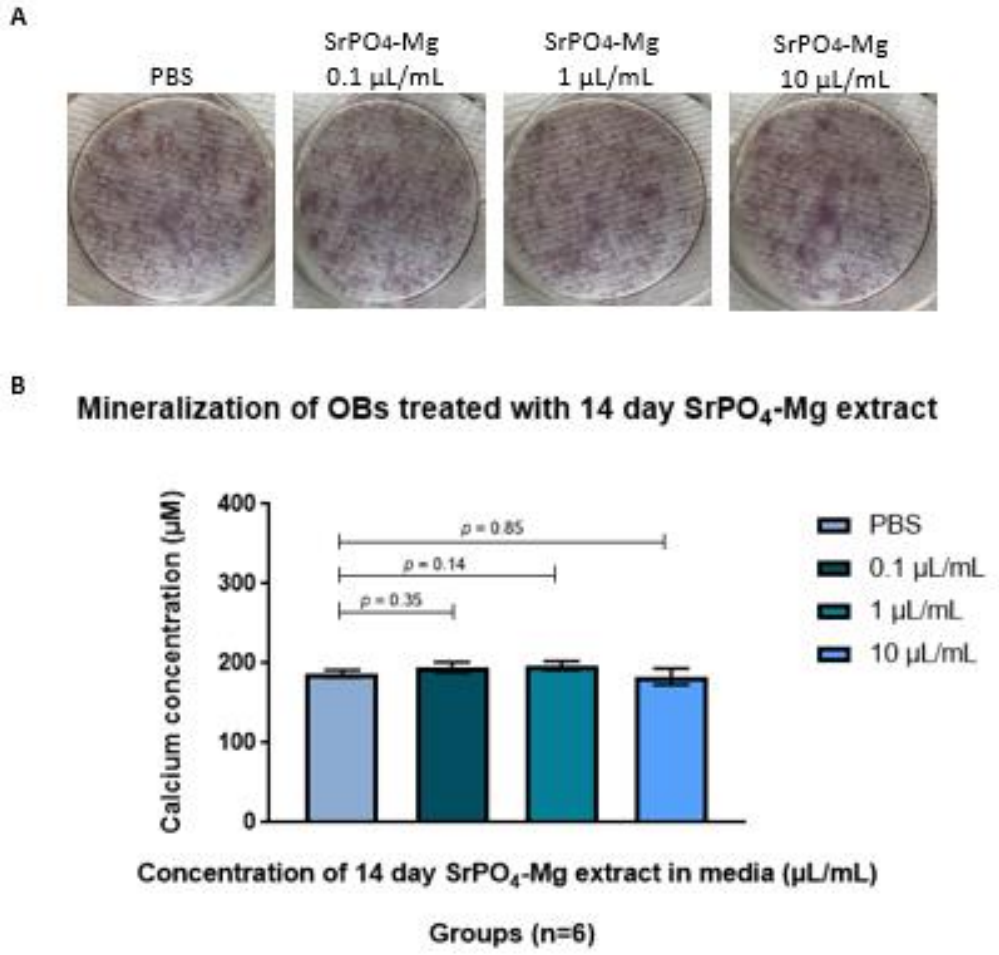

Figure 6.15 – **Mineralization of OBs treated with 14-day $SrPO_4$-Mg extracts (n=6).**

A. Photographs showing AR-S staining of OBs prior to the extraction with CPC: OBs treated with PBS control and 14-day $SrPO_4$-Mg extracts at concentrations of 0.1, 1 and 10 µL/mL from left to right. **B.** Concentrations of Ca in OBs treated with control and 14-hour $SrPO_4$-Mg extracts at concentrations of 0.1, 1 and 10 µL/mL were 187.2 ± 4.26, 195.2 ± 6.78, 197.2 ± 5.68 and 183.3 ± 10.26 µM respectively. None of the $SrPO_4$-Mg-treated samples had a statistically significant difference compared to the control sample OBs with *p*-values of 0.35, 0.14 and 0.85 respectively. All treatments had 6 replicates, performed over two experiments.

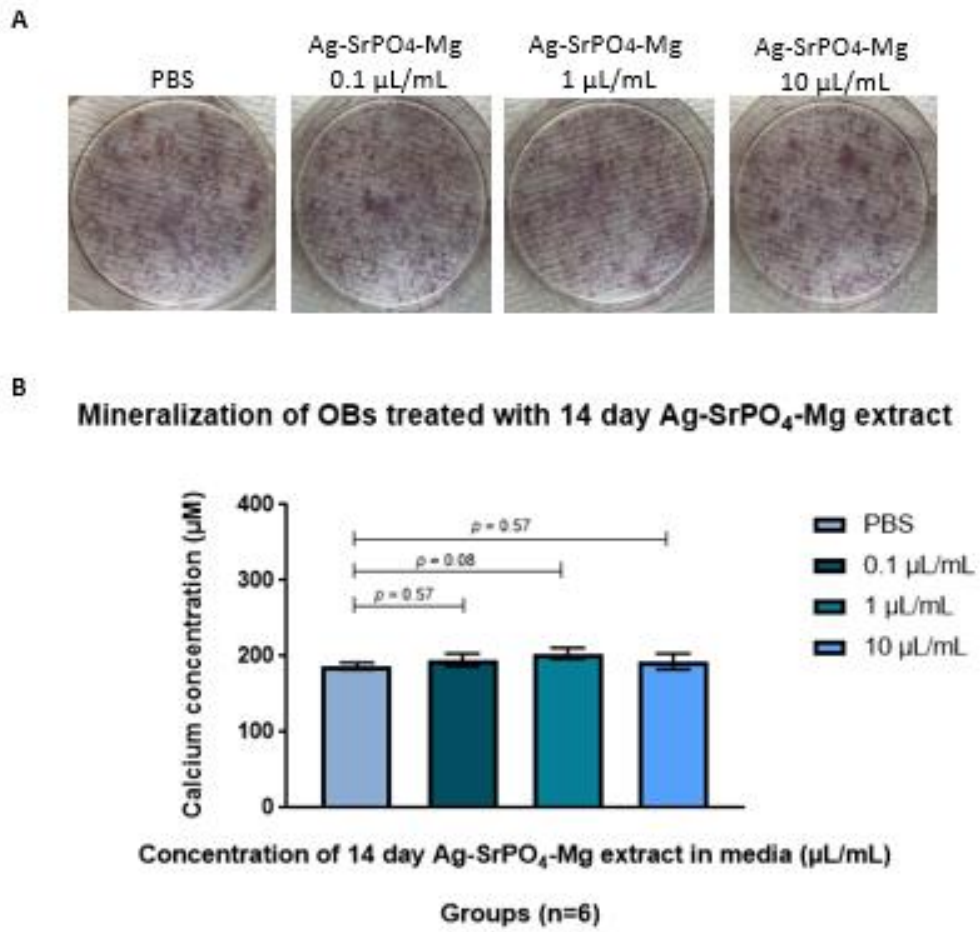

Figure 6.16 – **Mineralization of OBs treated with 14-day Ag-$SrPO_4$-Mg extracts (n=6).**

A. Photographs showing AR-S staining of OBs prior to the extraction with CPC: OBs treated with PBS control and 14-day Ag-$SrPO_4$-Mg extracts at concentrations of 0.1, 1 and 10 µL/mL from left to right. **B.** Concentrations of Ca in OBs treated with control and 14-day Ag-$SrPO_4$-Mg extracts at concentrations of 0.1, 1 and 10 µL/mL were 187.2 ± 4.26, 195.1 ± 8.48, 203.8 ± 7.4 and 193 ± 10.68 µM respectively. None of the Ag-$SrPO_4$-Mg-treated samples had a statistically significant difference compared to the control sample OBs with *p*-values of 0.57, 0.08 and 0.57 respectively. All treatments had 6 replicates, performed over two experiments.

6.3.5 - Inter-experiment variability between mineralization assay standards

Each experiment contained six standards, corresponding to six concentrations of ARS by absorbance measurement at 562 nm using the Infinite M200 PRO plate reader and i-control 1.9 program, were used to construct the standard curve from which the test sample Ca concentrations were interpolated. We compared the standards from six sets of mineralization assays with ANOVA and found there was no statistically significant inter-experiment variability between the standards, with a *p*-value >0.990 (**Table 6.10**).

Table 6.10 – Absorbance values of mineralization standards.

Standard Ca concentration (µM)	Assay 1	Assay 2	Assay 3	Assay 4	Assay 5	Assay 6
333	0.305	0.277	0.277	0.295	0.280	0.314
111	0.109	0.096	0.103	0.102	0.097	0.107
37	0.039	0.037	0.038	0.036	0.035	0.038
12	0.016	0.015	0.016	0.015	0.015	0.014
0.4	0.007	0.009	0.009	0.006	0.006	0.005
0.1	0.003	0.006	0.003	0.004	0.003	0.003

The six concentrations of ARS correspond to 333, 111, 37, 12, 0.4, and 0.1 µM of Ca with absorbance values measured at 562 nm using the Infinite M200 PRO plate reader and i-control 1.9 program. Inter-experiment variability between six assays had an ANOVA *p*-value > 0.999, showing no statistically significant difference between assays.

Chapter 7: Local tissue gene expression in response to PJI

7.1 - RNA quantification and quality

The concentration of the RNA extracted from capsular tissue of all patients was expressed in ng/µL and was shown in **Table 7.1**. Three out of the original fifteen patients were excluded from further analysis as two had insufficient levels of RNA and the third patient, from the PJI group, did not meet the MSIS criteria for a definitive PJI. All other RNA samples had A260/A280 and A260/A230 ratios greater than 2 and were deemed acceptable quality for cDNA synthesis further analysis with RT-qPCR and PCR-array.

7.2 - Differential gene expression using RT2 Profiler PCR Array

Quantitative PCR was performed on the cDNA samples using RT^2 Profiler PCR array Human Inflammatory Cytokines and Receptors and the data was entered into the Qiagen data analysis portal. The output data was examined, the outliers were eliminated, and data analysis performed again. A total of 58 genes were upregulated and 11 genes downregulated in the PJI group compared with the OA group, after normalizing to the GAPDH gene. Of the 58 upregulated genes, three had a statistically significant difference (p-value < 0.05). The genes were CCL20, CXCL6 and IL27 with upregulations of 6.58-fold, 6.81-fold, and 20.98-fold, respectively (**Table 7.2**). Of the downregulated genes, only TNFRSF11B was statistically significant and was downregulated 8.52-fold (**Table 7.3**).

Table 7.1 – Quantity and quality of mRNA isolated from joint capsular tissue of recruited patients.

Patient ID	RNA concentration (ng/µL)	A260/A280 ratio	A260/A230
Controls			
1	280.7	2.11	2.22
2	349.5	2.1	2.07
3	176.6	2.08	2.15
4	340.5	2.1	2.18
5	335.1	2.09	2.23
6	337.4	2.11	2.17
PJI			
7	376.2	2.13	2.16
8	606.87	2.11	2.29
9	673.1	2.11	2.24
10	669.9	2.11	2.31
11	874.7	2.10	2.07
12	773.5	2.08	2.16

Table 7.2 – Genes upregulated in PJI patients and degree of upregulation relative to control patients.

Gene symbol	Gene name	Fold up regulated	*p*-value
BMP2	Bone morphogenetic protein 2	3.00	0.30
CCL1	Chemokine (C-C motif) ligand 1	2.08	0.85
CCL11	Chemokine (C-C motif) ligand 11	6.60	0.36
CCL15	Chemokine (C-C motif) ligand 15	1.55	0.76
CCL16	Chemokine (C-C motif) ligand 16	5.50	0.28
CCL17	Chemokine (C-C motif) ligand 17	1.61	0.89

CCL20	**Chemokine (C-C motif) ligand 20**	**6.58**	**0.04**
CCL26	Chemokine (C-C motif) ligand 26	2.01	0.40
CCL3	Chemokine (C-C motif) ligand 3	1.76	0.56
CCL4	Chemokine (C-C motif) ligand 4	6.04	0.12
CCL5	Chemokine (C-C motif) ligand 5	2.6	0.41
CCL7	Chemokine (C-C motif) ligand 7	1.54	0.82
CCL8	Chemokine (C-C motif) ligand 8	1.55	0.47
CCR2	Chemokine (C-C motif) receptor 2	3.4	0.57
CCR3	Chemokine (C-C motif) receptor 3	2.5	0.20
CCR4	Chemokine (C-C motif) receptor 4	2.92	0.88
CCR5	Chemokine (C-C motif) receptor 5	4.53	0.74
CCR6	Chemokine (C-C motif) receptor 6	2.85	0.70
CCR8	Chemokine (C-C motif) receptor 8	2.49	0.70
CD40LG	CD40 ligand	2.35	0.44
CSF1	Colony stimulating factor 1 (macrophage)	2.28	0.71
CSF2	Colony stimulating factor 2 (granulocyte-macrophage)	2.70	0.39
CSF3	Colony stimulating factor 3 (granulocyte)	3.59	0.26
CX3CL1	Chemokine (C-X3-C motif) ligand 1	3.11	0.29
CX3CR1	Chemokine (C-X3-C motif) receptor 1	2.34	0.19
CXCL10	Chemokine (C-X-C motif) ligand 10	3.02	0.43
CXCL11	Chemokine (C-X-C motif) ligand 11	3.25	0.46
CXCL13	Chemokine (C-X-C motif) ligand 13	25.11	0.14
CXCL3	Chemokine (C-X-C motif) ligand 3	1.74	0.84
CXCL5	Chemokine (C-X-C motif) ligand 5	12.16	0.12
CXCL6	**Chemokine (C-X-C motif) ligand 6 (granulocyte chemotactic protein 2)**	**6.81**	**0.04**
CXCL9	Chemokine (C-X-C motif) ligand 9	1.74	0.89
CXCR1	Chemokine (C-X-C motif) receptor 1	2.24	0.58
CXCR2	Chemokine (C-X-C motif) receptor 2	21.25	0.21
IFNA2	Interferon, alpha 2	2	0.34
IFNG	Interferon, gamma	2.48	0.47
IL10RB	Interleukin 10 receptor, beta	1.50	0.57
IL13	Interleukin 13	3.67	0.22
IL16	Interleukin 16	2.83	0.62
IL17C	Interleukin 17C	15.18	0.21

IL17F	Interleukin 17F	4.75	0.64
IL1A	Interleukin 1, alpha	2.19	0.30
IL1B	Interleukin 1, beta	16.49	0.17
IL1RN	Interleukin 1 receptor antagonist	2	0.54
IL21	Interleukin 21	3.04	0.13
IL27	**Interleukin 27**	**20.98**	**0.03**
IL5RA	Interleukin 5 receptor, alpha	1.86	0.66
IL8	Interleukin 8	4.09	0.22
IL9	Interleukin 9	1.79	0.71
LTA	Lymphotoxin alpha (TNF superfamily, member 1)	1.97	0.43
LTB	Lymphotoxin beta (TNF superfamily, member 3)	4.08	0.44
MIF	Macrophage migration inhibitory factor (glycosylation-inhibiting factor)	1.59	0.53
OSM	Oncostatin M	2.69	0.47
SPP1	Secreted phosphoprotein 1	1.79	0.77
TNFSF11	Tumor necrosis factor (ligand) superfamily, member 11	2	0.57
TNFSF13	Tumor necrosis factor (ligand) superfamily, member 13	22.92	0.21
TNFSF13B	Tumor necrosis factor (ligand) superfamily, member 13b	3.6	0.49
TNFSF4	Tumor necrosis factor (ligand) superfamily, member 4	2.65	0.23

The genes CCL20, CXCL6 and IL27 in PJI patients were upregulated 6.58-fold, 6.81-fold and 20.98-fold respectively compared to controls, and all reached statistical significance (p-value < 0.05).

Table 7.3 – Genes downregulated in PJI patients and degree of downregulation relative to control patients.

Gene symbol	Gene name	Fold down regulated	*p*-value
C5	Complement component 5	-1.65	0.41
CCL2	Chemokine (C-C motif) ligand 2	-1.71	0.35
CCL22	Chemokine (C-C motif) ligand 22	-11.11	0.27
CCR1	Chemokine (C-C motif) receptor 1	-1.68	0.56

FASLG	Fas ligand (TNF superfamily, member 6)	-2.78	0.34
IL10RA	Interleukin 10 receptor, alpha	-2.23	0.27
IL33	Interleukin 33	-1.69	0.44
IL5	Interleukin 5 (colony-stimulating factor, eosinophil)	-4.50	0.36
TNFRSF11B	**Tumor necrosis factor receptor superfamily, member 11b**	**-8.52**	**0.03**
TNFSF10	Tumor necrosis factor (ligand) superfamily, member 10	-2.87	0.44
VEGFA	Vascular endothelial growth factor A	-1.56	0.35

The gene TNFRSF11B was downregulated 8.52-fold and reached statistical significance (*p*-value < 0.05).

Chapter 8: Thesis overview, limitations, and recommendations for future research directions

8.1 – Thesis overview

The emergence of antibiotic resistance is one that has well and truly transpired. Precipitating factors such as improper prescription of antimicrobials for non-bacterial infections as well as the gross overuse of antibiotics in the agricultural industry and diminished investment in novel agents by pharmaceutical companies have resulted in an ever-diminishing edge that mankind has enjoyed over bacterial infections over the past century. This is even more relevant in recent times as antimicrobial resistance has been exacerbated by the heavy use of antibiotics during the COVID-19 pandemic. Major advancements in nanotechnology have led to significant progress in designing antibacterial nanoparticles, of which Ag has been one of the most well-investigated. Antimicrobial properties alone, however, are no longer sufficient for biomaterials used in the field of orthopaedic surgery, particularly in arthroplasty where impacts are expected to provide a patient with satisfactory function of over a decade. A material should also have a similar Young's modulus to bone to prevent stress shielding, allows integration to promote bone healing, not stimulate the immune system to jeopardize implant longevity as well augment the natural function of the host.

There are currently no biomaterials used as a standard for comparing the antimicrobial properties of novel compounds. We found that Ag-$SrPO_4$-Mg had the greatest inhibitory effect against *S.aureus* and *E.coli* at 93.38 ± 1.31% and 85.8 ± 2.60% respectively, compared to the negative control. The inhibitory effect on *P.aeruginosa* and *S.epidermidis* were more modest, at 47.69 ± 13.27% and 32.09 ± 2.60% respectively. These differences may be explained by both the intrinsic characteristics of the bacteria, as well as the physical properties of the Ag-$SrPO_4$-Mg nanoparticles. In addition, we can further analyze the surface roughness of the Ag-$SrPO_4$-Mg and $SrPO_4$-Mg discs, both before and after immersion in BHI media using 3D measuring laser microscope to help us predict which bacteria are more likely to attach to the surface. The control metal discs utilized in our antibacterial experiments were stainless steel 316L discs which has not been shown in literature to possess antibacterial effects unless electrochemical modification has been performed on the surface, which was not the case for our stainless-steel samples.

8.1.1 – Antibacterial effect of Ag-$SrPO_4$-Mg on *S.aureus* and *S.epidermidis*

The degree of inhibition on *S.aureus* by Ag-$SrPO_4$-Mg is a clinically significant finding as it is the most common pathogen isolated in PJIs. There was no statistically significant difference in inhibition by Ag-$SrPO_4$-Mg, 0.5x MIC and MIC of oxacillin. Whereas antibiotics exert their effects on MSSA and MRSA through a single mode of action, such as inhibition of cell-wall synthesis, protein synthesis

or nucleotide synthesis, proteomic studies demonstrate that Ag and Ag^+ exert bactericidal properties by targeting multiple biological pathways, particularly the disruption of glycolysis and oxidative stress. Therefore theoretically, Ag-$SrPO_4$-Mg could overcome resistance in *S.aureus* since the probability of simultaneous mutation on multiple targets is much less likely than on a single target. It has been demonstrated that the mutation frequencies of resistance colonies of *S.aureus* against commonly used antibiotics including ampicillin, kanamycin, ciprofloxacin and tetracycline ranged from 2.9×10^{-8} to 6.3×10^{-6} compared to mutation frequencies of less than 1.0×10^{-10} for Ag^+ or AgNP and that ampicillin concentrations as high as 8-fold MIC failed to kill high-level resistant mutants of *S.aureus* whereas the number of mutant colonies decreased significantly when increasing concentrations of Ag^+ [264]. The development of Ag-resistance in *S.aureus* has been a subject of investigation: Randall et al [265] found that prolonged exposure to Ag^+ failed to select resistant mutants. The downside of utilizing Ag is that it can promote the co-emergence of antibiotic resistance in bacteria [266, 267].

The degree of inhibition of *S.epidermidis* by Ag-$SrPO_4$-Mg was significantly lower than that of all concentrations of oxacillin. We speculate that this was due to the size of the Ag-$SrPO_4$-Mg nanoparticles, as well as the strain of *S.epidermidis* used. A study by Swolana et al [270] showed that no antibacterial activity was observed using AgNPs above 40 nm against the ATCC 12228 strain of *S.epidermidis* whereas AgNPs 100 nm in diameter continued to have potent inhibitory effects against strains ATCC 36983 and ATCC 35984 of the same bacteria. We utilized the ATCC 1228 strain of *S.epidermidis* as this was the strain available at our research facility. However, literature suggests that this strain is a non-biofilm forming and non-infection associated strain [271] whereas the RP62A clinical isolate, synonymous with the ATCC 35984 strain, can form biofilms. Therefore, our findings may not be directly translatable to clinical findings in *S.epidermidis* PJI, as ATCC 12228 is not the predominant strain. The surface roughness of a material, as well as the material itself, also influences bacterial adhesion. In general, *S.epidermidis* has a greater affinity for rougher surfaces than finer surfaces and had a lower affinity for cobalt-chromium surfaces than pure titanium, titanium alloy, stainless steel and oxinium [272]. We found that the surface characteristics influenced bacterial adhesion tremendously, as demonstrated by the different densities of adherent *S.epidermidis* attached to different areas of the same Ag-$SrPO_4$-Mg disc, which may have been the result of the coating process. In addition, different bacterial species displayed different surface preferences: we observed that the same surface characteristics of the Ag-$SrPO_4$-Mg disc that favored *S.epidermidis* attachment inhibited *P.aeruginosa* attachment.

8.1.2 – Antibacterial effect of Ag-$SrPO_4$-Mg on *E.coli* and *P.aeruginosa*

We found that inhibition of *E.coli* by Ag-$SrPO_4$-Mg was profound and was significantly greater than that of gentamicin. However, a clinical consideration is that *E.coli* can develop Ag resistance with prolonged exposure to sublethal concentrations of Ag. Chronic exposure to $AgNO_3$ resulted in the downregulation of the major porins OmpF or both OmpF and OmpC which transport cations and small molecules, such as drugs and toxins, into the bacterial cells while simultaneously upregulating the expression of a natural copper binding/efflux (Cus) system which conferred cross resistance to Ag [268, 269]. This further supports the notion of combining intravenous antibiotics at the time of anaesthetic induction as well as Ag-$SrPO_4$-Mg coated prosthesis to eliminate all bacteria and not allow resistance to develop.

By its nature, *P.aeruginosa* is resistant to multiple antimicrobial agents and is extremely difficult to treat in PJIs. Therefore, the development of new therapies against *P.aeruginosa* is crucial. We have found that Ag-$SrPO_4$-Mg inhibited *P.aeruginosa* by 47.69 ± 13.27% and was significantly less than the MIC of gentamicin whereas $SrPO_4$-Mg showed almost no inhibition. Particle size of AgNPs seemed to have less influence on *P.aeruginosa* than on *S.epidermidis* due to the absence of the cell wall in Gram negative bacteria: studies have cited the MIC value of AgNPs at 40 nm and 121 nm at 12.5 µg/mL and 15 µg/mL respectively [273]. Based on these findings, we can conclude that AgNP size is not the only determining factor and the method of synthesis, capping agents and the presence of other elements were also important considerations. Areas on the Ag-$SrPO_4$-Mg disc with increased roughness and large irregular lattice structures harbored more bacteria than the less rough areas, consistent with previous findings that surface roughness correlates with bacterial adhesion.

We observed that $SrPO_4$-Mg also inhibited *S.aureus* by 41.3 ± 4.47% and *E.coli* by 46.46 ± 6.23%, a significant finding. There are currently conflicting findings in literature regarding the antibacterial role of Sr. Geng et al observed no inhibition of *S.aureus* or *E.coli* by pure Sr whereas Baheiraei et al showed that Sr doped bioactive glasses completely inhibited *E.coli* growth while partially inhibiting *S.aureus* [274, 275]. The inhibitory effect of $SrPO_4$-Mg on *S.epidermidis* and *P.aeruginosa* were minimal.

8.1.3 – Bioactivity of Ag-$SrPO_4$-Mg on OBs

The ALP assay demonstrated that OBs treated with 24-hour extracts of $SrPO_4$-Mg at 1 and 0.1 µL/mL had the greatest relative ALP expression at of 1.41 ± 0.16 and 1.48 ± 0.23 times respectively, compared to controls but neither reached statistical significance (*p*-values 0.20 and 0.06, respectively). All OBs treated with 7-day extracts had reduced relative ALP expression compared to controls but the Kruskal-Wallis test *p*-value between the 7-day extracts of Ag-$SrPO_4$-Mg, $SrPO_4$-Mg

and pure Mg at three concentrations did not reach statistical significance. The only statistically significance difference seen with 14-day extract was seen with $SrPO_4$-Mg at 0.1 µL/mL, where a relative expression of 0.74 was observed. Although the Mann-Whitney U-test showed statistically significant increases and decreases between the test samples and controls, the Kruskal-Wallis ANOVA test *p*-values between test samples did not reach significance and therefore the clinical significance of our findings is unclear.

The degree of mineralization of OBs in our experiments did not seem to be affected significantly by extracts of pure Mg, $SrPO_4$-Mg and Ag-$SrPO_4$-Mg at concentrations of 0.1, 1 and 10 µL/mL for all time points. The OBs treated with 14-day extract of Ag-$SrPO_4$-Mg at 1 µL/mL had a Ca concentration of 203.8 ± 7.4 µM compared to controls with a Ca concentration of 187.2 ± 4.26 µM. This difference approached, but did not reach, statistical significance (*p*-value 0.08). One of the concerns regarding Ag containing biomaterials is the potential implications of cytotoxicity but our experiments did not demonstrate reduced bioactivity to OBs compared to controls, Mg and $SrPO_4$-Mg. However, we also did not observe increased ALP expression or mineralization of OBs with $SrPO_4$-Mg treatment, which had been shown in previous studies performed by our group. One possible explanation is the Ag coating on the $SrPO_4$-Mg base continued to remain on the surface of the disc after 14 days, therefore very little Sr and Mg were released into the extract solution. However, this would not explain why the $SrPO_4$-Mg and Mg extracts also displayed no additional bioactivity compared to the PBS control. Another explanation is that we used primary human OBs in our experiments instead of a commonly used cell line, such as MC3T3-E1. These cells had been harvested from donors several years prior to our experiment and stored at -80 ^{o}C. We used primary human OBs between passages 2 and 6 in all our experiments as we wanted to simulate a more realistic host response to our novel compound. The characteristic trait of OB cell lines derived from osteosarcomas is the cells are selected for their oncogenic potential rather than to OB properties. One possible explanation for similar expression of ALP between treated samples and our control samples is that treatment extracts were added on day 3 after seeding of the cells to allow greater confluence. The literature suggest that the early proliferative phase of OBs continues for several days after confluence and begin to exit the cell cycle between days 3 and 7 [276] therefore addition of the extracts on day 3 should still influence ALP expression but a modification to the experiment would be addition of the extracts on day 0 or day 1 after seeding and is an area for future studies. We always sub-cultured the cells at approximately 80% confluence for ALP assay and mineralization assays to prevent over-confluence and progression of OB to osteocytes. Another explanation for the lack of increased bioactivity observed after treatment with extracts is the biology of the cells. Although the cell passages we used were within the recommended passages for primary cell culture, we noted that from passage 4 onwards, the OBs often lost their cuboid shapes and often assumed a more stellate shape seen in osteocytes, even before the cells became confluent, an observation that was consistent with all primary human OBs we used, regardless of the donor

patient. In addition, we noted that OBs from certain patients expressed lower levels of ALP compared to other patients, even when the passage number had been adjusted for, which may be attributed to genetic differences or medical conditions of the patient. Therefore, we used relative ALP expression of test samples compared to control samples, rather than absolute ALP levels, to minimize the effect of confounding between different patients. In the strict sense, we tested for the bioactivity of the treatment extracts on OBs only, based on ALP levels and mineralization, but not cytotoxicity, which would be more accurately tested with a cytotoxicity test such as the neutral red uptake assay. However, we did not observe gross signs of cell apoptosis such as cell-blebs forming when viewing the cells under light microscopy. Cytotoxicity studies using neutral red uptake assay is another study for future directions. It is also important to note that all cell culture experiments we conducted were with OBs whereas in an in-vivo environment, there is continuous co-regulation between OBs and OCs, in particular the RANK-RANKL-OPG pathway, and therefore another area of further study is the explore the effects of $SrPO_4$-Mg and $AgSrPO_4$-Mg on OB-OC co-cultures, as literature shows Sr reduces OC activity by decreasing differentiation and intensifying the apoptosis of mature OCs. In addition, adverse tissue reactions in response to the release of cobalt and chromium ions from metal-on-metal prosthesis generates aseptic lymphocyte-dominant vasculitis-associated lesions (ALVAL) culminating in detrimental local and systemic effects on the patient. It is therefore imperative for future studies to examine the in-vivo effects of $AgSrPO_4$-Mg using animal studies to determine if adverse local tissue reactions occur.

A challenge with Ag-coating that has been cited in literature is establishing a strong attachment of OBs to the surface. Geng et al [274] have demonstrated that OB attachment on Ag-coated HA was scant and displayed an elongated morphology with few filopodia compared to Sr-coated HA and uncoated HA. The addition of Sr to Ag-coated HA resulted in an increase in the confluence of OBs compared to Ag-HA but was still significantly less than pure HA and Sr-HA. The clinical implications of this observation in orthopaedics are that there will be reduced ongrowth and ingrowth of host bone onto the prosthesis, therefore increasing micromotion and instability of the prosthesis. We did not examine the attachment properties of OBs to the surface of Ag-$SrPO_4$-Mg and is therefore an area that requires further investigation.

8.1.4 – Genetic changes in capsular tissue of PJI patients

The patients in our PJI group were matched by age and gender to those in the control group and were not on immunosuppressive medications such as steroids or biologics as such agents inhibit the patient from mounting a normal immune response and alter gene expression. We noted that patient TC9 had a higher cycle number, and therefore lower expression of most of the genes in the PCR array compared to the other PJI patients. This may be explained by the fact that the patient sustained the neck of femur fracture six months prior to the time of tissue sampling, which required surgical fixation which failed

due to non-union of the fracture and collapse requiring a conversion to arthroplasty. The nature of the injury combined with multiple operations culminated in ample scar tissue formation in the hip, which may not be able to mount the expected immune response to an infection. However, despite having a lower expression of most genes, exclusion of this patient from the final analysis on GeneGlobe did not change the outcome for the genes we investigated.

Previous studies have identified several genes that were upregulated in PJI by a minimum of 2-fold [277]. These genes are primarily involved in immune function, cell development and repair function and include: Alpha-2-macroglobulin (A2M), B2M, BPI, Calcitonin receptor (CALCR), Cathelicidin antimicrobial peptide (CAMP/LL37), CCL3-5, CSF2RA, CSF2RB, CSF3, CXCL2, defensin (DEFA4), neutrophil elastase (ELANE), leukocyte esterase (ESD), Fc fragment of IgG receptor Ia (FCGR1A), FCGR1B, FGF2, intercellular adhesion molecule 1 (ICAM1), IFNG, IL10, IL10RA, IL10RB, IL17D, IL1A, IL1B, IL1RN, IL5RA, IL6, IL8, lipopolysaccharide binding protein (LBP), lipocalin 2 (LCN2), lactate dehydrogenase (LDH) A-D, lactotransferrin (LTF), MMP3, peptidase inhibitor 3 (PI3), resistin (RETN), thrombospondin 1 (THBS1), tissue inhibitor of metalloproteinase 1 (TIMP1), TNF, VEGFA-C and von Willebrand factor (VWF).

We have identified four genes that were expressed differentially between PJI cases and uninfected cases. CCL20, CXCL6 and IL27 were upregulated while TNFRSF11B was downregulated. CCL20 and CXCL6 expression in synovial fluid and sonicate fluid in PJI have only been mentioned recently. The expression of IL27 and TNFRSF11B, and expression of CCL20 and CXCL6 in capsule tissue, have not, to the best of our knowledge, been mentioned previously in literature to be associated with PJI.

CCL20, belonging to the CC chemokine family, is strongly chemotactic for lymphocytes but weakly attracts neutrophils and is implicated in several autoimmune processes including psoriasis, cancer, RA and diabetes via the STAT and Nfκβ signal pathways. Proinflammatory cytokines and lipopolysaccharide (LPS) induce the production of CCL20 by PBMCs, monocytes, macrophages, neutrophils, endothelial and epithelial cells. It binds to only to CCR6, expressed on T cells, B cells and dendritic cells to migrate towards CCL20 and induces a proinflammatory phenotype in macrophages [278]. Masters et al [277] have demonstrated recently that CCL20 was upregulated in sonicate fluid of patients with PJI compared to aseptic revisions making it a potential diagnostic marker for PJI. The specific binding of CCL20 to CCR6 carries the implication that CCL20 may be a future drug target. Indeed, modulation of the CCL20-CCR6 axis is already in its preclinical stages with biological agents such as infliximab and etanercept (279) but these applications in PJI is unclear: whilst inhibition of CCL20-CCR6 may dampen inflammation and osteolysis around the infected

implant, it may be simultaneously detrimental to immunosuppress the patient during an active infection.

The encoded protein of the CXCL6 gene is chemotactic for neutrophils and exhibits antibacterial properties against gram-negative and gram-positive bacteria. Binding of CXCL6 to its receptor CXCR2 has been implicated in the pathogenesis and disease progression of numerous disease states including IBD, lung cancer, endometriosis and gastrointestinal malignancies [280] although it's role in PJI is unknown and very scarcely mentioned in literature. Fisher et al [281] found that synovial fluid from patients with PJI contained higher levels of CXCL6 protein than those undergoing aseptic revisions. There have been no other studies examining the expression of CXCL6 in capsular tissue in PJI. It is important to note that both CCR6 and CXCR2, the receptors for CCL20 and CXCL6 respectively, were expressed to a greater extent in our PJI group but did not reach statistical significance. A possible explanation is that all the PJI patients we recruited had acute infections and the tissue samples were obtained before upregulation of cytokine receptors occurred. In addition, chemokines are rapidly inducible but may display temporal and spatial differences in expression to provide graded navigation of neutrophils through tissue which may not correspond with upregulation of their receptors. In the human skin blister model, CXCL6 and CXCL8 expression peak at 24 hours whereas complement and leukotrienes appear sooner [282], hence discrepancies in the expression of genes between our cohort of patients and those reported in other studies, as well as difference within our cohort, may be attributable to time of tissue obtained from time of the onset of infection.

We found that IL27 was upregulated almost 21-fold in our PJI cohort compared to the control group. The binding of IL27 to the IL27 receptor activates the Jak family kinases which in turn induces the phosphorylation of STAT1-STAT5 via the STAT signaling pathway. As part of the innate immune system response, IL27 induces the production of IL1, TNFα, IL18 and IL12 in monocytes and IL1 and TNFα in mast cells [283]. In the adaptive immune system, IL27 synergizes with IL12 to promote the production of IFNγ by CD4 and CD8 lymphocytes. In the rheumatoid arthritis model, IL27 exerts multiple regulatory functions via different mechanisms. On the one hand, it inhibits the formation of ectopic-like structures and OC differentiation to alleviate RA, it has also been shown to simultaneously promote Th1 cell differentiation which in turn exacerbates synovitis. Although our PJI group showed a significant increase in IL27 expression, we did not observe a downstream increase in TNF and while IL1A, IL1B and IFNγ were all elevated in the PJI group (2.19-fold, 16.49-fold and 2.48-fold respectively), none reached statistical significance. Other genes downstream including IL12 and IL18 were not available as part of our PCR array kit.

The TNFRSF11B gene, located on chromosome 8q24.12, encodes osteoprotegrin, an OB-secreted decoy receptor that binds RANKL to inhibit the activation of osteoclastogenesis. The role of the

RANK/RANKL/OPG is established in cases of aseptic loosening but is less clear in PJI. Wang et al [284] found that while the RANKL/OPG ratio from interface membrane from aseptic loosening was higher compared to that of septic loosening, which in turn was higher than controls, the expression of OPG did not differ significantly between the three groups. We found this gene was downregulated 8.52-fold in the PJI patients compared to controls, indicating that the downregulation of osteolysis suppression may further contribute to the septic loosening of implants seen in PJI by activation of osteoclasts, a new and significant finding. TNFSF11, the ligand for TNFRSF11B had increased expression in the PJI group but did not reach statistical significance. RANKL, the other ligand of TNFRSF11B, was not part of the PCR array. TNFRSF11B is involved in the canonical part of the Wingless and Int-1 (WNT) pathway in the suppression of osteoclastogenesis but upstream genes in the pathway, such as β-catenin and WNT antagonists such as secreted frizzled-related proteins (SFRPs), were not part of the PCR array we utilized. TNFRSF11B has been shown to be a gene target of, and is positively regulated by, β-catenin [285]. The WNT pathway is also involved in inflammation with higher levels of Wnt1, Wnt5 and frizzeled5 detected in the synovial tissue of RA patients than OA patients [286] and it is postulated that Wnt5a stimulates the production of pro-inflammatory cytokines Il6 and IL8 to enhance bone resorption through the production of RANKL [287].

The differentially expressed genes in our study are involved in different signaling pathways: CCL20, CXCL6 and IL27 are implicated in the STAT and Nfκβ pathways, while TNFRSF11B is involved with the WNT pathway. The WNT pathway is crucial for development and tissue regeneration while STAT, and particularly the Nfκβ pathways control inflammation. Both pathways are conserved but emerging evidence indicates that the two pathways cross-regulate. The Wnt/β-catenin pathway can negatively regulate Nfκβ: β-catenin forms a complex with RelA and p50 to decrease Nfκβ binding and downstream transcription [288]. We postulate that in PJI patients, there may be reduced WNT signaling, as indicated by reduction of TNFRSF11B expression, resulting in reduced negative regulation of the Nfκβ pathway, resulting in increased inflammation and elevated levels of inflammatory cytokines such as CCL20, CXCL6 and IL27 leading to OC activation. However, we need to investigate the expression of Wnt proteins and β-catenin to elucidate this link. The advantage of utilizing a PCR array to evaluate the changes in gene expression is that each real-time quantitative polymerase chain reaction (RT-qPCR) taking place within the PCR array is the equivalent as an individual qPCR for the gene, as the primer is embedded in the wells of the PCR array. Therefore, the differential expressions do not need to be confirmed with individual PCRs, as opposed to if a DNA microarray was utilized.

The patients recruited to our study were comprised of the control group and those with PJI. One possible confounding factor is that the control group were patients had OA undergoing primary

arthroplasty, instead of patients with well-functioning prosthesis in-situ not experiencing problems with aseptic loosening or infection. Inflammatory and destructive responses in the synovium play a role in the pathogenesis of OA [289] and therefore the change in expression-fold and magnitude of the difference between the OA and PJI groups may be under-represented compared to joints with no pathology. Studies have shown that synovial fluid concentrations of key proinflammatory cytokines (IL-1α, IL-18 and TNF-α) and serum levels of the chemokine CX3CL1 are all elevated significantly elevated in OA and RA compared to normal controls [290]. There is evidence that cartilage from OA knees had a more abundant expression of CCL20 than non-arthritis knees and the presence of CCL20 further promotes the release of IL-6, MMP-13 and ADAMTS-5 from chondrocytes [291]. In addition, even sterile tissue damage, such as fracture or trauma could activate macrophages and the innate immune system therefore obtaining tissue from a patient with no prior joint pathology, or one who has a stable prosthesis in-situ without problems would be extremely difficult to obtain, as it would pose multiple ethical dilemmas such as introducing a pathogen to a sterile joint and may cause donor site morbidity. It is plausible to obtain capsule tissue from healthy patients undergoing other surgeries, such as anterior cruciate ligament reconstruction however these are typically young patients who are not age-matched to patients undergoing joint arthroplasty. Our protocol controlled for a degree of confounding by excluding patients with inflammatory arthritis and malignancies as multiple cytokines, including CCL20 and CXCL6 are known to be upregulated in these conditions.

8.2 – Limitations

The findings from this project further build on the research conducted by members of our research group (R.W Li, P.N Smith, X Chen et al) as well as other scientists and clinicians dedicated to the research of antibacterial properties of biomaterials. However, it is imperative to recognize the limitations of our findings to aid in the interpretation of results, as well as guiding future studies to address knowledge gaps in the field. Our experiments were not without limitations:

- **Number of CFUs seeded in Ag-$SrPO_4$-Mg antibacterial assays**. An important determinant of the degree of inhibition is the number of CFUs seeded. We sought to seed 1 x 10^6 CFU per well in the bacterial viability assay and we did this by creating a bacterial suspension of 0.5 McFarland standard, but the exact number of CFUs seeded can never be guaranteed to be the same between serial experiments due to the small size of bacteria and the vast number of the CFUs.
- **Finite number of genes examined in capsular tissue.** A limitation of our study in elucidating the mechanism of septic loosening is the finite number of genes we examined. The RT^2 Profiler PCR array Human Inflammatory Cytokines and Receptors contained 84 genes within the inflammatory cascade but did not contain other genes upstream and

downstream in the inflammatory cascade in response to bacteria, found in the Toll-Like Receptor Signaling Pathway array, Antibacterial Response array, Innate and Adaptive Immune Responses array, and NFκβ signaling arrays. In addition, gene upregulation and downregulation should be confirmed by comparing the expression of a gene that has been proven to be a marker of PJI, such as α-defensin but this gene was not present in PCR array we utilized. Furthermore, the regulation of gene expression can be confirmed by encoded proteins with the Western Blot. This was a challenge as capsular tissue is largely collagen fibres with fewer interstitial cells, particularly in the case of PJI revision surgery where there was an abundance of scar tissue. We were limited by how much tissue we could take at the time of surgery, as a meticulous capsular closure contributes to the stability of the prosthesis and clinical outcome for the patient.

- **Patient recruitment numbers.** Another limitation of our study is the smaller sample size. The number of replicates in each group required to detect a change in gene expression through RNA sequencing varies in literature and a minimum of three samples per condition is required [293] whereas other sources site a minimum of six to twelve replicates per condition are required if identifying the majority of all differentially expressed genes is important [294]. We were limited in the recruitment of patients due to several factors. Our recruitment period coincided with the COVID-19 pandemic lockdown of Canberra in 2021 when elective surgery numbers were reduced, and we were not able to recruit more patients to the control group. In addition, patients between the PJI and control groups were matched based on gender and age but may have had surgeries on different joints, for example, a hip joint and a knee joint. This was once again due to a limited number of patients, but the clinical significance is unclear, as synovial tissue from different joints are expected to respond in the same way to infection. However, the control patients we did recruit were matched to the PJI group by age and gender to minimize differences in demographics. We could not utilize the tissue of a few PJI patients because they were infected with a multi-resistant organism (MRO) including MRSA and the handling of such organisms was strictly forbidden at our physical containment level 2 (PC2) laboratory. Because of this, RNA extraction from the tissue of several PJI patients were not processed immediately after the surgery because we did not know what pathogen was involved but we minimized RNA degradation by transferring the tissue immediately to a -80 ^{o}C freezer at the Canberra Hospital until the organism was identified. In the cases where an organism had already been identified from joint arthrocentesis, or tissue was obtained from the control group, RNA extraction was performed immediately.

8.3 – Future directions

The results from this project bring encouraging possibilities for the utilization of a novel biomaterial in orthopaedic implants. In addition, they open interesting questions and exciting possibilities for further studies with significant clinical implications.

- **Expansion of Ag-$SrPO_4$-Mg antibacterial assays to other bacterial strains.** We investigated the inhibition of four strains of bacteria in our project, namely *S.aureus*, *S.epidermidis*, *E.coli* and *P.aeruginosa*. Combined, these strains comprise the majority of PJIs involving TKA, THA and TSA. We could further expand our antibacterial assay for other strains including *Streptococci*, *Enterococci*, and in particular, *P.acnes*, which is a prominent offending organism in upper limb joint arthroplasty. In addition to the LIVE/DEAD assay, an additional test of bacterial viability would be to plate the bacterial suspension after treatment with antibiotics, Ag-$SrPO_4$-Mg and $SrPO_4$-Mg on agar plates after serial dilution. Another area of improvement in our study is utilizing more concentrations of antibiotics to construct a dose-response curve to extrapolate the effect of Ag-$SrPO_4$-Mg to a known concentration of antibiotic, particularly in the case of *E.coli* and gentamicin, where we did not observe the expected dose-response curve.
- **Synergistic effect between antibiotics and Ag-$SrPO_4$-Mg**. An area that requires further investigation is the combined effect of antibiotics and Ag-$SrPO_4$-Mg to ascertain if the two agents have an additive or synergistic effect as literature have demonstrated that there appears to be a synergistic effect between antibiotics and AgNPs whereby AgNPs disrupt the bacterial envelope which in turn assists the antibiotics in localizing to their cellular targets. Although the susceptibility of MRSA to Ag-$SrPO_4$-Mg could not be carried out at our PC2 facility, it is an area that requires further research and is clinically important as the incidence of MRSA PJI is increasing with the rise of antibiotic resistance.
- **Local tissue adverse reaction in an in-vivo model.** Another consideration is whether the generation of Ag-$SrPO_4$-Mg at concentrations high enough to inhibit bacterial growth can also elicit an adverse local tissue reaction including a pseudotumour and systemic toxicity, as seen when high concentrations of cobalt and chromium are released from metal-on-metal articulating prosthesis. As far as we are aware, there is a knowledge gap surrounding this clinical question and is a direction for future studies. We can further expand to animal studies whereby Ag-$SrPO_4$-Mg implants are inserted and bacteria are inoculated at the time of implantation to determine if the biomaterial inhibits bacterial proliferation in-situ, and this will also elucidate if Ag-$SrPO_4$-Mg elicits adverse local tissue reactions. Another advantage of animal studies is to examine the degree of bone ingrowth onto prosthesis coated with Ag-$SrPO_4$-Mg. Utilizing an in-vivo animal model would also demonstrate the effect of Ag-

$SrPO_4$-Mg on OCs, as our group has previously demonstrated an inhibitory effect on OCs in in-vitro studies.

- **Gene expression in capsular tissue of patients with aseptic loosening as comparison group.** Historically, aseptic loosening and septic loosening were regarded as two distinct entities with macrophages and foreign body giant cell seen in aseptic loosening whereas neutrophils and lymphocytes characterize septic loosening. There is mounting evidence that the two pathways have significant overlap. For example, TLRs are involved in the recognition and binding of not only PAMPs but also inorganic wear debris such as alkane polymers polymers released from UHMPE which can bind to TLR2 on macrophages to activate proinflammatory signaling [292] through secretion of IFNG as well as other proinflammatory cytokines. Therefore, we can further improve our study by recruiting patients undergoing revision arthroplasty for aseptic loosening as a comparison group to assess whether there is a statistically significant difference in the expression of TNFRSF11B between septic and aseptic loosening. Joint capsule and synovium are comprised of type A cells derived from macrophages with antigen presenting and phagocytosis ability, while type B cells are fibroblast-like cells that produce synovial fluid [295]. These cells are therefore the first to respond to a prosthetic joint infection. Therefore, histological analysis can also help confirm the presence of type A and B cells in the joint synovium, as well as the infiltration of proinflammatory cells following an infection.
- **Expand gene expression study and confirm with downstream protein expression.** As mentioned, one of the limitations of our study was the finite number of genes included in the PCR-array. A solution to this limitation is expanding to other PCR-arrays that includes genes upstream and downstream of CXCL6, CCL20, IL20 and TNFRSF11β. Alternatively, RNA sequencing will reveal genome-wide changes in gene expression and elucidate the inflammatory pathways involved in the process of septic osteolysis. Furthermore, gene-editing techniques such as clustered regularly interspaced short palindromic repeats (CRISPR) can be utilized to create transgenic animal models with knockouts of the aforementioned genes in which implanted biomaterials can be inoculated with bacteria to test if knockout of the relevant genes reduces the amount of periprosthetic osteolysis, as well as the possible detrimental effects of such gene knockouts given the multi-faceted functions of these genes in infections, autoimmune diseases and the development of malignancies. In addition, protein assays such as Western Blots and enzyme-linked immunosorbent assay (ELISA) can be utilized to confirm the upregulation of CCL20, CXCL6 and IL20 as well as the downregulation of TNFRSF11β.

References

1. Kelsey MC. The management and control of hospital-acquired infection in acute NHS trusts in England: a report by the Comptroller and Auditor General--the who, how and what. J Hosp Infect. 2000;44(3):157-9.
2. Donlan RM. Biofilms and device-associated infections. Emerg Infect Dis. 2001;7(2):277-81.
3. Weiner-Lastinger LM, Abner S, Edwards JR, Kallen AJ, Karlsson M, Magill SS, et al. Antimicrobial-resistant pathogens associated with adult healthcare-associated infections: Summary of data reported to the National Healthcare Safety Network, 2015-2017. Infect Control Hosp Epidemiol. 2020;41(1):1-18.
4. Percival SL, Sabbuba NA, Kite P, Stickler DJ. The effect of EDTA instillations on the rate of development of encrustation and biofilms in Foley catheters. Urol Res. 2009;37(4):205-9.
5. Donlan RM. Biofilms on central venous catheters: is eradication possible? Curr Top Microbiol Immunol. 2008;322:133-61.
6. Anaissie E, Samonis G, Kontoyiannis D, Costerton J, Sabharwal U, Bodey G, et al. Role of catheter colonization and infrequent hematogenous seeding in catheter-related infections. Eur J Clin Microbiol Infect Dis. 1995;14(2):134-7.
7. Talsma SS. Biofilms on medical devices. Home Healthc Nurse. 2007;25(9):589-94.
8. Stickler DJ. Bacterial biofilms in patients with indwelling urinary catheters. Nat Clin Pract Urol. 2008;5(11):598-608.
9. Percival SL, Suleman L, Vuotto C, Donelli G. Healthcare-associated infections, medical devices and biofilms: risk, tolerance and control. J Med Microbiol. 2015;64(Pt 4):323-34.
10. Chastre J, Fagon JY. Ventilator-associated pneumonia. Am J Respir Crit Care Med. 2002;165(7):867-903.
11. Bauer TT, Torres A, Ferrer R, Heyer CM, Schultze-Werninghaus G, Rasche K. Biofilm formation in endotracheal tubes. Association between pneumonia and the persistence of pathogens. Monaldi Arch Chest Dis. 2002;57(1):84-7.
12. Diaz E, Rodriguez AH, Rello J. Ventilator-associated pneumonia: issues related to the artificial airway. Respir Care. 2005;50(7):900-6; discussion 6-9.
13. Graves N. Economics and preventing hospital-acquired infection. Emerg Infect Dis. 2004;10(4):561-6.
14. Kathju S, Nistico L, Hall-Stoodley L, Post JC, Ehrlich GD, Stoodley P. Chronic surgical site infection due to suture-associated polymicrobial biofilm. Surg Infect (Larchmt). 2009;10(5):457-61.
15. Australian Orthopaedic Association. Hip, Knee & Shoulder Arthroplasty Annual Report - Annual Report 2019 2019 [Available from: https://aoanjrr.sahmri.com/documents/10180/668596/Hip%2C+Knee+%26+Shoulder+Arthroplasty/c287d2a3-22df-a3bb-37a2-91e6c00bfcf0.
16. Franceschini V, Chillemi C. Periprosthetic shoulder infection. Open Orthop J. 2013;7:243-9.
17. Gundtoft PH, Pedersen AB, Varnum C, Overgaard S. Increased Mortality After Prosthetic Joint Infection in Primary THA. Clin Orthop Relat Res. 2017;475(11):2623-31.
18. Kurtz SM, Lau E, Watson H, Schmier JK, Parvizi J. Economic burden of periprosthetic joint infection in the United States. J Arthroplasty. 2012;27(8 Suppl):61-5 e1.
19. Nguyen LL, Nelson CL, Saccente M, Smeltzer MS, Wassell DL, McLaren SG. Detecting bacterial colonization of implanted orthopaedic devices by ultrasonication. Clin Orthop Relat Res. 2002(403):29-37.
20. Zimmerli W. Infection and musculoskeletal conditions: Prosthetic-joint-associated infections. Best Pract Res Clin Rheumatol. 2006;20(6):1045-63.
21. Hoiby N, Bjarnsholt T, Givskov M, Molin S, Ciofu O. Antibiotic resistance of bacterial biofilms. Int J Antimicrob Agents. 2010;35(4):322-32.
22. Chen M, Yu Q, Sun H. Novel strategies for the prevention and treatment of biofilm related infections. Int J Mol Sci. 2013;14(9):18488-501.
23. Arsoy D, Woodcock JA, Lewallen DG, Trousdale RT. Outcomes and complications following total hip arthroplasty in the super-obese patient, BMI > 50. J Arthroplasty. 2014;29(10):1899-905.

24. Zmistowski B, Tetreault MW, Alijanipour P, Chen AF, Della Valle CJ, Parvizi J. Recurrent periprosthetic joint infection: persistent or new infection? J Arthroplasty. 2013;28(9):1486-9.
25. Greene KA, Wilde AH, Stulberg BN. Preoperative nutritional status of total joint patients. Relationship to postoperative wound complications. J Arthroplasty. 1991;6(4):321-5.
26. Bozic KJ, Lau E, Kurtz S, Ong K, Berry DJ. Patient-related risk factors for postoperative mortality and periprosthetic joint infection in medicare patients undergoing TKA. Clin Orthop Relat Res. 2012;470(1):130-7.
27. Dronge AS, Perkal MF, Kancir S, Concato J, Aslan M, Rosenthal RA. Long-term glycemic control and postoperative infectious complications. Arch Surg. 2006;141(4):375-80; discussion 80.
28. Marchant MH, Jr., Viens NA, Cook C, Vail TP, Bolognesi MP. The impact of glycemic control and diabetes mellitus on perioperative outcomes after total joint arthroplasty. J Bone Joint Surg Am. 2009;91(7):1621-9.
29. Tande AJ, Patel R. Prosthetic joint infection. Clin Microbiol Rev. 2014;27(2):302-45.
30. Marik PE. The hazards of blood transfusion. Br J Hosp Med (Lond). 2009;70(1):12-5.
31. Pulido L, Ghanem E, Joshi A, Purtill JJ, Parvizi J. Periprosthetic joint infection: the incidence, timing, and predisposing factors. Clin Orthop Relat Res. 2008;466(7):1710-5.
32. Ford PM. Arthropathies associated with renal disease including dialysis-related amyloid. Curr Opin Rheumatol. 1992;4(1):63-7.
33. Lieu D, Harris IA, Naylor JM, Mittal R. Review article: Total hip replacement in haemodialysis or renal transplant patients. J Orthop Surg (Hong Kong). 2014;22(3):393-8.
34. Rezapoor M, Parvizi J. Prevention of Periprosthetic Joint Infection. J Arthroplasty. 2015;30(6):902-7.
35. Zhu Y, Zhang F, Chen W, Liu S, Zhang Q, Zhang Y. Risk factors for periprosthetic joint infection after total joint arthroplasty: a systematic review and meta-analysis. J Hosp Infect. 2015;89(2):82-9.
36. Del Buono A, Denaro V, Maffulli N. Genetic susceptibility to aseptic loosening following total hip arthroplasty: a systematic review. Br Med Bull. 2012;101:39-55.
37. El-Helou O, Berbari EF, Brown RA, Gralewski JH, Osmon DR, Razonable RR. Functional assessment of Toll-like receptor 2 and its relevance in patients with Staphylococcus aureus infection of joint prosthesis. Hum Immunol. 2011;72(1):47-53.
38. Malik MH, Bayat A, Jury F, Kay PR, Ollier WE. Genetic susceptibility to total hip arthroplasty failure--positive association with mannose-binding lectin. J Arthroplasty. 2007;22(2):265-70.
39. Malik MH, Bayat A, Jury F, Ollier WE, Kay PR. Genetic susceptibility to hip arthroplasty failure--association with the RANK/OPG pathway. Int Orthop. 2006;30(3):177-81.
40. Malik MH, Jury F, Bayat A, Ollier WE, Kay PR. Genetic susceptibility to total hip arthroplasty failure: a preliminary study on the influence of matrix metalloproteinase 1, interleukin 6 polymorphisms and vitamin D receptor. Ann Rheum Dis. 2007;66(8):1116-20.
41. Navratilova Z, Gallo J, Mrazek F, Lostak J, Petrek M. MBL2 gene variation affecting serum MBL is associated with prosthetic joint infection in Czech patients after total joint arthroplasty. Tissue Antigens. 2012;80(5):444-51.
42. Navratilova Z, Gallo J, Mrazek F, Petrek M. Genetic variation in key molecules of the Th-17 immune response is not associated with risk for prosthetic joint infection in a Czech population. Biomed Pap Med Fac Univ Palacky Olomouc Czech Repub. 2012;156(3):248-52.
43. Stahelova A, Mrazek F, Smizansky M, Petrek M, Gallo J. Variation in the IL1B, TNF and IL6 genes and individual susceptibility to prosthetic joint infection. BMC Immunol. 2012;13:25.
44. Mrazek F, Gallo J, Stahelova A, Petrek M. Coding variants of TLR2 and TLR4 genes do not substantially contribute to prosthetic joint infection. Inflamm Res. 2013;62(5):483-7.
45. Association AO. Australian Orthopaedic Association National Joint Replacement Registry Annual Report 2021 2021 [Available from: https://aoanjrr.sahmri.com/annual-reports-2021.
46. Nelson CL, McLaren AC, McLaren SG, Johnson JW, Smeltzer MS. Is aseptic loosening truly aseptic? Clin Orthop Relat Res. 2005(437):25-30.
47. Phillips JE, Crane TP, Noy M, Elliott TS, Grimer RJ. The incidence of deep prosthetic infections in a specialist orthopaedic hospital: a 15-year prospective survey. J Bone Joint Surg Br. 2006;88(7):943-8.

48. Cheung E, Willis M, Walker M, Clark R, Frankle MA. Complications in reverse total shoulder arthroplasty. J Am Acad Orthop Surg. 2011;19(7):439-49.
49. Zumstein MA, Pinedo M, Old J, Boileau P. Problems, complications, reoperations, and revisions in reverse total shoulder arthroplasty: a systematic review. J Shoulder Elbow Surg. 2011;20(1):146-57.
50. Rudge WBJ, Eseonu K, Brown M, Warren S, Majed A, Bayley IL, et al. The management of infected elbow arthroplasty by two-stage revision. J Shoulder Elbow Surg. 2018;27(5):879-86.
51. Streubel PN, Simone JP, Morrey BF, Sanchez-Sotelo J, Morrey ME. Infection in total elbow arthroplasty with stable components: outcomes of a staged surgical protocol with retention of the components. Bone Joint J. 2016;98-B(7):976-83.
52. Kwak JM, Koh KH, Jeon IH. Total Elbow Arthroplasty: Clinical Outcomes, Complications, and Revision Surgery. Clin Orthop Surg. 2019;11(4):369-79.
53. Parikh MS, Antony S. A comprehensive review of the diagnosis and management of prosthetic joint infections in the absence of positive cultures. J Infect Public Health. 2016;9(5):545-56.
54. Hall-Stoodley L, Costerton JW, Stoodley P. Bacterial biofilms: from the natural environment to infectious diseases. Nat Rev Microbiol. 2004;2(2):95-108.
55. Costerton JW, Stewart PS, Greenberg EP. Bacterial biofilms: a common cause of persistent infections. Science. 1999;284(5418):1318-22.
56. O'Toole GA, Kolter R. Flagellar and twitching motility are necessary for Pseudomonas aeruginosa biofilm development. Mol Microbiol. 1998;30(2):295-304.
57. O'Toole G, Kaplan HB, Kolter R. Biofilm formation as microbial development. Annu Rev Microbiol. 2000;54:49-79.
58. Markowska K, Grudniak AM, Wolska KI. Silver nanoparticles as an alternative strategy against bacterial biofilms. Acta Biochim Pol. 2013;60(4):523-30.
59. Donlan RM. Biofilm formation: a clinically relevant microbiological process. Clin Infect Dis. 2001;33(8):1387-92.
60. Van Houdt R, Michiels CW. Role of bacterial cell surface structures in Escherichia coli biofilm formation. Res Microbiol. 2005;156(5-6):626-33.
61. Watnick P, Kolter R. Biofilm, city of microbes. J Bacteriol. 2000;182(10):2675-9.
62. Periasamy S, Joo HS, Duong AC, Bach TH, Tan VY, Chatterjee SS, et al. How Staphylococcus aureus biofilms develop their characteristic structure. Proc Natl Acad Sci U S A. 2012;109(4):1281-6.
63. Vuong C, Saenz HL, Gotz F, Otto M. Impact of the agr quorum-sensing system on adherence to polystyrene in Staphylococcus aureus. J Infect Dis. 2000;182(6):1688-93.
64. Boles BR, Thoendel M, Singh PK. Rhamnolipids mediate detachment of Pseudomonas aeruginosa from biofilms. Mol Microbiol. 2005;57(5):1210-23.
65. Angelini TE, Roper M, Kolter R, Weitz DA, Brenner MP. Bacillus subtilis spreads by surfing on waves of surfactant. Proc Natl Acad Sci U S A. 2009;106(43):18109-13.
66. Wang R, Khan BA, Cheung GY, Bach TH, Jameson-Lee M, Kong KF, et al. Staphylococcus epidermidis surfactant peptides promote biofilm maturation and dissemination of biofilm-associated infection in mice. J Clin Invest. 2011;121(1):238-48.
67. Flemming HC, Wingender J. The biofilm matrix. Nat Rev Microbiol. 2010;8(9):623-33.
68. Hoyle BD, Wong CK, Costerton JW. Disparate efficacy of tobramycin on Ca(2+)-, Mg(2+)-, and HEPES-treated Pseudomonas aeruginosa biofilms. Can J Microbiol. 1992;38(11):1214-8.
69. Anderl JN, Franklin MJ, Stewart PS. Role of antibiotic penetration limitation in Klebsiella pneumoniae biofilm resistance to ampicillin and ciprofloxacin. Antimicrob Agents Chemother. 2000;44(7):1818-24.
70. Johnson L, Mulcahy H, Kanevets U, Shi Y, Lewenza S. Surface-localized spermidine protects the Pseudomonas aeruginosa outer membrane from antibiotic treatment and oxidative stress. J Bacteriol. 2012;194(4):813-26.
71. Duguid IG, Evans E, Brown MR, Gilbert P. Effect of biofilm culture upon the susceptibility of Staphylococcus epidermidis to tobramycin. J Antimicrob Chemother. 1992;30(6):803-10.
72. Lewis K. Multidrug tolerance of biofilms and persister cells. Curr Top Microbiol Immunol. 2008;322:107-31.

73. Qu Y, Daley AJ, Istivan TS, Rouch DA, Deighton MA. Densely adherent growth mode, rather than extracellular polymer substance matrix build-up ability, contributes to high resistance of Staphylococcus epidermidis biofilms to antibiotics. J Antimicrob Chemother. 2010;65(7):1405-11.
74. Pringle JH, Fletcher M. Influence of substratum wettability on attachment of freshwater bacteria to solid surfaces. Appl Environ Microbiol. 1983;45(3):811-7.
75. Monroe D. Looking for chinks in the armor of bacterial biofilms. PLoS Biol. 2007;5(11):e307.
76. Song F, Koo H, Ren D. Effects of Material Properties on Bacterial Adhesion and Biofilm Formation. J Dent Res. 2015;94(8):1027-34.
77. Zhang X, Di Q, Zhu F, Sun G, Zhang H. Superhydrophobic micro/nano dual-scale structures. J Nanosci Nanotechnol. 2013;13(2):1539-42.
78. Anselme K, Davidson P, Popa AM, Giazzon M, Liley M, Ploux L. The interaction of cells and bacteria with surfaces structured at the nanometre scale. Acta Biomater. 2010;6(10):3824-46.
79. Teughels W, Van Assche N, Sliepen I, Quirynen M. Effect of material characteristics and/or surface topography on biofilm development. Clin Oral Implants Res. 2006;17 Suppl 2:68-81.
80. Quirynen M, Bollen CM, Papaioannou W, Van Eldere J, van Steenberghe D. The influence of titanium abutment surface roughness on plaque accumulation and gingivitis: short-term observations. Int J Oral Maxillofac Implants. 1996;11(2):169-78.
81. Poncin-Epaillard F, Herry JM, Marmey P, Legeay G, Debarnot D, Bellon-Fontaine MN. Elaboration of highly hydrophobic polymeric surface--a potential strategy to reduce the adhesion of pathogenic bacteria? Mater Sci Eng C Mater Biol Appl. 2013;33(3):1152-61.
82. Manabe K, Nishizawa S, Shiratori S. Porous surface structure fabricated by breath figures that suppresses Pseudomonas aeruginosa biofilm formation. ACS Appl Mater Interfaces. 2013;5(22):11900-5.
83. Pogodin S, Hasan J, Baulin VA, Webb HK, Truong VK, Phong Nguyen TH, et al. Biophysical model of bacterial cell interactions with nanopatterned cicada wing surfaces. Biophys J. 2013;104(4):835-40.
84. Lichter JA, Thompson MT, Delgadillo M, Nishikawa T, Rubner MF, Van Vliet KJ. Substrata mechanical stiffness can regulate adhesion of viable bacteria. Biomacromolecules. 2008;9(6):1571-8.
85. Saha N, Monge C, Dulong V, Picart C, Glinel K. Influence of polyelectrolyte film stiffness on bacterial growth. Biomacromolecules. 2013;14(2):520-8.
86. Arciola CR, Campoccia D, Gamberini S, Baldassarri L, Montanaro L. Prevalence of cna, fnbA and fnbB adhesin genes among Staphylococcus aureus isolates from orthopedic infections associated to different types of implant. FEMS Microbiol Lett. 2005;246(1):81-6.
87. Otto M. Staphylococcal biofilms. Curr Top Microbiol Immunol. 2008;322:207-28.
88. Novick RP. Autoinduction and signal transduction in the regulation of staphylococcal virulence. Mol Microbiol. 2003;48(6):1429-49.
89. Archer NK, Mazaitis MJ, Costerton JW, Leid JG, Powers ME, Shirtliff ME. Staphylococcus aureus biofilms: properties, regulation, and roles in human disease. Virulence. 2011;2(5):445-59.
90. Wang R, Braughton KR, Kretschmer D, Bach TH, Queck SY, Li M, et al. Identification of novel cytolytic peptides as key virulence determinants for community-associated MRSA. Nat Med. 2007;13(12):1510-4.
91. Grice EA, Segre JA. The skin microbiome. Nat Rev Microbiol. 2011;9(4):244-53.
92. Sugimoto S, Iwamoto T, Takada K, Okuda K, Tajima A, Iwase T, et al. Staphylococcus epidermidis Esp degrades specific proteins associated with Staphylococcus aureus biofilm formation and host-pathogen interaction. J Bacteriol. 2013;195(8):1645-55.
93. Heilmann C, Hussain M, Peters G, Gotz F. Evidence for autolysin-mediated primary attachment of Staphylococcus epidermidis to a polystyrene surface. Mol Microbiol. 1997;24(5):1013-24.
94. Mack D, Davies AP, Harris LG, Knobloch JK, Rohde H. Staphylococcus epidermidis Biofilms: Functional Molecules, Relation to Virulence, and Vaccine Potential. Top Curr Chem. 2009;288:157-82.
95. Josefsson E, McCrea KW, Ni Eidhin D, O'Connell D, Cox J, Hook M, et al. Three new members of the serine-aspartate repeat protein multigene family of Staphylococcus aureus. Microbiology. 1998;144 (Pt 12):3387-95.

96. Christner M, Heinze C, Busch M, Franke G, Hentschke M, Bayard Duhring S, et al. sarA negatively regulates Staphylococcus epidermidis biofilm formation by modulating expression of 1 MDa extracellular matrix binding protein and autolysis-dependent release of eDNA. Mol Microbiol. 2012;86(2):394-410.
97. O'Gara JP, Humphreys H. Staphylococcus epidermidis biofilms: importance and implications. J Med Microbiol. 2001;50(7):582-7.
98. Anderson GG, Palermo JJ, Schilling JD, Roth R, Heuser J, Hultgren SJ. Intracellular bacterial biofilm-like pods in urinary tract infections. Science. 2003;301(5629):105-7.
99. Clarke SR, Harris LG, Richards RG, Foster SJ. Analysis of Ebh, a 1.1-megadalton cell wall-associated fibronectin-binding protein of Staphylococcus aureus. Infect Immun. 2002;70(12):6680-7.
100. Rohde H, Burandt EC, Siemssen N, Frommelt L, Burdelski C, Wurster S, et al. Polysaccharide intercellular adhesin or protein factors in biofilm accumulation of Staphylococcus epidermidis and Staphylococcus aureus isolated from prosthetic hip and knee joint infections. Biomaterials. 2007;28(9):1711-20.
101. Christner M, Franke GC, Schommer NN, Wendt U, Wegert K, Pehle P, et al. The giant extracellular matrix-binding protein of Staphylococcus epidermidis mediates biofilm accumulation and attachment to fibronectin. Mol Microbiol. 2010;75(1):187-207.
102. Hussain M, Herrmann M, von Eiff C, Perdreau-Remington F, Peters G. A 140-kilodalton extracellular protein is essential for the accumulation of Staphylococcus epidermidis strains on surfaces. Infect Immun. 1997;65(2):519-24.
103. Macintosh RL, Brittan JL, Bhattacharya R, Jenkinson HF, Derrick J, Upton M, et al. The terminal A domain of the fibrillar accumulation-associated protein (Aap) of Staphylococcus epidermidis mediates adhesion to human corneocytes. J Bacteriol. 2009;191(22):7007-16.
104. Pruss BM, Besemann C, Denton A, Wolfe AJ. A complex transcription network controls the early stages of biofilm development by Escherichia coli. J Bacteriol. 2006;188(11):3731-9.
105. Wood TK. Insights on Escherichia coli biofilm formation and inhibition from whole-transcriptome profiling. Environ Microbiol. 2009;11(1):1-15.
106. Beloin C, Roux A, Ghigo JM. Escherichia coli biofilms. Current topics in microbiology and immunology. 2008;322:249-89.
107. Ryder C, Byrd M, Wozniak DJ. Role of polysaccharides in Pseudomonas aeruginosa biofilm development. Curr Opin Microbiol. 2007;10(6):644-8.
108. Sutherland I. Biofilm exopolysaccharides: a strong and sticky framework. Microbiology. 2001;147(Pt 1):3-9.
109. Colvin KM, Gordon VD, Murakami K, Borlee BR, Wozniak DJ, Wong GC, et al. The pel polysaccharide can serve a structural and protective role in the biofilm matrix of Pseudomonas aeruginosa. PLoS Pathog. 2011;7(1):e1001264.
110. Deziel E, Lepine F, Milot S, Villemur R. rhlA is required for the production of a novel biosurfactant promoting swarming motility in Pseudomonas aeruginosa: 3-(3-hydroxyalkanoyloxy)alkanoic acids (HAAs), the precursors of rhamnolipids. Microbiology. 2003;149(Pt 8):2005-13.
111. Davies DG, Parsek MR, Pearson JP, Iglewski BH, Costerton JW, Greenberg EP. The involvement of cell-to-cell signals in the development of a bacterial biofilm. Science. 1998;280(5361):295-8.
112. Ha KY, Chung YG, Ryoo SJ. Adherence and biofilm formation of Staphylococcus epidermidis and Mycobacterium tuberculosis on various spinal implants. Spine (Phila Pa 1976). 2005;30(1):38-43.
113. Zimmerli W, Sendi P. Pathogenesis of implant-associated infection: the role of the host. Semin Immunopathol. 2011;33(3):295-306.
114. Bernard L, Vaudaux P, Merle C, Stern R, Huggler E, Lew D, et al. The inhibition of neutrophil antibacterial activity by ultra-high molecular weight polyethylene particles. Biomaterials. 2005;26(27):5552-7.
115. Zimmerli W, Waldvogel FA, Vaudaux P, Nydegger UE. Pathogenesis of foreign body infection: description and characteristics of an animal model. J Infect Dis. 1982;146(4):487-97.

116. Lucke M, Schmidmaier G, Sadoni S, Wildemann B, Schiller R, Stemberger A, et al. A new model of implant-related osteomyelitis in rats. J Biomed Mater Res B Appl Biomater. 2003;67(1):593-602.
117. Chang S, Popowich Y, Greco RS, Haimovich B. Neutrophil survival on biomaterials is determined by surface topography. J Vasc Surg. 2003;37(5):1082-90.
118. Seebach E, Kubatzky KF. Chronic Implant-Related Bone Infections-Can Immune Modulation be a Therapeutic Strategy? Front Immunol. 2019;10:1724.
119. Watters C, Fleming D, Bishop D, Rumbaugh KP. Host Responses to Biofilm. Prog Mol Biol Transl Sci. 2016;142:193-239.
120. Nishitani K, Sutipornpalangkul W, de Mesy Bentley KL, Varrone JJ, Bello-Irizarry SN, Ito H, et al. Quantifying the natural history of biofilm formation in vivo during the establishment of chronic implant-associated Staphylococcus aureus osteomyelitis in mice to identify critical pathogen and host factors. J Orthop Res. 2015;33(9):1311-9.
121. Thurlow LR, Hanke ML, Fritz T, Angle A, Aldrich A, Williams SH, et al. Staphylococcus aureus biofilms prevent macrophage phagocytosis and attenuate inflammation in vivo. J Immunol. 2011;186(11):6585-96.
122. Massaccesi L, Ragone V, Papini N, Goi G, Corsi Romanelli MM, Galliera E. Effects of Vitamin E-Stabilized Ultra High Molecular Weight Polyethylene on Oxidative Stress Response and Osteoimmunological Response in Human Osteoblast. Front Endocrinol (Lausanne). 2019;10:203.
123. Montanaro L, Campoccia D, Arciola CR. Nanostructured materials for inhibition of bacterial adhesion in orthopedic implants: a minireview. Int J Artif Organs. 2008;31(9):771-6.
124. Raimondo T, Puckett S, Webster TJ. Greater osteoblast and endothelial cell adhesion on nanostructured polyethylene and titanium. Int J Nanomedicine. 2010;5:647-52.
125. Webster TJ, Siegel RW, Bizios R. Osteoblast adhesion on nanophase ceramics. Biomaterials. 1999;20(13):1221-7.
126. Ferraz N, Nilsson B, Hong J, Karlsson Ott M. Nanoporesize affects complement activation. J Biomed Mater Res A. 2008;87(3):575-81.
127. Groll J, Fiedler J, Engelhard E, Ameringer T, Tugulu S, Klok HA, et al. A novel star PEG-derived surface coating for specific cell adhesion. J Biomed Mater Res A. 2005;74(4):607-17.
128. Gottenbos B, Grijpma DW, van der Mei HC, Feijen J, Busscher HJ. Antimicrobial effects of positively charged surfaces on adhering Gram-positive and Gram-negative bacteria. J Antimicrob Chemother. 2001;48(1):7-13.
129. Li B, Jiang B, Boyce BM, Lindsey BA. Multilayer polypeptide nanoscale coatings incorporating IL-12 for the prevention of biomedical device-associated infections. Biomaterials. 2009;30(13):2552-8.
130. Zimmerli W, Trampuz A, Ochsner PE. Prosthetic-joint infections. N Engl J Med. 2004;351(16):1645-54.
131. Parvizi J, Zmistowski B, Berbari EF, Bauer TW, Springer BD, Della Valle CJ, et al. New definition for periprosthetic joint infection: from the Workgroup of the Musculoskeletal Infection Society. Clin Orthop Relat Res. 2011;469(11):2992-4.
132. Parvizi J, Tan TL, Goswami K, Higuera C, Della Valle C, Chen AF, et al. The 2018 Definition of Periprosthetic Hip and Knee Infection: An Evidence-Based and Validated Criteria. J Arthroplasty. 2018;33(5):1309-14 e2.
133. Ghanem E, Parvizi J, Burnett RS, Sharkey PF, Keshavarzi N, Aggarwal A, et al. Cell count and differential of aspirated fluid in the diagnosis of infection at the site of total knee arthroplasty. J Bone Joint Surg Am. 2008;90(8):1637-43.
134. Della Valle CJ, Sporer SM, Jacobs JJ, Berger RA, Rosenberg AG, Paprosky WG. Preoperative testing for sepsis before revision total knee arthroplasty. J Arthroplasty. 2007;22(6 Suppl 2):90-3.
135. Schinsky MF, Della Valle CJ, Sporer SM, Paprosky WG. Perioperative testing for joint infection in patients undergoing revision total hip arthroplasty. J Bone Joint Surg Am. 2008;90(9):1869-75.
136. Boisrenoult P. Cutibacterium acnes prosthetic joint infection: Diagnosis and treatment. Orthop Traumatol Surg Res. 2018;104(1S):S19-S24.

137. Garrigues GE, Zmistowski B, Cooper AM, Green A, Group ICMS. Proceedings from the 2018 International Consensus Meeting on Orthopedic Infections: evaluation of periprosthetic shoulder infection. J Shoulder Elbow Surg. 2019;28(6S):S32-S66.
138. Bejon P, Berendt A, Atkins BL, Green N, Parry H, Masters S, et al. Two-stage revision for prosthetic joint infection: predictors of outcome and the role of reimplantation microbiology. J Antimicrob Chemother. 2010;65(3):569-75.
139. Zmistowski B, Della Valle C, Bauer TW, Malizos KN, Alavi A, Bedair H, et al. Diagnosis of periprosthetic joint infection. J Arthroplasty. 2014;29(2 Suppl):77-83.
140. Parvizi J, Erkocak OF, Della Valle CJ. Culture-negative periprosthetic joint infection. J Bone Joint Surg Am. 2014;96(5):430-6.
141. Malekzadeh D, Osmon DR, Lahr BD, Hanssen AD, Berbari EF. Prior use of antimicrobial therapy is a risk factor for culture-negative prosthetic joint infection. Clin Orthop Relat Res. 2010;468(8):2039-45.
142. Peel TN, Dylla BL, Hughes JG, Lynch DT, Greenwood-Quaintance KE, Cheng AC, et al. Improved Diagnosis of Prosthetic Joint Infection by Culturing Periprosthetic Tissue Specimens in Blood Culture Bottles. mBio. 2016;7(1):e01776-15.
143. Abdulmassih R, Makadia J, Como J, Paulson M, Min Z, Bhanot N. Propionibacterium acnes: Time-to-Positivity in Standard Bacterial Culture From Different Anatomical Sites. J Clin Med Res. 2016;8(12):916-8.
144. Larsen LH, Lange J, Xu Y, Schonheyder HC. Optimizing culture methods for diagnosis of prosthetic joint infections: a summary of modifications and improvements reported since 1995. J Med Microbiol. 2012;61(Pt 3):309-16.
145. Nace J, Siddiqi A, Talmo CT, Chen AF. Diagnosis and Management of Fungal Periprosthetic Joint Infections. J Am Acad Orthop Surg. 2019;27(18):e804-e18.
146. Jakobs O, Schoof B, Klatte TO, Schmidl S, Fensky F, Guenther D, et al. Fungal periprosthetic joint infection in total knee arthroplasty: a systematic review. Orthop Rev (Pavia). 2015;7(1):5623.
147. Schoof B, Jakobs O, Schmidl S, Klatte TO, Frommelt L, Gehrke T, et al. Fungal periprosthetic joint infection of the hip: a systematic review. Orthop Rev (Pavia). 2015;7(1):5748.
148. Garcia-Vidal C, Viasus D, Carratala J. Pathogenesis of invasive fungal infections. Curr Opin Infect Dis. 2013;26(3):270-6.
149. Azzam K, Parvizi J, Jungkind D, Hanssen A, Fehring T, Springer B, et al. Microbiological, clinical, and surgical features of fungal prosthetic joint infections: a multi-institutional experience. J Bone Joint Surg Am. 2009;91 Suppl 6:142-9.
150. Lee YS, Koo KH, Kim HJ, Tian S, Kim TY, Maltenfort MG, et al. Synovial Fluid Biomarkers for the Diagnosis of Periprosthetic Joint Infection: A Systematic Review and Meta-Analysis. J Bone Joint Surg Am. 2017;99(24):2077-84.
151. Deirmengian C, Kardos K, Kilmartin P, Gulati S, Citrano P, Booth RE, Jr. The Alpha-defensin Test for Periprosthetic Joint Infection Responds to a Wide Spectrum of Organisms. Clin Orthop Relat Res. 2015;473(7):2229-35.
152. Tsaras G, Maduka-Ezeh A, Inwards CY, Mabry T, Erwin PJ, Murad MH, et al. Utility of intraoperative frozen section histopathology in the diagnosis of periprosthetic joint infection: a systematic review and meta-analysis. J Bone Joint Surg Am. 2012;94(18):1700-11.
153. Deirmengian C, Kardos K, Kilmartin P, Cameron A, Schiller K, Parvizi J. Diagnosing periprosthetic joint infection: has the era of the biomarker arrived? Clin Orthop Relat Res. 2014;472(11):3254-62.
154. Bonanzinga T, Zahar A, Dutsch M, Lausmann C, Kendoff D, Gehrke T. How Reliable Is the Alpha-defensin Immunoassay Test for Diagnosing Periprosthetic Joint Infection? A Prospective Study. Clin Orthop Relat Res. 2017;475(2):408-15.
155. Shahi A, Parvizi J, Kazarian GS, Higuera C, Frangiamore S, Bingham J, et al. The Alpha-defensin Test for Periprosthetic Joint Infections Is Not Affected by Prior Antibiotic Administration. Clin Orthop Relat Res. 2016;474(7):1610-5.
156. Wyatt MC, Beswick AD, Kunutsor SK, Wilson MJ, Whitehouse MR, Blom AW. The Alpha-Defensin Immunoassay and Leukocyte Esterase Colorimetric Strip Test for the Diagnosis of Periprosthetic Infection: A Systematic Review and Meta-Analysis. J Bone Joint Surg Am. 2016;98(12):992-1000.

157. Deirmengian C, Kardos K, Kilmartin P, Cameron A, Schiller K, Parvizi J. Combined measurement of synovial fluid alpha-Defensin and C-reactive protein levels: highly accurate for diagnosing periprosthetic joint infection. J Bone Joint Surg Am. 2014;96(17):1439-45.
158. Ganz T, Selsted ME, Szklarek D, Harwig SS, Daher K, Bainton DF, et al. Defensins. Natural peptide antibiotics of human neutrophils. J Clin Invest. 1985;76(4):1427-35.
159. Chen Y, Kang X, Tao J, Zhang Y, Ying C, Lin W. Reliability of synovial fluid alpha-defensin and leukocyte esterase in diagnosing periprosthetic joint infection (PJI): a systematic review and meta-analysis. J Orthop Surg Res. 2019;14(1):453.
160. Qasim SN, Swann A, Ashford R. The DAIR (debridement, antibiotics and implant retention) procedure for infected total knee replacement - a literature review. SICOT J. 2017;3:2.
161. Segawa H, Tsukayama DT, Kyle RF, Becker DA, Gustilo RB. Infection after total knee arthroplasty. A retrospective study of the treatment of eighty-one infections. J Bone Joint Surg Am. 1999;81(10):1434-45.
162. Kuiper JW, Vos SJ, Saouti R, Vergroesen DA, Graat HC, Debets-Ossenkopp YJ, et al. Prosthetic joint-associated infections treated with DAIR (debridement, antibiotics, irrigation, and retention): analysis of risk factors and local antibiotic carriers in 91 patients. Acta Orthop. 2013;84(4):380-6.
163. Azzam KA, Seeley M, Ghanem E, Austin MS, Purtill JJ, Parvizi J. Irrigation and debridement in the management of prosthetic joint infection: traditional indications revisited. J Arthroplasty. 2010;25(7):1022-7.
164. Cobo J, Miguel LG, Euba G, Rodriguez D, Garcia-Lechuz JM, Riera M, et al. Early prosthetic joint infection: outcomes with debridement and implant retention followed by antibiotic therapy. Clin Microbiol Infect. 2011;17(11):1632-7.
165. George DA, Haddad FS. One-Stage Exchange Arthroplasty: A Surgical Technique Update. J Arthroplasty. 2017;32(9S):S59-S62.
166. Pangaud C, Ollivier M, Argenson JN. Outcome of single-stage versus two-stage exchange for revision knee arthroplasty for chronic periprosthetic infection. EFORT Open Rev. 2019;4(8):495-502.
167. Escudero-Sanchez R, Senneville E, Digumber M, Soriano A, Del Toro MD, Bahamonde A, et al. Suppressive antibiotic therapy in prosthetic joint infections: a multicentre cohort study. Clin Microbiol Infect. 2020;26(4):499-505.
168. Pradier M, Robineau O, Boucher A, Titecat M, Blondiaux N, Valette M, et al. Suppressive antibiotic therapy with oral tetracyclines for prosthetic joint infections: a retrospective study of 78 patients. Infection. 2018;46(1):39-47.
169. Goulet JA, Pellicci PM, Brause BD, Salvati EM. Prolonged suppression of infection in total hip arthroplasty. J Arthroplasty. 1988;3(2):109-16.
170. Wouthuyzen-Bakker M, Nijman JM, Kampinga GA, van Assen S, Jutte PC. Efficacy of Antibiotic Suppressive Therapy in Patients with a Prosthetic Joint Infection. J Bone Jt Infect. 2017;2(2):77-83.
171. Hake ME, Young H, Hak DJ, Stahel PF, Hammerberg EM, Mauffrey C. Local antibiotic therapy strategies in orthopaedic trauma: Practical tips and tricks and review of the literature. Injury. 2015;46(8):1447-56.
172. Gonzalez Della Valle A, Bostrom M, Brause B, Harney C, Salvati EA. Effective bactericidal activity of tobramycin and vancomycin eluted from acrylic bone cement. Acta Orthop Scand. 2001;72(3):237-40.
173. Sasaki T, Ishibashi Y, Katano H, Nagumo A, Toh S. In vitro elution of vancomycin from calcium phosphate cement. J Arthroplasty. 2005;20(8):1055-9.
174. Anagnostakos K, Wilmes P, Schmitt E, Kelm J. Elution of gentamicin and vancomycin from polymethylmethacrylate beads and hip spacers in vivo. Acta Orthop. 2009;80(2):193-7.
175. Penner MJ, Duncan CP, Masri BA. The in vitro elution characteristics of antibiotic-loaded CMW and Palacos-R bone cements. J Arthroplasty. 1999;14(2):209-14.
176. Cook GE, Markel DC, Ren W, Webb LX, McKee MD, Schemitsch EH. Infection in Orthopaedics. J Orthop Trauma. 2015;29 Suppl 12:S19-23.
177. Ma Y, Chen M, Jones JE, Ritts AC, Yu Q, Sun H. Inhibition of Staphylococcus epidermidis biofilm by trimethylsilane plasma coating. Antimicrob Agents Chemother. 2012;56(11):5923-37.

178. Lee JH, Kim YG, Cho MH, Lee J. ZnO nanoparticles inhibit Pseudomonas aeruginosa biofilm formation and virulence factor production. Microbiol Res. 2014;169(12):888-96.
179. Applerot G, Lellouche J, Lipovsky A, Nitzan Y, Lubart R, Gedanken A, et al. Understanding the antibacterial mechanism of CuO nanoparticles: revealing the route of induced oxidative stress. Small. 2012;8(21):3326-37.
180. Seil JT, Webster TJ. Antimicrobial applications of nanotechnology: methods and literature. Int J Nanomedicine. 2012;7:2767-81.
181. Qing Y, Cheng L, Li R, Liu G, Zhang Y, Tang X, et al. Potential antibacterial mechanism of silver nanoparticles and the optimization of orthopedic implants by advanced modification technologies. Int J Nanomedicine. 2018;13:3311-27.
182. Seong M, Lee DG. Silver Nanoparticles Against Salmonella enterica Serotype Typhimurium: Role of Inner Membrane Dysfunction. Curr Microbiol. 2017;74(6):661-70.
183. Khalandi B, Asadi N, Milani M, Davaran S, Abadi AJ, Abasi E, et al. A Review on Potential Role of Silver Nanoparticles and Possible Mechanisms of their Actions on Bacteria. Drug Res (Stuttg). 2017;67(2):70-6.
184. Quinteros MA, Cano Aristizabal V, Dalmasso PR, Paraje MG, Paez PL. Oxidative stress generation of silver nanoparticles in three bacterial genera and its relationship with the antimicrobial activity. Toxicol In Vitro. 2016;36:216-23.
185. Klueh U, Wagner V, Kelly S, Johnson A, Bryers JD. Efficacy of silver-coated fabric to prevent bacterial colonization and subsequent device-based biofilm formation. J Biomed Mater Res. 2000;53(6):621-31.
186. Holt KB, Bard AJ. Interaction of silver(I) ions with the respiratory chain of Escherichia coli: an electrochemical and scanning electrochemical microscopy study of the antimicrobial mechanism of micromolar Ag+. Biochemistry. 2005;44(39):13214-23.
187. Monteiro DR, Gorup LF, Takamiya AS, de Camargo ER, Filho AC, Barbosa DB. Silver distribution and release from an antimicrobial denture base resin containing silver colloidal nanoparticles. J Prosthodont. 2012;21(1):7-15.
188. Sun D, Zhang W, Mou Z, Chen Y, Guo F, Yang E, et al. Transcriptome Analysis Reveals Silver Nanoparticle-Decorated Quercetin Antibacterial Molecular Mechanism. ACS Appl Mater Interfaces. 2017;9(11):10047-60.
189. Singh N, Rajwade J, Paknikar KM. Transcriptome analysis of silver nanoparticles treated Staphylococcus aureus reveals potential targets for biofilm inhibition. Colloids Surf B Biointerfaces. 2019;175:487-97.
190. Franci G, Falanga A, Galdiero S, Palomba L, Rai M, Morelli G, et al. Silver nanoparticles as potential antibacterial agents. Molecules. 2015;20(5):8856-74.
191. Du J, Singh H, Yi TH. Antibacterial, anti-biofilm and anticancer potentials of green synthesized silver nanoparticles using benzoin gum (Styrax benzoin) extract. Bioprocess Biosyst Eng. 2016;39(12):1923-31.
192. van Hengel IAJ, Riool M, Fratila-Apachitei LE, Witte-Bouma J, Farrell E, Zadpoor AA, et al. Selective laser melting porous metallic implants with immobilized silver nanoparticles kill and prevent biofilm formation by methicillin-resistant Staphylococcus aureus. Biomaterials. 2017;140:1-15.
193. Kalishwaralal K, BarathManiKanth S, Pandian SR, Deepak V, Gurunathan S. Silver nanoparticles impede the biofilm formation by Pseudomonas aeruginosa and Staphylococcus epidermidis. Colloids Surf B Biointerfaces. 2010;79(2):340-4.
194. Chen X, Schluesener HJ. Nanosilver: a nanoproduct in medical application. Toxicol Lett. 2008;176(1):1-12.
195. Tang J, Xiong L, Zhou G, Wang S, Wang J, Liu L, et al. Silver nanoparticles crossing through and distribution in the blood-brain barrier in vitro. J Nanosci Nanotechnol. 2010;10(10):6313-7.
196. Akter M, Sikder MT, Rahman MM, Ullah A, Hossain KFB, Banik S, et al. A systematic review on silver nanoparticles-induced cytotoxicity: Physicochemical properties and perspectives. J Adv Res. 2018;9:1-16.
197. Ahamed M, Karns M, Goodson M, Rowe J, Hussain SM, Schlager JJ, et al. DNA damage response to different surface chemistry of silver nanoparticles in mammalian cells. Toxicol Appl Pharmacol. 2008;233(3):404-10.

198. van Aerle R, Lange A, Moorhouse A, Paszkiewicz K, Ball K, Johnston BD, et al. Molecular mechanisms of toxicity of silver nanoparticles in zebrafish embryos. Environ Sci Technol. 2013;47(14):8005-14.
199. Visse R, Nagase H. Matrix metalloproteinases and tissue inhibitors of metalloproteinases: structure, function, and biochemistry. Circ Res. 2003;92(8):827-39.
200. Miethling-Graff R, Rumpker R, Richter M, Verano-Braga T, Kjeldsen F, Brewer J, et al. Exposure to silver nanoparticles induces size- and dose-dependent oxidative stress and cytotoxicity in human colon carcinoma cells. Toxicol In Vitro. 2014;28(7):1280-9.
201. Li Y, Guo M, Lin Z, Zhao M, Xiao M, Wang C, et al. Polyethylenimine-functionalized silver nanoparticle-based co-delivery of paclitaxel to induce HepG2 cell apoptosis. Int J Nanomedicine. 2016;11:6693-702.
202. You F, Tang W, Yung LL. Real-time monitoring of the Trojan-horse effect of silver nanoparticles by using a genetically encoded fluorescent cell sensor. Nanoscale. 2018;10(16):7726-35.
203. Choi JE, Kim S, Ahn JH, Youn P, Kang JS, Park K, et al. Induction of oxidative stress and apoptosis by silver nanoparticles in the liver of adult zebrafish. Aquat Toxicol. 2010;100(2):151-9.
204. Zielinska E, Tukaj C, Radomski MW, Inkielewicz-Stepniak I. Molecular Mechanism of Silver Nanoparticles-Induced Human Osteoblast Cell Death: Protective Effect of Inducible Nitric Oxide Synthase Inhibitor. PLoS One. 2016;11(10):e0164137.
205. Sengstock C, Diendorf J, Epple M, Schildhauer TA, Koller M. Effect of silver nanoparticles on human mesenchymal stem cell differentiation. Beilstein J Nanotechnol. 2014;5:2058-69.
206. Berry CC, de la Fuente JM, Mullin M, Chu SW, Curtis AS. Nuclear localization of HIV-1 tat functionalized gold nanoparticles. IEEE Trans Nanobioscience. 2007;6(4):262-9.
207. Pauksch L, Hartmann S, Rohnke M, Szalay G, Alt V, Schnettler R, et al. Biocompatibility of silver nanoparticles and silver ions in primary human mesenchymal stem cells and osteoblasts. Acta Biomater. 2014;10(1):439-49.
208. Lu W, Senapati D, Wang S, Tovmachenko O, Singh AK, Yu H, et al. Effect of Surface Coating on the Toxicity of Silver Nanomaterials on Human Skin Keratinocytes. Chem Phys Lett. 2010;487(1-3).
209. Hackenberg S, Scherzed A, Kessler M, Hummel S, Technau A, Froelich K, et al. Silver nanoparticles: evaluation of DNA damage, toxicity and functional impairment in human mesenchymal stem cells. Toxicol Lett. 2011;201(1):27-33.
210. Inkielewicz-Stepniak I, Santos-Martinez MJ, Medina C, Radomski MW. Pharmacological and toxicological effects of co-exposure of human gingival fibroblasts to silver nanoparticles and sodium fluoride. Int J Nanomedicine. 2014;9:1677-87.
211. Pascarelli NA, Moretti E, Terzuoli G, Lamboglia A, Renieri T, Fioravanti A, et al. Effects of gold and silver nanoparticles in cultured human osteoarthritic chondrocytes. J Appl Toxicol. 2013;33(12):1506-13.
212. Ates M, Daniels J, Arslan Z, Farah IO. Effects of aqueous suspensions of titanium dioxide nanoparticles on Artemia salina: assessment of nanoparticle aggregation, accumulation, and toxicity. Environ Monit Assess. 2013;185(4):3339-48.
213. Petosa AR, Jaisi DP, Quevedo IR, Elimelech M, Tufenkji N. Aggregation and deposition of engineered nanomaterials in aquatic environments: role of physicochemical interactions. Environ Sci Technol. 2010;44(17):6532-49.
214. Sharma VK. Aggregation and toxicity of titanium dioxide nanoparticles in aquatic environment--a review. J Environ Sci Health A Tox Hazard Subst Environ Eng. 2009;44(14):1485-95.
215. Carlson C, Hussain SM, Schrand AM, Braydich-Stolle LK, Hess KL, Jones RL, et al. Unique cellular interaction of silver nanoparticles: size-dependent generation of reactive oxygen species. J Phys Chem B. 2008;112(43):13608-19.
216. Singh RP, Ramarao P. Cellular uptake, intracellular trafficking and cytotoxicity of silver nanoparticles. Toxicol Lett. 2012;213(2):249-59.
217. Stoehr LC, Gonzalez E, Stampfl A, Casals E, Duschl A, Puntes V, et al. Shape matters: effects of silver nanospheres and wires on human alveolar epithelial cells. Part Fibre Toxicol. 2011;8:36.

218. Samberg ME, Oldenburg SJ, Monteiro-Riviere NA. Evaluation of silver nanoparticle toxicity in skin in vivo and keratinocytes in vitro. Environ Health Perspect. 2010;118(3):407-13.
219. Suresh AK, Pelletier DA, Wang W, Morrell-Falvey JL, Gu B, Doktycz MJ. Cytotoxicity induced by engineered silver nanocrystallites is dependent on surface coatings and cell types. Langmuir. 2012;28(5):2727-35.
220. Gliga AR, Skoglund S, Wallinder IO, Fadeel B, Karlsson HL. Size-dependent cytotoxicity of silver nanoparticles in human lung cells: the role of cellular uptake, agglomeration and Ag release. Part Fibre Toxicol. 2014;11:11.
221. Albers CE, Hofstetter W, Siebenrock KA, Landmann R, Klenke FM. In vitro cytotoxicity of silver nanoparticles on osteoblasts and osteoclasts at antibacterial concentrations. Nanotoxicology. 2013;7(1):30-6.
222. Mahmood M, Li Z, Casciano D, Khodakovskaya MV, Chen T, Karmakar A, et al. Nanostructural materials increase mineralization in bone cells and affect gene expression through miRNA regulation. J Cell Mol Med. 2011;15(11):2297-306.
223. Qing T, Mahmood M, Zheng Y, Biris AS, Shi L, Casciano DA. A genomic characterization of the influence of silver nanoparticles on bone differentiation in MC3T3-E1 cells. J Appl Toxicol. 2018;38(2):172-9.
224. Niinomi M, Nakai M. Titanium-Based Biomaterials for Preventing Stress Shielding between Implant Devices and Bone. Int J Biomater. 2011;2011:836587.
225. Montoya C, Du Y, Gianforcaro AL, Orrego S, Yang M, Lelkes PI. On the road to smart biomaterials for bone research: definitions, concepts, advances, and outlook. Bone Res. 2021;9(1):12.
226. Niinomi M, Nakai M, Hieda J. Development of new metallic alloys for biomedical applications. Acta Biomater. 2012;8(11):3888-903.
227. Staiger MP, Pietak AM, Huadmai J, Dias G. Magnesium and its alloys as orthopedic biomaterials: a review. Biomaterials. 2006;27(9):1728-34.
228. Wang N, Maskomani S, Meenashisundaram GK, Fuh JYH, Dheen ST, Anantharajan SK. A study of Titanium and Magnesium particle-induced oxidative stress and toxicity to human osteoblasts. Mater Sci Eng C Mater Biol Appl. 2020;117:111285.
229. Ajib FA, Childress JM. Magnesium Toxicity. StatPearls. Treasure Island (FL)2021.
230. Chaya A, Yoshizawa S, Verdelis K, Myers N, Costello BJ, Chou DT, et al. In vivo study of magnesium plate and screw degradation and bone fracture healing. Acta Biomater. 2015;18:262-9.
231. Saris NE, Mervaala E, Karppanen H, Khawaja JA, Lewenstam A. Magnesium. An update on physiological, clinical and analytical aspects. Clin Chim Acta. 2000;294(1-2):1-26.
232. Okuma T. Magnesium and bone strength. Nutrition. 2001;17(7-8):679-80.
233. Zreiqat H, Howlett CR, Zannettino A, Evans P, Schulze-Tanzil G, Knabe C, et al. Mechanisms of magnesium-stimulated adhesion of osteoblastic cells to commonly used orthopaedic implants. J Biomed Mater Res. 2002;62(2):175-84.
234. Li RW, Kirkland NT, Truong J, Wang J, Smith PN, Birbilis N, et al. The influence of biodegradable magnesium alloys on the osteogenic differentiation of human mesenchymal stem cells. J Biomed Mater Res A. 2014;102(12):4346-57.
235. Witte F, Kaese V, Haferkamp H, Switzer E, Meyer-Lindenberg A, Wirth CJ, et al. In vivo corrosion of four magnesium alloys and the associated bone response. Biomaterials. 2005;26(17):3557-63.
236. Maradze D, Musson D, Zheng Y, Cornish J, Lewis M, Liu Y. High Magnesium Corrosion Rate has an Effect on Osteoclast and Mesenchymal Stem Cell Role During Bone Remodelling. Sci Rep. 2018;8(1):10003.
237. Huehnerschulte TA, Reifenrath J, von Rechenberg B, Dziuba D, Seitz JM, Bormann D, et al. In vivo assessment of the host reactions to the biodegradation of the two novel magnesium alloys ZEK100 and AX30 in an animal model. Biomed Eng Online. 2012;11:14.
238. Zhang S, Zhang X, Zhao C, Li J, Song Y, Xie C, et al. Research on an Mg-Zn alloy as a degradable biomaterial. Acta Biomater. 2010;6(2):626-40.
239. Li Z, Gu X, Lou S, Zheng Y. The development of binary Mg-Ca alloys for use as biodegradable materials within bone. Biomaterials. 2008;29(10):1329-44.

240. Mori H, Suzuki H, Hirai Y, Okuzawa A, Kayashima A, Kubosawa Y, et al. Clinical features of hypermagnesemia in patients with functional constipation taking daily magnesium oxide. J Clin Biochem Nutr. 2019;65(1):76-81.
241. Centers for Disease Control and Prevention. Chronic Kidney Disease in the United States, 2021 2021, March 4 [Available from: https://www.cdc.gov/kidneydisease/publications-resources/ckd-national-facts.html.
242. Contreras K, Rodriguez D, Bernal-Gutierrez M, Villamizar JP, Baquero-Galvis R, Arguello-Morales O, et al. Incidence of chronic kidney disease in patients undergoing arthroplasty: A systematic review of the literature. Orthop Rev (Pavia). 2019;11(4):8157.
243. Blake GM, Zivanovic MA, McEwan AJ, Ackery DM. Sr-89 therapy: strontium kinetics in disseminated carcinoma of the prostate. Eur J Nucl Med. 1986;12(9):447-54.
244. Pors Nielsen S. The biological role of strontium. Bone. 2004;35(3):583-8.
245. Meunier PJ. [Strontium ranelate: new therapeutic agent for postmenopausal osteoporosis]. Med Sci (Paris). 2004;20(6-7):631-3.
246. Bonnelye E, Chabadel A, Saltel F, Jurdic P. Dual effect of strontium ranelate: stimulation of osteoblast differentiation and inhibition of osteoclast formation and resorption in vitro. Bone. 2008;42(1):129-38.
247. Ding YF, Li RW, Nakai M, Majumdar T, Zhang DH, Niinomi M, et al. Osteoanabolic Implant Materials for Orthopedic Treatment. Adv Healthc Mater. 2016;5(14):1740-52.
248. Ni GX, Lu WW, Chiu KY, Li ZY, Fong DY, Luk KD. Strontium-containing hydroxyapatite (Sr-HA) bioactive cement for primary hip replacement: an in vivo study. J Biomed Mater Res B Appl Biomater. 2006;77(2):409-15.
249. Pina S, Torres PM, Goetz-Neunhoeffer F, Neubauer J, Ferreira JM. Newly developed Sr-substituted alpha-TCP bone cements. Acta Biomater. 2010;6(3):928-35.
250. Oliveira AL, Reis RL, Li P. Strontium-substituted apatite coating grown on Ti6Al4V substrate through biomimetic synthesis. J Biomed Mater Res B Appl Biomater. 2007;83(1):258-65.
251. Chen XB, Nisbet DR, Li RW, Smith PN, Abbott TB, Easton MA, et al. Controlling initial biodegradation of magnesium by a biocompatible strontium phosphate conversion coating. Acta Biomater. 2014;10(3):1463-74.
252. Kukurba KR, Montgomery SB. RNA Sequencing and Analysis. Cold Spring Harb Protoc. 2015;2015(11):951-69.
253. Stefani G, Slack FJ. Small non-coding RNAs in animal development. Nat Rev Mol Cell Biol. 2008;9(3):219-30.
254. Goodman SB, Gibon E, Yao Z. The basic science of periprosthetic osteolysis. Instr Course Lect. 2013;62:201-6.
255. Gallo J, Goodman SB, Konttinen YT, Raska M. Particle disease: biologic mechanisms of periprosthetic osteolysis in total hip arthroplasty. Innate Immun. 2013;19(2):213-24.
256. Ingham E, Fisher J. The role of macrophages in osteolysis of total joint replacement. Biomaterials. 2005;26(11):1271-86.
257. Konttinen YT, Pajarinen J. Adverse reactions to metal-on-metal implants. Nat Rev Rheumatol. 2013;9(1):5-6.
258. Goodman SB, Ma T. Cellular chemotaxis induced by wear particles from joint replacements. Biomaterials. 2010;31(19):5045-50.
259. Tunney MM, Patrick S, Curran MD, Ramage G, Anderson N, Davis RI, et al. Detection of prosthetic joint biofilm infection using immunological and molecular techniques. Methods Enzymol. 1999;310:566-76.
260. Tunney MM, Patrick S, Curran MD, Ramage G, Hanna D, Nixon JR, et al. Detection of prosthetic hip infection at revision arthroplasty by immunofluorescence microscopy and PCR amplification of the bacterial 16S rRNA gene. J Clin Microbiol. 1999;37(10):3281-90.
261. Pajarinen J, Cenni E, Savarino L, Gomez-Barrena E, Tamaki Y, Takagi M, et al. Profile of toll-like receptor-positive cells in septic and aseptic loosening of total hip arthroplasty implants. J Biomed Mater Res A. 2010;94(1):84-92.
262. Chakravarti A, Raquil MA, Tessier P, Poubelle PE. Surface RANKL of Toll-like receptor 4-stimulated human neutrophils activates osteoclastic bone resorption. Blood. 2009;114(8):1633-44.

263. Testing ECoAS. Clinical breakpoints - bacteria v 11.0 2021 [updated 06/01/2021. Available from: https://www.eucast.org/clinical_breakpoints/.
264. Wang H, Wang M, Xu X, Gao P, Xu Z, Zhang Q, et al. Author Correction: Multi-target mode of action of silver against Staphylococcus aureus endows it with capability to combat antibiotic resistance. Nat Commun. 2021;12(1):4140.
265. Randall CP, Oyama LB, Bostock JM, Chopra I, O'Neill AJ. The silver cation (Ag+): antistaphylococcal activity, mode of action and resistance studies. J Antimicrob Chemother. 2013;68(1):131-8.
266. Villapun VM, Balacco DL, Webber MA, Hall T, Lowther M, Addison O, et al. Repeated exposure of nosocomial pathogens to silver does not select for silver resistance but does impact ciprofloxacin susceptibility. Acta Biomater. 2021;134:760-73.
267. Pietsch F, O'Neill AJ, Ivask A, Jenssen H, Inkinen J, Kahru A, et al. Selection of resistance by antimicrobial coatings in the healthcare setting. J Hosp Infect. 2020;106(1):115-25.
268. Randall CP, Gupta A, Jackson N, Busse D, O'Neill AJ. Silver resistance in Gram-negative bacteria: a dissection of endogenous and exogenous mechanisms. J Antimicrob Chemother. 2015;70(4):1037-46.
269. Radzig MA, Nadtochenko VA, Koksharova OA, Kiwi J, Lipasova VA, Khmel IA. Antibacterial effects of silver nanoparticles on gram-negative bacteria: influence on the growth and biofilms formation, mechanisms of action. Colloids Surf B Biointerfaces. 2013;102:300-6.
270. Swolana D, Kepa M, Idzik D, Dziedzic A, Kabala-Dzik A, Wasik TJ, et al. The Antibacterial Effect of Silver Nanoparticles on Staphylococcus epidermidis Strains with Different Biofilm-Forming Ability. Nanomaterials (Basel). 2020;10(5).
271. Zhang YQ, Ren SX, Li HL, Wang YX, Fu G, Yang J, et al. Genome-based analysis of virulence genes in a non-biofilm-forming Staphylococcus epidermidis strain (ATCC 12228). Mol Microbiol. 2003;49(6):1577-93.
272. Yoda I, Koseki H, Tomita M, Shida T, Horiuchi H, Sakoda H, et al. Effect of surface roughness of biomaterials on Staphylococcus epidermidis adhesion. BMC Microbiol. 2014;14:234.
273. de Lacerda Coriolano D, de Souza JB, Bueno EV, Medeiros S, Cavalcanti IDL, Cavalcanti IMF. Antibacterial and antibiofilm potential of silver nanoparticles against antibiotic-sensitive and multidrug-resistant Pseudomonas aeruginosa strains. Braz J Microbiol. 2021;52(1):267-78.
274. Geng Z, Cui Z, Li Z, Zhu S, Liang Y, Liu Y, et al. Strontium incorporation to optimize the antibacterial and biological characteristics of silver-substituted hydroxyapatite coating. Mater Sci Eng C Mater Biol Appl. 2016;58:467-77.
275. Baheiraei N, Eyni H, Bakhshi B, Najafloo R, Rabiee N. Effects of strontium ions with potential antibacterial activity on in vivo bone regeneration. Sci Rep. 2021;11(1):8745.
276. Beck GR, Jr., Zerler B, Moran E. Gene array analysis of osteoblast differentiation. Cell Growth Differ. 2001;12(2):61-83.
277. Masters TL, Bhagwate AV, Dehankar MK, Greenwood-Quaintance KE, Abdel MP, Mandrekar JN, et al. Human transcriptomic response to periprosthetic joint infection. Gene. 2022;825:146400.
278. Rabin RL. CC, C and CX3C Chemokines. Encyclopedia of Hormones2003. p. 255.
279. Ranasinghe R, Eri R. Modulation of the CCR6-CCL20 Axis: A Potential Therapeutic Target in Inflammation and Cancer. Medicina (Kaunas). 2018;54(5).
280. Mittal P, Romero R, Kusanovic JP, Edwin SS, Gotsch F, Mazaki-Tovi S, et al. CXCL6 (granulocyte chemotactic protein-2): a novel chemokine involved in the innate immune response of the amniotic cavity. Am J Reprod Immunol. 2008;60(3):246-57.
281. Fisher CR, Salmons HI, Mandrekar J, Greenwood-Quaintance KE, Abdel MP, Patel R. A 92 protein inflammation panel performed on sonicate fluid differentiates periprosthetic joint infection from non-infectious causes of arthroplasty failure. Sci Rep. 2022;12(1):16135.
282. Murphy PM. Clinical Immunology - Principles and Practice. Fifth ed2019 2019.
283. Carl JW, Bai XF. IL27: its roles in the induction and inhibition of inflammation. Int J Clin Exp Pathol. 2008;1(2):117-23.
284. Wang L, Dai Z, Xie J, Liao H, Lv C, Hu Y. Alteration of the RANKL/RANK/OPG System in Periprosthetic Osteolysis with Septic Loosening. Inflammation. 2016;39(1):218-27.

285. Glass DA, 2nd, Bialek P, Ahn JD, Starbuck M, Patel MS, Clevers H, et al. Canonical Wnt signaling in differentiated osteoblasts controls osteoclast differentiation. Dev Cell. 2005;8(5):751-64.
286. Sen M, Lauterbach K, El-Gabalawy H, Firestein GS, Corr M, Carson DA. Expression and function of wingless and frizzled homologs in rheumatoid arthritis. Proc Natl Acad Sci U S A. 2000;97(6):2791-6.
287. Kobayashi Y. [Roles of Wnt signaling in bone metabolism]. Clin Calcium. 2012;22(11):1701-6.
288. Deng J, Miller SA, Wang HY, Xia W, Wen Y, Zhou BP, et al. beta-catenin interacts with and inhibits NF-kappa B in human colon and breast cancer. Cancer Cell. 2002;2(4):323-34.
289. Daghestani HN, Kraus VB. Inflammatory biomarkers in osteoarthritis. Osteoarthritis Cartilage. 2015;23(11):1890-6.
290. Guo H, Luo Q, Zhang J, Lin H, Xia L, He C. Comparing different physical factors on serum TNF-alpha levels, chondrocyte apoptosis, caspase-3 and caspase-8 expression in osteoarthritis of the knee in rabbits. Joint Bone Spine. 2011;78(6):604-10.
291. Alaaeddine N, Antoniou J, Moussa M, Hilal G, Kreichaty G, Ghanem I, et al. The chemokine CCL20 induces proinflammatory and matrix degradative responses in cartilage. Inflamm Res. 2015;64(9):721-31.
292. Pajarinen J, Jamsen E, Konttinen YT, Goodman SB. Innate immune reactions in septic and aseptic osteolysis around hip implants. J Long Term Eff Med Implants. 2014;24(4):283-96.
293. Soneson C, Delorenzi M. A comparison of methods for differential expression analysis of RNA-seq data. BMC Bioinformatics. 2013;14:91.
294. Schurch NJ, Schofield P, Gierlinski M, Cole C, Sherstnev A, Singh V, et al. How many biological replicates are needed in an RNA-seq experiment and which differential expression tool should you use? RNA. 2016;22(6):839-51.

295. Iwanaga T, Shikichi M, Kitamura H, Yanase H, Nozawa-Inoue K. Morphology and functional roles of synoviocytes in the joint. Arch Histol Cytol. 2000 Mar;63(1):17-31.